



**Biogeochemical mechanisms of P and C cycling
in rice-paddy systems driven by enzymatic reactions and
the Fe(III)-Fe(II) redox wheel**

Dissertation

to attain the Dr. rer. nat. degree

of the Faculty of Agricultural Sciences

Georg-August-Universität Göttingen

Submitted by

Chaoqun Wang

born on the 1993.06.12 in Henan Province, China

Göttingen, September 2022

1st Referee: Prof. Dr. Michaela A. Dippold

2nd Referee: Prof. Dr. Martin Maier

Date of oral examination: 2022.09.29

Summary

Rice (*Oryza sativa* L.) is one of the predominant food sources and is mainly cultivated on flooded paddy soils. However, finite and dwindling phosphate rock, the main source of phosphorus (P) fertilizer, becomes increasingly a threat to rice yield. Moreover, sustainable rice cultivation requires techniques that consume less irrigation water, i.e., alternate wetting and drying (AWD) regime, to cope with increasing water scarcity due to population growth, climate change, and water pollution. Soil flooding or drying leads to the rapid onset of reducing or oxidizing conditions, respectively. Changing redox conditions significantly affect the characteristics of redox-sensitive iron (Fe) minerals, which in turn influence the cycling of important elements such as P and carbon (C) in the soils by a multitude of redox, sorption/desorption, and (co)precipitation/dissolution processes. Biotic processes of the hydrolysis of organic P (P_o) and C by enzymes play a key role in P and C dynamics. Although the ‘enzyme latch’ and ‘iron gate’ theories for regulating soil organic matter (SOM) transformation under changing redox conditions were proposed, it remains unclear whether these mechanisms require time (weeks to months) to have clear effects on enzymatic reactions, or whether a short-term oxygen (O_2) exposure of samples adapted to anoxic conditions to O_2 can elicit a rapid specific response in enzyme assays. This rapid response is expected to be negative due to the O_2 toxicity for active anoxic microbial communities. Therefore, this thesis aims to exploring the biogeochemical mechanisms of the P and C cycling in rice-paddy soil ecosystem under fluctuating redox conditions. We hypothesized that (i) short-term (minutes to hours) aeration suppresses the activities of hydrolytic enzymes that catalyze organic matter mineralization, while medium-term (days to weeks) aeration has contrasting effects due to the adaptation of anoxic microbial communities to oxic conditions; (ii) the reductive dissolution of ferric Fe (Fe(III))-bound inorganic P (Fe-P) can contribute to the P nutrition of plants and microorganisms; and (iii) the AWD regime increases the contribution of P_o from organic residues to P nutrition of rice plants and microorganisms.

Flooded paddy rice soil mesocosms were established to investigate (i) aeration effects on the activities of three hydrolytic enzymes contributing to P (phosphomonoesterase), C (β -glucosidase), and nitrogen (N; leucine aminopeptidase) turnover (Study 1 and 2) and two oxidative enzymes mainly involved in C cycling (phenol oxidases and peroxidases) (Study 1), (ii) aeration effects on the rhizosphere extent of growing rice and the percentage of hotspot area of three hydrolytic enzyme activities (Study 3), (iii) the quantitative contribution of the Fe-P dissolution to the demands of rice plants and microorganisms (Study 4 and 5), and (iv) the effects of the Fe(III) reduction on rice root growth and the allocation dynamics of P released from Fe-P with root growth (Study 6). Additionally, a mesocosm experiment with rice plants grown either in continuous flooding (CF) or AWD paddy soils was conducted to explore the effects of these water regimes on the dynamics of P release from the Fe-P and wheat straw (Study 7). For the latter, the quantitative contributions of the Fe-P dissolution and P_o mineralization to the P nutrition of rice plants and microorganisms were estimated.

Short-term aeration (for ca. 2–2.5 h) suppressed the maximal reaction rate (V_{\max}) of hydrolytic enzymes by 5–43% but increased oxidative enzyme activities by 2–14 times in the Study 1. Short-term aeration (for 35 min) in the Study 3 decreased the *in-situ* activity of three hydrolytic enzymes by 4–61% and increased the percentage of hotspot area of enzyme activities by 3–158%. In contrast, medium-term aeration (after 10-day oxic vs. anoxic pre-incubation) increased V_{\max} of hydrolytic enzymes by 12–253% in the Study 2. Thus, the activation of oxidative enzymes by short-term aeration was uncoupled from the hydrolytic enzymes. This put to a question both the “iron gate” and “enzyme latch” mechanisms. The effect of aeration on anoxic enzyme activities ultimately depends on the aeration duration and controls sequential mechanisms starting from suppression of microbial activity and enzyme production followed by adaptation of microbial communities to newly established conditions.

To quantify relevance of the Fe-P dissolution for plant and microbial P uptake in the Studies 4 and 5, ^{32}P -labeled ferrihydrite (31 mg P kg^{-1}) was supplied either (1) in polyamide mesh bags ($30 \mu\text{m}$ mesh size) to prevent roots but not microorganisms from direct Fe-P mobilization, or (2) directly mixed with soil to enable roots and microorganisms unrestricted access to the Fe-P. The contribution of Fe-P to microbial biomass P (MBP) remarkably decreased from 4.5% to almost zero from day 10 to 33 after rice transplantation. Nearly 2% of Fe-P compensated up to 16% of the plant P uptake 33 days after rice transplantation. Microbial biomass C (MBC) and dissolved organic C contents decreased from day 10 to 33 by 8–54% and 68–77%, respectively, suggesting that the microbially-mediated Fe(III) reduction was C-limited. A novel *in-situ* ^{32}P phosphor-imaging approach under flooding was developed in the Study 6 to estimate P uptake by rice roots released from Fe-P dissolution. Direct root access to Fe-P raised both the number and mean diameter of crown roots and root tips, and increased P uptake by 149–231%. Therefore, rice varieties with extended crown root densities will increase P uptake when P is limiting in paddy soils.

To estimate the contributions of the Fe-P dissolution and P_o mineralization to the P nutrition of plants and microorganisms under different water regimes in the Study 7, pre-germinated rice plants were grown for 40 days in rhizoboxes under either CF or AWD. ^{32}P -labeled ferrihydrite (30 mg P kg^{-1}) and ^{33}P -labeled wheat straw ($10 \text{ g straw kg}^{-1}$) were added. Continuous flooding stimulated P release to the soil solution by increasing Fe(III) reduction and wheat straw mineralization compared to AWD. The proportions of P from Fe-P and straw in rice plants and MBP were 5–64% higher under CF vs. AWD regime. The contributions of Fe-P and straw to MBP were 72–78% lower and 16–42% higher in rooted vs. bulk soil, respectively, suggesting a strong competition between plants and microorganisms for P. The Fe-P and straw compensated up to 16% and 20% of the plant P uptake and 15% and 35% microbial P uptake 40 days after rice transplantation, respectively. Relatively high contribution of P_o to the P nutrition of plants and microorganisms calls for the adaptation of the P fertilization strategies to avoid excess chemical P fertilizer inputs.

In summary, short-term and medium-term aeration had contrasting effects on hydrolytic enzyme activities, thus supporting the first hypothesis. The

underestimation of hydrolytic enzyme activities due to short-term aeration bias may lead to a strongly skewed mechanistic understanding of SOM transformations in anoxic environments with follow-up complications for process-based modeling. The sensitivity of anoxic enzymes to the O₂ adaptation mechanisms requires strong consideration for understanding the SOM dynamics in fluctuating O₂ environments. Fe-P and wheat straw compensated up to 16% and 20% of plant P demand, respectively, thereby supporting the second hypothesis that Fe-P can serve as a P source. In reality higher than expected hydrolytic enzyme activities lead to considerable decomposition of fresh organic matter – one of the underlying mechanisms making straw as a P source even in anoxic systems. An increase in C availability for microorganisms intensifies P mobilization, which is especially critical at early stages of rice growth. Continuous flooding increased the contributions of P released from Fe-P and wheat straw to P nutrition compared to AWD, thus is against the third hypothesis that AWD increases the contribution of P_o to P nutrition. This can be attributed to (i) decreased P availability caused by increasing P sorption capacity of soils after drying and (ii) increased competition between plants and microorganisms for P. Microorganisms appear to be more competitive for P_o than rice plants, and rice plants are more competitive than microorganisms for P released from the Fe-P dissolution. Therefore, the P fertilization strategies should consider the P mobilization from Fe (oxyhydr)oxides and straw under different water regimes in paddy soils during rice growth.

Finally, this thesis developed new approaches dedicated to accuracy of enzyme activity measurements and to quantitative assessment of the dynamics of P uptake by plants under low redox conditions. Our studies also open further perspectives for the investigation of (i) the mechanisms of aeration effects on enzyme activities and (ii) the contribution of inorganic P and organic P to the nutrition balance and competition between microorganisms and plants under changing redox conditions.

Acknowledgements

Nearly three years of my PhD study at University of Goettingen have taught me that life always teaches you more than you can imagine. This is a great journey that makes me stronger.

First and foremost, I would like to express my deepest appreciation to my supervisor, Dr. Maxim Dorodnikov, who offered me a chance to finish my PhD study at University of Goettingen and provided continuous support for my study. He not only provided professional advice, brilliant ideas, and critical recommendations on my PhD project and manuscripts, but also gave an unforgettable memory of his kindness, patience, intelligence, and diligence. I could not have imagined how lucky I am to have such a good advisor.

I gratefully acknowledge the rest of my thesis committee, Prof. Michaela Dippold, and Prof. Georg Guggenberger. Special thanks to Prof. Dippold for helping me get away from that dark period and for her insightful advice and continuously creative suggestions on my PhD project and manuscripts. My sincere thanks also go to Prof. Guggenberger for offering partly financial support for my PhD study and for providing excellent suggestions on my manuscripts. Furthermore, I would thank Prof. Martin Maier for his help on my thesis.

Besides my thesis committee members, I sincerely thank Prof. Yakov Kuzyakov and Dr. Evgenia Blagodatskaya for their insightful advice and creative suggestions on my PhD project and manuscripts. Thanks also to Dr. Callum C. Banfield for his kind support in advising in ^{32}P and ^{33}P measurements and image analyses. I also would take this opportunity to thank my colleagues from the Biogeochemistry of Agroecosystems group, in particular Karin Schmidt and Susann Enzmann for their kind help in sample measurements. I also thank Bernd Kopka, Jan Muhr, and Marvin Blaue of the Laboratory for Radioisotopes (LARI) of the University of Goettingen for their advice, support, and measurements.

Last but not the least, I sincerely thank my family for their unconditional love, care, and spiritual support throughout my life. I am most grateful to my girlfriend, Lin Xue, for her continuous accompany, patience, and encouragement.

Table of contents

Summary.....	1
Acknowledgements.....	4
Table of contents.....	5
List of Figures.....	7
List of Tables.....	16
Abbreviations.....	17
1. Extended summary.....	18
1.1 Introduction.....	18
1.2 Objectives.....	21
1.3 Hypotheses.....	22
1.4 Material and methods.....	22
1.5 Results and discussion.....	29
1.6 Conclusions.....	36
References.....	39
Contributions to the included manuscripts.....	45
2. Publications and manuscripts.....	48
Study 1 Keep oxygen in check: contrasting effects of short-term aeration on hydrolytic versus oxidative enzymes in paddy soils.....	48
Study 2 Oxygen matters: Short- and medium-term effects of aeration on hydrolytic enzymes in a paddy soil.....	71

Study 3 Keep oxygen in check: an improved in-situ zymography approach for mapping anoxic hydrolytic enzyme activities in a paddy soil.....	102
Study 4 Can the reductive dissolution of ferric iron in paddy soils compensate phosphorus limitation of rice plants and microorganisms?.....	128
Study 5 Microbial iron reduction compensates for phosphorus limitation in paddy soils.....	157
Study 6 Reductive dissolution of iron phosphate modifies rice root morphology in phosphorus-deficient paddy soils.....	177
Study 7 The wetter the better: continuous flooding promoted phosphorus uptake by rice from ³³ P-organic and ³² P-inorganic phosphorus sources compared to alternate wetting and drying.....	209
Curriculum vitae.....	234
Declaration.....	236

List of Figures

Extended summary:

Fig. ES1 The dimensions of a rhizobox with plexiglas cover on top, sealed with rubber gasket (not visible on photo) and fixed by thumbscrews (a), sampling of soil from compartments of a rhizobox, glass bottles for soil suspension preparation and the level of O₂ as indicated by an O₂-sensor (b), the sampling locations of three soil compartments 48 hours after water drainage (c), and a substrate saturated zymography membrane and the O₂ level as indicated by an O₂-sensor (d). In subfigure c, the level of flooded water maintained during experiment is shown schematically by a dashed line. Shaded spots within each compartment correspond to the removed soil.....23

Fig. ES2 Diagram of the experimental design to test the effects of medium-term (10-day pre-incubation) and short-term (2-h assay) aeration (red boxes) vs. anoxic controls (blue boxes) on activities of three hydrolytic enzymes (phosphomonoesterase, β -glucosidase, and leucine aminopeptidase) in soils from three rhizobox compartments (top bulk, rooted, and bottom bulk) collected at three rice growth stages (seedling stage, 10 days after rice transplantation; early tillering stage, 16–20 days; late tillering stage, 28–31 days). Photos of rice are examples of growth stages (there were 9 rhizoboxes with plants for each of the three enzymes tested)..... 25

Fig. ES3 Diagram of the experimental design. MicroRhizon® samplers were placed at the P-rich patch zone, and a platinum electrode for measuring redox potential (E_h) was installed in each rhizobox. Pre-filled soil corresponds to paddy soil filled into rhizoboxes 16–24 h prior the addition of ferric iron-bound P. Filled soil is the paddy soil added during Fe–P placement and rice seedlings transplantation..... 26

Fig. ES4 Mechanisms of hydrolytic enzymes suppression by short-term (during 2 hours) O₂ exposure. Left side (a): enzymatic reactions conducted by hydrolytic enzymes under anoxic conditions. Right side (b): reduction of microbial activity (pathway I), toxicity of reactive oxygen species (ROS) to microbial cells (pathway II), and compensatory mechanism of anti-stress enzyme production, e.g. catalase, superoxide dismutase (pathway III). Size of arrows corresponds to relative intensity of enzyme production or reaction rates. Triangles on top reflect the relative increase of the short-term suppressive effect of oxygen (brown) and the concurrent relative decrease of enzymatic maximal reaction rate (V_{max}, blue) with O₂..... 30

Fig. ES5 Mechanisms of hydrolytic enzymes suppression by short-term aeration due to (1) toxicity of reactive oxygen species (ROS) to microbial cells, (2) decreasing efficiency of phenol oxidase because of Fe (II) oxidation and accumulation of phenolics (“iron-gate”), and activation by medium-term aeration due to cancelling of suppressive factors. Arrow size: relative intensity of active enzyme production, reaction rates, or substrate turnover rate. Triangles with color gradients: the intensity of O₂ effects on enzyme activities from low (blueish) to high (reddish)..... 31

Fig. ES6 Effects of short-term aeration on *in-situ* hydrolytic enzyme activities,

hotspot area, and rhizosphere extent in a flooded paddy soil.....32

Fig. ES7 Conceptual scheme demonstrating the shift from microorganisms outcompeting rice plants for phosphorus to rice plants outcompeting microorganisms. Red solid line demonstrates the dynamics of microbially driven Fe(III) reduction. Blue lines show ³²P recovery either in rice plants (dashed line) or in microbial biomass (solid line) with rice plant growth..... 33

Fig. ES8 Conceptual scheme demonstrating the shift from P-limitation to C-limitation for microorganisms during 33 days of rice growth. Blue lines show either microbial biomass C (MBC) or redox potential E_h dynamics with rice growth. Red dashed line demonstrates the dynamics of microbially-mediated Fe(III) reduction. Green dashed line shows ³²P recovery in rice plants with rice plant growth..... 34

Fig. ES9 A schematic diagram of the effects of direct accessibility of ferric iron-bound phosphate (Fe-P) by rice roots on root architecture under low phosphate conditions. With the application of Fe-P directly to the soil, Fe-P pellet re-distribution resulted in a large area, where roots were directly in contact with Fe-P. When Fe-P was not restricted by mesh bags, roots could provide carbon to Fe-reducing microorganisms to boost microbial growth and activity (blue circles)..... 35

Fig. ES 10 Conceptual scheme demonstrating the effects of water regimes on mineral phosphorus (P) availability and the contributions of ferric iron-bound P (Fe-P) and wheat straw-driven P to P uptake by rice plants and microorganisms. Trapezoids with color gradients demonstrate either the relative P availability in soil solution or the relative contributions of Fe-P and wheat straw to microbial biomass P from high (dark) to low (light)..... 36

Study 1:

Fig. 1 (a) Sampling locations in the three soil compartments 48 hours after flood water drainage for the Research task 1: moderate O₂ limitation; shaded spots within each compartment correspond to the removed soil; the level of flooded water maintained during experiment is shown schematically by a dashed line. (b) Incubation set-up for the Research task 2: strong O₂ limitation with water-saturated soil in a bottle sealed with a thick air-impermeable butyl rubber septum..... 54

Fig. 2 The maximum reaction rate (V_{max}) of phosphomonoesterase (PME, a), β-glucosidase (BG, b), and leucine aminopeptidase (LAP, c) and the affinity to a substrate (K_m) of PME (d), BG (e), and LAP (f) at the top bulk, rooted, and bottom bulk soil of rhizoboxes with growing rice under moderate O₂ limitation (research task 1) in oxic (+O₂, dashed lines) and anoxic (-O₂, solid lines) assays. The data are means ± standard deviations (n = 3)..... 58

Fig. 3 The maximum reaction rate (V_{max}) of phosphomonoesterase (PME, a), β-glucosidase (BG, b), and leucine aminopeptidase (LAP, c) and the affinity to a substrate (K_m) of PME (d), BG (e), and LAP (f) in soils under strong O₂ limitation (research task 2) in oxic (+O₂, dashed lines) and anoxic (-O₂, solid lines) assays. The

data are means \pm standard deviations ($n = 4$). The vertical red lines correspond to the duration of autofluorescence when enzyme activity is not measurable. Downward arrows represent the negative aeration effect on V_{max} . Size of a arrow indicate the relative intensity of the aeration..... 59

Fig. 4 The activity (a) of phenol oxidases (yellow lines) and peroxidases (blue lines) and the concentration dynamics (b) of soluble Fe(II) (blue) and Fe(III) (yellow) in soil suspension either in oxic (+O₂) or anoxic (-O₂) assays. The data are means \pm standard deviations ($n = 4$). Solid lines in subFig. b indicate significant linear correlations. Arrows represent the aeration effect on either the activity of phenol oxidases and peroxidases or the concentration dynamics of soluble Fe(II) and Fe(III) in soil suspension. Size of arrows indicates the relative intensity and direction corresponds to a positive or a negative aeration effect on a parameter..... 60

Fig. 5 Mechanisms of hydrolytic enzymes suppression by short-term (during 2 hours) O₂ exposure. Left side (a): enzymatic reactions conducted by hydrolytic enzymes under anoxic conditions. Right side (b): reduction of microbial activity (pathway I), toxicity of reactive oxygen species (ROS) to microbial cells (pathway II), and compensatory mechanism of anti-stress enzyme production, e.g. catalase, superoxide dismutase (pathway III). Size of arrows corresponds to relative intensity of enzyme production or reaction rates. Triangles on top reflect the relative increase of the short-term suppressive effect of oxygen (brown) and the concurrent relative decrease of enzymatic maximal reaction rate (V_{max} , blue) with O₂..... 62

Study 2:

Fig. 1 Diagram of the experimental design to test the effects of medium-term (10-day pre-incubation) and short-term (2-h assay) aeration (red boxes) vs. anoxic controls (blue boxes) on activities of three hydrolytic enzymes (phosphomonoesterase, β -glucosidase, and leucine aminopeptidase) in soils from three rhizobox compartments (top bulk, rooted, and bottom bulk) collected at three rice growth stages (seedling stage, 10 days after rice transplantation; early tillering stage, 16-20 days; late tillering stage, 28-31 days). Photos of rice are examples of growth stages (there were 9 rhizoboxes with plants for each of the three enzymes tested)..... 78

Fig. 2 The maximum reaction rate (V_{max}) and the inverse of the affinity to a substrate (K_m) of phosphomonoesterase (a, b, c), β -glucosidase (d, e, f), and leucine aminopeptidase (g, h, i) of samples after anoxic (blue) and oxic (red) pre-incubation at the top bulk-, rooted-, and bottom bulk soil during rice plant growth (seeding (triangle), early- (diamond), and late tillering (stars) stages) in oxic (+O₂, filled symbols) and anoxic (-O₂, open symbols) assays. The data are the means \pm standard deviations ($n = 3$). Arrows: the effect of medium-term (10-day) aeration on V_{max} and K_m during pre-incubation. Significance of the effect is denoted by P values in bold font. Missing arrows: no effect. Original data are shown in Supplementary tables 1, 2, and 3..... 80

Fig. 3 Relative difference ($\Delta\%$) for catalytic efficiency of enzymes (K_a) due to

short-term aeration during assays (2-h) after anoxic pre-incubation (a, left) and oxic pre-incubation O₂ (a, right), and relative difference ($\Delta\%$) for K_a in -O₂ (b, unshaded) and +O₂ (b, shaded) assays due to medium-term (10-day) oxic and anoxic pre-incubation in top bulk, rooted, and bottom bulk soil compartments. Values are means between seedling, early- and late tillering stages of rice growth. Original data are shown in Supplementary tables 4, 5, and 6. Asterisks: significant differences ($P < 0.05$) between oxic and anoxic pre-incubation as well as between -O₂ and +O₂ assays. 82

Fig. 4 The turnover time (T_1) of respective substrates catalyzed by phosphomonoesterase (left), β -glucosidase (middle), and leucine aminopeptidase (right) after anoxic and oxic pre-incubation of the top bulk-, rooted-, and bottom bulk soil during rice plant growth (seedling, early-, and late tillering stages) in oxic (+O₂) and anoxic (-O₂) assays. The data are the means of three replicates ($n = 3$). Original data are shown in Supplementary tables 4, 5, and 6.....84

Fig. 5 Mechanisms of hydrolytic enzymes suppression by short-term aeration due to (1) toxicity of reactive oxygen species (ROS) to microbial cells, (2) decreasing efficiency of phenol oxidase because of Fe (II) oxidation and accumulation of phenolics (“iron-gate”), and activation by medium-term aeration due to cancelling of suppressive factors. Arrow size: relative intensity of active enzyme production, reaction rates, or substrate turnover rate. Triangles with color gradients: the intensity of O₂ effects on enzyme activities from low (blueish) to high (reddish)..... 86

Study 3:

Fig. 1 Examples of zymograms with spatial distribution of phosphomonoesterase (PME), β -glucosidase (BG), and leucine aminopeptidase (LAP) activities under oxic (+O₂) and anoxic (-O₂) conditions at seedling, early-, and late tillering stages of rice growth. Cavities (poor attachment) are shown as black area. Calibration scale bars on the right side correspond to 4-methylumbelliferone (MUF) representing PME and BG activities (top) and to 7-amino-4-methylcomarin (AMC) representing LAP activity (bottom). Triangles and percentage values below images correspond either to suppression of enzyme activities due to aeration or activation of enzyme activities due to removal of O₂. For demonstration, one of three replicates and one of rice growth stages were chosen; the complete set of zymograms is shown on Fig. S3.....111

Fig. 2 The zymogram-based activities of phosphomonoesterase (PME), β -glucosidase (BG), and leucine aminopeptidase (LAP) at three soil compartments (top bulk, rooted, and bottom bulk soils) under oxic (+O₂) and anoxic (-O₂) conditions at three stages (seedling (I), early- (II) and late tillering (III) stage) of rice growth. The data are shown as the means \pm standard deviations ($n = 3$) of respective zymograms (Fig. 1 and S3). The results of effects of assay condition, rice growth stage, soil compartment, and their interactions on enzyme activities analyzed by three-way ANOVA can be found in Table 1. Different uppercase or lowercase letters represent significant differences ($p < 0.05$) among three compartments at the same rice growth stage or among three rice growth stages of each compartment, respectively. Significant differences ($p < 0.05$) between +O₂ and -O₂ assays are indicated by asterisk..... 112

Fig. 3 The percentage of hotspot area per rhizobox surface for phosphomonoesterase, β -glucosidase, and leucine aminopeptidase under oxic (+O₂) and anoxic (-O₂) conditions at the three rice growth stages. Significant differences ($p < 0.05$) between oxic and anoxic assays are indicated by asterisk. Different uppercase or lowercase letters represent significant differences ($p < 0.05$) among three rice growth stages under +O₂ or -O₂ conditions, respectively..... 113

Fig. 4 The rhizosphere gradient and extent of phosphomonoesterase (a), β -glucosidase (b), and leucine aminopeptidase (c) activities as a function of distance from root center under oxic (+O₂) and anoxic (-O₂) conditions, and the difference in rhizosphere extent (%) between -O₂ and +O₂ assays depending on initial conditions – either first -O₂ and then +O₂ (transition from anoxic to oxic) or *vice versa* (transition from oxic to anoxic) (d). Each curve refers to the mean activity of each enzyme measured at 9-15 roots in the three replicated zymograms. The vertical lines (dashed for +O₂ and solid for -O₂) mark the border between rhizosphere and bulk soil as defined by one-way ANOVA. The differences in rhizosphere extent are shown as the means \pm standard deviations of the three rice growth stages ($n = 5$ (rhizoboxes) under the transition from anoxic to oxic conditions and $n = 4$ (rhizoboxes) under the transition from oxic to anoxic conditions). Significant differences ($p < 0.05$) between the transition from anoxic to oxic conditions and the transition from oxic to anoxic conditions are indicated by asterisk..... 114

Study 4:

Fig. 1 Diagram of the experimental design. MicroRhizon® samplers were placed at the P-rich patch zone, and a platinum electrode for measuring redox potential (E_h) was installed in each rhizobox. Pre-filled soil corresponds to paddy soil filled into rhizoboxes 16–24 h prior the addition of ferric iron-bound P. Filled soil is the paddy soil added during Fe-P placement and rice seedlings transplantation..... 134

Fig. 2 Soil redox potential E_h (top), the recovery of ³²P (middle) and total soluble Fe concentration (bottom) in soil solution during the first (DS1), second (DS2), and third (DS3) periods of rice growth before destructive sampling. The data are the means \pm standard errors ($n = 4$). Letters represent significant differences ($p < 0.05$) among sampling dates of each period of rice growth under Pellets-in-mesh bag (uppercase) or Pellets-no-mesh bag (lowercase) treatment, respectively. Significant differences ($p < 0.05$) between Pellets-in-mesh bag and Pellets-no-mesh bag treatments are indicated by asterisk..... 139

Fig. 3 Relationships between redox potential E_h and ³²P recovery in soil solution under Pellets-in-mesh bag and Pellets-no-mesh bag treatments in the first 10 days after rice transplantation of the 1st destructive sampling (DS1, a), 10 days of the DS2 (b), and 11 days of DS3 (c), respectively. Solid lines indicate significant non-linear correlations..... 140

Fig. 4 Microbial biomass carbon (MBC, a), nitrogen (MBN, b), and phosphorus (MBP, c) content in the top bulk, rooted, and bottom bulk soil under Pellets-in-mesh

bag (left side) and Pellets-no-mesh bag treatment (right side) of the first (DS1, 10 days), second (DS2, 18 days), and third destructive sampling (DS3, 33 days) after rice transplantation. The data are the means \pm standard errors ($n = 4$)..... 141

Fig. 5 Proportion of phosphorus (P) derived from applied ferric iron-bound P (Fe-P) in shoots or roots (a) and microbial biomass P (MBP, b), and the ratio of ^{32}P recovery in MBP in rooted soil and that in root P (c) under Pellets-in-mesh bag (solid lines) and Pellets-no-mesh bag treatment (dashed lines) of the first (DS1, 10 days), second (DS2, 18 days), and third destructive sampling (DS3, 33 days) after rice transplantation. The data are the means \pm standard errors ($n = 4$). Significant differences ($p < 0.05$) between Pellets-in-mesh bag and Pellets-no-mesh bag treatments are indicated by asterisk..... 142

Fig. 6 Maximum reaction rate (V_{\max}) and the affinity to a substrate (K_m) of phosphomonoesterase (PME, a, b, c), β -glucosidase (BG, d), and leucine aminopeptidase (LAP, e) in the top bulk, rooted, and bottom bulk soil under Pellets-in-mesh bag and Pellets-no-mesh bag treatments of the first (DS1, 10 days for PME), second (DS2, 18 days for PME), and third destructive sampling (DS3, 33 days for PME, BG, and LAP) after rice transplantation. The data are the means \pm standard errors ($n = 4$). Table inside shows p values of the effects of treatment (Pellets-in-mesh bag vs. Pellets-no-mesh bag), soil compartment, and their interactions on V_{\max} and K_m of PME, BG, and LAP analyzed by a two-way ANOVA. Additionally, the V_{\max} and K_m of PME were analyzed by a two-way ANOVA with repeated measures (destructive sampling, $n = 3$). The p values in bold in the table inside indicate significant effects of treatments and their interactions on V_{\max} or K_m 143

Fig. 7 Conceptual scheme demonstrating the shift from microorganisms outcompeting rice plants for phosphorus to rice plants outcompeting microorganisms. Red solid line demonstrates the dynamics of microbially driven Fe(III) reduction. Blue lines show ^{32}P recovery either in rice plants (dashed line) or in microbial biomass (solid line) with rice plant growth..... 147

Study 5:

Fig. 1 Dynamics of soil redox potential E_h (a), total iron (Fe) concentration (b), and ^{32}P recovery in soil solution (c, based on Eq.1) after rice transplantation. The data are mean \pm standard error ($n = 24$ during 10 days after rice transplantation, $n = 16$ during 10–18 days, and $n = 8$ during 18–32 days). Lowercase letters represent significant differences ($p < 0.05$) among the three sampling dates. The orange shaded area in ‘a’ shows the redox potential area where Fe(III) or Fe(II) exists at a soil pH of 6.2..... 165

Fig. 2 Dissolved carbon (C; a) and phosphorus (P; b), and microbial biomass carbon (MBC; c) and phosphorus (MBP; d) at the top bulk-, rooted-, and bottom bulk soil in rhizoboxes after 10, 18, and 33 days of rice growth. The data are mean \pm standard error ($n = 8$). The p values show the effects of rice growth or soil compartment on the respective parameter..... 166

Fig. 3 ^{32}P recovery from applied ferric iron-bound phosphorus (Fe(III)- ^{32}P) in plant

(black solid line) and microbial biomass (MBP, black dashed line, left Y-axis) and the uptake rate of Fe(III)-³²P in total plant P (red solid line) and MBP (red dashed line, right Y-axis). The data are mean ± standard error (n = 8). Uppercase or lowercase letters represent significant differences ($p < 0.05$) in the recovery of Fe(III)-³²P in total plant P and MBP or the recovery rate of Fe(III)-³²P in total plant P and MBP among three sampling dates, respectively..... 167

Fig. 4 Proportion of total phosphorus (P) from the applied ferric iron-bound P (Fe(III)-P) to total P in plant shoots and roots (a, based on Eq. 2) or total P in microbial biomass (MBP, b, based on Eq. 3). The data are mean ± standard error (n = 8)..... 167

Fig. 5 Relationships between shoot (green) and root (yellow) C:N, C:P, and N:P ratios to the respective ratios in dissolved organic matter in rooted soil (n = 24). Solid lines indicate linear correlations significant at $p < 0.05$ 168

Fig. 6 Conceptual scheme demonstrating the shift from P-limitation to C-limitation for microorganisms during 33 days of rice growth. Blue lines show either microbial biomass C (MBC) or redox potential E_h dynamics with rice growth. Red dashed line demonstrates the dynamics of microbially-mediated Fe(III) reduction. Green dashed line shows ³²P recovery in rice plants with rice plant growth..... 170

Study 6:

Fig. 1 Soil redox potential E_h (a), ³²P recovery (b), and total soluble Fe concentration (c) in soil solution after rice transplantation. The data are the means ± standard errors (n = 24 during 10 d after rice transplantation, n = 16 during 14–18 d, and n = 8 during 24–32 d) and are modified from Wang et al., 2022. Soil Bio. Biochem., Fig.2. The orange shaded area in a, b, and c shows the redox potential area where Fe(III) or Fe(II) exist for the soil pH of 6.2..... 188

Fig. 2 Examples of spatial distribution of ³²P activities during 32 days of the experiment under Pellets-in-mesh bag (top) or Pellets-no-mesh bag (bottom) treatment. Calibration scale bar on the right side represents ³²P activity per mm⁻². For demonstration, one of four replicates of each treatment was chosen..... 188

Fig. 3 Examples of spatial distribution of ³²P activities (in Bq per mm⁻² of rhizobox area) under Pellets-in-mesh bag (left side) or Pellets-no-mesh bag (right side) treatment. Calibration scale bar on the right side represents ³²P activity. For demonstration, one of four replicates of each treatment at 32 d after rice transplantation was chosen; full set of images of these two rhizoboxes demonstrating the dynamics of spatial distribution of ³²P activities are shown on Fig. 2. Red dashed lines represent borders of the maximally rooted zone of rice under two treatments. A or B is an example of root tip under Pellets-in-mesh bag or Pellets-no-mesh bag treatment, respectively..... 189

Fig. 4 Detectable root number on the soil surface (a), crown root diameter (b), crown root elongation rate (c), detectable root tip number on the soil surface (d), root tip

diameter (e), and maximally rooted soil area (f) under Pellets-in-mesh bag (blue lines) and Pellets-no-mesh bag (yellow lines) treatments calculated from rhizoboxes of the third destructive sampling (DS3, 33 days) at 15, 19, 24, 28, and 32 d after rice transplantation. The data are means \pm standard errors ($n = 4$). Solid lines indicate correlations significant at $p < 0.05$. The orange shaded area in b and e shows the period when most of crown roots distributed either in the applied Fe-P patch (b) or towards the rhizobox bottom (e)..... 190

Fig. 5 (a) Examples of the profiles of ^{32}P activity as a function of distance along soil through a root rip to crown root (see inlet as an example on subFig. a) under Pellets-in-mesh bag (blue lines) and Pellets-no-mesh bag (yellow lines) treatments calculated from rhizoboxes for the third destructive sampling (DS3, 33 days) at 24 d after rice transplantation. (b) Mean ^{32}P activities in soil (0–0.5 cm away from root tip), root tips, and roots (0–3 cm away from root tip) under Pellets-in-mesh bag (solid lines) and Pellets-no-mesh bag (dashed lines) treatments calculated from rhizoboxes for the third destructive sampling (DS3, 33 days) at 15, 19, 24, 28, and 32 d after rice transplantation. Data are radial means \pm standard errors ($n = 12$)..... 191

Fig. 6 Radial profiles of ^{32}P activities as a function of the distance from the crown root center at a position of ca. 1 cm away from root tips under Pellets-in-mesh bag (blue lines) and Pellets-no-mesh bag (yellow lines) treatments calculated from rhizoboxes for the third destructive sampling (DS3, 33 days) at 15 (a), 19 (b), 24 (c), 28 (d), and 32 (e) d after rice transplantation. Data are the means \pm standard errors ($n = 12$)..... 192

Fig. 7 ^{32}P recovery from applied ferric iron-bound phosphate ($\text{Fe-}^{32}\text{P}$) in microbial biomass (MBP, a) and shoots or roots (b), the ratio of ^{32}P recovery in MBP in rooted soil and that in roots (c), and Fe content in shoots or roots (d) under Pellets-in-mesh bag and Pellets-no-mesh bag treatments of the first (DS1, 10 d), second (DS2, 18 d), and third destructive sampling (DS3, 33 d) after rice transplantation. The data are the means \pm standard errors ($n = 4$)..... 193

Fig. 8 A schematic diagram of the effects of direct accessibility of ferric iron-bound phosphate (Fe-P) by rice roots on root architecture under low phosphate conditions. With the application of Fe-P directly to the soil, Fe-P pellet re-distribution resulted in a large area, where roots were directly in contact with Fe-P. When Fe-P was not restricted by mesh bags, roots could provide carbon to Fe-reducing microorganisms to boost microbial growth and activity (blue circles)..... 196

Study 7:

Fig. 1 Diagram of the experimental design. ^{32}P -labeled ferrihydrite (Fe-P) and ^{33}P -labeled wheat straw were evenly mixed with the soil. The rhizoboxes were filled with water to a depth of 2–3 cm from soil surface from day 1 to day 40 under continuously flooding and at wetting phase from day 11 to day 20 and from day 31 to day 40 under alternate wetting and drying regime. Microrhizon samplers were placed at the middle of rhizoboxes, and a platinum electrode for measuring redox potential

(E_h) was installed in each rhizobox..... 214

Fig. 2 Soil redox potential E_h (a), the recovery of ³²P (b) and ³³P (c), and the concentrations of Fe(II) (solid lines) and Fe(III) (dash lines) (d) in soil solution under continuous flooding (CF) (blue lines) and alternate wetting and drying (AWD) (yellow lines) regimes. The blue and orange shaded areas show the wetting and drying phases under AWD regime, respectively. Under AWD regime, the absence of data on day 40 indicates failure of soil solution collection due to increased evaporation and rice plant transpiration. The data are the means ± standard errors (n = 4). Two-way ANOVA revealed significant effects (*p* < 0.001) of water regimes and rice growth on E_h values, the proportions of ³²P and ³³P, and the concentrations of Fe(II) and Fe(III) in soil solution..... 220

Fig. 3 Relationships between redox potential (E_h values) and either ³²P (a) or ³³P (b) proportions in soil solution under continuous flooding (CF) and alternate wetting and drying (AWD) regimes..... 221

Fig. 4 Microbial biomass carbon (MBC, a), nitrogen (MBN, b), and phosphorus (MBP, c) contents in the top bulk, rooted, and bottom bulk soils under continuous flooding (CF) and alternate wetting and drying (AWD) regimes. The data are the means ± standard errors (n = 4). The *p* values show the effects of water regime or rice growth on the respective parameter..... 221

Fig. 5 Maximum reaction rate (V_{max}) and the affinity to a substrate (K_m) of phosphomonoesterase (PME) in the top bulk, rooted, and bottom bulk soil under continuous flooding (CF) (filled symbols) and alternate wetting and drying (AWD) (open symbols) regimes. The data are the means ± standard errors (n = 4). Uppercase and lowercase letters represent significant differences (*p* < 0.05) in V_{max} and K_m between CF and AWD regimes, respectively. Significant differences (*p* < 0.05) in V_{max} and K_m values among the soil compartments were observed..... 222

Fig. 6 Proportions of phosphorus (P) derived from applied ferric iron-bound P (Fe-P) and wheat straw in shoots or roots (a, b) and microbial biomass P (MBP, c, d) under continuous flooding (CF) and alternate wetting and drying (AWD) regimes. The data are the means ± standard errors (n = 4). Uppercase or lowercase letters represent significant differences (*p* < 0.05) in the proportions of P derived from applied Fe-P and wheat straw in shoots or roots between CF and AWD regimes, respectively. The *p* values show the effects of water regime or rice growth on the respective parameter..... 223

Fig. 7 Conceptual scheme demonstrating the effects of water regimes on mineral phosphorus (P) availability and the contributions of ferric iron-bound P (Fe-P) and wheat straw-driven P to P uptake by rice plants and microorganisms. Trapezoids with color gradients demonstrate either the relative P availability in soil solution or the relative contributions of Fe-P and wheat straw to microbial biomass P from high (dark) to low (light)..... 226

List of Tables

Study 2:

Table 1 Effects of medium-term aeration (MTA), short-term aeration (STA), soil compartment (SC), and their interactions on the maximum reaction rate (V_{max}), the affinity to a substrate (K_m), the catalytic efficiency (K_a), and the turnover time (T_i) of respective substrates of phosphomonoesterase (PME), β -glucosidase (BG), and leucine aminopeptidase (LAP) analyzed by three-way ANOVA with repeated measures (rice growth stage, $n = 3$).....83

Study 3:

Table 2 Effects of assay condition (AC), rice growth stage (RGS), soil compartment (SC), and their interactions on the activities of phosphomonoesterase (PME), β -glucosidase (BG), and leucine aminopeptidase (LAP) analyzed by three-way ANOVA.....111

Abbreviations

P	Phosphorus
C	Carbon
N	Nitrogen
SOM	Soil organic matter
MBC	Microbial biomass carbon
MBN	Microbial biomass nitrogen
MBP	Microbial biomass phosphorus
Fe	Iron
Fe(III)	Ferric iron
Fe(II)	Ferrous iron
Fe-P	Ferric iron-bound phosphate
PME	Phosphomonoesterase
BG	β -glucosidase
LAP	Leucine aminopeptidase
O ₂	Oxygen
+O ₂	Oxic assay
-O ₂	Anoxic assay
ROS	Reactive oxygen species
MUF	4-methylumbelliferone
AMC	7-amino-4-methylcomarin
DS	Destructive sampling
CF	Continuous flooding
AWD	Alternate wetting and drying
ANOVA	Analysis of variance

1. Extended summary

1.1 Introduction

The typical cultivation techniques of rice (*Oryza sativa* L.) on paddy soils involve flooding the fields during the vegetation period (Lampayan et al., 2015). However, sustainable rice cultivation requires techniques that consume less irrigation water to cope with increasing water scarcity due to population growth, climate change, and water pollution (Belder et al., 2005; Wu et al., 2017). Alternate wetting and drying (AWD) water regime adopted for paddy soils could serve as a water-saving technique compared to the traditionally continuous flooding (CF) water regime (Bouman and Tuong, 2001; Chen et al., 2021). Soil flooding leads to the shift from oxic to anoxic conditions, while water drainage under the AWD rice cultivation shifts the system from anoxic to oxic conditions. This creates dynamically fluctuating environment in these soils. The changing redox conditions significantly influence microbial activities and the characteristics of redox-sensitive iron (Fe) minerals (Li et al., 2012). These Fe minerals control the cycling of important elements such as phosphorus (P) and carbon (C) in the soils additionally to a multitude of biotic processes of the hydrolysis of organic P and C by enzymes, microbial P immobilization, and plant P uptake (Richardson and Simpson, 2011) as well as abiotic sorption/desorption and co-precipitation/dissolution processes (Frossard et al., 2000).

1.1.1 P and C cycling driven by enzymatic reactions

Soil enzymes, produced mainly by microorganisms and plant roots, are central to a large variety of soil biogeochemical processes (Kunito et al., 2018; Wang et al., 2021). Independent of soil sample origin, enzyme activity assays are commonly performed under oxic conditions (Keiluweit et al., 2017; Wei et al., 2019b), albeit oxygen (O₂) is a known suppressor for putative anaerobic microorganisms (Dellwig et al., 2012). The effects of short-term aeration (minutes to hours) on the hydrolytic and oxidative enzymes in anoxic systems are still unclear. This key gap in current methods was clarified by measuring the kinetics of hydrolytic phosphomonoesterase (PME), β-glucosidase (BG), and leucine aminopeptidase (LAP) and the activities of oxidative phenol oxidases and peroxidases in a rice-planted paddy soil by fluorogenic substrates under oxic (+O₂) and anoxic conditions (–O₂) (Study 1).

Although the redox-induced transformation of Fe plays a key role in biogeochemical processes driven by enzymatic reactions during wetting and drying cycles (Kleber, 2010; Davidson et al., 2012), only a few studies have systematically quantified and proposed explanations of such effects of redox changes on hydrolytic enzyme activities. For example, the “iron gate” paradigm proposed that the accumulation of phenol due to inactivated phenol oxidases by ferrous Fe (Fe(II)) oxidation in Fe-rich ecosystems with aeration may inhibit the activities of hydrolytic enzymes (Wang et al., 2017). In contrast, the “enzymatic latch” mechanism concluded that the decomposition of soil organic matter (SOM) in peatlands is controlled by the

activation or inactivation of phenol oxidase depending on O₂ availability (Freeman et al., 2001). In addition to indirect effects of O₂ on soil hydrolytic enzymes in anoxic systems, the production of reactive oxygen species (ROS) as a result of molecular O₂ reduction may directly suppress microorganisms and enzymatic activities during the transition from anoxic to oxic conditions (Fenchel and Finlay, 2010). Therefore, we lack experimental data to predict the effects of the dramatic increase in O₂ concentration on hydrolytic enzyme activities in anoxic systems. This knowledge gap was filled by evaluating the effects of short-term (2-h oxic (+O₂) vs. anoxic (-O₂) assays) and medium-term aeration (after 10-day oxic vs. anoxic pre-incubation) on the kinetic parameters (V_{\max} and K_m) of PME, BG, and LAP in top bulk, rooted, and bottom bulk paddy soil of flooded rice microcosms (Study 2).

The high heterogeneity of bioavailable substrates results in the spatial heterogeneity of microbial activities (Kuzyakov and Blagodatskaya, 2015; Tecon and Or, 2017). Rhizosphere with a higher labile C input is microbial activity hotspots compared to bulk soil microzones with scarce substrate resources (Hinsinger et al., 2009). Microorganisms producing hydrolytic enzymes in flooded rice paddy systems can be affected by O₂ via two pathways (i) O₂ diffusion belowground from atmosphere and dissolution in surface water, and (ii) O₂ delivery belowground into rhizosphere through aerenchyma of plants (Larsen et al., 2015). However, *in-situ* soil zymography – a screening method applied to reveal the spatial distribution of enzyme activities and to localize enzymatic hotspots in anoxic systems including flooded rice paddy soils – has commonly been conducted under oxic conditions (Ge et al., 2017; Wei et al., 2019a, b). Therefore, understanding how aeration affects the distribution and intensity of the enzymatic hotspots is of utmost importance for predicting the nutrient flows in plant-soil-microorganism continuum. This knowledge gap was closed by adapting the conventional zymography technique developed under the ambient laboratory atmosphere (Spohn et al., 2013; Razavi et al. 2016) to the anoxic conditions by means of a portable glovebox to map the activity of PME, BG, and LAP under +O₂ and -O₂ conditions during 30 days of rice growth (Study 3).

Under P deficiency, organic P plays a central role in P cycling in soils because of its large pool size (Pistocchi et al., 2018). To increase P bioavailability, microorganisms and plants produce and release phosphatases, such as acid phosphomonoesterase, alkaline phosphatase, phytase, and phosphodiesterases, to hydrolyze organic P (Razavi et al. 2016; Kunito et al., 2018). Soil flooding creates the rapid onset of reducing conditions, thereby decreasing the P deficiency because ferric Fe (Fe(III)) reduction promotes the P solubility at low-redox conditions (redox potential ranging from -314 mV to +14 mV) (Saleque et al., 1996; Weber et al., 2006). In contrast, P solubility decreases under oxidizing conditions at drying phases that occur during AWD water regimes due to increasing P sorption capacity of soils (Olsen and Court, 1982). Soil P availability also affects C cycling by changing soil nutrient stoichiometry (Wei et al., 2019b) and by structuring microbial communities (Tang et al., 2016). In paddy soils, the C availability increases during flooding due to a larger proportion of water-soluble microbial metabolites produced under anaerobic

SOM decomposition (Drake et al., 2009), which in turn controls the activity of microorganisms associated with the Fe cycling. Therefore, knowledge of how changing redox conditions affect Fe(III) reduction and subsequent dissolution of Fe(III)-bound P (Fe-P), which in turn influences organic P and C mineralization, can uncover biogeochemical mechanisms of P and C cycling. This knowledge gap was filled by exploring the release of P from the Fe(III)-bound phase on the activities of PME and BG under low-redox conditions and by comparing PME activities under CF vs. AWD regimes (Study 4 and 7).

1.1.2 P and C cycling driven by the Fe(III)-Fe(II) redox wheel

Besides its influence on hydrolytic enzymes by direct and indirect effects, the presence or absence of O₂ also affects P and C cycles via the Fe(III)-Fe(II) redox wheel. Iron phases in paddy soils are of utmost importance for P and C cycling associated with rice cultivation. Under oxidizing conditions prior to flooding, Fe(III) in paddy soils is present either as low-crystalline minerals such as ferrihydrite or as high-crystalline goethite and hematite (Vogelsang et al., 2016). Under reducing conditions after flooding, these minerals can be dissolved driven by microbially mediated processes because Fe(III) is the most common terminal electron acceptor for anaerobic microorganisms to maintain their metabolism, especially in strongly weathered acidic soils (Lovley et al., 1998; Weber et al., 2006).

Soil P cycling is strongly controlled by its specific interactions with redox-sensitive Fe(III) and Fe(II) minerals. Under oxidizing conditions, inorganic P is precipitated by Fe and aluminum (Al) (oxyhydr)oxides in acidic soils, or calcium (Ca) in neutral and alkaline soils or absorbed to clay mineral surfaces (Elser et al., 2007; Wang et al., 2019). Inorganic P in paddy soils largely appears in the form of Fe-P, which accounts for approximately 30% of the total P in the soils where rice has been planted for more than 20 years (Darilek, 2010). Therefore, one of key strategies to decrease P deficiency is to solubilize the P precipitated on minerals or absorbed P and to minimize the re-precipitation of solubilized P on minerals before it is taken up by microorganisms and plants. However, knowledge gaps in tracing the dynamics of P released from Fe(III) reduction and subsequent Fe-P dissolution in paddy soils are associated with (i) alternative electron acceptors (e.g., NO₃⁻) that maintain high redox potentials even in the absence of O₂ and (ii) various forms of Fe(III) (oxyhydr)oxides with considerable differences in their dissolution kinetics. These knowledge gaps were narrowed by tracing the dynamics of P uptake by plants and competition between plants and microorganisms based on ³²P-labeling of Fe-P during first 33 days after rice transplantation (Study 4 and 5).

Plants evolved various mechanisms to cope with P deficiency including morphological and physiological modifications (Lynch et al., 2019). Root growth and development play key roles in the improvement of foraging and exploitation (Walk et al., 2006; Sun et al., 2018). However, the responses of rice roots in flooded paddy soils to the reductive dissolution of Fe-P remains unclear. This is because the Fe-P displays contrasting availabilities depending on redox potentials, and a magnitude of

factors such as O₂ release by roots leading to a high spatio-temporal variability in redox potentials in paddy soils. *In-situ* imaging methods, like phosphor imaging, enable to document the development of root systems (Sakuraba et al., 2018). However, it has been challenging to image roots at low redox conditions, as phosphor imaging requires direct contact of imaging plates and the soil surface to minimize scattering. Previously, rhizoboxes had to be opened for imaging, thereby strongly and rapidly changing the redox state of the soil. These knowledge gaps were filled by developing and applying a novel *in-situ* ³²P-imaging method with minimal disturbance for low-redox conditions (Study 6).

Microbially-mediated Fe(III) reduction largely depends on the availability of C, which is used as a substrate and an energy source by microorganisms in paddy soils (Kögel-Knabner et al., 2010; Liu et al., 2022). Increased C availability accelerates the reductive dissolution of Fe(III) (oxyhydr)oxides mediated by microorganisms (Scalenghe et al., 2002; Rakotoson et al., 2015). Thus, P release from Fe-P dissolution mediated by microorganisms is expected to be stimulated in soils with high labile C availability under reducing conditions. Crop straw is an important source of both organic C and P. Rice straw incorporation accelerated Fe(III) reduction and increased P availability in flooded paddy soils (Rakotoson et al., 2015). In contrast, the AWD regime is expected to accelerate organic P mineralization due to the lower Fe(III) reduction under oxidizing conditions at drying phases. However, rapid changes in water potential during wetting and drying cycles may also decrease microbial biomass because of the dehydration of microbial cells (Fierer et al., 2003), thus decreasing phosphatase activities. Therefore, there is a clear research need in estimation of P uptake by plants and microorganisms derived from Fe(III) reduction and SOM (e.g. crop straw) mineralization under different water regimes. This knowledge gap was addressed by tracing the dynamics of P uptake by microorganisms and plants based on ³²P-labeling of Fe-P and ³²P-labeling of wheat straw under CF and AWD regimes 40 days after rice transplantation (Study 7).

1.2 Objectives

This thesis generally aims to explore the biogeochemical mechanisms of P and C cycling in paddy soils driven by enzymatic reactions and the Fe(III)-Fe(II) redox wheel under changing redox conditions. Specifically, the following tasks were put forward:

- (i) To verify how short-term aeration (minutes to hours) regulates the key hydrolytic (PME, BG, and LAP) and oxidative (phenol oxidases and peroxidases) enzymes (Study 1).
- (ii) To compare the effects of short-term (2-h oxic vs. anoxic assays) and medium-term aeration (after 10-day oxic vs. anoxic pre-incubation) on the kinetic parameters (V_{\max} , K_m) of hydrolytic enzymes (Study 2).
- (iii) To quantify the effects of short-term presence of O₂ on *in-situ* microbial hotspots

and enzyme activities (Study 3).

(iv) To test whether microbially-driven Fe(III) reduction and dissolution can cover the P demand of microorganisms and growing rice plants (Study 4).

(v) To quantify the relevance of the reductive dissolution of Fe-P for plant and microbial P uptake (Study 5).

(vi) To reveal the mechanisms adopted by rice roots in response to improved P availability after Fe-P dissolution (Study 6).

(vii) To quantify contributions of the reductive dissolution of Fe-P and organic P mineralization to the P nutrition of rice plants and microorganisms under different water regimes in paddy soils (Study 7).

1.3 Hypotheses

To fill the above knowledge gaps, we formulated the following hypotheses:

(1) Short-term (minutes to hours) aeration suppresses the activities of hydrolytic enzymes due to the O₂ toxicity to the active anoxic microbial communities, while medium-term (days to weeks) aeration will cause anoxic microbial communities to adapt reducing the impact of O₂ exposure during enzyme assays with absence or presence of O₂.

(2) In addition to the organic matter-derived P, the reductive dissolution of Fe-P can contribute to the P nutrition of plants and microorganisms.

(3) The direct accessibility of Fe-P by rice roots stimulates their growth due to increased plant P foraging and uptake.

(4) Alternate wetting and drying increases the phosphomonoesterase activity and the contribution of organic P to P nutrition of rice plants and microorganisms.

1.4 Material and methods

1.3.1 Soil description

The low available P soil (available P content < 10 mg kg⁻¹ according to the Chinese soil nutrient classification standard) was collected from 0–20 cm of a paddy rice field at the Changsha Agricultural and Environmental Monitoring Station, Hunan Province, China (113°19'52" E, 28°33'04" N). This region is characterized by a subtropical monsoon climate with an annual average temperature of 17.5 °C and an annual average precipitation of 1300 mm. The soil is a typical Stagnic Anthrosol developed from highly weathered granite (Gong et al., 2007), and is under paddy cultivation with double-cropping rice. The soil was collected with a corer at five locations in the field, combined, sieved through a 2 mm mesh, air-dried, and homogenized. The soil texture was 26.7% clay, 29.2% silt, and 44.2% sand. The main soil physico-chemical properties were as follows: pH 6.2, soil organic C 13.1 g kg⁻¹,

total N 1.4 g kg⁻¹, available N 18.0 mg kg⁻¹, total P 0.3 g kg⁻¹, Olsen-P 3.7 mg kg⁻¹, and total Fe 15.7 g kg⁻¹ (Zhu et al., 2018).

1.3.2 Experimental design

All studies were conducted in mesocosms of rice (*Oryza sativa* L. ‘Two-line hybrid rice Zhongzao 39’) grown in water-tight PVC-rhizoboxes with the inner dimensions of 24.0 × 20.5 × 1.5 cm (height × width × depth) (Fig. ES1a) except for the research task 2 in the Study 1. For the latter, an incubation experiment with soil microcosms was conducted. Briefly, four 100 ml Kimble KIMAX borosilicate laboratory glass bottles (Kimble Chase Life Science and Research Products, LLC., Meiningen, Germany) were filled with 20 g (dry weight) water-saturated soil each. Additionally, 10 ml deionized water were added to each bottle. The soil was pre-incubated anaerobically in the dark for 10 days at 25 °C in a climate chamber (KBF-S 720, Binder GmbH, Tuttlingen, Germany) to establish strong anoxic conditions. After incubation, all the bottles were opened inside a portable PVC glovebox (Captair® Pyramid Glovebox 3015-00, Erlab DFS, Saint-Maurice, France) (Fig. ES1c) evacuated with a vacuum pump (Ilmvac MP 301 Vp, Ilmvac GmbH, Ilmenau, Germany) and then back-flushed with nitrogen to O₂ concentrations lower than 0.2% as indicated by an O₂-sensor (Greisinger GOX 100, GHM Messtechnik GmbH, Remscheid, Germany) (Fig. ES1b). Soil in each bottle was stirred with a spoon and two subsamples ca. 0.5 g moist soil were collected individually for oxic and anoxic assays, respectively.

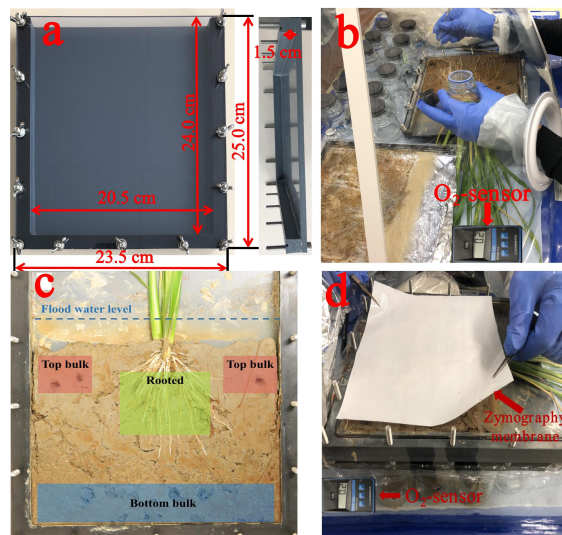


Fig. ES1 The dimensions of a rhizobox with plexiglas cover on top, sealed with rubber gasket (not visible on photo) and fixed by thumbscrews (a), sampling of soil from compartments of a rhizobox, glass bottles for soil suspension preparation and the level of O₂ as indicated by an O₂-sensor (b), the sampling locations of three soil compartments 48 hours after water drainage (c), and a substrate saturated zymography membrane and the O₂ level as indicated by an O₂-sensor (d). In subfigure c, the level of flooded water maintained during experiment is shown schematically by a dashed line. Shaded spots within each compartment correspond to the removed soil.

For Study 1, 2, and 3, three rice mesocosms were established for each of the three enzymes (PME, BG, and LAP) (9 in total) and were adjusted with deionized water ca. 2 cm above the soil surface and the water level was maintained throughout the experiment except the dates of soil sampling. Soil sampling was performed at the seedling (with 2 ± 1 tillers), early- (4 ± 1), and late (6 ± 1) tillering stages of rice plants 10, 16–20, and 28–31 days after rice transplantation. Three compartments, top bulk (2–5 cm), rooted (5–15 cm), and bottom bulk (15–18 cm), were sampled after opening a rhizobox inside the glovebox as explained above (Fig. ES1c). For each compartment, the soil collected in three random locations was pooled into one approximately 0.5 g sample in 100 ml Kimble KIMAX borosilicate laboratory glass bottles. In total, six samples were collected per compartment of a rhizobox at each rice growth stage: two for oxic and anoxic assays in the Study 1 and four (two for oxic and two for anoxic) for pre-incubation in the Study 2. For the Study 2, every enzyme activity assay was conducted on one corresponding soil sample. Below, for simplicity, we explain the treatments for soil samples taken from a compartment for an individual enzyme and rice growth stage, whereas in total there were 324 samples ($3 \text{ compartments} \times 3 \text{ enzymes} \times 3 \text{ stages} \times 3 \text{ replicates} \times 2 \text{ pre-incubation conditions} \times 2 \text{ assay conditions}$) assayed in the experiment (Fig. ES2). The bottles for anoxic pre-incubation were sealed with thick air-impermeable butyl rubber septa, while the bottles for oxic pre-incubation were closed with plastic screw caps. Then, the “anoxic” samples were flushed for 20 min with N_2 and the “oxic” samples were aerated and left loosely closed to ensure gas exchange but prevent drying. Both treatments were pre-incubated in the dark for 10 days at 22 °C in an incubator chamber (FKS 3600 Index 20B/001, Liebherr, Germany). After pre-incubation, one anoxic and one oxic bottle were filled with N_2 -bubbled deionized sterile water in a ratio of 100 v/v to the soil sample and closed with thick air-impermeable butyl rubber septa in the glovebox. Another anoxic and oxic bottle were filled with deionized sterile water (with dissolved O_2) and closed with plastic screw caps. Thereafter, the bottles for $-O_2$ assay (one from anoxic pre-incubation and the other from oxic pre-incubation) were additionally flushed with N_2 for 30 min. No specific manipulations were conducted for the bottles of the $+O_2$ assay.

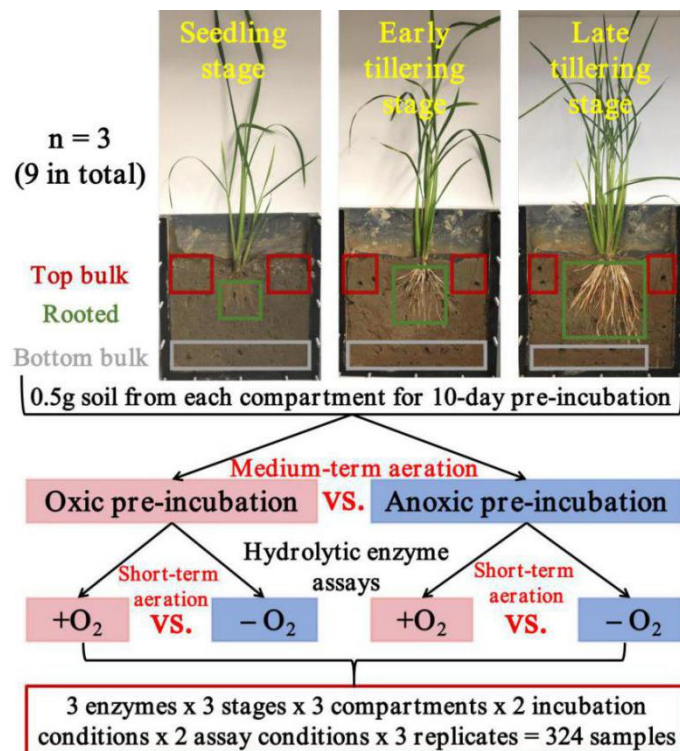


Fig. ES2 Diagram of the experimental design to test the effects of medium-term (10-day pre-incubation) and short-term (2-h assay) aeration (red boxes) vs. anoxic controls (blue boxes) on activities of three hydrolytic enzymes (phosphomonoesterase, β -glucosidase, and leucine aminopeptidase) in soils from three rhizobox compartments (top bulk, rooted, and bottom bulk) collected at three rice growth stages (seedling stage, 10 days after rice transplantation; early tillering stage, 16–20 days; late tillering stage, 28–31 days). Photos of rice are examples of growth stages (there were 9 rhizoboxes with plants for each of the three enzymes tested).

To map enzyme activities at soil-root interface in the Study 3, we applied *in situ* imaging method – soil zymography. In contrast to the conventional zymography approach conducted under the ambient laboratory atmosphere (Spohn et al., 2013; Razavi et al. 2016), the anoxic zymography was performed here for the first time. To keep anoxic conditions during soil zymography, the rhizoboxes were placed inside the glovebox as described above (Fig. ES1d). The details of zymography are described in the Study 3.

For the Study 4 and 6, pre-germinated rice plants were grown for 33 days in flooded rhizoboxes supplied with ^{32}P -labeled ferrihydrite (31 mg P kg^{-1}) either (i) in polyamide mesh bags ($30 \mu\text{m}$ mesh size; $5.0 \times 5.0 \text{ cm}$, height \times width) to prevent roots from directly mobilizing Fe–P (pellets-in-mesh bag treatment), or (ii) in the same pellet form but without a mesh bag to enable roots accessing the Fe–P (pellets-no-mesh bag treatment) (Fig. ES3). For the Study 5, only the rhizoboxes without mesh bags were used. To perform ^{32}P imaging under low redox conditions, a transparent, colorless, and 0.2-mm thin rigid-PVC film (Modular Material Total, Berlin, Germany) was installed approximately 2 mm below the sturdy plexiglass front

cover of the rhizobox. This 2-mm gap (and the good seal) allowed to insert the moisture-sensitive imaging plate with minimum scatter. Destructive samplings were conducted after 10, 18, and 33 days after rice transplanting, respectively. The details of ^{32}P labeling of Fe-P are described in the Study 4, 5, and 6.

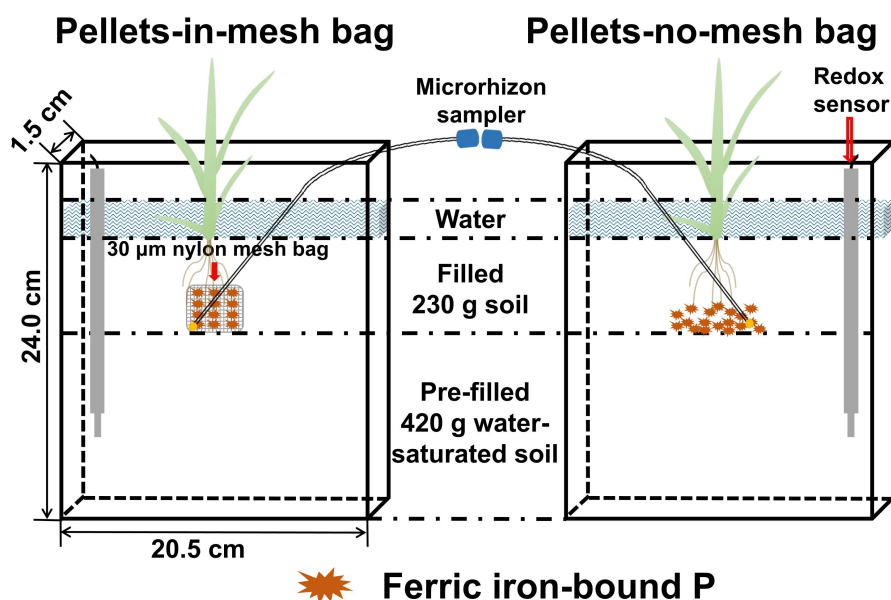


Fig. ES3 Diagram of the experimental design. MicroRhizon® samplers were placed at the P-rich patch zone, and a platinum electrode for measuring redox potential (E_h) was installed in each rhizobox. Pre-filled soil corresponds to paddy soil filled into rhizoboxes 16–24 h prior the addition of ferric iron-bound P. Filled soil is the paddy soil added during Fe–P placement and rice seedlings transplantation.

For the Study 7, the experimental design included two water regimes with four replicates (eight rhizoboxes in total). Two water regimes included continuous flooding (CF, the rhizoboxes were always filled with water to a depth of 2–3 cm from the soil surface) and alternate wetting and drying (AWD, the rhizoboxes were flooded for 10 days as described above for CF, then the top water layer was drained for 10 days, and then the above procedure was repeated again). ^{32}P -labeled ferrihydrite (30 mg P kg⁻¹) and ^{33}P -labeled wheat straw (10 g straw kg⁻¹) were evenly added. Destructive sampling was conducted 40 days after rice transplantation. The details of ^{32}P labeling of Fe-P and ^{32}P labeling of wheat straw are described in the Study 7.

1.3.3 Analytical methods

The kinetics parameters of PME, BG, and LAP were measured using fluorogenically labeled substrates of 4-methylumbelliferyl-phosphate, 4-methylumbelliferyl- β -D-glucoside, and L-leucine-7-amino-4-methylcoumarin hydrochloride (all substrates were purchased from Sigma-Aldrich Co. Ltd), respectively, according to the established method (Marx et al., 2001). Phenol oxidase activity and peroxidase activity were measured using a substrate Amplex Red (10-acety-3,7-dihydroxyphenoxazine, purchased from Sigma-Aldrich Co. Ltd), according to Khosrozadeh et al. (2022).

Microbial biomass C (MBC) and N (MBN) were measured using the chloroform-fumigation-extraction method (Vance et al., 1987). The organic C and total N contents in each extract were measured by an elemental analyzer (Multi N/C 2100S, Analytik, Germany). The contents of MBC and MBN were calculated as the difference between the content of organic C and the difference between the content of total N extracted from the fumigated and non-fumigated soils, respectively, using a conversion factor of 0.40 (Brookes et al., 1985; Vance et al., 1987). Soil microbial biomass P (MBP) was determined in the Study 4 and 5 with the anion exchange resin method by adding hexanol as fumigant according to Kouno et al. (1995). The P concentration was measured with the colorimetric method on a spectrophotometer (NanoPhotometer® NP80, IMPLEN, Munich, Germany). MBP was calculated as the difference between anion exchange P without hexanol and P extracted with hexanol, corrected by the recovery of a P spike in each soil sample. The content of MBP in the Study 7 was measured according to Brookes et al. (1984). Phosphorus was extracted with 0.5 M NaHCO₃ solution and was measured with the colorimetric method on a spectrophotometer. MBP was calculated as the difference between the content of P extracted from the fumigated and non-fumigated soils and corrected for the recovery of a P spike in each soil sample.

Zymograms were transformed to 8-bit gray scale images in ImageJ (Schindelin et al., 2012). Then, gray values were transformed to enzyme activities based on the calibration curves for 4-methylumbelliferone (MUF) or 7-amino-4-methylcomarin (AMC) concentrations. Determination and separation of hotspots and cavities (poor or no attachment areas between soil surface and membrane) in images were processed in R (version 3.5.1, R development core team, 2014) according to the method proposed by Bilyera et al. (2020). We plotted the profiles of the enzyme activity distribution as a function of distance from a geometrical root center on 3–5 visible and randomly selected roots, not overlapping with each other, and without cavities within 1 cm distance away from them. The geometrical root center and not a root surface was chosen as a starting point of a profile because of the inability to correctly define the exact root diameter due to the relatively low resolution of light images under high moisture conditions. The rhizosphere boundaries were set using a one-way ANOVA, followed by a Tukey's HSD test, to assess the differences between independent variables (mean enzyme activity of five adjacent pixels). Significant differences ($p < 0.05$) between two adjacent groups of 5 pixels were then considered as a boundary of rhizosphere extent (Hoang et al., 2016).

To measure Fe(II) concentration in soil solution, 2 ml sample were mixed with 500 µl ammonium acetate buffer (pH 4.5) and 500 µl phenanthroline solution (0.5%) in a 10-mm polystyrene cuvette (Th. Geyer GmbH & Co. KG, Renningen, Germany) and then measured at 512 nm on a spectrophotometer (NanoPhotometer® NP80, Implen GmbH, Munich, Germany). Then, 200 µl 10% ascorbic acid were added to each cuvette to completely reduce Fe(III) to Fe(II) after a 30-min reaction. Total Fe concentration was measured as Fe(II) as above (Elrod et al., 1991). Fe(III) concentration was calculated as the difference between total Fe and Fe(II)

concentrations. Calibration was done by external FeCl₃ standards ranging from 5 to 300 µM.

For the Study 4, 5, and 6, the ³²P activity in soil solution was measured in the Liquid Scintillation Analyser (LSA) (Tri-Carb® 2800 TR, PerkinElmer, Shelton, CT, US), corrected for isotope decay, and back-calculated to a reference date. Briefly, 0.75 ml soil solution was mixed with 10 ml cocktail (Carl Roth GmbH + Co. KG, Germany) in a scintillation vial and then counted for 5 min. To measure ³²P activity in MBP, 1 ml sample was mixed with 10 ml cocktail in a scintillation vial and then measured for 5 min on the LSA. The ³²P activity in MBP was also calculated as the difference in ³²P activity between samples extracted without and with hexanol and corrected for the recovery of a P spike in each soil sample. To measure ³²P activity in shoots and roots, approximately 100 mg of each sample were digested with 2 ml of 65% HNO₃ at 180 °C for 8 h in a PTFE digestion block. Each digested sample was filtered and filled up to 25 ml volume with milli-Q (highly purified) water. A subsample (1 ml) was mixed with 10 ml scintillation cocktail in a 20-ml scintillation vial, and then counted for 5 min on the LSA. For the Study 7, the ³²P and ³³P activities in all samples were determined using a dual-labeling (³²P/³³P) counting procedure on the LSA, corrected for respective isotope radioactive decays, and back-calculated to a reference date. Briefly, 1 ml sample was mixed with 10 ml scintillation cocktail and then counted for 10 min. The details of radioactivity measurements are described in the Study 4, 5, 6, and 7.

In the Study 6, a novel *in-situ* ³²P phosphor-imaging approach under flooding were developed and applied to estimate P uptake by rice roots released from Fe-P dissolution. A phosphor imaging plate (20 × 40 cm; BAS-IP MS 2040 E, Cytiva, Marlborough, MA, USA) was inserted into the gap between the PVC film and the front cover of each rhizobox (see section 1.3.2). Exposure in the dark was 1 h. The imaging system Fujifilm FLA-5100 (FUJIFILM Life Science, Stamford, CT, USA) was used to read the plates with a spatial resolution of 100 µm. The emitted β⁻ radiation from the decay of ³²P was stored in 16-bit digital images and converted (by log-linearization) to standardized photo-stimulated luminescence (PSL) units (Fuji Photo Film Co. Ltd. 2003). Image processing was performed with an open-source software Fiji (Schindelin et al., 2012). The PSL values were transformed to ³²P activities based on the calibration and corrected for isotope radioactive decay. All images of each rhizobox were aligned by defining one image the reference and applying geometric transformations to other images. The profiles of ³²P activity were plotted as a function of distance from a geometrical crown root center at a position of 1 cm away from root tips. For every crown root, the profile of mean ³²P activity was presented as a function of distance from a crown root center determined at given pixels from a root center (Zarebanadkouki et al., 2016) assuming radial symmetry of a crown root. The boundaries between root and soil were set using a one-way ANOVA, followed by a Tukey's HSD test, to assess the differences between the independent variables (mean ³²P activity of five adjacent pixels). Significant differences ($p < 0.05$) between two adjacent groups of 5 pixels were considered the boundary between root

and soil (Hoang et al., 2016). To explore ^{32}P activity distribution along the root, the profiles of ^{32}P activity were plotted as a function of distance along a crown root through a root rip to the soil by drawing a segment line. The boundaries between root and root tip and between root tip and soil were determined using a one-way ANOVA as described above. Root tip diameter of each root was calculated as a distance from the boundary between root and root tip to the boundary between root tip and soil. The details of image processing are described in the Study 6.

1.5 Results and discussion

1.4.1 Effects of short-term aeration on hydrolytic versus oxidative enzymes

The activities of hydrolytic enzymes (PME, BG, and LAP) were lower by 5–43% under $+\text{O}_2$ compared to $-\text{O}_2$ (Fig. 2 and 3 in the Study 1). In contrast, the activities of peroxidases and phenol oxidases were 2–14 times higher under $+\text{O}_2$ than under $-\text{O}_2$ (Fig. 4 in the Study 1). Thus, the activation of oxidative enzymes under $+\text{O}_2$ was uncoupled from the hydrolytic activities. This contradicts both the “iron gate” and the “enzyme latch” concepts. We propose three mechanisms, which in our view may most comprehensively explain the observed short-term suppressive effect of O_2 on hydrolytic reactions (Fig. ES4):

(i) Abrupt aeration inhibited the activity of obligate anaerobic microorganisms and initiated a shift in microbial metabolic pathways, restricting the secretion of *de novo* formed enzymes. Facultative anaerobes and micro-aerophilic groups can adapt to common O_2 fluctuations (Yadav et al., 2014). However, the abrupt exposure of an established anoxic environment to air will most probably cause a direct suppressive effect on active anaerobic microorganisms and strongly reduce *de novo* enzymes synthesis (Fig. ES4b, pathway I).

(ii) The reactive oxygen species (ROS) can be produced as a result of molecular O_2 reduction by Fe(II) and may directly suppress microorganisms after the transition from anoxic to oxic conditions (Fenchel and Finlay, 2010). Stimulated oxidative enzyme activities (Fig. 4 in the Study 1), which use ROS such as H_2O_2 as co-substrates, support the concept of increased ROS formation. An abrupt aeration can therefore suppress the entire metabolic activity of anaerobes, including the production of hydrolytic enzymes (Fig. ES4b, pathway II), at least until sufficient agents are synthesized to protect cells from ROS damages.

(iii) Aerobes and facultative anaerobes may respond to oxidative stress caused by ROS by redirecting their resources from the secretion of hydrolases to protection. To protect themselves against oxidative stress, the compensatory mechanisms established by microorganisms include production of catalase, superoxide dismutase, glutaredoxin, and thioredoxin (Cabiscol et al., 2000). Along with such a direct compensatory mechanism, the indirect effect will be driven by the need of microorganisms to overuse their resources in dealing with the stress (Schimel et al., 2007). If this energy is devoted to compensatory production of catalases and

ferroxidases to resist oxidative stress, then there could be a concurrent decrease in hydrolases production (Fig. ES4b, pathway III).

Suggested mechanisms of enzyme activities with aeration

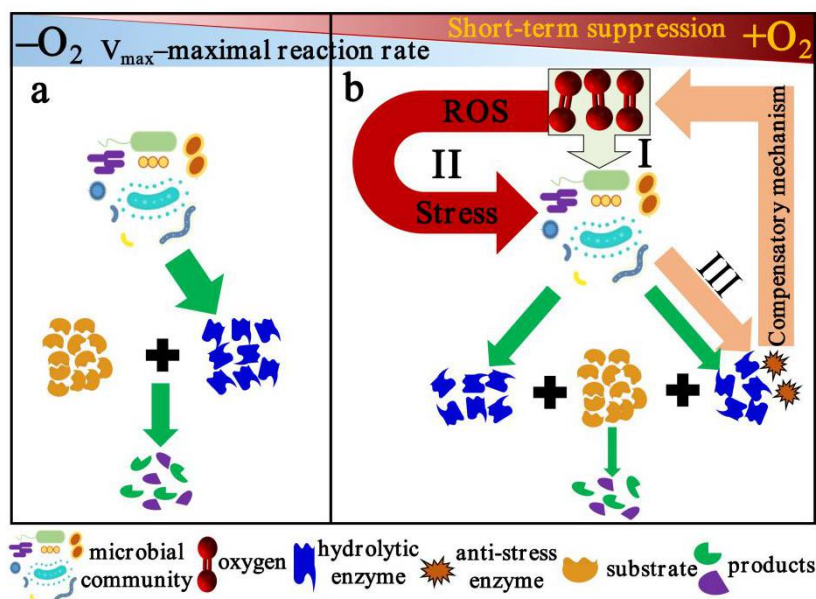


Fig. ES4 Mechanisms of hydrolytic enzymes suppression by short-term (during 2 hours) O₂ exposure. Left side (a): enzymatic reactions conducted by hydrolytic enzymes under anoxic conditions. Right side (b): reduction of microbial activity (pathway I), toxicity of reactive oxygen species (ROS) to microbial cells (pathway II), and compensatory mechanism of anti-stress enzyme production, e.g. catalase, superoxide dismutase (pathway III). Size of arrows corresponds to relative intensity of enzyme production or reaction rates. Triangles on top reflect the relative increase of the short-term suppressive effect of oxygen (brown) and the concurrent relative decrease of enzymatic maximal reaction rate (V_{max} , blue) with O₂.

1.4.2 Short- and medium-term effects of aeration on hydrolytic enzymes

Overall, 2-h aeration suppressed V_{max} values by 7–43% and catalytic efficiency K_a (V_{max}/K_m) by 3–22%, and extended the substrate turnover time T_t (7–33%) of three tested enzymes in all soil compartments pre-incubated without O₂ (Fig. 2, 3, 4 in the study 2). These findings fully supported those obtained in the Study 1. In contrast, no short-term suppressive effect of O₂ was observed on three tested enzymes after oxie pre-incubation (Fig. 2, 3, 4 in the Study 2). Medium-term aeration increased V_{max} (by 12–253%) and K_a (by 3–78%) of the enzymes and shortened T_t (4–42%) as compared to the anoxic counterpart (Fig. 2, 3, 4 in the Study 2).

The opposite effects of 2-h and 10-day aeration on hydrolytic enzyme kinetic parameters indicated that the microbial community exploited different strategies to acclimatize their anoxic metabolisms and enzymes to oxic conditions (Fig. ES5). Two-hour aeration may inactivate or kill obligate anaerobes due to O₂ toxicity, i.e. the effect of stress (Fenchel and Finlay, 1995) described in the Study 1, an interpretation supported by the about 30% decrease in living bacteria number in sediments after 2-h

aeration (Ma et al., 2019). Aeration for 12 h was insufficient to trigger aerobic respiration by microorganisms, but 4 days was sufficient (Pett-Ridge and Firestone, 2005). Accordingly, 10-day pre-incubation in our study was long enough for microbial communities to acclimate to oxic conditions and to exploit an aerobic metabolism either by a metabolic switch by facultative anaerobes or by growth of aerobic community members. Significant changes in community structure were detected in paddy soils after 7 days of incubation under oxic vs. anoxic conditions (Lüdemann et al., 2000). We therefore assume that 10-day aeration induced the changes in community structure, which was responsible for the overall increase in hydrolytic enzyme activities.

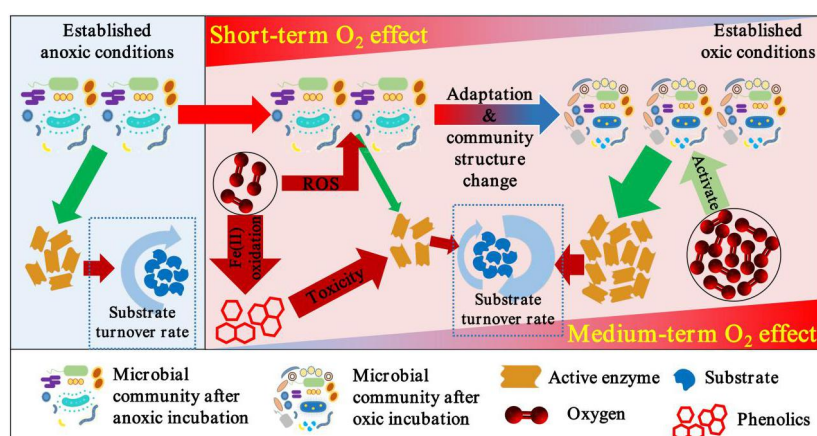


Fig. ES5 Mechanisms of hydrolytic enzymes suppression by short-term aeration due to (1) toxicity of reactive oxygen species (ROS) to microbial cells, (2) decreasing efficiency of phenol oxidase because of Fe (II) oxidation and accumulation of phenolics (“iron-gate”), and activation by medium-term aeration due to cancelling of suppressive factors. Arrow size: relative intensity of active enzyme production, reaction rates, or substrate turnover rate. Triangles with color gradients: the intensity of O₂ effects on enzyme activities from low (blueish) to high (reddish).

1.4.3 Short-term aeration effects on *in-situ* microbial hotspots and enzyme activities

Short-term (35 min) aeration decreased the activities of three hydrolytic enzymes 4–61% as compared with $-O_2$ (Fig. ES6). These findings demonstrated that *in-situ* zymography method of intact soil screening for enzyme activities also revealed the short-term suppressive effect of O₂ which therefore can’t be occasional or a method-dependent. The percentage of hotspot area was higher by 3–158% under $+O_2$ vs. $-O_2$ conditions depending on a rice growth stage (Fig. ES6). Irrespective of the aeration conditions, the rhizosphere extent of rice plants for three enzymes was generally greater under higher moisture conditions and at earlier growth stage (Fig. ES6).

In addition to the overall suppression of enzymes by aeration, zymography revealed spatial inhomogeneity of enzyme activity hotspots in paddy soils. We suggest two possible reasons of the increased percentage of hotspot area by short-term aeration. (i) Enzymatic hotspots are mainly attributed to rhizosphere with overall

higher microbial abundance and activity due to continuous input of root exudates as compared to the bulk soil (Kuzyakov and Blagodatskaya, 2015). Roots of wetland plants including rice are supplied via aerenchyma with atmospheric O₂ which is diffusing into the anoxic environment. Long-term availability of O₂ in the close vicinity to roots of rice should cause an adaptive effect on rhizosphere microorganisms and enzyme activities. This is why anoxic bulk soil microbial communities were suppressed by aeration during zymography, while rhizosphere microbial activities were weakly affected (Fig. 1 in the Study 3). This explains the finding that no differences in the percentage of hotspot area were observed at a tillering stage of rice growth (Fig. 3 in the Study 3). (ii) Another reason is related to the algorithm of hotspots identification. Thus, we estimated a decreased threshold for the identification of hotspots by 0–12% mainly due to differences in bulk soil activities between +O₂ and –O₂ assays. By definition, the hotspot is an area of enzyme activity that is higher by three times of a standard deviation than mean enzyme activity estimated for the whole zymogram (Bilyera et al., 2020). The lower the difference between hotspot activity and the mean activity of a zymogram, the smaller is the hotspot area. Short-term aeration resulted in a narrower enzymatic rhizosphere extent as compared to anoxic assays (Fig. 4 in the Study 3). This may have implications for other studies where the actual rhizosphere extent was most probably underestimated for paddy soils when measured under oxic conditions (Ge et al., 2017). Accordingly, incorrect rhizosphere extents will give biased input to the models established for anoxic ecosystems (Ge et al., 2017) due to the underestimation of the area with a high reaction rate on the premise that oxygen and hydrolytic enzymes are completely decoupled at a biochemical level.

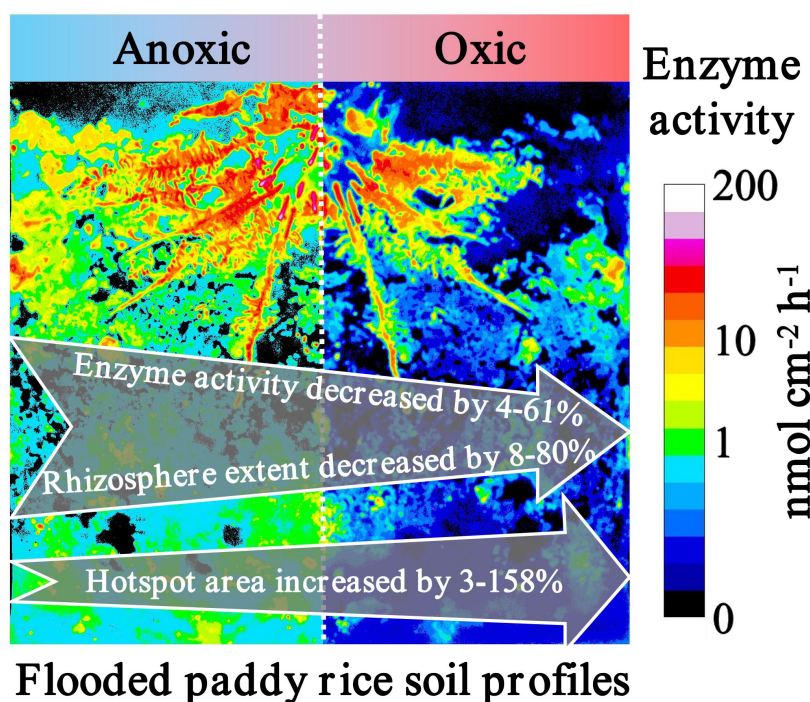


Fig. ES6 Effects of short-term aeration on *in-situ* hydrolytic enzyme activities, hotspot area, and rhizosphere extent in a flooded paddy soil

1.4.4 Microbial iron reduction compensates for phosphorus limitation

Mineralization of SOM catalyzed by extracellular enzymes couldn't alone explain in full the demand of rice plants and microorganisms for P in studied paddy soils. Accessible P from Fe-P after the dissolution was a substantial pool in the total P uptake. The higher MBC, MBN, and MBP contents were observed when Fe-P was root-accessible compared to the soil surrounding pellets in mesh bags (Fig. 4 in the Study 4). Likewise, the accessibility of Fe-P to rice roots may also have facilitated their colonization with Fe reducers. Above- and especially belowground rice growth at the tillering stage resulted in the decrease of MBC and MBP contents in the rooted soil by 28–56% (Fig. 4a and c in the Study 4). Such a pattern can be attributed to an increased competition between rice plants and microorganisms for the available P (Fig. ES7). The contribution of Fe-P to MBP remarkably decreased from 4.5% to almost zero from 10 to 33 days after rice transplantation, while Fe-P compensated up to 16% of the plant P uptake at 33 days after rice transplantation (Fig. 5a and b in the study 4), thus outcompeting microorganisms (Fig. ES7).

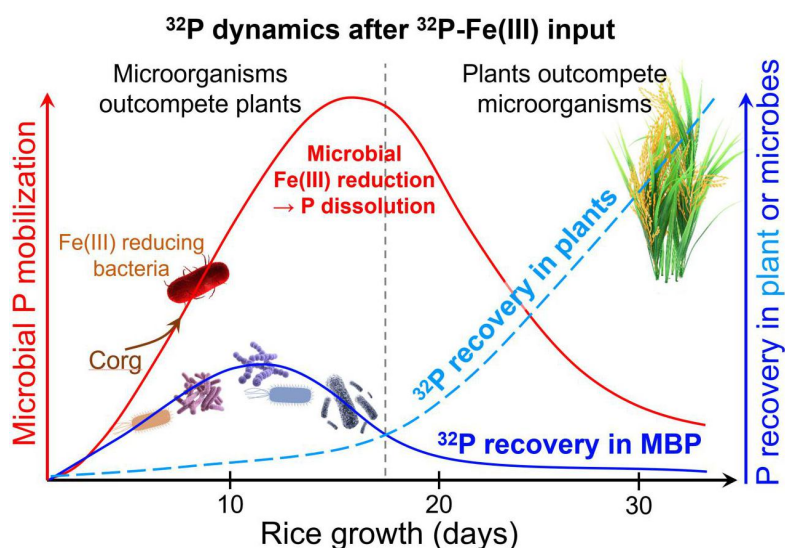


Fig. ES7 Conceptual scheme demonstrating the shift from microorganisms outcompeting rice plants for phosphorus to rice plants outcompeting microorganisms. Red solid line demonstrates the dynamics of microbially driven Fe(III) reduction. Blue lines show ^{32}P recovery either in rice plants (dashed line) or in microbial biomass (solid line) with rice plant growth.

Without mesh bags, P was more available leading to increases in the V_{\max} of PME and BG as compared to P pellets not directly available to roots (Fig. 6 in the Study 4). Such nutrient mining, i.e., the promotion of organic P mineralization due to an insufficient amount of P released from the added Fe(III)-bound P source, often linked to the priming effect (Kuzyakov and Blagodatskaya, 2015). In our case, roots eventually outcompeted microorganisms in P uptake especially when in direct access to P source (Fig. ES7). Therefore, P deficient microbes compensated their demand from the recent plant-derived deposits and SOM-derived organic P sources.

Microbial biomass C and dissolved organic C content decreased from day 10 to

33 by 8–54% and 68–77%, respectively (Fig. 2 a and c in the Study 5), suggesting that the microbial-mediated Fe(III) reduction was C-limited (Fig. ES8). The much faster decrease of MBC in rooted (by 54%) vs. bulk soil (8–36%) (Fig. 2 a and c in the Study 5) reflects very fast microbial turnover in the rice rhizosphere (high C and oxygen inputs) resulting in the mineralization of the microbial necromass (Loppmann et al., 2020).

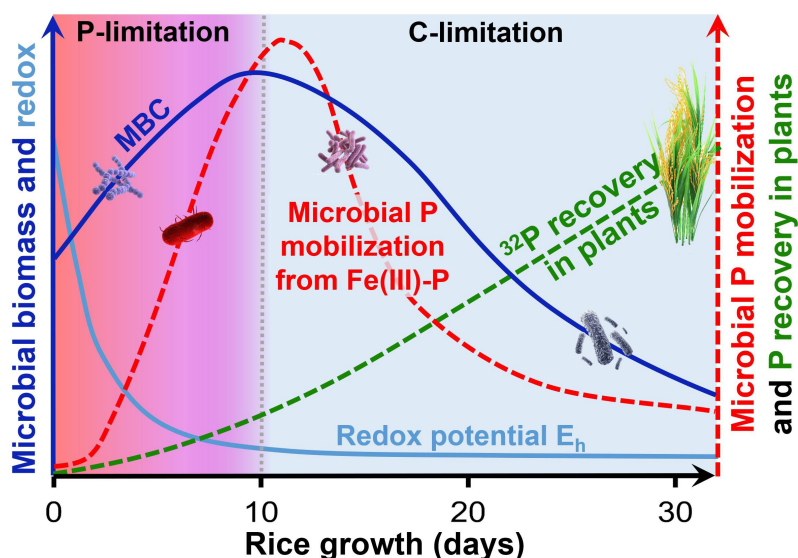


Fig. ES8 Conceptual scheme demonstrating the shift from P-limitation to C-limitation for microorganisms during 33 days of rice growth. Blue lines show either microbial biomass C (MBC) or redox potential E_h dynamics with rice growth. Red dashed line demonstrates the dynamics of microbially-mediated Fe(III) reduction. Green dashed line shows ^{32}P recovery in rice plants with rice plant growth.

1.4.5 Reductive dissolution of iron phosphate modifies rice root morphology

Direct root access to Fe-P raised both the number and mean diameter of crown roots and root tips, and increased P uptake by 149–231% (Fig. 4, 5, and 7 in the Study 6). A higher number of crown roots indicates more intensive root foraging. This was also shown in P-limited upland soils, when a greater number of roots and higher root density increased P acquisition by maize (*Zea mays*) phenotypes (Jia et al., 2018). Crown root elongation rate, ^{32}P activities along roots and root tips were 5–133% higher when roots directly accessed Fe-P (Fig. 4c and 5b in the Study 6). Thus, the reductive dissolution of Fe-P can mitigate P limitation and thereby increase the P uptake by rice plants. Plant-derived organic acids alone did not cause Fe-P dissolution, suggesting Fe(III) reduction is a predominately microbially-mediated process (tested in a preliminary experiment, data not shown here). Therefore, the higher ^{32}P recovery in roots in the soil without mesh bags may be mostly attributed to the increased colonization of rice roots with Fe reducers compared to the pellets isolated in mesh bags (Fig. ES9).

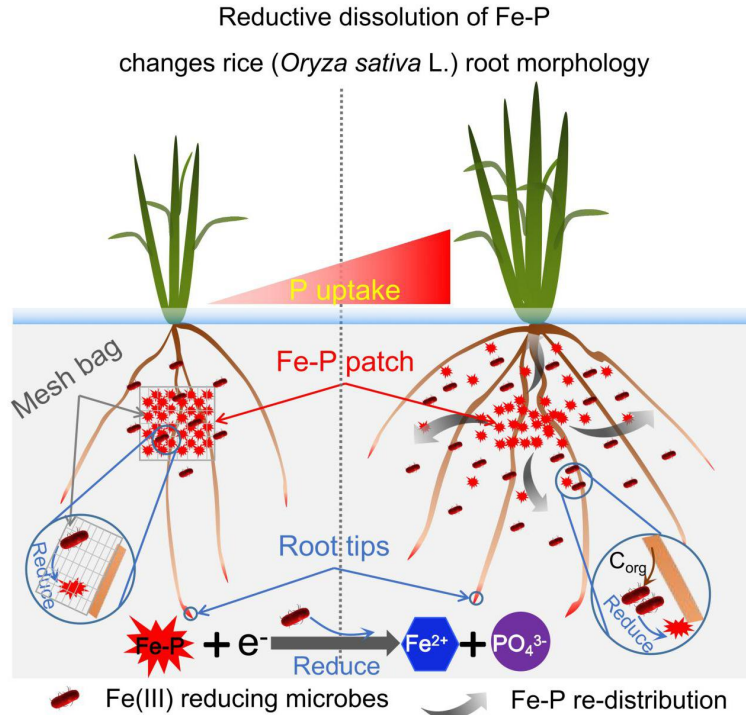


Fig. ES9 A schematic diagram of the effects of direct accessibility of ferric iron-bound phosphate (Fe-P) by rice roots on root architecture under low phosphate conditions. With the application of Fe-P directly to the soil, Fe-P pellet re-distribution resulted in a large area, where roots were directly in contact with Fe-P. When Fe-P was not restricted by mesh bags, roots could provide carbon to Fe-reducing microorganisms to boost microbial growth and activity (blue circles).

1.4.6 Effects of water regimes on the contributions of iron phosphate and wheat straw to phosphorus nutrition

The effects of water regimes on microbial biomass and PME activities were soil depth-dependent and were most pronounced in top bulk soil where microbial biomass and PME activities were 9–56% higher under CF vs. AWD regime (Fig. 4 and 5 in the Study 7). The decrease of microbial biomass in top bulk soil under AWD regime is most likely due to the rapid dehydration of microbial cells after soil drying (Fierer et al., 2003; Bagheri-Novair, et al., 2020). Sudden and high drying intensities induced by a low relative humidity (35%) in our study may result in drought stress on microorganisms in top bulk soil (Blackwell et al., 2010), thus decreasing PME activities.

The proportions of P derived from Fe-P and wheat straw in rice plants and MBP were 5–64% higher under CF vs. AWD regime (Fig. 6 in the Study 7). Continuous flooding increased the contribution of Fe-P to rice plant and microbial P uptake (Fig. 6a, c in the Study 7) because of the increased rates of the reductive dissolution of Fe-P under low-redox conditions after flooding (Fig. 2a and 2b in the Study 7). In contrast to our expectations, AWD regime decreased the contribution of wheat straw-derived P to the P nutrition of rice plants compared to CF regime (Fig. 6b in the Study 7). This

means that microorganisms immobilized most of P derived from wheat straw mineralization to their biomass, thus decreasing P availability to plants (Fig. ES10). Phosphorus uptake by rice plants is controlled not only by the P availability in soil solution, but also by the processes of P transport to the root surface (Jungk and Claasen, 1989). For example, the P uptake by rice plants increased with increasing moisture levels in paddy soils (Turner and Gilliam, 1976). Thus, continuously flooding increased plant available P by faster P diffusion compared to alternate wetting and drying regime (Fig. ES10).

The contribution of Fe-P to MBP was 72–78% lower and wheat straw-P to MBP was 16–42% higher in rooted soil than in bulk soil, respectively (Fig. 6 in the Study 7), suggesting a strong competition between plants and microorganisms for P. Microorganisms appear to be more competitive for organic P than rice plants, and rice plants are more competitive than microorganisms for P released from the reductive dissolution of Fe-P (Fig. ES10).

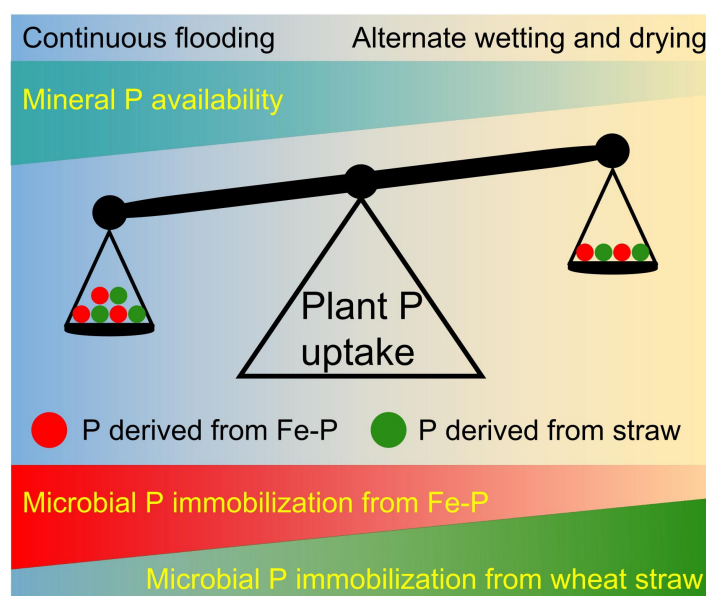


Fig. ES10 Conceptual scheme demonstrating the effects of water regimes on mineral phosphorus (P) availability and the contributions of ferric iron-bound P (Fe-P) and wheat straw-driven P to P uptake by rice plants and microorganisms. Trapezoids with color gradients demonstrate either the relative P availability in soil solution or the relative contributions of Fe-P and wheat straw to microbial biomass P from high (dark) to low (light).

1.6 Conclusions and outlook

The main conclusions of this thesis are as follows:

- (i) Anoxic conditions and soil moisture should be kept constant during enzyme assays and zymography when studying anoxic systems to avoid underestimation due to rapid suppression of hydrolytic enzyme activities by O₂. The short-term suppressive effect

of O₂ on hydrolytic enzyme activities in assays was most probably caused by increased ROS concentrations, which decreased microbial activity. In contrast, anoxic microbial community adapt to oxic conditions over the medium-term aeration (10 days for the studied paddy soil), thus **supporting the Hypothesis 1**.

(ii) The reductive dissolution of ferrihydrite-bound P under low redox conditions can not only serve as a P source to increase rice root growth but also to induce root morphological changes, thereby **supporting the Hypotheses 2 and 3**. Rice varieties with extended crown root densities will increase P uptake when P is limiting in paddy soils.

(iii) Rice plants outcompeted microorganisms for P released from the reductive dissolution of Fe-P, and microorganisms increased the immobilization of wheat straw-derived P to their biomass.

(iv) Although the P released by the reductive dissolution of ferrihydrite and wheat straw mineralization could not fully meet the P requirements of both rice plants and microorganisms, this P amount was accessible to plants and microorganisms. Alternate wetting and drying increased phosphomonoesterase activities only in the rooted soil generally decreasing the contribution of wheat straw-derived P to the P nutrition of rice plants compared to continuous flooding. This was **against the Hypothesis 4**. Still, phosphate fertilization strategies should be adapted considering the rates of P mobilization from Fe (oxyhydr)oxides and straw under different water regimes in paddy soils.

In summary, these studies demonstrated for the first time the clear need to consider *in-situ* conditions for the soil enzyme assays. Improved estimation of enzyme activity in anoxic environments is an important step forward to more adequately assess SOM turnover in anoxic systems and to more accurately represent these ecosystems in modern enzyme-catalyzed process-based models from the local to the global scale. The proposed mechanisms should be further proven by (i) in-depth verification based on ROS identification and concentration measurements and (ii) the long-term effects of aeration on enzyme kinetic parameters during the shift from anoxic to oxic conditions, e.g. after water drainage or under the alternative wetting and drying rice cultivation management. The effect of medium-term aeration on the enzyme kinetics points to a potential problem: the prolonged storage (for months or years) of soil samples taken from anoxic systems may cause the slow adaptation of the microbial community to oxic conditions and to a biased estimation of enzyme activities and element turnover rates in such samples. The mineralization of organic matter-derived P sources catalyzed by hydrolytic enzymes and the microbially-mediated Fe-P dissolution are two key mechanisms for P mobilization for plants and microorganisms in paddy soils. The reductive dissolution of Fe-P and wheat straw mineralization compensated up to 36% and 40% of the plant and microbial P uptake, respectively. Microbial biomass and enzyme activities were linked to the rice growth in this nutrient-limited low-redox environment and their dynamics was strongly depended on P availability. We have proven that rice plants

outcompeted microorganisms for P released from the Fe-P dissolution, and wheat straw incorporation could intensify P mobilization from Fe (oxyhydr)oxides due to increased C availability for microorganisms. Alternate wetting and drying decreased the contributions of Fe-P dissolution to P nutrition, but unexpectedly wheat straw decomposition could also not increase P availability as compared to continuous flooding. This can be attributed to increased P sorption capacity of soils during drying phases. As one of the main outcomes, alternate wetting and drying had no preferences for P uptake by rice plants from organic and inorganic P sources. But relatively high contribution of organic P to the total P nutrition of plants and microorganisms calls for the adaptation of the P fertilization strategies in paddy soils to avoid excess chemical P fertilizer inputs especially under continuous water flooding. In conclusion, this thesis did not only propose urgent modifications to the methods of enzyme kinetic assays and *in-situ* zymography to quantify realistic enzyme activities in anoxic systems, but also primarily uncovered for the first time the dynamics of P in the interface between precipitation, dissolution, mineralization, and immobilization as affected directly and indirectly by redox conditions controlling Fe(II)/Fe(III) dynamics. Thereby, a new conceptual framework of P interaction among the plant-microorganism-iron mineral interface was developed identifying the strong competition between rice plants and microorganisms for P released from the reduction and dissolution of Fe-P and organic matter-derived P sources.

References

- Bagheri-Novair, S., Hosseini, H.M., Etesami, H., Razavipour, T., Lajayer, B.A., Astatkie, T., 2020. Short-term soil drying–rewetting effects on respiration rate and microbial biomass carbon and phosphorus in a 60-year paddy soil. *3 Biotech* 10(11), 1–11.
- Belder, P., Bouman, B.A.M., Cabangon, R., Guoan, L., Quilang, E.J.P., Li, Y., Spiertz, J.H.J., Tuong, T.P., 2004. Effect of water-saving irrigation on rice yield and water use in typical lowland conditions in Asia. *Agricultural Water Management* 65, 193–210.
- Bilyera, N., Kuyzakova, I., Guber, A., Razavi, B.S., Kuzyakov, Y., 2020. How “hot” are hotspots: statistically localizing the high-activity areas on soil and rhizosphere images. *Rhizosphere* 16, 100259.
- Blackwell, M.S.A., Brookes, P.C., de la Fuente-Martinez, N., Gordon, H., Murray, P.J., Snars, K.E., Williams, J.K., Bol, R., Haygarth, P.M., 2010. Phosphorus solubilization and potential transfer to surface waters from the soil microbial biomass following drying-rewetting and freezing-thawing. *Advances in Agronomy* 106, 1–35.
- Bouman, B.A.M., Tuong, T.P., 2001. Field water management to save water and increase its productivity in irrigated lowland rice. *Agricultural Water Management* 49, 11–30.
- Brookes, P.C., Landman, A., Pruden, G., Jenkinson, D., 1985. Chloroform fumigation and the release of soil nitrogen: a rapid direct extraction method to measure microbial biomass nitrogen in soil. *Soil Biology and Biochemistry* 17, 837–842.
- Brookes, P.C., Powlson, D.S., Jenkinson, D.S., 1984. Phosphorus in the soil microbial biomass. *Soil Biology and Biochemistry* 16, 169–175.
- Cabiscol, E., Tamarit, J., Ros, J., 2000. Oxidative stress in bacteria and protein damage by reactive oxygen species. *International Microbiology* 3, 3–8.
- Chen, H., Jarosch, K.A., Mészáros, É., Frossard, E., Zhao, X., Oberson, A., 2021. Repeated drying and rewetting differently affect abiotic and biotic soil phosphorus (P) dynamics in a sandy soil: A ³³P soil incubation study. *Soil Biology and Biochemistry* 153, 108079.
- Darilek, J.L., 2010. Effect of land use conversion from rice paddies to vegetable fields on soil phosphorus fractions. *Pedosphere* 2, 137–145.
- Davidson, E.A., Samanta, S., Caramori, S.S., Savage, K., 2012. The Dual Arrhenius and Michaelis-Menten kinetics model for decomposition of soil organic matter at hourly to seasonal time scales. *Global Change Biology* 18 (1), 371–384.
- Dellwig, O., Schnetger, B., Brumsack, H.J., Grossart, H.P., Umlauf, L., 2012.

- Dissolved reactive manganese at pelagic redoxclines (part II): hydrodynamic conditions for accumulation. *Journal of Marine Systems* 90, 31–41.
- Drake, H.L., Horn, M.A., Wüst, P.K., 2009. Intermediary ecosystem metabolism as a main driver of methanogenesis in acidic wetland soil. *Environmental microbiology reports* 1(5), 307–318.
- Elrod, V.A., Johnson, K.S., Coale, K.H., 1991. Determination of subnanomolar levels of iron(II) and total dissolved iron in seawater by flow injection analysis with chemiluminescence detection. *Analytical Chemistry* 63 (9), 893–898.
- Elser, J.J., Bracken, M., Cleland, E.E., Gruner, D.S., Harpole, W.S., Hillebrand, H., Ngai, J.T., Seabloom, E.W., Shurin, J.B., Smith, J.E., 2007. Global analysis of nitrogen and phosphorus limitation of primary producers in freshwater, marine and terrestrial ecosystems. *Ecology Letters* 10 (12), 1135–1142.
- Fenchel, T., Finlay, B.J., 1995. *Ecology and Evolution in Anoxic Worlds*. Oxford University Press, New York.
- Fenchel, T., Finlay, B.J., 2010. Oxygen and the spatial structure of microbial communities. *Biological Reviews* 83 (4), 553–569.
- Fierer, N., Schimel, J.P., Holden, P.A., 2003. Variations in microbial community composition through two soil depth profiles. *Soil Biology and Biochemistry* 35 (1), 167–176.
- Freeman, C., Ostle, N., Kang, H., 2001. An enzymic ‘latch’ on a global carbon store — a shortage of oxygen locks up carbon in peatlands by restraining a single enzyme. *Nature* 409, 149.
- Frossard, E., Condron, L.M., Oberson, A., Sinaj, S., Fardeau, J.C., 2000. Processes governing phosphorus availability in temperate soils. *Journal of Environmental Quality* 29, 15–23.
- Ge, T.D., Wei, X.M., Razavi, B.S., Zhu, Z.K., Hu, Y.J., Kuzyakov, Y., Jones D.L., Wu, J.S., 2017. Stability and dynamics of enzyme activity patterns in the rice rhizosphere: Effects of plant growth and temperature. *Soil Biology and Biochemistry* 113, 108–115.
- Gong, Z.T., Zhang, G.L., Chen, Z.C. (Eds.), 2007. *Pedogenesis and Soil Taxonomy*. Science Press, Beijing, China, pp. 613–626.
- Hinsinger, P., Bengough, A., Vetterlein, D., Young, I., 2009. Rhizosphere: biophysics, biogeochemistry and ecological relevance. *Plant and Soil* 321, 117–152.
- Hoang, D.T.T., Razavi, B.S., Kuzyakov, Y., Blagodatskaya, E., 2016. Earthworm burrows: kinetics and spatial distribution of enzymes of C-, N- and P- cycles. *Soil Biology and Biochemistry* 99, 94–103.
- Jia, X.C., Liu, P., Lynch, J.P., 2018. Greater lateral root branching density in maize improves phosphorus acquisition from low phosphorus soil. *Journal of*

- Experimental Botany 69, 4961–4970.
- Jungk, A., Claassen, N., 1989. Availability in soil and acquisition by plant as the basis for phosphorus and potassium supply to plants. *Zeitschrift für Pflanzenernährung und Bodenkunde* 152(2), 151–157.
- Keiluweit, M., Wanzek, T., Kleber, M., Nico, P., Fendorf, S., 2017. Anaerobic microsites have an unaccounted role in soil carbon stabilization. *Nature Communications* 8 (1), 1771.
- Khosrozadeh, S., Dorodnikov, M., Reitz, T., Blagodatskaya, E., 2022. An improved Amplex Red-based fluorometric assay of phenol oxidases and peroxidases activity: a case study on Haplic Chernozem. *European Journal of Soil Science* 73 (2), e13225.
- Kleber, M., 2010. What is recalcitrant soil organic matter? *Environmental Chemistry* 7, 320–332.
- Kögel-Knabner, I., Amelung, W., Cao, Z.H., Fiedler, S., Frenzel, P., Jahn, R., Kalbitz, K., Kölbl, A., Schloter, M., 2010. Biogeochemistry of paddy soils. *Geoderma* 157, 1–14.
- Kunito, T., Hiruta, N., Miyagishi, Y., Sumi, H., Moro, H., 2018. Changes in phosphorus fractions caused by increased microbial activity in forest soil in a short-term incubation study. *Chemical Speciation and Bioavailability* 30, 9–13.
- Kouno, K., Tuchiya, Y., Ando, T., 1995. Measurement of soil microbial biomass phosphorus by an anion exchange membrane method. *Soil Biology and Biochemistry* 27, 1353–1357.
- Kuzyakov, Y., Blagodatskaya, E., 2015. Microbial hotspots and hot moments in soil: Concept & review. *Soil Biology and Biochemistry* 83, 184–199.
- Lampayan, R.M., Rejesus, R.M., Singleton, G.R., Bouman, B.A., 2015. Adoption and economics of alternate wetting and drying water management for irrigated lowland rice. *Field Crops Research* 170, 95–108.
- Larsen, M., Santner, J., Oburger, E., Wenzel, W.W., Glud, R.N., 2015. O₂ dynamics in the rhizosphere of young rice plants (*Oryza sativa* L.) as studied by planar optodes. *Plant and Soil* 390(1), 279.
- Li, Y., Yu, S., Strong, J., Wang, H., 2012. Are the biogeochemical cycles of carbon, nitrogen, sulfur, and phosphorus driven by the “FeIII-FeII redox wheel” in dynamic redox environments? *Journal of Soils and Sediments* 12, 683–693.
- Liu, Q., Li, Y., Liu, S., Gao, W., Zhang, G., Xu, H., Zhu, Z., Ge, T., Wu, J., 2022. Anaerobic primed CO₂ and CH₄ in paddy soil are driven by Fe reduction and stimulated by biochar. *Science of the Total Environment* 808, 151911.
- Loeppmann, S., Breidenbach, A., Spielvogel, S., Dippold, M.A., Blagodatskaya, E., 2020. Organic nutrients induced coupled C-and P-cycling enzyme activities

- during microbial growth in forest soils. *Frontier for Global Change* 3, 100.
- Lovley, D.R., Fraga, J.L., Blunt-Harris, E.L., Hayes, L.A., Phillips, E.J.P. Coates, J.D., 1998. Humic substances as a mediator for microbially catalyzed metal reduction. *Acta Hydrochimica et Hydrobiologica* 26, 152–157.
- Lüdemann, H., Arth, I., Liesack, W., 2000. Spatial changes in the bacterial community structure along a vertical oxygen gradient in flooded paddy soil cores. *Applied and Environmental Microbiology* 66 (2), 754–762.
- Lynch, J.P., 2019. Root phenotypes for improved nutrient capture: an underexploited opportunity for global agriculture. *New Phytologist* 223, 548–564.
- Ma, S., Tong, M., Yuan, S., Liu, H., 2019. Responses of microbial community structure in Fe(II)-bearing sediments to oxygenation: the role of reactive oxygen species. *ACS Earth and Space Chemistry* 3, 738–747.
- Marx, M., Wood, M., Jarvis, S., 2001. A microplate fluorimetric assay for the study of enzyme diversity in soils. *Soil Biology and Biochemistry* 33, 1633–1640.
- Olsen, R., Court, M., 1982. Effect of wetting and drying of soils on phosphate adsorption and resin extraction of soil phosphate. *Journal of Soil Science* 33, 709–717.
- Pett-Ridge, J., Firestone, M.K., 2005. Redox fluctuation structures microbial communities in a wet tropical soil. *Applied and Environmental Microbiology* 71 (11), 6998–7007.
- Pistocchi, C., Mészáros, É., Tamburini, F., Frossard, E., Bünemann, E.K., 2018. Biological processes dominate phosphorus dynamics under low phosphorus availability in organic horizons of temperate forest soils. *Soil Biology and Biochemistry* 126, 64–75.
- R Development Core Team, 2014. R: a language and environment for statistical computing, R Foundation for Statistical Computing.
- Rakotoson, T., Six, L., Razafimanantsoa, M.P., Rabeharisoa, L., Smolders, E., 2015. Effects of organic matter addition on phosphorus availability to flooded and nonflooded rice in a P-deficient tropical soil: a greenhouse study. *Soil Use and Management* 31, 10–18.
- Razavi, B.S., Zarebanadkouki, M., Blagodatskaya, E., Kuzyakov, Y., 2016. Rhizosphere shape of lentil and maize: spatial distribution of enzyme activities. *Soil Biology and Biochemistry* 96, 229–237.
- Richardson, A.E., Simpson, R.J., 2011. Soil microorganisms mediating phosphorus availability. *Plant Physiology* 156, 989–996.
- Sakuraba, Y., Kanno, S., Mabuchi, A., Monda, K., Iba, K., Yanagisawa, S., 2018. A phytochrome-B-mediated regulatory mechanism of phosphorus acquisition. *Nature Plants* 4(12), 1089–1101.

- Saleque, M.A., Abedin, M.J., Bhuiyan, N.I., 1996. Effect of moisture and temperature regimes on available phosphorus in wetland rice soils. *Communications in Soil Science and Plant Analysis* 27, 2017–2023.
- Scalenghe, R., Edwards, A., Ajmone Marsan, F., Barberis, E., 2002. The effect of reducing conditions on the solubility of phosphorus in a diverse range of European agricultural soils. *European Journal of Soil Science* 53, 1–9.
- Schimel, J., Balsler, T.C., Wallenstein, M., 2007. Microbial stress-response physiology and its implications for ecosystem function. *Ecology* 88, 1386–1394.
- Schindelin, J., Arganda-Carreras, I., Frise, E., Kaynig, V., Longair, M., Petzsch, T., Preibisch, S., Rueden, C., Saalfeld, S., Schmid, B., Tinevez, J.Y., White, D.J., Hartenstein, V., Eliceiri, K., Tomancak, P., Cardona, A., 2012. Fiji: an open-source platform for biological-image analysis. *Nature Methods* 9(7), 676–682.
- Spohn, M., Carminati, A., Kuzyakov, Y., 2013. Soil zymography – a novel *in situ* method for mapping distribution of enzyme activity in soil. *Soil Biology and Biochemistry* 58, 275–280.
- Sun, B., Gao, Y., Lynch, J., 2018. Large crown root number improves topsoil foraging and phosphorus acquisition. *Plant Physiology* 177, 90–104.
- Tang, Y.Q., Zhang, X.Y., Li, D.D., Wang, H.M., Chen, F.S., Fu, X.L., Fang, X.M., Sun, X.M., Yu, G.R., 2016. Impacts of nitrogen and phosphorus additions on the abundance and community structure of ammonia oxidizers and denitrifying bacteria in Chinese fir plantations. *Soil Biology and Biochemistry* 103, 284–293.
- Tecon, R., Or, D., 2017. Biophysical processes supporting the diversity of microbial life in soil. *FEMS Microbiology Reviews* 41, 599–623.
- Turner, F.A., Gilliam, J.W., 1976. Increased P diffusion as an explanation of increased P availability in flooded rice soils. *Plant and Soil* 45, 365–377.
- Vance, E., Brookes, P., Jenkinson, D., 1987. An extraction method for measuring soil microbial biomass C. *Soil Biology and Biochemistry* 19, 703–707.
- Vogelsang, V., Fiedler, S., Jahn, R., Kaiser, K., 2016. *In-situ* transformation of iron - bearing minerals in marshland-derived paddy subsoil. *European Journal of Soil Science* 67(5), 676–685.
- Walk, T.C., Jaramillo, R., Lynch, J.P., 2006. Architectural tradeoffs between adventitious and basal roots for phosphorus acquisition. *Plant and Soil* 279, 347–366.
- Wang, C.Q., Xue, L., Dong, Y.H., Jiao, R.Z., 2021. Effects of stand density on soil microbial community composition and enzyme activities in subtropical *Cunninghamia lanceolata* (Lamb.) Hook plantations. *Forest Ecology and Management* 479, 118559.

- Wang, Y., Wang, H., He, J.S., Feng, X., 2017. Iron-mediated soil carbon response to water-table decline in an alpine wetland. *Nature Communications* 8, 1–9.
- Wang, Y., Yuan, J.H., Chen, H., Zhao, X., Wang, D., Wang, S.Q., Ding, S.M., 2019. Small-scale interaction of iron and phosphorus in flooded soils with rice growth. *The Science of the Total Environment* 669, 911–919.
- Weber, K.A., Achenbach, L.A., Coates, J.D., 2006. Microorganisms pumping iron: anaerobic microbial iron oxidation and reduction. *Nature Reviews Microbiology* 4 (10), 752–764.
- Wei, X., Ge, T., Zhu, Z., Hu, Y., Liu, S., Li, Y., Wu, J., Razavi, B., 2019a. Expansion of rice enzymatic rhizosphere: temporal dynamics in response to phosphorus and cellulose application. *Plant and Soil* 445, 169–181.
- Wei, X., Razavi, B.S., Hu, Y., Xu, X., Zhu, Z., Liu, Y., Kuzyakov, Y., Li, Y., Wu, J.S., Ge, T. D., 2019. C/P stoichiometry of dying rice root defines the spatial distribution and dynamics of enzyme activities in root-detritusphere. *Biology and Fertility of Soils* 55, 251–263.
- Wu, X.H., Wang, W., Yin, C.M., Hou, H.J., Xie, K.J., Xie, X.L., 2017. Water consumption, grain yield, and water productivity in response to field water management in double rice systems in China. *PLoS ONE* 12, e0189280.
- Yadav, T.C., Khardenavis, A.A., Kapley, A., 2014. Shifts in microbial community in response to dissolved oxygen levels in activated sludge. *Bioresource Technology* 165, 257–264.
- Zarebanadkouki, M., Ahmed, M.A., Carminati, A., 2016. Hydraulic conductivity of the root-soil interface of lupin in sandy soil after drying and rewetting. *Plant and Soil* 398, 267–280.
- Zhu, Z., Ge, T., Luo, Y., Liu, S., Xu, X., Tong, C., Shibistova, O., Guggenberger, G., Wu, J., 2018. Microbial stoichiometric flexibility regulates rice straw mineralization and its priming effect in paddy soil. *Soil Biology and Biochemistry* 121, 67–76.

Contributions to the included publications and manuscripts

This thesis comprises five publications and two manuscripts which were elaborated in cooperation with various coauthors. The coauthors listed in these publications and manuscripts contributed as follows:

Study 1 Keep oxygen in check: contrasting effects of short-term aeration on hydrolytic versus oxidative enzymes in paddy soils

Status: Published in Soil Biology and Biochemistry (2022)

Wang C.Q.: Conceptualization, Methodology, Formal analysis, Data curation, Writing – original draft, Writing – review & editing, Visualization

Blagodatskaya E.: Writing – review & editing

Dippold M.A.: Writing – review & editing

Dorodnikov M.: Conceptualization, Methodology, Resources, Writing – review & editing, Supervision, Funding acquisition

Study 2 Oxygen matters: Short- and medium-term effects of aeration on hydrolytic enzymes in a paddy soil

Status: Published in Geoderma (2022)

Wang C.Q.: Conceptualization, Methodology, Formal analysis, Data curation, Writing – original draft, Writing – review & editing, Visualization

Dippold M.A.: Writing – review & editing

Blagodatskaya E.: Writing – review & editing

Dorodnikov M.: Conceptualization, Methodology, Resources, Writing – review & editing, Supervision, Funding acquisition

Study 3 Keep oxygen in check: an improved *in-situ* zymography approach for mapping anoxic hydrolytic enzyme activities in a paddy soil

Status: Published in Science of the Total Environment (2022)

Wang C.Q.: Conceptualization, Methodology, Formal analysis, Data curation, Writing – original draft, Writing – review & editing, Visualization

Bilyear N.: Writing – review & editing

Blagodatskaya E.: Writing – review & editing

Zhang X.C.: Writing – review & editing

Dippold M.A.: Writing – review & editing

Dorodnikov M.: Conceptualization, Methodology, Resources, Writing – review & editing, Supervision, Funding acquisition

Study 4 Can the reductive dissolution of ferric iron in paddy soils compensate phosphorus limitation of rice plants and microorganisms?

Status: Published in Soil Biology and Biochemistry (2022)

Wang C.Q.: Conceptualization, Methodology, Formal analysis, Data curation, Writing – original draft, Writing – review & editing, Visualization

Thielemann L.: Writing – review & editing

Dippold M.A.: Writing – review & editing

Guggenberger G.: Writing – review & editing

Kuzyakov Y.: Writing – review & editing

Banfield C.C.: Writing – review & editing

Ge T.D.: Writing – review & editing

Guenther S.: Writing – review & editing

Horn M.A.: Writing – review & editing

Bork P.: Writing – review & editing

Dorodnikov M.: Conceptualization, Methodology, Resources, Writing – review & editing, Supervision, Funding acquisition

Study 5 Microbial iron reduction compensates for phosphorus limitation in paddy soils

Status: Published in Science of the Total Environment (2022)

Wang C.Q.: Conceptualization, Methodology, Formal analysis, Data curation, Writing – original draft, Writing – review & editing, Visualization

Thielemann L.: Writing – review & editing

Dippold M.A.: Writing – review & editing

Guggenberger G.: Writing – review & editing

Kuzyakov Y.: Writing – review & editing

Banfield C.C.: Writing – review & editing

Ge T.D.: Writing – review & editing

Guenther S.: Writing – review & editing

Horn M.A.: Writing – review & editing

Bork P.: Writing – review & editing

Dorodnikov M.: Conceptualization, Methodology, Resources, Writing – review & editing, Supervision, Funding acquisition

Study 6 Reductive dissolution of iron phosphate modifies rice root morphology in phosphorus-deficient paddy soils

Status: Under review in Soil Biology and Biochemistry

Wang C.Q.: Conceptualization, Methodology, Formal analysis, Data curation, Writing – original draft, Writing – review & editing, Visualization

Thielemann L.: Writing – review & editing

Dippold M.A.: Writing – review & editing

Guggenberger G.: Writing – review & editing

Kuzyakov Y.: Writing – review & editing

Banfield C.C.: Writing – review & editing

Ge T.D.: Writing – review & editing

Guenther S.: Writing – review & editing

Dorodnikov M.: Conceptualization, Methodology, Resources, Writing – review & editing, Supervision, Funding acquisition

Study 7 The wetter the better: continuous flooding promoted phosphorus uptake by rice from ³³P-organic and ³²P-inorganic phosphorus sources compared to alternate wetting and drying

Status: In preparing

Wang C.Q.: Conceptualization, Methodology, Formal analysis, Data curation, Writing – original draft, Writing – review & editing, Visualization

Dippold M.A.: Writing – review & editing

Guggenberger G.: Writing – review & editing

Kuzyakov Y.: Writing – review & editing

Banfield C.C.: Writing – review & editing

Guenther S.: Writing – review & editing

Dorodnikov M.: Conceptualization, Methodology, Resources, Writing – review & editing, Supervision, Funding acquisition

2. Publications and manuscripts

Study 1 Keep oxygen in check: contrasting effects of short-term aeration on hydrolytic versus oxidative enzymes in paddy soils

Chaoqun Wang^{a,*}, Evgenia Blagodatskaya^b, Michaela A. Dippold^{a,c}, Maxim Dorodnikov^{a,d}

^a Biogeochemistry of Agroecosystems, University of Goettingen, 37077 Goettingen, Germany

^b Department of Soil Ecology, Helmholtz Center for Environmental Research, 06120 Halle/Saale, Germany

^c Geo-Biosphere Interactions, University of Tuebingen, 72076 Tuebingen, Germany

^d Department of Soil Science of Temperate Ecosystems, University of Goettingen, 37077 Goettingen, Germany

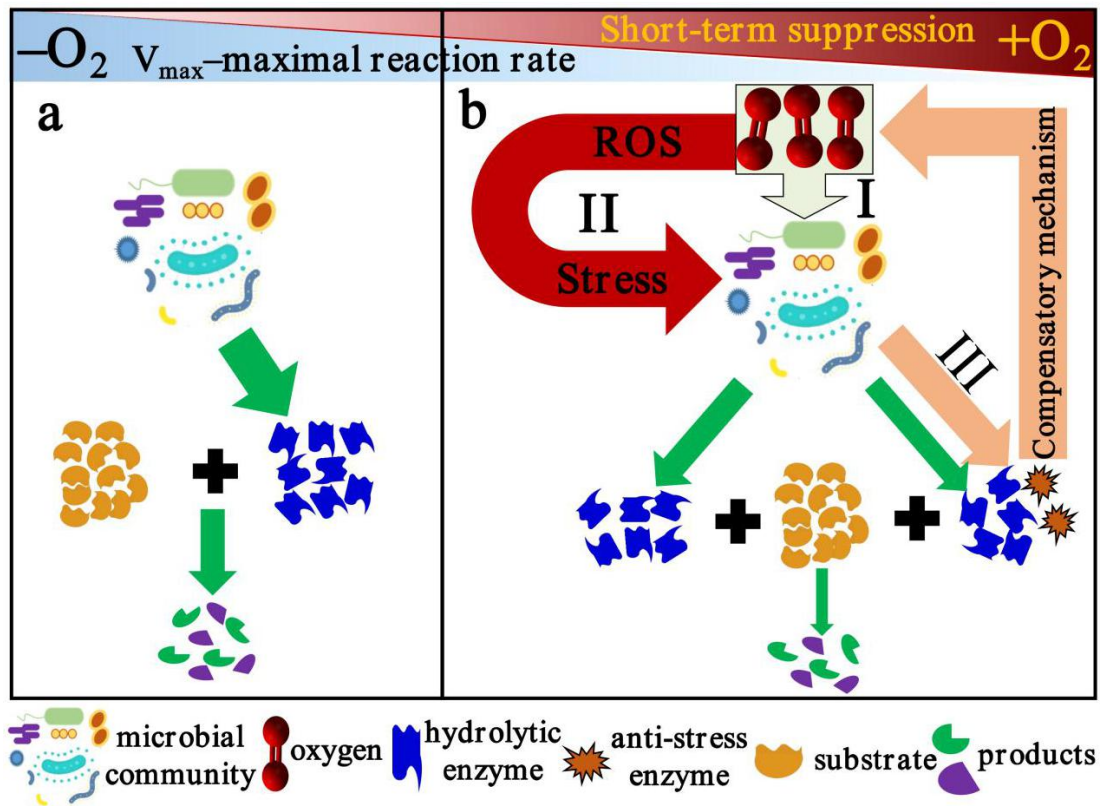
* **Correspondence:** chaoqun.wang@forst.uni-goettingen.de

Status: Published in Soil Biology and Biochemistry

Wang, C.Q., Blagodatskaya, E., Dippold, M.A., Dorodnikov, M. 2022. Keep oxygen in check: Contrasting effects of short-term aeration on hydrolytic versus oxidative enzymes in paddy soils. *Soil Biology and Biochemistry* 169, 108690.

Graphical abstract

Suggested mechanisms of enzyme activities with aeration



Mechanisms of hydrolytic enzymes suppression by short-term (during 2 hours) O_2 exposure. Left side (a): enzymatic reactions conducted by hydrolytic enzymes under anoxic conditions. Right side (b): reduction of microbial activity (pathway I), toxicity of reactive oxygen species (ROS) to microbial cells (pathway II), and compensatory mechanism of anti-stress enzyme production, e.g. catalase, superoxide dismutase (pathway III). Size of arrows corresponds to relative intensity of enzyme production or reaction rates. Triangles on top reflect the relative increase of the short-term suppressive effect of oxygen (brown) and the concurrent relative decrease of enzymatic maximal reaction rate (V_{max} , blue) with O_2 .

Abstract: Enzymes produced by microorganisms and plants are very sensitive to variations in soil microclimate, yet most enzyme assays are conducted under oxic conditions irrespective of the origin of environmental samples. It remains unclear how short-term aeration (minutes to hours) affects the hydrolytic and oxidative enzymes in anoxic systems. This key gap in current methods was addressed by measuring the kinetics of hydrolytic phosphomonoesterase, β -glucosidase, and leucine aminopeptidase and the activities of oxidative phenol oxidases and peroxidases by fluorogenic substrates under oxic (+O₂) and anoxic conditions (-O₂). Aeration effects were tested in a flooded paddy soil with growing rice (research task 1: moderate O₂ limitation) and without rice (research task 2: strong O₂ limitation). We tested two hypotheses explaining possible effects of short-term aeration on hydrolytic versus oxidative enzymes. (1) Aeration promotes Fe(II) oxidation, which leads to the accumulation of phenolics through the “iron-gate” mechanism, thus suppressing the activities of hydrolytic enzymes compared to the anoxic conditions. (2) Aeration stimulates phenol oxidases that degrade phenolics according to the “enzyme latch” concept, thus eliminating the suppression of hydrolytic enzymes. The activities of hydrolytic enzymes were lower by 5–43% in both experiments under +O₂ compared to -O₂. In contrast, the activities of peroxidases and phenol oxidases were 2 to 14 times higher under +O₂ than under -O₂. Thus, the activation of oxidative enzymes under +O₂ was uncoupled from the hydrolytic activities. This contradicts both the “iron gate” and the “enzyme latch” mechanisms. We explain the short-term suppressive effect of O₂ in assays by increased concentrations of reactive oxygen species, which decreased microbial activity. We conclude that our modification of enzyme assays under anoxic conditions is required for samples taken from low-oxygen environments to avoid underestimation due to rapid suppression of hydrolytic enzyme activities by O₂.

Keywords: anoxic conditions; suppression by oxygen; paddy soil; phosphomonoesterase; β -glucosidase; leucine aminopeptidase

1. Introduction

A large variety of biogeochemical processes in soil is mediated by enzymes, produced mainly by microorganisms, plant roots, and fauna (Kunito et al., 2018; Wang et al., 2021). Hydrolytic enzymes such as β -glucosidase, phosphatase, and leucine aminopeptidase catalyze the decomposition of organic polymers in soils to cover the demand by plants and microorganisms for carbon (C), phosphorus (P), and nitrogen (N), respectively (Alexander, 1977; Cosgrove, 1980; Hanson and Frohne, 1976). In contrast, oxidative enzymes such as phenol oxidases and peroxidases are expressed for a variety of purposes including ontogeny, defense, and the acquisition of C and nutrients from recalcitrant organic matter pool (Ladd, 1978; Sinsabaugh, 2010). Independent of soil sample origin, enzymatic activity assays are commonly performed under aerobic conditions (Wei et al., 2019; Parvin et al., 2018; Keiluweit et al., 2017), albeit oxygen (O_2) is a known suppressor for putative anaerobic microorganisms (Dellwig et al., 2012). The prevailing paradigm claims that O_2 and hydrolytic enzymes are decoupled at a biochemical level, so that the respective enzyme activities are commonly measured under oxic conditions (Huang et al., 2021; Wei et al., 2019; Li et al., 2019a; Peacock et al., 2015). Moreover, the terrestrial ecosystem models and the mechanisms controlling the transformation of soil organic matter (SOM) have been explored predominately under oxic conditions; the anoxic legacy effect is existing, yet, even within well-drained soil systems but is largely overlooked in previous studies (Keiluweit et al., 2017).

A general concept of the long-term effects of fluctuating oxic and anoxic conditions on enzyme activities in soils has been described in the “enzyme latch” hypothesis proposed by Freeman et al. (2001). It postulates that increased phenol oxidase activity under O_2 exposure leads to the degradation of phenolics, which inhibit hydrolytic enzyme activities, thereby stimulating SOM mineralization. Positive relationships between O_2 availability and organic carbon mineralization rate (Waldrop et al., 2004; Keiluweit et al., 2017) have also been reported for the upland ecosystems. In contrast, reduced O_2 availability in humid tropical forest soils did not limit the activity of hydrolytic enzymes, which was higher under anoxic vs. oxic conditions (Hall et al., 2014). As opposed to oxidoreductases (e.g., phenol oxidase or peroxidase), the functioning of soil hydrolytic enzymes does not require O_2 (Hall et al., 2014). In addition to the “enzyme latch” concept, the “iron gate” paradigm proposes that the oxidation of ferrous iron (Fe(II)) and C-complexation by ferric iron (Fe(III)) are the main protective mechanisms against C loss in wetlands under O_2 exposure (Wang et al., 2017). This in turn was attributed to the accumulation of phenolics caused by the decreasing Fe(II) contents with aeration, as Fe(II) oxidation inhibits the oxidative activity of phenols and promotes Fe-lignin phenol association. Thus, the “enzyme latch” and “iron gate” may simultaneously control phenol oxidative activity and C loss rates under O_2 exposure in peatlands, but it depends on the trade-off between O_2 and Fe(II) (Wen et al., 2019). Whether the mechanisms described require time (weeks to months) to have clear effects on enzymatic reactions, or whether a short-term O_2

exposure of environmental samples adapted to anoxic conditions to O₂ can elicit a rapid specific response in hydrolytic enzyme assays, remains uncertain. This calls for evaluating the enzyme activities of samples from semi- or fully anoxic environments, such as flooded rice paddy soils, and investigating how the measurement conditions may influence enzyme activities in such ecosystems.

To address these apparent knowledge gaps, we adapted a commonly used enzyme activity assay based on fluorogenically labeled substrates (Marx et al., 2001) to the anoxic conditions by means of a portable glovebox. We applied the Michaelis-Menten kinetic approach to calculate the maximal rate of an enzymatic reaction (V_{\max}) and the Michaelis constant (K_m) for three hydrolytic enzymes contributing to C, N, and P turnover. The activities were measured at three dates of rice plants growth (research task 1: moderate O₂ limitation due to diffusion from the atmosphere and in the rhizosphere) and in combination with hydrolytic, two oxidative extracellular enzymes measured in the same Fe-rich paddy soil without growing rice (research task 2: strong O₂ limitation). The key aim of the study was to evaluate whether enzyme activities in flooded paddy soils differ under anoxic and oxic short-term (45–150 min) assay conditions. Based on the proposed “enzyme latch” and “iron-gate” concepts, we hypothesized that short-term aeration (minutes to hours) either (1) stimulates the oxidative enzymes that degrade phenolics according to the “enzyme latch” concept, thus reinforcing hydrolytic enzymes, or (2) promotes Fe(II) oxidation, which leads to the accumulation of phenolics through the “iron-gate” mechanism, thus suppressing the activities of hydrolytic enzymes compared to the anoxic control. The following additional research questions were addressed: would the expected effects of short-term aeration on enzyme activities be modified with (1) a spatial natural aeration gradient from top via rooted to bottom soil in a rhizobox, and (2) a temporal natural aeration gradient arising from the age of the rice plants, which contributes to soil aeration via their aerenchyma as root biomass increases but also provide more C through higher exudation.

2. Materials and methods

2.1. Soil description

The soil was collected from the 0–20 cm depth in a paddy rice field at the Changsha Agricultural and Environmental Monitoring Station, Hunan Province, China (113°19'52" E, 28°33'04" N). The main soil physicochemical properties were pH 6.2, soil organic C 13.1 g kg⁻¹, total N 1.4 g kg⁻¹, available N 18.0 mg kg⁻¹, total P 0.3 g kg⁻¹, Olsen-P 3.7 mg kg⁻¹, and total Fe 15.7 g kg⁻¹ (Zhu et al., 2018). The soil was passed through a 2 mm sieve and homogenized.

2.2. Research task 1: moderate O₂ limitation

2.2.1. Experimental setup

For each of the three enzyme assays, three PVC-rhizoboxes (9 in total) with inner dimensions of 20.5 × 24.0 × 1.5 cm closed with a transparent, removable

plexiglas front cover were set as replicates. Rhizoboxes were specially constructed to be water-tight using rubber sealing and screw-holders. One 20-day-old rice seedling (*Oryza sativa* L. ‘Two-line hybrid rice Zhongzao 39’) was transplanted into a rhizobox prefilled with water-saturated soil. After transplanting, all rhizoboxes were adjusted with deionized water ca. 2 cm above the soil surface and the water level was maintained throughout the experiment (except the dates of soil sampling; see section 2.2. below). Despite of flooding, moderate O₂ limitation in the Experiment 1 was achieved through the diffusion of air to the water and topsoil as well as through releasing of O₂ to the rhizosphere soil via aerenchymatous rice roots (Larsen et al., 2015). All seedlings were grown in a climate chamber (KBF-S 720, Binder GmbH, Tuttlingen, Germany) with 28 ± 1 °C day temperature and 24 ± 1 °C night temperature, 70% relative humidity, and 12-h photoperiod. After transplanting, 30 mg N as urea, 25 mg K and 20 mg P as KH₂PO₄ per kg dry soil were added to each rhizobox as background fertilizers.

2.2.2. Soil sampling

Soil was collected at three consecutive dates of rice growth, i.e. after 10, 16–20, and 28–31 days from rice transplanting. These ages of rice plants roughly corresponded to a seedling (with 1 tiller), early (4 ± 1) and late (6 ± 1) tillering stages of the vegetative phase of rice growth. Two days before each sampling date, the soil in rhizoboxes was preconditioned by draining the flooding water to omit the loss at the moment of opening. To maintain anoxic conditions in the moist soil, all the rhizoboxes were opened inside a portable PVC glovebox (Captair® Pyramid Glovebox 3015-00, Erlab DFS, Saint-Maurice, France) evacuated with a vacuum pump (Ilmvac MP 301 Vp, Ilmvac GmbH, Ilmenau, Germany) and then back-flushed with nitrogen to O₂ concentrations lower than 0.2%. The O₂ concentrations were determined with an O₂-sensor (Greisinger GOX 100, GHM Messtechnik GmbH, Remscheid, Germany).

After opening a rhizobox, the soil was collected from three compartments roughly reflecting the gradient of natural aeration from higher to lower: top bulk (2–5 cm), rooted (5–15 cm), and bottom bulk (15–18 cm) (Fig. 1a). In each compartment, soil was collected from three random locations and then mixed into one sample of ca. 0.5 g moist weight. The sampling per compartment was repeated two times in the glovebox – for oxic and anoxic assay – and the collected soil was placed into two 100 ml Kimble KIMAX borosilicate laboratory glass bottles (Kimble Chase Life Science and Research Products, LLC., Meiningen, Germany), respectively. Depending on the aeration treatment, either N₂-bubbled (anoxic) or normal deionized sterile water (with dissolved O₂) was added to the respective bottles with soils at a soil-water ratio of 1:100. Before opening the glovebox, the bottles for the anoxic assay were tightly sealed with thick air-impermeable butyl rubber septa. The glovebox was opened and air filled the headspace of oxic bottles. Thereafter, the anoxic treatment was additionally flushed with N₂ for 30 min. At the same time, the oxic treatment remained open without additional manipulations. After slaking the soil, the oxic bottles were closed with butyl septa and the suspension was prepared in oxic and

anoxic bottles simultaneously by shaking on a rotator (200 rpm) for 30 min before the enzyme activity assays. A preliminary experiment has shown that the contribution of enzymes bound to soil particles to the total enzyme activity is not significant after a mild sonication (De Cesare et al., 2000) compared to a 30-min shaking without sonication (data not shown). This suggested that the 30-min shaking was sufficient to detect the majority of extracellular enzymes, both those released by active cells and those enzymes stabilized on soil particles and colloids.

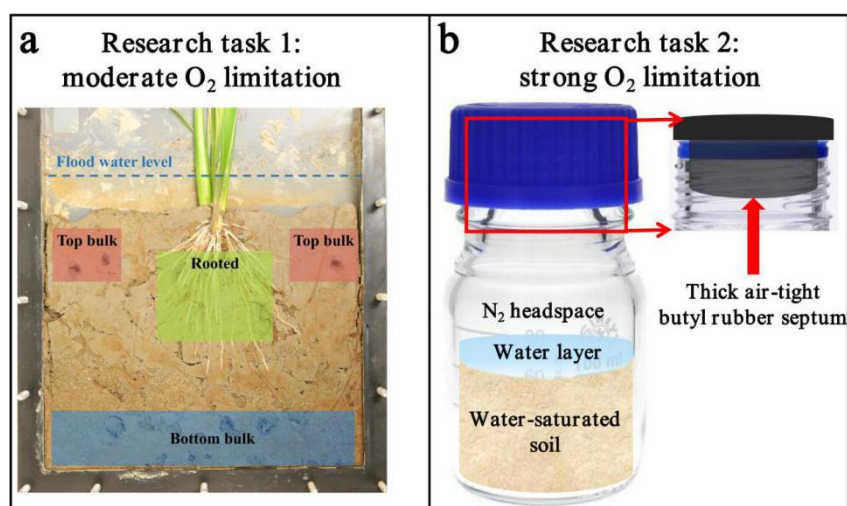


Fig. 1 (a) Sampling locations in the three soil compartments 48 hours after flood water drainage for the Research task 1: moderate O₂ limitation; shaded spots within each compartment correspond to the removed soil; the level of flooded water maintained during experiment is shown schematically by a dashed line. (b) Incubation set-up for the Research task 2: strong O₂ limitation with water-saturated soil in a bottle sealed with a thick air-impermeable butyl rubber septum.

2.2.3. Hydrolytic enzyme assays

The activities of phosphomonoesterase (PME), β -glucosidase (BG), and leucine aminopeptidase (LAP) were measured in independent variants (3 rhizoboxes per enzyme) using fluorogenically labelled substrates of 4-methylumbelliferyl-phosphate, 4-methylumbelliferyl- β -D-glucoside, and L-leucine-7-amino-4-methylcoumarin hydrochloride (all substrates were purchased from Sigma-Aldrich Co. Ltd), respectively, according to the established method (Marx et al., 2001). We measured enzyme kinetics according to the Michaelis-Menten approach with a saturating range of substrate concentrations: 0, 5, 10, 20, 50, 100, 150, and 200 μ M. Substrate and buffer (see below) were prepared in duplicate, one replicate was flushed with N₂ for 20 min and then used for enzyme determination under anoxic conditions in the glovebox ($-O_2$ assay) and the other replicate without any pretreatment was used for enzyme determination under oxic conditions ($+O_2$ assay). For both assay treatments, 50 μ l soil suspension, 100 μ l 4-methylumbelliferone (MUF) or 7-amino-4-methylcoumarin (AMC)-based substrate, and 50 μ l MES or TRIZMA buffer were added into a 96-well black microplate (Brand GmbH, Wertheim,

Germany). After addition, microplates were incubated for enzymatic reaction development. To maintain anoxic conditions during incubation, anoxic microplates were prepared in the glovebox with O₂ concentrations lower than 0.2% from the atmospheric level. For +O₂ assay, the preparation and incubation of microplates were done outside the glovebox. The difference in enzyme kinetic parameters between oxic and anoxic assays was termed as “aeration effect”. Pre-tests were made to define a period of time between 0 and 120 min after addition of substrates ensuring linear development of fluorescent signal. So, the fluorescence was measured at 30 and 60 min after addition of substrates to soil on a Victor 1420-050 Multi label counter (PerkinElmer, USA) using a protocol with the excitation and emission wavelengths at 355 nm and 460 nm, respectively. The duration of reading per well was 0.1 s, so full measuring of microplates was completed within 10 s. The effect of such a short period of time compared with the total time of exposure to O₂ for the oxic assay including suspension preparation (ca. 2 h) was assumed to be negligible during anoxic assays. The total time of exposure to O₂ for the oxic assay including suspension preparation was ca. 2 h.

2.3. Research task 2: strong O₂ limitation

2.3.1. Experimental setup

Strong O₂ limitation in the paddy soil was tested in an incubation experiment without rice plants. The research task 2 comprised two objectives: (1) to reveal the earliest effect of aeration on enzyme activities by measuring the signal during the first 45 min incubation of soil and substrates, (2) to estimate the aeration effects on the activities of phenol oxidases and peroxidases and to correlate the activities with the concentrations of Fe(II) and Fe(III) in soil suspensions of oxic and anoxic assays.

Same paddy soil was used for the research tasks 1 and 2 (see section 2.1.). Four 100 ml Kimble KIMAX borosilicate laboratory glass bottles (Kimble Chase Life Science and Research Products, LLC., Meiningen, Germany) were filled with 20 g (dry weight) water-saturated soil each (Fig. 1b). Additionally, 10 ml deionized water was added to each bottle. The soil was pre-incubated anaerobically in the dark for 10 days at 25 °C in a climate chamber (KBF-S 720, Binder GmbH, Tuttlingen, Germany) to establish strong anoxic conditions.

2.3.2. Soil sampling

After incubation, all the bottles were opened inside the glovebox as explained above (section 2.2.2.). Soil in each bottle was stirred with a spoon and two subsamples ca. 0.5 g moist soil were collected individually for oxic and anoxic assays, respectively. The soil suspension was prepared as described above (section 2.2.2.).

2.3.3. Hydrolytic enzyme assays

Same hydrolytic enzymes – PME, BG, and LAP – were assayed as described above (see 2.2.3. section). To reveal the earliest effect of aeration on enzyme activities, the fluorescence was measured at 0, 15, 30, 60, 90, and 120 min after the

addition of substrates to microplates under oxic and anoxic conditions.

2.3.4. Phenol oxidase and peroxidase activity assays

Phenol oxidase activity and peroxidase activity were measured using a substrate Amplex Red (10-acety-3,7-dihydroxyphenoxazine, purchased from Sigma-Aldrich Co. Ltd), according to Khosrozadeh et al. (2022). Briefly, 1 mg Amplex Red was dissolved in 300 μl dimethyl sulfoxide (DMSO, Zhou et al., 1997), and then TRIZMA buffer was added to obtain a final concentration of 500 μM . The Amplex Red solution was prepared in duplicate and was flushed with N_2 for 5 min. For both assay treatments (anoxic and oxic), 50 μl soil suspension, 100 μl Amplex Red solution, and 50 μl TRIZMA buffer were added into a 96-well black microplate (Brand GmbH, Wertheim, Germany). To distinguish peroxidase activity from phenol oxidase in total oxidative enzymatic reaction with Amplex Red, 10 μl of 0.3% H_2O_2 were added to each well of a separate microplate after the soil suspension, Amplex Red solution, and TRIZMA buffer were added as described above. The anoxic conditions during respective assay, including the incubation period of soil and substrate in microplates, were maintained using the glovebox. All manipulations of the oxic treatment were conducted in a similar way but under the room conditions. The fluorescence was measured at 0, 15, 30, 60, 90, and 120 min after the addition of substrates to microplates on a TECAN Infinite 200[®] PRO (Tecan Austria GmbH, Austria) using a protocol with the excitation and emission wavelengths at 530 nm and 585 nm, respectively.

2.3.5. Fe(II) and Fe(III) concentration measurement

Determination of Fe(II) and Fe(III) concentrations in oxic and anoxic soil suspensions was done according to Elrod et al. (1991). Before analysis, all soil suspensions were filtered through a filter paper (Whatman No. 42). For oxic assay, 2 ml filtrate were mixed with 500 μl ammonium acetate buffer (pH 4.5) and 500 μl 1,10-phenanthroline solution (0.5%) in a transparent cuvette (Th. Geyer GmbH & Co. KG, Renningen, Germany) and then measured at 512 nm on a spectrophotometer (NanoPhotometer[®] NP80, Implen GmbH, Munich, Germany). Then, 200 μl ascorbic acid solution (10%) was added to cuvettes to completely reduce Fe(III) to Fe(II). After 30-min reaction, total Fe concentration was measured as described above. Fe(III) concentration was calculated as the difference between total Fe and Fe(II) concentrations. The measurement was repeated after 15, 30, 60, 90, and 120 min incubation of soil suspensions. For anoxic assay, the described procedure was conducted inside the glovebox and the measurement was conducted immediately after the cuvettes were removed from the glovebox. Determination of Fe(II) and total Fe was done on the same anoxic suspension but in separate runs to exclude effect of aeration during 30 min Fe (III) reduction by ascorbic acid. Calibration was performed with FeCl_3 at increasing concentrations of 0, 5, 10, 25, 50, 100, 200, and 300 μM .

2.4. Enzyme kinetics

To estimate the rate of hydrolytic enzyme activities in the research tasks 1 and 2,

the assays were calibrated using either MUF or AMC pure substances at increasing concentrations of 0, 100, 200, 500, 800, and 1200 pmol well⁻¹ of a microplate. For phenol oxidative and peroxidase activity estimation, the assays were calibrated using resorufin at increasing concentrations of 0, 500, 1000, 1500, and 2000 nmol well⁻¹. Calibration was conducted in parallel under oxic and anoxic conditions. All pure substances were purchased from Sigma Aldrich Co. Ltd.

Based on the calibration, the rates of three hydrolytic enzyme activities were calculated as nmol MUF or AMC per g soil on a dry weight basis per hour at each of the substrate concentrations added (in $\mu\text{mol g}^{-1}$ dry soil). The Michaelis-Menten equation was used to calculate the kinetic parameters V_{max} and K_m for each enzyme:

$$v = (V_{\text{max}} * S)/(K_m + S) \quad (1)$$

where v is the reaction rate (nmol g^{-1} soil h^{-1}), S is the substrate concentration, V_{max} is the maximum reaction rate of enzymatic activity at saturated substrate concentration calculated from the increment of fluorescence values between the selected time intervals (0–15, 15–30, 30–60, 60–90, and 90–120 min), and K_m is the substrate concentration at half-maximal rate ($1/2 V_{\text{max}}$). V_{max} and K_m were estimated using non-linear curve fitting in GraphPad Prism 8 (GraphPad Software, Inc., San Diego, USA). Oxidative enzymes were calculated based on a single saturating concentration ($v = V_{\text{max}}$) from a linear regression of calibration and presented as nmol resorufin per g soil on a dry weight basis per hour.

2.5. Statistical analysis

For the research task 1, a two-way ANOVA with repeated measures (rice growth stage, $n = 3$) was used to test the effects of (i) assay condition (+O₂ vs. -O₂ assays) and (ii) soil compartment on V_{max} and K_m . For the research task 2, a two-way ANOVA was used to test the effects of (i) assay condition (+O₂ vs. -O₂ assays) and (ii) incubation time on V_{max} and K_m of hydrolytic enzymes, the activity of phenol oxidases and peroxidases, and the concentration of Fe(II) and Fe(III) in soil suspensions. Linear regression analysis was used to determine the relationships between Fe(II) or Fe(III) concentrations and incubation time in soil suspensions. All statistical tests were conducted using SPSS (Version 21, IBM, Armonk, NY, USA).

3. Results

3.1. Calibration of assays under anoxic and oxic conditions

Calibration curves of MUF (Fig. S1a), AMC (Fig. S1b), or resorufin (Fig. S1c) obtained under -O₂ and +O₂ demonstrated strong linearity ($r^2 \sim 0.967\text{--}0.999$) with given concentrations. The slopes of the MUF and AMC calibration lines varied by 0.1% and 1.7% under -O₂ vs. +O₂ assays, respectively. The differences between the slopes in -O₂ and +O₂ assays were not statistically significant for MUF, AMC, or resorufin (Fig. S1).

3.2. Kinetic parameters of the hydrolytic enzymes

3.2.1. Research task 1: moderate O₂ limitation

The activities of the three tested enzymes demonstrated the saturation pattern with increasing substrate concentrations from 0 to 200 $\mu\text{mol g}^{-1}$ soil under both aeration treatments (Fig. S2, S3). V_{max} was most strongly suppressed by O₂ for BG (28–43%), followed by PME (12–27%) and LAP (9–22%) (Fig. 2a, b, c). This was more pronounced in rooted soil than in bulk soil (Fig. 2a, b, c). The suppression effect by O₂ demonstrated diverse patterns (increase, decrease, or no change) with rice growth for all tested enzymes (Fig. 2a, b, c). Compared with V_{max} , the affinity of enzymes to substrates (K_m values) was generally less affected by O₂. Only the affinity of PME decreased (higher K_m) by 11–17% under –O₂ vs. +O₂ (Fig. 2d). Between the compartments, the K_m values were overall higher in rooted vs. top bulk soil and especially bottom bulk soil for all enzymes in both aeration assays (Fig. 2d, e, f). The substrate affinity dynamics of PME increased with rice growth, except for rooted soil under +O₂ conditions (Fig. 2, bottom row).

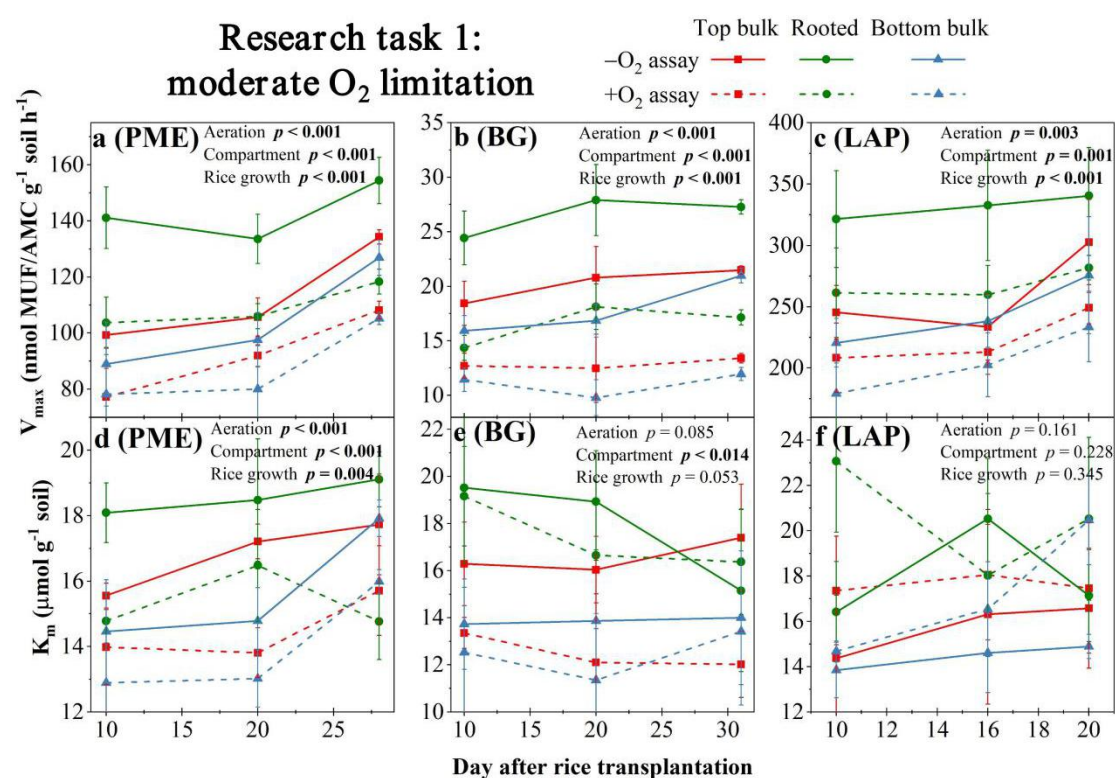


Fig. 2 The maximum reaction rate (V_{max}) of phosphomonoesterase (PME, a), β -glucosidase (BG, b), and leucine aminopeptidase (LAP, c) and the affinity to a substrate (K_m) of PME (d), BG (e), and LAP (f) at the top bulk, rooted, and bottom bulk soil of rhizoboxes with growing rice under moderate O₂ limitation (research task 1) in oxic (+O₂, dashed lines) and anoxic (–O₂, solid lines) assays. The data are means \pm standard deviations ($n = 3$).

3.2.2. Research task 2: strong O₂ limitation

V_{max} was suppressed by 6–26% for BG, 8–24% for PME, and 5–23% for LAP under +O₂ vs. –O₂ (Fig. 3a, b, c). The difference in V_{max} between +O₂ vs. –O₂

increased from 5–8% to 20–24% with incubation time from 15 to 60 min and then stabilized between 19–26% after 1-h incubation (Fig. 3a, b, c). The increased activities of all three enzymes at initial 15–30 min (for PME and BG) and up to 60 min (for LAP) was attributed to high autofluorescence of substrates (fluorescence during solubilization of substrates which was not caused by an enzymatic reaction) (Fig. 3, red arrows). In contrast to V_{\max} , the aeration had no effects on the affinity of enzymes to substrates (Fig. 3d, e, f), except for PME which affinity to the substrate increased with incubation time (Fig. 3d).

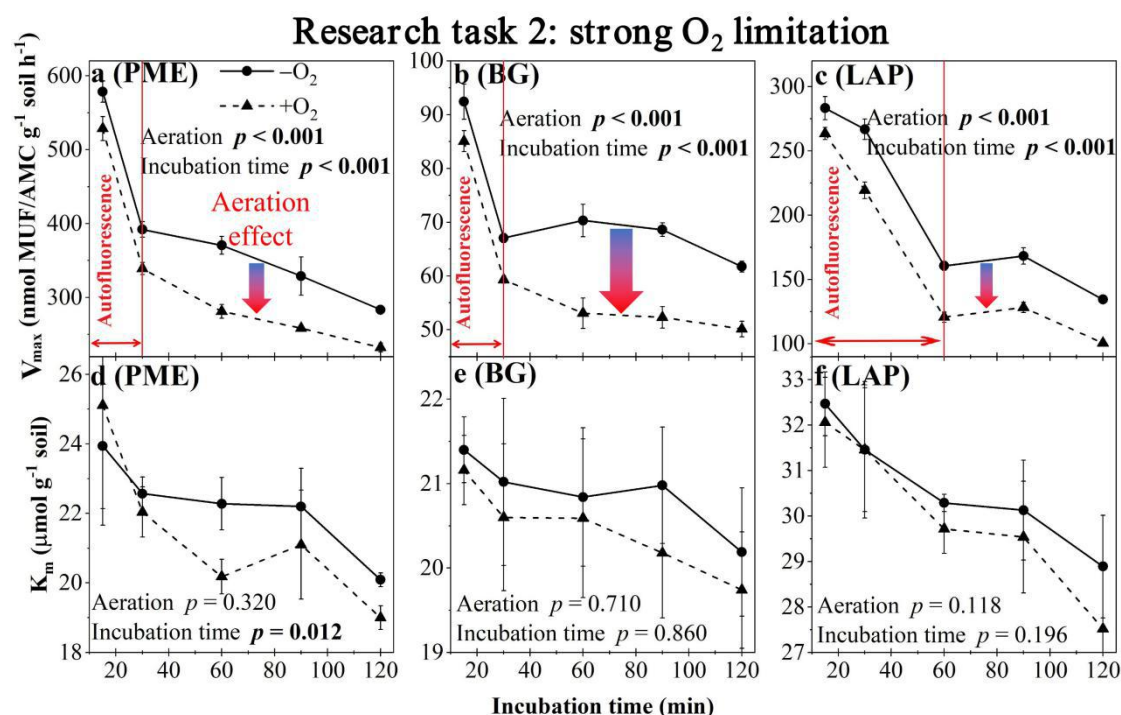


Fig. 3 The maximum reaction rate (V_{\max}) of phosphomonoesterase (PME, a), β -glucosidase (BG, b), and leucine aminopeptidase (LAP, c) and the affinity to a substrate (K_m) of PME (d), BG (e), and LAP (f) in soils under strong O₂ limitation (research task 2) in oxic (+O₂, dashed lines) and anoxic (–O₂, solid lines) assays. The data are means \pm standard deviations ($n = 4$). The vertical red lines correspond to the duration of autofluorescence when enzyme activity is not measurable. Downward arrows represent the negative aeration effect on V_{\max} . Size of a arrow indicate the relative intensity of the aeration.

3.3. The activity of phenol oxidases and peroxidases and the concentration of Fe(II) and Fe(III) in the research task 2

In contrast to hydrolytic enzymes, oxidative phenol oxidase and peroxidase activities were up to 14 and 2 times higher under +O₂ than –O₂, respectively (Fig. 4a). Fe(II) concentration in soil suspension gradually decreased at a rate of 0.02 $\mu\text{M min}^{-1}$ under +O₂ assays during 150 min exposure to air (Fig. 4b). In contrast, Fe(III) concentrations gradually increased at a rate of 0.014 $\mu\text{M min}^{-1}$ under +O₂ assays (Fig. 4b).

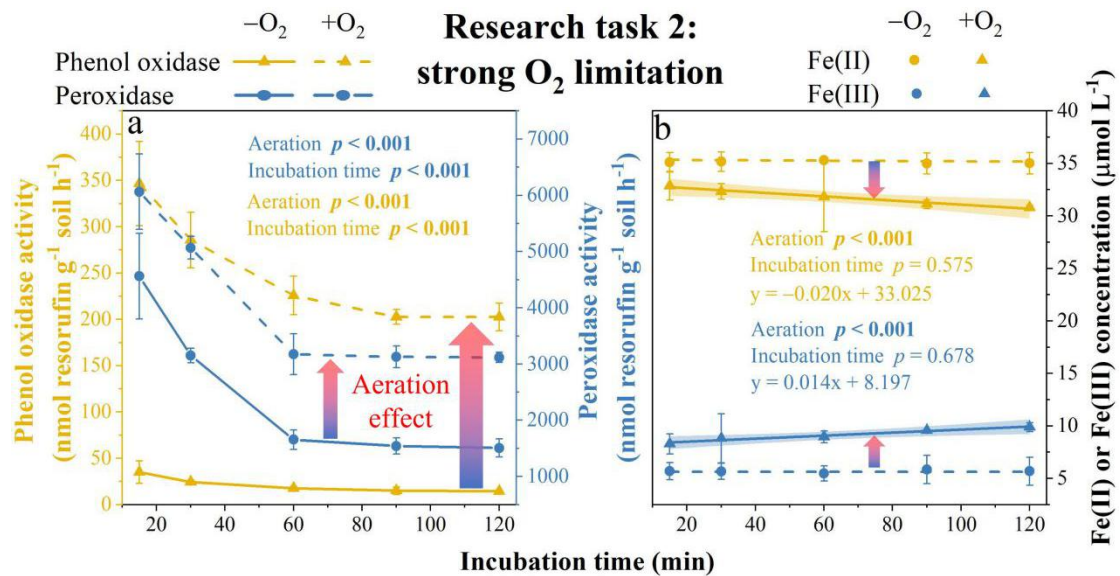


Fig. 4 The activity (a) of phenol oxidases (yellow lines) and peroxidases (blue lines) and the concentration dynamics (b) of soluble Fe(II) (blue) and Fe(III) (yellow) in soil suspension either in oxic (+O₂) or anoxic (-O₂) assays. The data are means ± standard deviations (n = 4). Solid lines in subFig. b indicate significant linear correlations. Arrows represent the aeration effect on either the activity of phenol oxidases and peroxidases or the concentration dynamics of soluble Fe(II) and Fe(III) in soil suspension. Size of arrows indicates the relative intensity and direction corresponds to a positive or a negative aeration effect on a parameter.

4. Discussion

4.1. Effects of short-term aeration on hydrolytic enzymes, phenol oxidases, and peroxidases

Incubation strategies under moderate (research task 1) and strong O₂ limitation (research task 2) both independently revealed the short-term suppressive effect of aeration on hydrolytic enzyme activities in a paddy soil. So, in soils subjected to moderate O₂ limitation, activities of hydrolytic enzymes were suppressed by 9–43% by aeration (Fig. 2a, b, c). Similarly, for soils incubated under strong O₂ limitation, the maximal enzymatic reaction rate after a reduction of autofluorescence (from 60–90 min depending on an enzyme) decreased by 19–26% with aeration of the enzyme assay (Fig. 3a, b, c). This contradicted the first hypothesis that hydrolytic enzyme activities would increase after the transition from anoxic to oxic conditions. The decrease in V_{max} by aeration in the assays was greater by 6–57% in rooted vs. bulk soil under the moderate O₂ limitation. This answered our first research question that the suppressive effects of short-term aeration on hydrolytic enzyme activities are modified along natural aeration gradient. This means, the natural aeration gradient (Lüdemann et al., 2000; Bai et al., 2015) in the paddy soil from top bulk through rooted and down to bottom bulk soil could not alleviate the suppression of enzymes by aeration.

Regarding the second research question, no clear patterns of V_{\max} by aeration of the assays with rice growth were observed, suggesting that the suppressive effects of short-term aeration on hydrolytic enzymes are independent of plant root biomass and amount of provided exudates. The short-term aeration only affected the affinity of phosphomonoesterase to substrates (K_m values) (Fig. 2d), indicating that the effects of moderate O_2 limitation are enzyme-specific. Moreover, the phosphomonoesterase K_m values decreased with the duration of aeration under strong O_2 limitation (Fig. 3d). This can be interpreted as (1) a selective suppression of less effective enzymatic systems, and/or (2) the production of a set of isoenzymes of phosphomonoesterase with the same function but different chemical structure resulting in higher affinity to substrate under oxic conditions (Hochachka and Somero 2002). The latter can be in turn interpreted as a quick feedback mechanism and physiological response of the microorganisms to the decreasing phosphate availability in soil solution due to the immobilization of phosphates on Fe(III) from Fe(II) oxidation under oxic conditions.

Long-term oxic conditions and the removal of phenolics have been suggested to increase hydrolytic enzyme activities in paddy soils (Wang et al., 2022), wetlands (Wang et al., 2017), and peatlands (Freeman et al., 2001). However, we found that short-term (2.5 h) aeration during enzymatic assays under strong O_2 limitation had an overall negative effect on V_{\max} values of the three tested hydrolytic enzymes in naturally anoxic flooded paddy soil. In contrast, oxic conditions stimulated phenol oxidase activity (Fig. 4a) and may therefore suggest an increased removal rate of phenolics. Thus, our findings could not support the proposed “enzyme latch” mechanism, which states that the suppression of hydrolytic enzymes is associated with decreased activity of oxidative enzymes and the accumulation of phenolics. Moreover, the Fe(II) oxidation rate of $0.02 \mu\text{M min}^{-1}$ observed in the present study was lower than the values ($0.1\text{--}0.5 \mu\text{M min}^{-1}$) found in other studies on paddy soils (Li et al., 2016; Li et al., 2019b). As a result, the production of Fe(III) at such a low rate cannot strongly affect the phenolics stoichiometrically, thereby contradicting the second hypothesis. This confirms the inability of “iron gate” to explain short-term aeration effects. Therefore, neither “enzyme latch” nor “iron gate” can explain the suppression of hydrolytic enzyme activities in the short-term.

4.2. Mechanisms of the short-term effects of aeration on hydrolytic enzymes

Enzyme activities are the net effect of complex processes including enzyme production, stabilization, degradation, and inhibition (Allison, 2006). Below, we propose three mechanisms, which in our view may most comprehensively explain the observed short-term suppressive effect of O_2 on hydrolytic reactions (Fig. 5):

(1) Abrupt aeration inhibited the activity of obligate anaerobic microorganisms and initiated a shift in microbial metabolic pathways, restricting the secretion of *de novo* formed enzymes. Generally, O_2 could affect microbial communities in two ways: (i) long-term change in microbial community structure if redox conditions persist longer than the average generation time of organisms, (ii) short-term change in the activity and metabolic pathways of the community if the redox conditions persist

shorter than organisms' average generation times (Deangelis et al., 2010). Although we did not determine the microbial community changes, there is evidence that such changes are not essential within a timeframe of 2.5 h, given the 4–11 h time lag preceding microbial growth and the 1.8–2.8 h generation time of growing microorganisms in soil (Bååth, 1992; Blagodatskaya et al., 2009). Microbial biomass and community structure did also not change in a humid tropical soil with short-term redox fluctuation under alternating flushing of air and N₂ every 12 h (Pett-Ridge et al., 2006). Therefore, 2.5-h aeration in our both experiments should rather cause short-term changes in activity than shifts in microbial community structure (Fig. 5b, pathway I). Facultative anaerobes and micro-aerophilic groups can adapt to common O₂ fluctuations (Yadav et al., 2014). However, the abrupt exposure of an established anoxic environment to air will most probably cause a direct suppressive effect on active anaerobic microorganisms and strongly reduce *de novo* enzymes synthesis. This was indirectly confirmed by the fact that the negative effect of aeration on hydrolytic enzyme activities increased with increasing duration of O₂ exposure, during which enzyme turnover and degradation continued but no new enzymes were supplied by the highly O₂-stressed microbial community (Fig. 3).

Suggested mechanisms of enzyme activities with aeration

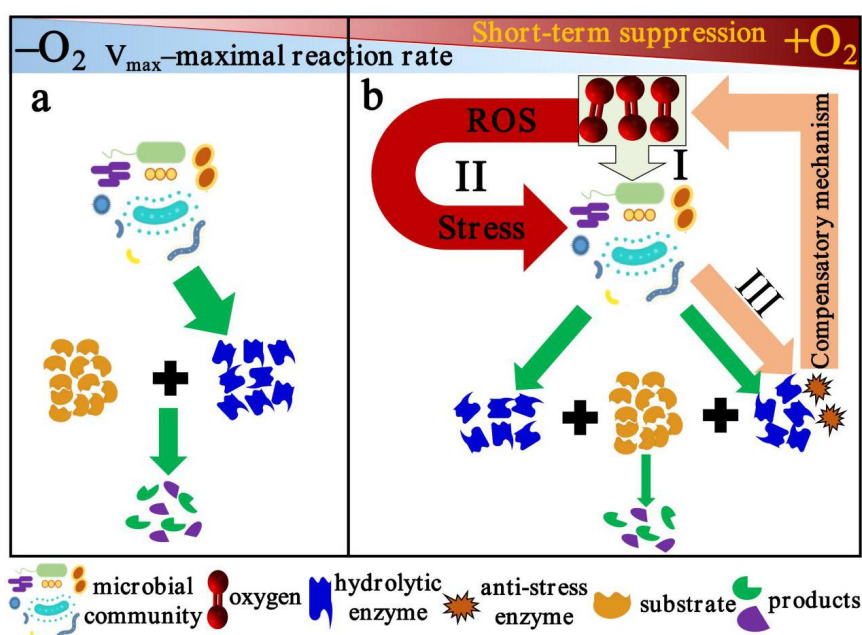
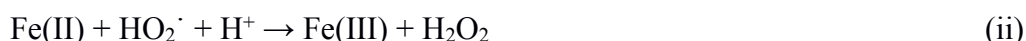
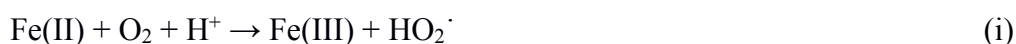


Fig. 5 Mechanisms of hydrolytic enzymes suppression by short-term (during 2 hours) O₂ exposure. Left side (a): enzymatic reactions conducted by hydrolytic enzymes under anoxic conditions. Right side (b): reduction of microbial activity (pathway I), toxicity of reactive oxygen species (ROS) to microbial cells (pathway II), and compensatory mechanism of anti-stress enzyme production, e.g. catalase, superoxide dismutase (pathway III). Size of arrows corresponds to relative intensity of enzyme production or reaction rates. Triangles on top reflect the relative increase of the short-term suppressive effect of oxygen (brown) and the concurrent relative decrease of enzymatic maximal reaction rate (V_{max} , blue) with O₂.

(2) The reactive oxygen species (ROS), such as superoxide anions ($O_2^{\cdot-}$), hydroxyl radicals (HO^{\cdot}), and hydroperoxyl (HO_2^{\cdot}), can be produced as a result of molecular O_2 reduction by Fe(II) and may directly suppress microorganisms after the transition from anoxic to oxic conditions (Fenchel and Finlay, 2010). Importantly, ROS could be generated quickly initially (Grant and Loake, 2000). For example, H_2O_2 -mediated oxidative cross-linking of bean cells was initiated within 2 min (Bradley et al., 1992). ROS can be generated through Fenton and Fenton-like reactions (Hall and Silver, 2013):



Although ROS species and their concentration dynamics were not measured in the current experiment, estimates based on Fe(II) oxidation rate of $0.02 \mu M \text{ min}^{-1}$ confirm the stoichiometric generation of 0.06 nmol of cumulative ROS in each well of a microplate per hour. Stimulated oxidative enzyme activities, which use ROS such as H_2O_2 as co-substrates, support the concept of increased ROS formation, which may be responsible for exertion of a negative effect on microbial activities after an abrupt aeration. Aerobes and facultative anaerobes possessed complex protective mechanisms such as the production of catalase, superoxide dismutase, and other compounds to reduce ROS (Fenchel and Finlay, 2010). However, these protective enzymes are generally lacking or occur at very low concentrations in anaerobes (Fenchel and Finlay, 1994). An abrupt aeration can therefore suppress the entire metabolic activity of anaerobes, including the production of hydrolytic enzymes (Fig. 5b, pathway II), at least until sufficient agents are synthesized to protect cells from ROS damages.

(3) Aerobes and facultative anaerobes may respond to oxidative stress caused by ROS by redirecting their resources from the secretion of hydrolases to protection. Microbial functions are prone to immediate changes, especially under conditions where stress becomes intolerable (Tikariha et al., 2018). For example, the ammonia-oxidizers (Bodelier et al., 1996) and the nitrifying bacterial community (Jensen, 1993) in fresh water sediments resumed nitrification within 1 h upon exposure to O_2 . This and other examples (Kalia et al., 2011; Tan et al., 2014; Cabisco et al., 2000) confirm that the 2-h aeration likely exerted intolerable stress on the microbial community and caused changes in enzyme kinetic parameters. To protect themselves against oxidative stress, the compensatory mechanisms established by microorganisms include production of catalase, superoxide dismutase, glutaredoxin, and thioredoxin (Cabisco et al., 2000). For example, manganese-containing superoxide dismutases and hydroperoxidase I were produced by *Escherichia coli* in response to oxidative stress (Compan and Touati, 1993; Finn and Condon, 1975). Along with such a direct compensatory mechanism, the indirect effect will be driven by the need of microorganisms to overuse their resources in dealing with the stress (Schimel et al., 2007). Apparently, the production and release of enzymes by

microorganisms are costly, energy-consuming processes (Schimel and Weintraub, 2003). If this energy is devoted to compensatory production of catalases and ferroxidases to resist oxidative stress, then there could be a concurrent decrease in hydrolases production (Fig. 5b, pathway III).

In summary, this study demonstrated for the first time the clear need to consider *in situ* conditions for the soil enzyme assays. The proposed mechanisms should be further proven by (i) in-depth verification based on ROS identification and concentration measurements and (ii) the long-term effects of aeration on enzyme kinetic parameters during the shift from anoxic to oxic conditions, e.g. after water drainage or under the alternative wetting/drying rice cultivation management.

5. Conclusions

We evaluated the effect of short-term aeration (for ca. 2–2.5 h) on activities of three common hydrolytic enzymes catalyzing the decomposition of C-, N-, and P-containing organic compounds in flooded paddy soil. Our study demonstrated for the first time that measuring the enzyme kinetics in natively low-oxygen systems under anoxic conditions e.g. in a glovebox is an essential methodological requirement to assess enzymatic reaction rates and affinity to substrates of this oxygen-sensitive biological soil feature. Overall, the potential activities (V_{\max}) of phosphomonoesterase, β -glucosidase, and leucine aminopeptidase in a paddy soil were underestimated under oxic conditions by 5–43% as compared to anoxic conditions. In contrast, phenol oxidases were up to 14 times higher and peroxidases 2 times higher after an abrupt aeration. Thus, short-term (a few hours) aeration strongly affected the enzymatically-mediated processes of enzymes produced under shortage of O_2 . We therefore suggest that enzymatic assays for anoxic (e.g. humid tropical soils, rice paddies) and especially more strict anaerobic environments (e.g. wetlands, peatlands, and sediments) should be conducted under controlled, O_2 -free conditions. Moreover, the underestimation of hydrolytic enzyme activities due to an aeration bias in enzyme assays may lead to a strongly skewed mechanistic understanding of SOM transformations in anoxic environments with follow-up complications for process-based modeling.

Acknowledgements

The authors gratefully acknowledge the China Scholarship Council (CSC) for financial support for Chaoqun Wang. The study was supported by the research grant from German Research Foundation (DFG Do 1533/3-1). Michaela Dippold was supported by the Bosch foundation in the framework of the Robert-Bosch Junior Professorship 2017. We also wish to thank a technical staff of the Department of Agricultural Soil Science, Susann Enzmann, for helpful hints in enzyme kinetic measurements.

References

- Alexander, M., 1977. An introduction to soil microbiology. Wiley, New York.
- Allison, S.D., 2006. Soil minerals and humic acids alter enzyme stability: implications for ecosystem processes. *Biogeochemistry* 81, 361–373.
- Bååth, E., 1992. Thymidine incorporation into macromolecules of bacteria extracted from soil by homogenization-centrifugation. *Soil Biol. Biochem.* 24, 1157–1165.
- Bai, R., Xi, D., He, J.Z., Hu, H.W., Fang, Y.T., Zhang, L.M., 2015. Activity, abundance and community structure of anammox bacteria along depth profiles in three different paddy soils. *Soil Biol. Biochem.* 91, 212–221.
- Blagodatskaya, E.V., Blagodatsky, S.A., Anderson, T.H., Kuzyakov, Y., 2009. Contrasting effects of glucose, living roots and maize straw on microbial growth kinetics and substrate availability in soil. *Eur. J. Soil Sci.* 60, 186–197.
- Bodelier, P.L.E., Libochant, J.A., Blom, C.W.P.M., Laanbroek, H.J., 1996. Dynamics of nitrification and denitrification in root-oxygenated sediments and adaptation of ammonia-oxidizing bacteria to low-oxygen or anoxic habitats. *Appl. Environ. Microbiol.* 62(11), 4100–4107.
- Bradley, D.J., Kjellbom, P., Lamb, C.J., 1992. Elicitor- and wound-induced oxidative cross-linking of a proline-rich plant-cell wall protein: a novel, rapid defense response. *Cell* 70, 21–30.
- Cabiscol, E., Tamarit, J., Ros, J., 2000. Oxidative stress in bacteria and protein damage by reactive oxygen species. *Int. Microbiol.* 3, 3–8.
- Compan, I., Touati, D., 1993. Interaction of six global transcription regulatorooted soil in expression of manganese superoxide dismutase in *Escherichia coli* K-12. *J. Bacteriol.* 175, 1687–1696.
- Cosgrove, D.J., 1980. Inositol phosphates—their chemistry, biochemistry and physiology. Amsterdam: Elsevier Scientific.
- De Cesare, F., Garzillo, A.M.V., Buonocore, V., Badalucco, L., 2000. Use of sonication for measuring acid phosphatase activity in soil. *Soil Biol. Biochem.* 32, 825–832.
- Deangelis, K.M., Silver, W.L., Thompson, A.W., Firestone, M.K., 2010. Microbial communities acclimate to recurring changes in soil redox potential status. *Environ. Microbiol.* 12(12), 3137–3149.
- Dellwig, O., Schnetger, B., Brumsack, H.J., Grossart, H.P., Umlauf, L., 2012. Dissolved reactive manganese at pelagic redoxclines (part II): hydrodynamic conditions for accumulation. *J. Mar. Syst.* 90, 31–41.
- Elrod, V.A., Johnson, K.S., Coale, K.H., 1991. Determination of subnanomolar levels

- of iron(II) and total dissolved iron in seawater by flow injection analysis with chemiluminescence detection. *Anal. Chem.* 63(9), 893–898.
- Fenchel, T., Finlay, B., 1994. The evolution of life without oxygen. *Am. Sci.* 82(1), 22–29.
- Fenchel, T., Finlay, B., 2010. Oxygen and the spatial structure of microbial communities. *Biol. Rev.* 83(4), 553–569.
- Finn, G.J., Condon, S., 1975. Regulation of catalase synthesis in *Salmonella typhimurium*. *J. Bacteriol.* 123, 570–579.
- Freeman, C., Ostle, N., Kang, H., 2001. An enzymatic “latch” on a global carbon store. *Nature* 409, 149.
- Grant, J.J., Loake, G.J., 2000. Role of reactive oxygen intermediates and cognate redox signaling in disease resistance. *Plant Physiol.* 124, 21–29.
- Hall, S.J., Silver, W.L., 2013. Iron oxidation stimulates organic matter decomposition in humid tropical forest soils. *Glob. Chang. Biol.* 19, 2804–2813.
- Hall, S.J., Treffkorn, J., Silver, W.L., 2014. Breaking the enzymatic latch: impacts of reducing conditions on hydrolytic enzyme activity in tropical forest soils. *Ecology* 95(10), 2964–2973.
- Hanson, H., Frohne, M., 1976. Crystalline leucine aminopeptidase from lens (α -aminoacyl-peptide hydrolase; EC 3.4.11.1). *Methods Enzymol.* 45, 504–521.
- Hochachka, P.W., Somero, G.N., 2002. *Biochemical Adaptation*. New York, NY: Oxford University Press.
- Huang, W., Wu, J., Pan, X.H., Tan, X.M., Zeng, Y.H., 2021. Effects of long-term straw return on soil organic carbon fractions and enzyme activities in a double-cropped rice paddy in south china. *J. Integr. Agr.* 20(1), 236–247.
- Jensen, K., 1993. Microscale distribution of nitrification activity in sediment determined with a shielded microsensor for nitrate. *Appl. Environ. Microbiol.* 59(10), 3287–96.
- Kalia, V.C., Raju, S.C., Purohit, H.J., 2011. Genomic analysis reveals verooted soilatile organisms for quorum quenching enzymes: acyl-homoserine lactone-acylase and -lactonase. *Open Microbiol. J.* 5, 1–13.
- Keiluweit, M., Wanzek, T., Kleber, M., Nico, P., Fendorf, S., 2017. Anaerobic microsites have an unaccounted role in soil carbon stabilization. *Nat. Commun.* 8(1), 1771.
- Khosrozadeh, S., Dorodnikov, M., Reitz, T., Blagodatskaya, E., 2022. An improved Amplex Red-based fluorometric assay of phenol oxidases and peroxidases activity: A case study on Haplic Chernozem. *Eur. J. Soil Sci.*
- Kunito, T., Hiruta, N., Miyagishi, Y., Sumi, H., Moro, H., 2018. Changes in

- phosphorus fractions caused by increased microbial activity in forest soil in a short-term incubation study. *Chem. Speciat. Bioavailab.* 30, 9–13.
- Ladd, J.N., 1978. Origin and range of enzymes in soil. In: Burns, R.G. (Ed.), *Soil Enzymes*. Academic Press, London, pp. 51–96.
- Larsen, M., Santner, J., Oburger, E., Wenzel, W.W., Glud, R.N., 2015. O₂ dynamics in the rhizosphere of young rice plants (*Oryza sativa* L.) as studied by planar optodes. *Plant Soil* 390 279–292.
- Li, T., Gao, J., Bai, L., Wang, Y., Zeng, X., 2019a. Influence of green manure and rice straw management on soil organic carbon, enzyme activities, and rice yield in red paddy soil. *Soil Till. Res.* 195, 104428.
- Li, X., Mou, S., Chen, Y., Liu, T., Dong, J., Li, F., 2019b. Microaerobic Fe(II) oxidation coupled to carbon assimilation processes driven by microbes from paddy soil. *Sci. China Earth Sci.* 62, 1719–1729.
- Li, X.M., Zhang, W., Liu, T.X., Chen, L.X., Chen, P.C., Li, F.B., 2016. Changes in the composition and diversity of microbial communities during anaerobic nitrate reduction and Fe(II) oxidation at circumneutral pH in paddy soil. *Soil Biol. Biochem.* 94, 70–79.
- Lüdemann, H., Arth, I., Liesack, W., 2000. Spatial changes in the bacterial community structure along a vertical oxygen gradient in flooded paddy soil cores. *Appl. Environ. Microbiol.* 66, 754–762.
- Marx, M., Wood, M., Jarvis, S., 2001. A microplate fluorimetric assay for the study of enzyme diversity in soils. *Soil Biol. Biochem.* 33, 1633–1640.
- Parvin, S., Blagodatskaya, E., Becker, J.N., Kuzyakov, Y., Uddin, S., Dorodnikov, M., 2018. Depth rather than microrelief controls microbial biomass and kinetics of C-, N-, P- and S-cycle enzymes in peatland. *Geoderma* 324, 67–76.
- Peacock, M., Jones, T.G., Airey, B., Johncock, A., Evans, C.D., Lebron, I., Fenner, N., Freeman, C., 2015. The effect of peatland drainage and rewetting (ditch blocking) on extracellular enzyme activities and water chemistry. *Soil Use Manag.* 31(1), 67–76.
- Pett-Ridge, J., Silver, W.L., Firestone, M.K., 2006. Redox fluctuations frame microbial community impacts on N-cycling rates in a humid tropical forest soil. *Biogeochemistry* 81(1), 95–110.
- Schimel, J., Balsler, T.C., Wallenstein, M., 2007. Microbial stress-response physiology and its implications for ecosystem function. *Ecology* 88, 1386–1394.
- Schimel, J.P., Weintraub, M.N., 2003. The implications of exoenzyme activity on microbial carbon and nitrogen limitation in soil: a theoretical model. *Soil Biol. Biochem.* 35, 549–563.

- Sinsabaugh, R.L., 2010. Phenol oxidase, peroxidase and organic matter dynamics of soil. *Soil Biol. Biochem.* 42, 391–404.
- Tan, C.H., Koh, K.S., Xie, C., Tay, M., Zhou, Y., Williams, R., Ng, W.J., Rice, S.A., Kjelleberg, S., 2014. The role of quorum sensing signalling in EPS production and the assembly of a sludge community into aerobic granules. *ISME J.* 8(6), 1186–1197.
- Tikariha, H., Khardenavis, A., Purohit, H.J., 2018. Dissolved oxygen-mediated enrichment of quorum-sensing phenomenon in the bacterial community to combat oxidative stress. *Arch. Microbiol.* 200, 1371–1379.
- Waldrop, M.P., Zak, D.R., Sinsabaugh, R.L., Gallo, M., Lauber, C., 2004. Nitrogen deposition modifies soil carbon storage through changes in microbial enzymatic activity. *Ecol. Appl.* 14, 1172–1177.
- Wang, C.Q., Dippold, M.A., Blagodatskaya, E., Dorodnikov, M., 2022. Oxygen matters: Short- and medium-term effects of aeration on hydrolytic enzymes in a paddy soil. *Geoderma* 407, 115548.
- Wang, C.Q., Xue, L., Dong, Y.H., Jiao, R.Z., 2021. Effects of stand density on soil microbial community composition and enzyme activities in subtropical *Cunninghamia lanceolata* (Lamb.) Hook plantations. *For. Ecol. Manag.* 479, 118559.
- Wang, Y., Wang, H., He, J.S., Feng, X., 2017. Iron-mediated soil carbon response to water-table decline in an alpine wetland. *Nat. Commun.* 8, 15972.
- Wei, X., Razavi, B.S., Hu, Y., Xu, X., Zhu, Z., & Liu, Y., Kuzyakov, Y., Li, Y., Wu, J.S., Ge, T.D., 2019. C/P stoichiometry of dying rice root defines the spatial distribution and dynamics of enzyme activities in root-detritusphere. *Biol. Fert. Soils* 55, 251–263.
- Wen, Y., Zang, H.D., Ma, Q.X., Evans, C.D., Chadwick, D.R., Jones, D.J., 2019. Is the ‘enzyme latch’ or ‘iron gate’ the key to protecting soil organic carbon in peatlands? *Geoderma* 349, 107–113.
- Yadav, T.C., Khardenavis, A.A., Kapley, A., 2014. Shifts in microbial community in response to dissolved oxygen levels in activated sludge. *Bioresour. Technol.* 165, 257–264.
- Zhou, M., Diwu, Z., Panchuk-Voloshina, N., Haugland, R.P., 1997. A stable nonfluorescent derivative of resorufin for the fluorometric determination of trace hydrogen peroxide: Applications in detecting the activity of phagocyte NADPH oxidase and other oxidases. *Anal. Biochem.* 253, 162–168.
- Zhu, Z., Ge, T., Luo, Y., Liu, S., Xu, X., Tong, C., Shibistova, O., Guggenberger, G., Wu, J., 2018. Microbial stoichiometric flexibility regulates rice straw mineralization and its priming effect in paddy soil. *Soil Biol. Biochem.* 121, 67–76.

Supplementary

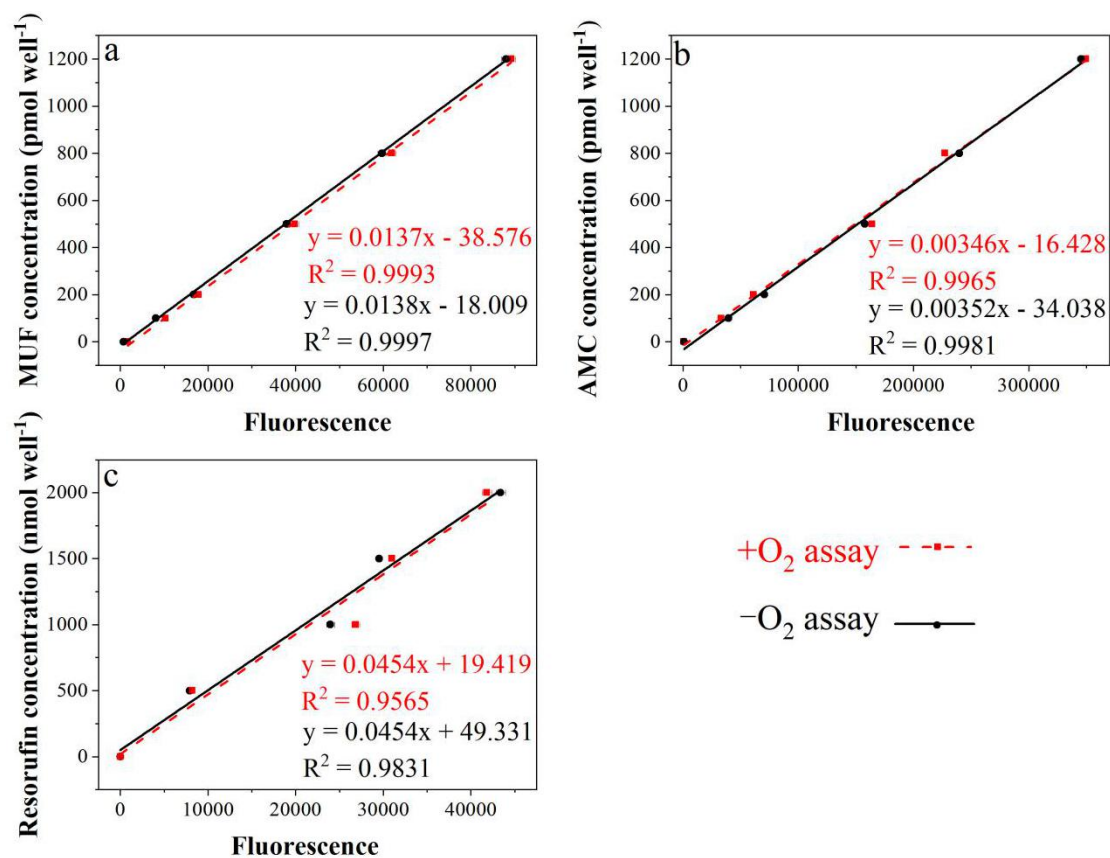


Fig. S1 Calibrations of phosphomonoesterase and β -glucosidase activities by 4-methylumbelliferone (MUF, a), leucine aminopeptidase activities by 7-amino-4-methylcoumarin (AMC, b), and phenol oxidase and peroxidase activities by resorufin (c) fluorogenic dyes under anoxic ($-O_2$) and oxic ($+O_2$) conditions. The data are means \pm standard deviations ($n = 6$).

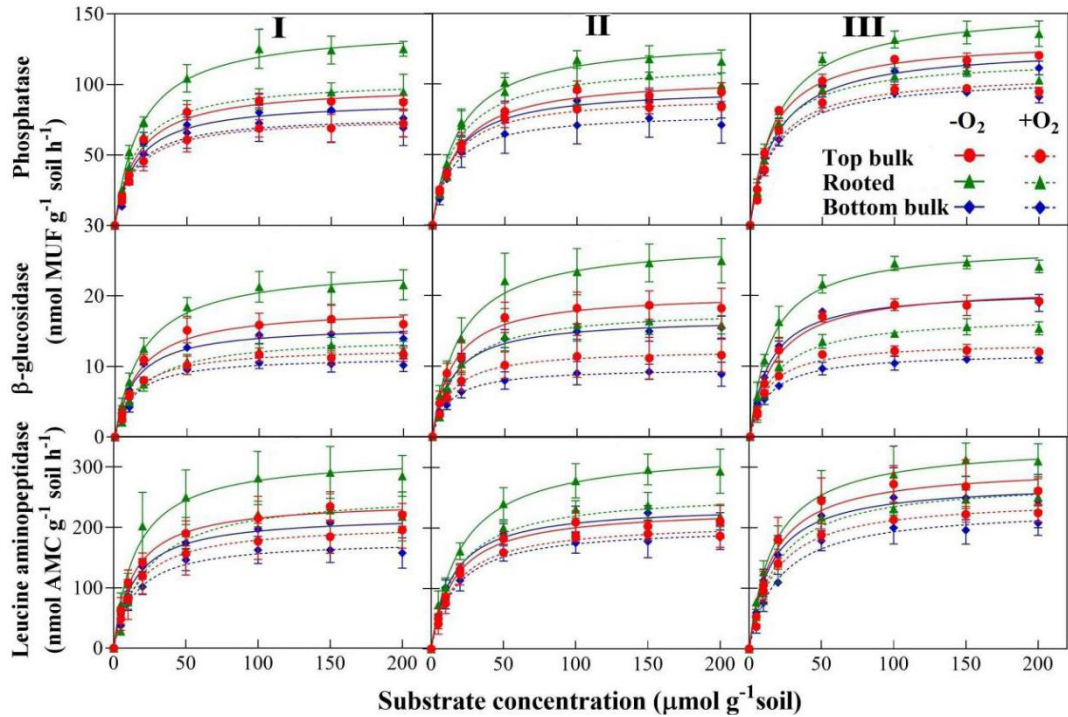


Fig. S2 The kinetics of phosphomonoesterase, β -glucosidase, and leucine aminopeptidase activities at the top bulk, rooted, and bottom bulk soil compartments of a rhizobox in oxic (+O₂) and anoxic (-O₂) assays from the research task 1: moderate O₂ limitation. The data are means \pm standard deviations ($n = 3$). I, II, and III represent seedling, early-, and late tillering stages of rice growth, respectively.

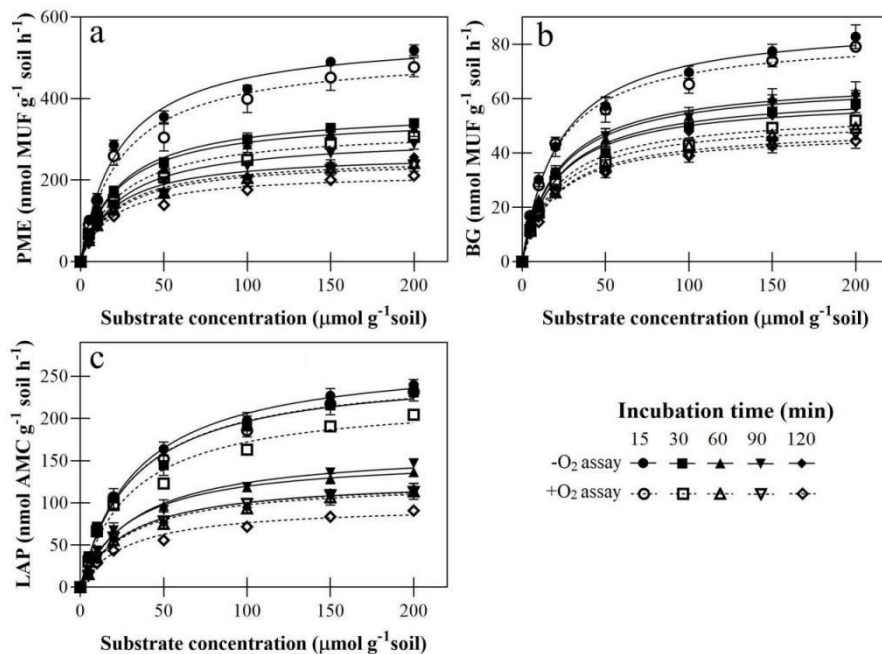


Fig. S3 The kinetics of phosphomonoesterase (PME, a), β -glucosidase (BG, b), and leucine aminopeptidase (LAP, c) activities in oxic (+O₂) and anoxic (-O₂) assays from the research task 2: strong O₂ limitation. The data are means \pm standard deviations ($n = 4$).

Study 2 Oxygen matters: Short- and medium-term effects of aeration on hydrolytic enzymes in a paddy soil

Chaoqun Wang^{a,*}, Michaela A. Dippold^{a,b}, Evgenia Blagodatskaya^{c,d}, Maxim Dorodnikov^{a,e}

^a Biogeochemistry of Agroecosystems, University of Goettingen, 37077 Goettingen, Germany

^b Geo-Biosphere Interactions, University of Tuebingen, 72076 Tuebingen, Germany

^c Department of Soil Ecology, Helmholtz Centre for Environmental Research, 06120 Halle/Saale, Germany

^d RUDN University, 6 Miklukho-Maklaya St, 117198 Moscow, Russia

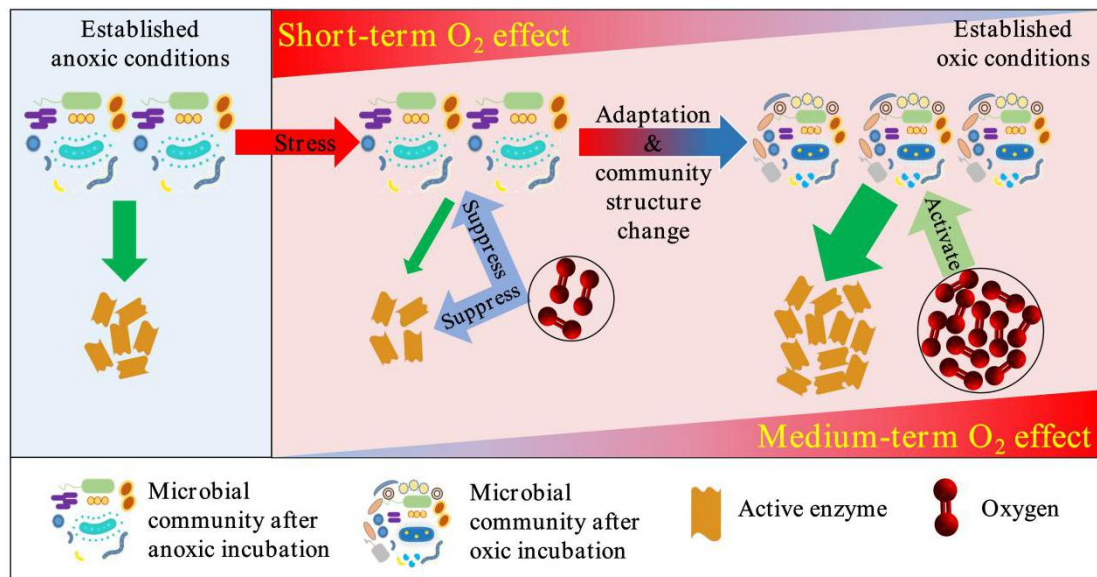
^e Department of Soil Science of Temperate Ecosystems, University of Goettingen, 37077 Goettingen, Germany

* **Correspondence:** chaoqun.wang@forst.uni-goettingen.de

Status: Published in Geoderma

Wang, C.Q., Dippold, M.A., Blagodatskaya, E., Dorodnikov, M., 2022. Oxygen matters: Short-and medium-term effects of aeration on hydrolytic enzymes in a paddy soil. *Geoderma* 407, 115548.

Graphical abstract



Mechanisms of hydrolytic enzymes suppression by short-term aeration due to (1) toxicity of reactive oxygen species (ROS) to microbial cells, (2) decreasing efficiency of phenol oxidase because of Fe (II) oxidation and accumulation of phenolics (“iron-gate”), and activation by medium-term aeration due to cancelling of suppressive factors. Arrow size: relative intensity of active enzyme production, reaction rates, or substrate turnover rate. Triangles with color gradients: the intensity of O₂ effects on enzyme activities from low (blueish) to high (reddish).

Abstract: Rapid exposure of anoxic microbial communities to oxygen (O₂) can have unpredictable effects, including strong suppression of their enzymatic activity. Nonetheless, most medium- and long-term incubation studies on soil organic matter transformations fail to consider aeration effects during sample post-processing and/or assays. Moreover, it remains unclear whether anoxic enzymatic systems are adapted to quick switch to oxic conditions. We evaluated the effects of short-term (2-h oxic (+O₂) vs. anoxic (-O₂) assays) and medium-term aeration (after 10-day oxic vs. anoxic pre-incubation) on the kinetic parameters (V_{\max} , K_m) of phosphomonoesterase, β -glucosidase, and leucine aminopeptidase in top bulk, rooted, and bottom bulk paddy soil of flooded rice microcosms. We hypothesized contrasting short- and medium-term responses of hydrolytic enzyme activities to aeration (i) a negative short-term effect caused by reactive O₂ species toxicity and/or other mechanisms, and (ii) adaptation of anoxic microbial communities to medium-term aeration reducing the impact of ongoing O₂ exposure.

Overall, 2-h aeration suppressed V_{\max} values by 7-43% and catalytic efficiency K_a (V_{\max}/K_m) by 3-22%, and extended the substrate turnover time T_t (7-33%) of three tested enzymes in all soil compartments pre-incubated without O₂. In contrast, no short-term suppressive effect of O₂ was observed on three tested enzymes after oxic pre-incubation. Medium-term aeration increased V_{\max} (by 12-253%) and K_a (by 3-78%) of the enzymes and shortened T_t (4-42%) as compared to the anoxic counterpart. These findings support our hypothesis about anoxic microbial community adaptation over the medium-term aeration. Accordingly, the sensitivity of anoxic hydrolytic enzymes to a short-term O₂ exposure and the O₂ adaptation mechanisms require strong consideration (i) for enzyme assays of anoxic soils and (ii) for understanding the soil organic matter dynamics in environments with O₂ fluctuations.

Keywords: anaerobes; aerobes; microbial community shift; enzyme system; suppression by oxygen; adaptation to oxygen

1. Introduction

Soil enzymes, excreted mainly by microorganisms and plant roots, are central to the cycling of nutrients. Among different types of enzymes, the hydrolytic group plays the most important role in mineralizing the organic matter (Burns et al., 2013). For example, the transformation of organic phosphorus to bioavailable forms in soil is driven by phosphatases secreted by plant roots and microorganisms (Cosgrove, 1980; Spohn and Kuzyakov, 2013; Kunito et al., 2018). β -glucosidase produced by microorganisms catalyzes the last step of carbohydrate degradation and thus provides crucial carbon sources for microbial life (Alexander, 1977; Kumar et al., 2018). Leucine aminopeptidase controls the degradation of amide-linked polypeptides, the primary form of organic nitrogen (Hanson and Frohne, 1976; Finzi et al., 2015). A solid understanding how biotic and abiotic factors affect enzyme activities is essential to predict biogeochemical processes contributing to soil nutrient cycling. The effects of biotic factors such as plant species (Caravaca et al., 2005) and microbial communities (Wang et al., 2021a, 2021b) – as well as of numerous abiotic factors such as soil moisture (Sanauallah et al., 2011), pH (Sinsabaugh, 2010), nutrient contents (Keuskamp et al., 2015), or element stoichiometry (Hartman et al., 2017; Zhou et al., 2017) – on potential enzyme activities have been well documented. Although the availability of oxygen (O_2) has been proposed as a potential limitation in the enzyme-regulated decomposition process (Kleber, 2010; Davidson et al., 2012), only a few studies have systematically quantified and proposed explanations of such O_2 effects on hydrolytic enzyme activities. For example, according to the “enzymatic latch” mechanism, decomposition of organic matter in peatlands is controlled by activation or inactivation of phenol oxidase depending on O_2 availability (Freeman et al., 2001). In turn, the accumulation of phenol may inhibit the activities of hydrolytic enzymes (Wang et al., 2017). A linkage between inactivation of phenol oxidase and Fe(II) oxidation in Fe-rich ecosystems with aeration is described in the “iron gate” concept (Wang et al., 2017; Wen et al., 2019). According to the latter, both decrease of Fe(II) and accumulation of phenol control carbon sequestration in ecosystems with fluctuating redox conditions but also affect N cycling (Matus et al., 2019). In addition to indirect effects of dissolved oxygen on hydrolytic enzymes in anoxic soil systems, the reactive oxygen species (ROS) can be produced as a result of molecular O_2 reduction. The ROS, such as superoxide anions, hydroxyl radicals, and peroxide may directly suppress microorganisms and enzymatic activities during the transition from anoxic to oxic conditions (Fenchel and Finlay, 2010). We therefore lack experimental data to predict the effects of the dramatic increase in O_2 concentration on hydrolytic enzyme activities in anoxic systems.

Changes in soil redox status can trigger the activation or inactivation of microbial populations (Deangelis et al., 2010; Pett-Ridge et al., 2006), which can in turn change soil enzyme systems. For putative anaerobic microorganisms, aeration kills cells in anoxic soils because O_2 is highly toxic for them (Moat and Foster, 1988; Fenchel and Finlay, 1995). For example, *Thiovulum majus* and *Candidatus Thioturbo*

danicus rapidly died under an atmospheric O₂ saturation (Fenchel and Finlay, 2010). Such toxicity is mainly due to the formation of ROS, which is produced by the incomplete reduction of the O₂ molecule, inside or outside cells (Fenchel and Finlay, 2010). In contrast, aerobic and facultative anaerobic microorganisms possess a set of mechanisms enabling them to protect their cells from detrimental O₂. Superoxide dismutase, catalase, and other compounds secreted by aerobic microorganisms counteract the O₂ toxicity. Thus, the tolerance of some microaerophilic bacteria to O₂ increased when superoxide dismutase and catalase were added to the growth medium (Krieg & Hoffman, 1986). Despite redox fluctuations are detrimental to strictly aerobic or anaerobic heterotrophs, they may promote facultative anaerobes with lower growth potential (Yang et al., 2021).

Enzymes can also be directly or indirectly affected when microorganisms respond to oxidative stress. There is contrasting evidence on the effects of aeration on enzymatic reactions in various ecosystems. The aminopeptidase activity in intertidal sediments (McKew et al., 2013), the protease activity in sludge (Jang et al., 2014; Ayol et al., 2008), and the activities of phosphatases and glucosidases in food waste (Henry et al., 2018) were lower in anoxic than oxic microcosms. In contrast, the activity of hydrolytic enzymes was higher without O₂ in humid tropical forest soils (Hall et al., 2014). Despite such inconsistency, enzymatic activity assays of soils from continuous or temporal anoxic systems such as paddy soils (Wei et al., 2019b), peatlands (Parvin et al., 2018), wetlands (Xu et al., 2020), and marine sediments (Cao et al., 2011) are usually performed under oxic conditions. Accordingly, the contrasting results reported in the literature may well reflect this anoxic-oxic shift shortly before or during the enzyme assay. This clearly calls for research to systematically evaluate the influence of O₂ on enzyme activities. This will help to decrease the uncertainty in the results or even reconsider previous findings with regard to methodological artefacts arising from changing O₂ levels during enzyme assays.

We, therefore, hypothesize that, in contrast to a negative short-term effect on the hydrolytic enzyme activities caused by reactive O₂ species toxicity and/or other mechanisms, such as inhibition of hydrolytic enzymes by accumulating phenolics, medium-term aeration will cause anoxic microbial communities to adapt reducing the impact of O₂ exposure during enzyme assays with absence or presence of O₂. To test this hypothesis, we measured the maximal reaction rate (V_{\max}) and Michaelis-Menten constant (K_m) of three common hydrolytic enzymes – phosphomonoesterase (PME), β -glucosidase (BG), and leucine aminopeptidase (LAP) – using fluorogenically labeled substrates (Marx et al., 2001). We compared enzyme assays conducted during 2 hours under oxic and anoxic conditions in soil samples along an aeration gradient (from high to low O₂ exposure: top bulk, rooted, and bottom bulk) of flooded paddy microcosms with growing rice. Rice plants can deliver O₂ to roots via aerenchyma, so the larger root system the stronger the O₂ allocation belowground. Samples collected at three periods of rice growth were pre-incubated for 10 days under oxic and anoxic conditions before their characterization by the enzyme assays to answer the following

questions:

- (1) Which of the enzyme kinetic parameters are most sensitive to stress and adaptation of microorganisms to aeration?
- (2) Do V_{\max} and K_m change independently of each other in response to aeration?
- (3) Will the natural soil aeration gradient between compartments (from top bulk through rooted down to bottom bulk soil) and with the rice plant growth stage (from seedling to late tillering stages) affect the enzyme kinetic parameters?

2. Materials and methods

2.1. Soil description and experimental setup

The topsoil (0-20 cm) was collected from a paddy rice field located at the Changsha Agricultural and Environmental Monitoring Station, Hunan Province, China (113°19'52" E, 28°33'04" N). The soil has a pH of 6.2 and contains 13.1 g·kg⁻¹ soil organic C, 1.4 g·kg⁻¹ total N, 18.0 mg·kg⁻¹ available N, 0.3 g·kg⁻¹ total P, and 3.7 mg·kg⁻¹ Olsen-P (Zhu et al., 2018). The soil was sampled after the second rice harvest (November-December 2017), sieved < 2 mm, homogenized, and air-dried prior to transportation to Germany.

Three rice microcosms were established in PVC rhizoboxes for each of the three enzymes (9 in total) to increase the statistical power of the observations related to medium- and short-term aeration effects on enzyme activities. Rhizoboxes with inner dimensions of 20.5 × 24.0 × 1.5 cm were made water-tight using rubber sealing and screw-holders closed with a transparent, removable plexiglas front cover (Fig. S1A). One 20-day-old rice seedling (*Oryza sativa* L. 'Two-line hybrid rice Zhongzao 39') was transplanted into the center of a rhizobox prefilled with 1.0 kg water-saturated soil. After transplanting, deionized water was added to rhizoboxes to maintain a 2-3 cm water layer above the soil surface during whole period of rice growth except for the sampling dates (see section 2.2 below). All seedlings were grown in a climate chamber (KBF-S 720, Binder GmbH, Tuttlingen, Germany) with 28 ± 1 day/24 ± 1 °C night temperatures, 70% relative humidity, and 12-h photoperiod (08:00 to 20:00). After transplanting, 30 mg N as urea, 25 mg K, and 20 mg P as KH₂PO₄ per kg dry soil were added to each rhizobox.

2.2. Soil sampling and pre-incubation

Soil sampling was performed at the seedling (with 2±1 tillers), early- (4±1), and late (6±1) tillering stages of rice plants 10, 16-20, and 28-31 days after rice transplantation. To prevent soil loss during opening, the rhizoboxes were preconditioned by draining floodwater two days before each sampling date. The drainage did not change soil redox potential (E_h values) at a 5-cm depth within 2 days (preliminary experiment, data not shown). To maintain anoxic conditions in the moist soil, all the rhizoboxes were opened inside a portable PVC glovebox (Captair® Pyramid Glovebox 3015-00, Erlab DFS, Saint-Maurice, France) (Fig. S1B) evacuated

with a vacuum pump (Ilmvac MP 301 Vp, Ilmvac GmbH, Ilmenau, Germany) and then back-flushed with nitrogen to levels of O₂ lower than 0.2% as indicated by an O₂-sensor (Greisinger GOX 100, GHM Messtechnik GmbH, Remscheid, Germany) (Fig. S1C).

Three compartments, top bulk (2-5 cm), rooted (5-15 cm), and bottom bulk (15-18 cm), were sampled after opening a rhizobox (Fig. S1D). For each compartment, the soil collected in three random locations was pooled into one approximately 0.5 g sample. In total, four samples were collected per compartment of a rhizobox at each rice growth stage: two for oxic and two for anoxic pre-incubation. The paired samples in each pre-incubation were used for -O₂ and +O₂ assays, respectively (Fig. 1). Every enzyme activity assay was conducted on one corresponding soil sample. Below, for simplicity, we explain the treatments for soil samples taken from a compartment for an individual enzyme and rice growth stage, whereas in total there were 324 samples (3 compartments x 3 enzymes x 3 stages x 3 replicates x 2 pre-incubation conditions x 2 assay conditions) assayed in the experiment (Fig. 1). The collected soil was placed into four 100-mL Kimble KIMAX borosilicate laboratory glass bottles (GL 45, Kimble Chase Life Science and Research Products, LLC., Meiningen, Germany). "Anoxic" bottles were sealed with thick air-impermeable butyl rubber septa, while the "oxic" bottles were closed with plastic screw caps. Then, the "anoxic" samples were flushed for 20 min with N₂ and the "oxic" samples were aerated and left loosely closed to ensure gas exchange but prevent drying. Both treatments were pre-incubated in the dark for 10 days at 22 °C in an incubator chamber (FKS 3600 Index 20B/001, Liebherr, Germany). After pre-incubation, one anoxic and one oxic bottle were filled with N₂-bubbled deionized sterile water in a ratio of 100 v/v to the soil sample and closed with thick air-impermeable butyl rubber septa in the glovebox. Another anoxic and oxic bottle were filled with deionized sterile water (with dissolved O₂) and closed with plastic screw caps. Thereafter, the bottles for -O₂ assay (one from anoxic pre-incubation and the other from oxic pre-incubation) were additionally flushed with N₂ for 30 minutes. No specific manipulations were conducted for the bottles of the +O₂ assay. Soil was slaked in bottles and the slurry was prepared during 30 min shaking on a rotator (200 rpm) before enzyme activity assays.

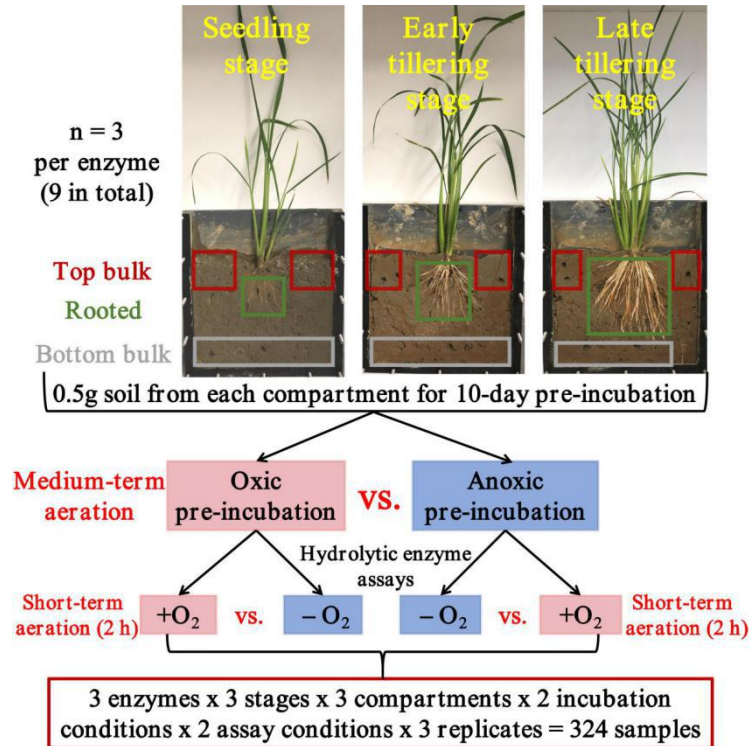


Fig. 1 Diagram of the experimental design to test the effects of medium-term (10-day pre-incubation) and short-term (2-h assay) aeration (red boxes) vs. anoxic controls (blue boxes) on activities of three hydrolytic enzymes (phosphomonoesterase, β -glucosidase, and leucine aminopeptidase) in soils from three rhizobox compartments (top bulk, rooted, and bottom bulk) collected at three rice growth stages (seedling stage, 10 days after rice transplantation; early tillering stage, 16-20 days; late tillering stage, 28-31 days). Photos of rice are examples of growth stages (there were 9 rhizoboxes with plants for each of the three enzymes tested).

2.3. Enzyme assays

The activities of PME, BG, and LAP were determined using fluorogenically labeled substrates (Sigma-Aldrich Co. Ltd): 4-methylumbelliferyl-phosphate, 4-methylumbelliferyl- β -D-glucoside, and L-Leucine-7-amino-4-methylcomarin hydrochloride, respectively (Marx et al., 2001; German et al., 2011). The Michaelis-Menten approach with substrate concentrations ranging from 0, 5, 10, 20, 50, 100, 150, to 200 $\mu\text{mol}\cdot\text{L}^{-1}$ was applied to determine enzyme kinetic parameters. Substrates and buffer (see below) were prepared in duplicate; one part was flushed with N₂ for 20 minutes and then used for enzyme assays under anoxic conditions in the glovebox, and the other part without any pretreatment was used for enzyme assays under oxic conditions. For both assay treatments, 50 μl soil suspension, 50 μl MES or TRIZMA buffer, and 100 μl 4-methylumbelliferone (MUF) or 7-amino-4-methylcomarin (AMC)-based substrate were added into a 96-well black microplate (Brand GmbH, Wertheim, Germany). The fluorescence was repeatedly measured at 355 nm and 460 nm (1.0 s) excitation and emission wavelengths, respectively, on a Victor 1420-050 Multi label counter (PerkinElmer, USA) after 30

and 60 min of incubation under oxic and anoxic conditions. Two sets of microplates for each sample were prepared at a 30-min interval to maintain anoxic conditions during incubation. After opening the glovebox, all anoxic plates were measured simultaneously within 5 min. The same approach was used for oxic assays.

2.4. Enzyme kinetics

To estimate the rate of enzyme activities measured by fluorescence, the assays were calibrated either using MUF or AMC pure substances at increasing concentrations of 0, 100, 200, 500, 800, and 1200 pmol·well⁻¹. Calibrations were conducted in parallel under oxic and anoxic conditions. Based on the calibration, the rates of three enzyme activities were calculated as nmol MUF or AMC per g soil on a dry weight basis per hour in relation to the substrate added (in $\mu\text{mol g}^{-1}$ dry soil). The Michaelis-Menten equation was used to calculate the kinetic parameters V_{max} and K_m for each enzyme:

$$v = (V_{\text{max}} * S)/(K_m + S) \quad (1)$$

where v is the reaction rate ($\text{nmol g}^{-1} \text{ soil h}^{-1}$), S is the substrate concentration, V_{max} is the maximum reaction rate of enzymatic activity at saturated substrate concentration, and K_m is the substrate concentration at half-maximal rate ($1/2 V_{\text{max}}$). V_{max} and K_m were estimated using non-linear curve fitting in GraphPad Prism 8 (GraphPad Software, Inc., San Diego, USA). The catalytic efficiency (K_a) of enzymes was expressed by the ratio of V_{max} and K_m (Tischer et al., 2015). The turnover time (T_t) was calculated according to the following equation (Tischer et al., 2015):

$$T_t \text{ (days)} = (K_m + S)/V_{\text{max}} \quad (2)$$

where S was equal to $K_m/10$ assuming substrate limitation and the identical degree of enzyme saturation by substrate (Basova et al., 2000).

2.5. Statistical analysis

A three-way ANOVA with repeated measures (rice growth stage, $n = 3$) was used to test the effects of (i) medium-term aeration (MTA, oxic vs. anoxic pre-incubation), (ii) short-term aeration (STA, $+O_2$ vs. $-O_2$ assays), and (iii) soil compartment (SC) on V_{max} , K_m , K_a , and T_t . A one-way ANOVA, followed by the least significant difference (LSD) test, was used to evaluate the significance of differences ($P < 0.05$) between the relative changes ($\Delta\%$) in K_a due to short-term aeration as well as medium-term aeration in top bulk, rooted, and bottom bulk soil compartments. All statistical tests as well as linear regression analysis to determine the relationship between V_{max} and K_m were conducted using SPSS (Version 21, IBM, Armonk, NY, USA).

3. Results

3.1. Enzyme activities and affinity of enzymes to substrates

Calibration of assays by MUF and AMC pure substances under $-O_2$ and $+O_2$

revealed no significant differences between conditions (Fig. S2), indicating no pronounced chemical oxidation (or reduction) during the 2-h assay. The rates of enzymatic reactions determined by oxic and anoxic conditions demonstrated a typical saturation pattern with increasing substrate concentration from 0 to 200 $\mu\text{mol}\cdot\text{g}^{-1}$ soil (Fig. S3), enabling use of the Michaelis-Menten equation to estimate V_{max} and K_{m} values.

The effect of medium-term aeration (oxic vs. anoxic pre-incubation) on enzyme activity (V_{max}) and the affinity of enzymes to substrates (the inverse of K_{m}) was more pronounced than those of short-term aeration (+ O_2 vs. $-\text{O}_2$ assays), and soil compartment (Table 1, Fig. 2). Moreover, the effects of medium-term aeration, short-term aeration, soil compartment, and their interactions on V_{max} were stronger as compared to K_{m} (Table 1). The V_{max} and K_{m} values of PME and BG increased at medium-term aeration, indicating that PME and BG were more sensitive to medium-term aeration than LAP (Fig. 2).

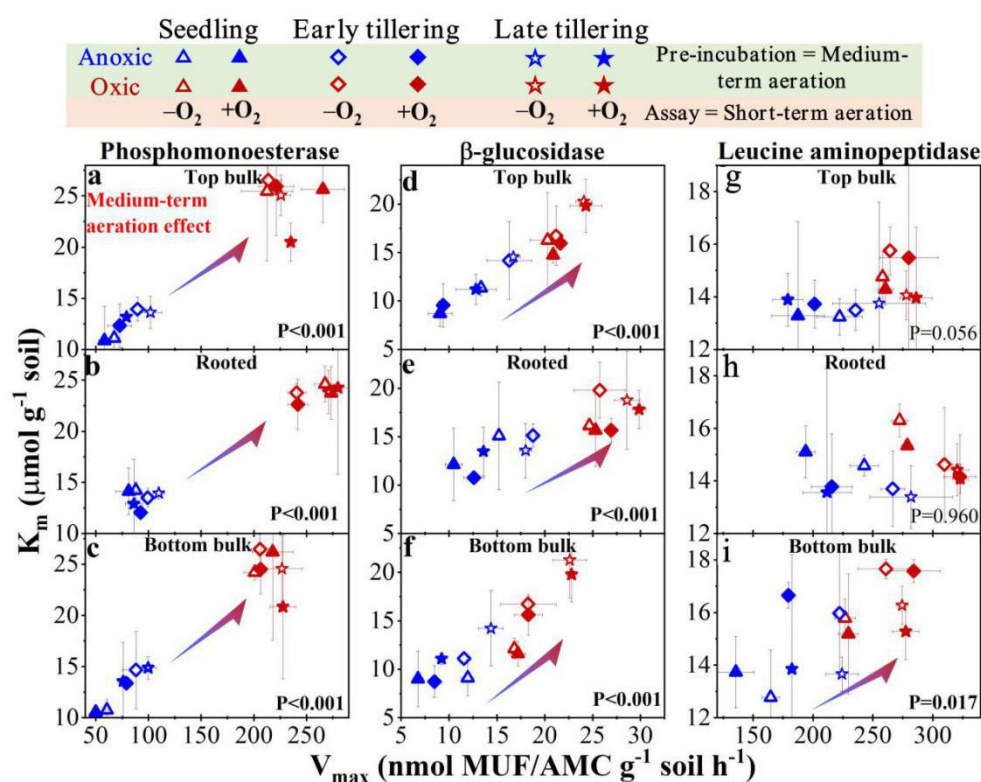


Fig. 2 The maximum reaction rate (V_{max}) and the inverse of the affinity to a substrate (K_{m}) of phosphomonoesterase (a, b, c), β -glucosidase (d, e, f), and leucine aminopeptidase (g, h, i) of samples after anoxic (blue) and oxic (red) pre-incubation at the top bulk-, rooted-, and bottom bulk soil during rice plant growth (seeding (triangle), early- (diamond), and late tillering (stars) stages) in oxic (+ O_2 , filled symbols) and anoxic ($-\text{O}_2$, open symbols) assays. The data are the means \pm standard deviations ($n = 3$). Arrows: the effect of medium-term (10-day) aeration on V_{max} and K_{m} during pre-incubation. Significance of the effect is denoted by P values in bold font. Missing arrows: no effect. Original data are shown in Supplementary tables 1, 2, and 3.

The highest activation by medium-term aeration was observed in bottom bulk soil for all three enzymes (Fig. 2c, f, i) and the largest relative increment of V_{\max} by medium-term aeration was detected for PME (Fig. 2a, b, c). Medium-term aeration substantially decreased the affinity to substrates of the PME and BG in all rhizobox compartments, whereas this decrease in LAP was significant only in bottom bulk. Short-term aeration suppressed V_{\max} of all enzymes after anoxic pre-incubation (Fig. 2, comparison of blue open vs. filled symbols). After oxalic pre-incubation this suppression was insignificant (Fig. 2, red open symbols vs. filled symbols). Rice growth generally stimulated the activities of all enzymes, but decreased the affinity to the substrates (Fig. 2, growth stage increase in the order triangles to diamonds to stars). Rice growth effects were observed after both oxalic- and anoxic pre-incubations.

3.2. Catalytic efficiency of enzymes and turnover time of substrates

Medium-term aeration, soil compartment, and their interactions had significant effects on the catalytic efficiency (K_a values) of the three tested enzymes (Table 1). Effects of short-term aeration on the K_a values were significant only for LAP (Table 1). After anoxic pre-incubation, short-term aeration reduced the K_a values of PME by 3-11%, BG by 9-22%, and LAP by 20%, depending on soil compartment (Fig. 3a, left). In contrast, after oxalic pre-incubation, the K_a values of PME increased by 10-19% in the $+O_2$ assay, BG by 4-15%, and LAP by 6-9% as compared to the $-O_2$ assay (Fig. 3a, right). After medium-term aeration in oxalic pre-incubation, the K_a values of PME, BG, and LAP increased by 29-52% in the $-O_2$ assay and by 73-78% in the $+O_2$ assay (Fig. 3b). The increase was less pronounced for the K_a of BG (3-20% and 26-61%, respectively) and LAP (3-5% and 39-43%). Among the three compartments, K_a values were higher overall in rooted vs. bulk soil for the three tested enzymes (Tables S4, S5, S6). With rice growth, short-term aeration increased the K_a values of PME in the three compartments and LAP in rooted and bottom bulk soil after anoxic pre-incubation (Tables S4, S5, S6). Moreover, medium-term aeration increased the K_a values of LAP in the three compartments, but decreased the K_a values of BG in bulk soil with rice growth (Tables S4, S5, S6).

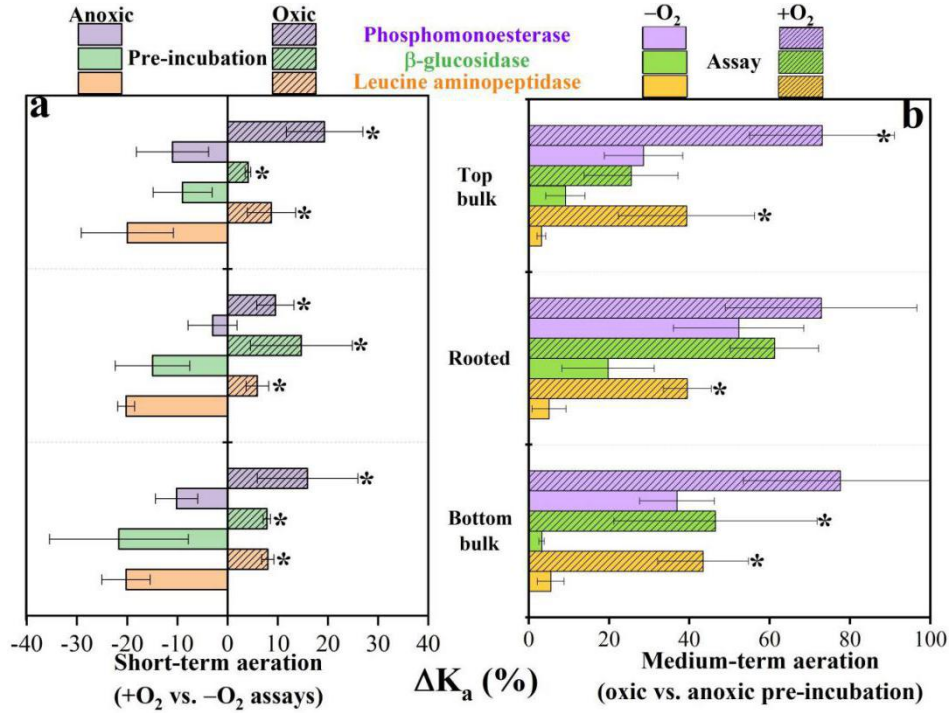


Fig. 3 Relative difference ($\Delta\%$) for catalytic efficiency of enzymes (K_a) due to short-term aeration during assays (2-h) after anoxic pre-incubation (a, left) and oxic pre-incubation O_2 (a, right), and relative difference ($\Delta\%$) for K_a in $-O_2$ (b, unshaded) and $+O_2$ (b, shaded) assays due to medium-term (10-day) oxic and anoxic pre-incubation in top bulk, rooted, and bottom bulk soil compartments. Values are means between seedling, early- and late tillering stages of rice growth. Original data are shown in Supplementary tables 4, 5, and 6. Asterisks: significant differences ($P < 0.05$) between oxic and anoxic pre-incubation as well as between $-O_2$ and $+O_2$ assays.

Medium-term aeration, soil compartment, and their interactions significantly affected the turnover time of corresponding substrates (T_t values) of three tested enzymes (Table 1). However, effects of short-term aeration on the T_t values were significant for LAP only (Table 1). In consequence, short-term aeration extended the T_t values under substrate deficiency ($\sim 10\%$ of K_m) of PME by 7-15%, BG by 10-33%, and LAP by 28-29% after anoxic pre-incubation (Fig. 4, Table S4, S5, S6). In contrast, the T_t values for PME, BG, and LAP shortened by 5-15%, 7-14%, and 6-7% in the $+O_2$ vs. $-O_2$ assay after oxic pre-incubation (Fig. 4, Tables S4, S5, S6). Moreover, medium-term aeration shortened the T_t values for PME (by 22-34% in the $-O_2$ assay, 40-42% in the $+O_2$ assay), BG (4-16% and 20-40%, respectively), and LAP (4-6% and 26-32%) (Fig. 4, Tables S4, S5, S6). Among the three compartments, T_t values were overall lower in rooted vs. bulk soil for the three tested enzymes (Fig. 4, Tables S4, S5, and S6). With rice growth, short-term aeration decreased the T_t values of PME in all three compartments, BG in rooted soil, and LAP in rooted and bottom bulk soil after anoxic pre-incubation (Fig. 4, Table S4, S5, and S6). Finally, medium-term aeration increased the T_t values of BG in bulk soil and LAP in rooted and bottom bulk soil with rice growth (Fig. 4, Tables S4, S5, and S6).

Table 1 Effects of medium-term aeration (MTA), short-term aeration (STA), soil compartment (SC), and their interactions on the maximum reaction rate (V_{\max}), the affinity to a substrate (K_m), the catalytic efficiency (K_a), and the turnover time (T_t) of respective substrates of phosphomonoesterase (PME), β -glucosidase (BG), and leucine aminopeptidase (LAP) analyzed by three-way ANOVA with repeated measures (rice growth stage, $n = 3$).

	Statistic	MTA	STA	SC	MTA \times STA	MTA \times SC	STA \times SC	MTA \times STA \times SC	
PME	V_{\max}	F	6852.098	0.627	112.022	49.609	23.578	1.774	3.441
		P	< 0.001	0.436	< 0.001	< 0.001	< 0.001	0.191	0.049
	K_m	F	348.907	2.682	0.006	0.061	0.896	0.065	0.085
		P	< 0.001	0.115	0.994	0.807	0.421	0.937	0.919
	K_a	F	142.736	2.023	11.517	10.377	1.482	0.003	0.361
		P	< 0.001	0.168	< 0.001	0.004	0.247	0.997	0.701
T_t	F	233.503	1.151	16.967	15.178	0.358	0.166	1.103	
	P	< 0.001	0.294	< 0.001	0.001	0.703	0.848	0.348	
BG	V_{\max}	F	1052.666	48.575	123.507	76.504	10.716	0.070	0.465
		P	< 0.001	< 0.001	< 0.001	< 0.001	< 0.001	0.933	0.634
	K_m	F	67.109	9.780	3.333	1.196	0.856	0.155	0.260
		P	< 0.001	0.005	0.053	0.285	0.437	0.857	0.773
	K_a	F	41.205	0.648	10.865	12.209	3.248	0.403	0.709
		P	< 0.001	0.429	< 0.001	0.002	0.056	0.673	0.502
T_t	F	31.736	1.180	5.699	11.431	1.410	0.600	0.671	
	P	< 0.001	0.191	0.009	0.002	0.264	0.557	0.520	
LAP	V_{\max}	F	298.376	25.439	51.767	52.495	1.566	0.623	0.383
		P	< 0.001	< 0.001	< 0.001	< 0.001	0.230	0.545	0.686
	K_m	F	7.753	0.024	2.652	0.786	0.461	0.014	0.058
		P	0.010	0.879	0.091	0.384	0.636	0.986	0.944
	K_a	F	39.826	4.983	29.665	24.400	0.227	0.097	0.122
		P	< 0.001	0.035	< 0.001	< 0.001	0.799	0.908	0.886
T_t	F	50.650	13.363	30.572	32.135	1.275	0.121	0.359	
	P	< 0.001	0.001	< 0.001	< 0.001	0.298	0.887	0.702	

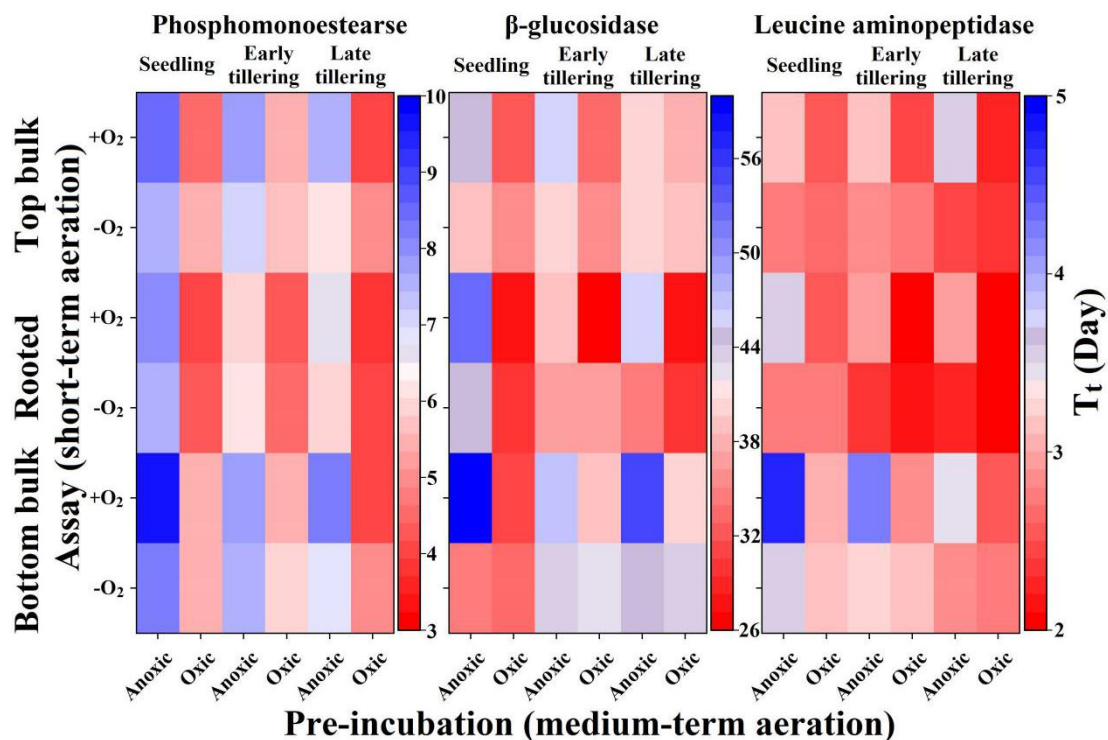


Fig. 4 The turnover time (T_t) of respective substrates catalyzed by phosphomonoesterase (left), β -glucosidase (middle), and leucine aminopeptidase (right) after anoxic and oxic pre-incubation of the top bulk-, rooted-, and bottom bulk soil during rice plant growth (seedling, early-, and late tillering stages) in oxic (+O₂) and anoxic (-O₂) assays. The data are the means of three replicates ($n = 3$). Original data are shown in Supplementary tables 4, 5, and 6.

4. Discussion

4.1. Effects of aeration on enzyme kinetic parameters

The activities (V_{max}) of phosphomonoesterase, β -glucosidase, and leucine aminopeptidase demonstrated contrasting responses to short- (during 2-h assays) and medium-term (10-day pre-incubation) O₂ exposure: short-term aeration suppressed all tested enzyme activities after anoxic pre-incubation (Fig. 2, blue empty vs. filled symbols). In contrast, medium-term aeration strongly increased V_{max} of the three studied enzymes irrespective of the oxygen level during the enzyme assay (Fig. 2, red symbols). This therefore supports the hypothesis that short-term aeration suppresses enzyme activities, whereas adaptation of microorganisms to medium-term aeration stimulates the enzyme activities. Interestingly, among the four kinetic parameters, the effects of short- and medium-term aeration were most pronounced for V_{max} vs. the affinity to substrate (K_m), the catalytic efficiency (K_a), and the turnover time of substrates (T_t). This therefore answers our first research question and suggests that most likely the enzyme activity itself is strongly affected by aeration. Thus, beyond temperature (Razavi et al., 2015), we demonstrate that aeration is another important environmental factor that affects V_{max} more strongly than K_m and K_a of hydrolytic

enzymes. We observed significant positive relationships between V_{\max} and K_m values under medium-term aeration for phosphomonoesterase and β -glucosidase in all three soil compartments and leucine aminopeptidase in bottom bulk soil (Fig. 2). This demonstrates a coupling response of the kinetic parameters to O_2 availability and represents a possible adaptation mechanism reducing the sensitivity of enzymatic reactions to oxygen, i.e., so-called cancelling effect (Razavi et al., 2015). Additionally, the medium-term aeration did not significantly change the K_a values of β -glucosidase and leucine aminopeptidase in $-O_2$ assays (Tables S5, S6). Thus, the adaptation of K_m of β -glucosidase and leucine aminopeptidase to alternating irrigation and drainage may be a potential mechanism for regulating the transformation of soil organic matter when anoxic and oxic conditions fluctuate. Accordingly, in response to short-term aeration, the enzyme systems with higher affinity to substrate were selected, whereas in response to medium-term aeration, anoxic enzymes demonstrated higher affinity to substrate than did oxic ones.

The K_m values between the soil compartments revealed no pronounced pattern following the proposed natural soil aeration gradient (Ludemann et al., 2000; Bai et al., 2015) from top bulk soil through rooted and down to bottom bulk soil. Nonetheless, the activities of the three tested enzymes were higher in the rooted zone than in bulk soil, which more likely reflects root exudation than an oxygen effect. Moreover, V_{\max} and K_m values showed an increasing trend with the vegetative stage of the rice plants (Fig. 2, triangles-diamonds-stars). In answer to our third research question, accelerated enzyme activity during the course of growth of above- and belowground plant biomass was a consequence of relatively high substrate availability in rooted vs. bulk soil (Wei et al., 2019b), rather than any adaptation of microorganisms to short- or even medium-term aeration.

4.1. Mechanisms of effects of short-term aeration on enzyme kinetic parameters

Short-term O_2 exposure in the $+O_2$ assay suppressed maximal reaction rates and the catalytic efficiency of studied enzymes compared to the $-O_2$ assay after anoxic pre-incubation, while short-term lack of O_2 played a less significant role for enzyme kinetic parameters after oxic pre-incubation (Figs 2, 3). This means that short-term aeration has a greater impact on enzyme kinetic parameters under anoxic than oxic soil conditions, and anoxically produced enzymes were more sensitive to short-term O_2 availability than oxic enzymes to O_2 deficiency (Fig. 5). Short-term O_2 availability after anoxic pre-incubation could stress enzyme functioning by: (1) decreased efficiency of phenol oxidase because Fe(II) oxidation inhibits the process of catalyzing additional OH radical production (Van Bodegom et al., 2005), thus accumulating phenolics that are toxic to hydrolases (“iron-gate” paradigm) (Wang et al., 2017), (2) production of ROS, such as (O_2^-) ion and hydrogen peroxide (H_2O_2), which both may suppress the activity of microorganisms producing enzymes (Deangelis et al., 2010; Imlay et al., 2008), (3) triggering the compensation mechanism established by microorganisms to allocate more energy and resources to produce oxidative enzymes, e.g., catalase and ferroxidases in response to the accumulation of ROS and thus decreasing the production of hydrolytic enzymes

(Cabisco et al., 2000), (4) non-competitive O₂-binding of the inactive sites of enzymes to unfavorably change their structure for substrate conformation (Bradford, 2013), (5) O₂ reacting with the enzyme-substrate complexes, thereby slowing down or even terminating the catalytic processes (Unno et al., 2007). Therefore, suppression of microbial activity by O₂, isoenzymes production, production of enzymes against reactive oxygen species, and reaction of O₂ with enzyme or enzyme-substrate complexes may together explain the suppression effect of short-term aeration on enzymatic activity (Fig. 5). Therefore, our findings may have implications for other studies where enzyme activities were most probably underestimated for paddy soils (Wei et al., 2019b), wetlands (Wang et al., 2017), and peatlands (Parvin et al., 2018) when measured under oxic conditions. Accordingly, underestimated enzyme activities will give biased input to the models established for anoxic ecosystems (Wei et al., 2019a).

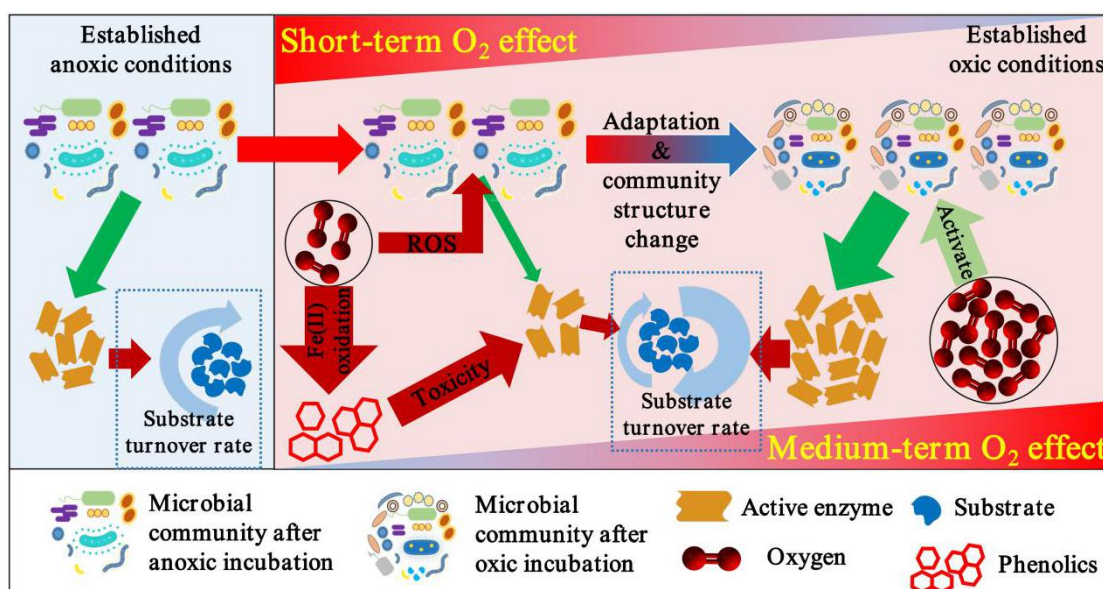


Fig. 5 Mechanisms of hydrolytic enzymes suppression by short-term aeration due to (1) toxicity of reactive oxygen species (ROS) to microbial cells, (2) decreasing efficiency of phenol oxidase because of Fe (II) oxidation and accumulation of phenolics (“iron-gate”), and activation by medium-term aeration due to cancelling of suppressive factors. Arrow size: relative intensity of active enzyme production, reaction rates, or substrate turnover rate. Triangles with color gradients: the intensity of O₂ effects on enzyme activities from low (blueish) to high (reddish).

4.2. Mechanisms of effects of medium-term aeration on enzyme kinetic parameters

The V_{max} and K_a of the three studied enzymes increased 12-253% and 3-78%, respectively, after 10-day oxic vs. anoxic pre-incubation (Figs. 2, 3). This is in line with further findings in paddy soils (Wang and Lu, 2006), peatlands (Fenner and Freeman, 2011), and other anoxic systems (Henry et al., 2018; Martínez-Valdez et al., 2016). However, in contrast to the stimulating effect of aeration, increased cellobiohydrolase, β -glucosidase, β -xylosidase, and N-acetyl β -D-glucosaminidase in

humid tropical forest soils was reported under anaerobic conditions compared to aerobic controls during 6-18 days of incubation (Hall et al., 2014). Such a difference could partly reflect the distinct environmental characteristics of flooded systems (i.e., paddy soils and peatlands vs. humid forest soils). In comparison to the short-term aeration, oxic enzyme systems with higher affinity to substrate were produced after oxic pre-incubation. Therefore, the canceling effect by decreasing the affinity of enzymes to substrates can be considered to be a natural mechanism for reducing the influence of medium-term aeration on the microbial decomposition of soil organic matter under oxic conditions.

The opposite effects of 2-h and 10-day aeration on enzyme kinetic parameters indicated that the microbial community exploited different strategies to acclimatize their anoxic metabolisms and enzymes to oxic conditions (Fig. 5). Two-hour aeration may inactivate or kill obligate anaerobes due to O₂ toxicity, i.e. the effect of stress (Fenchel and Finlay, 1995), an interpretation supported by the about 30% decrease in living bacteria number in sediments after 2-h aeration (Ma et al., 2019). Furthermore, aeration for 12 h was insufficient to trigger aerobic respiration by microorganisms, but 4 days was sufficient (Pett-Ridge and Firestone, 2005). Accordingly, 10-day pre-incubation in our study was long enough for microbial communities to acclimate to oxic conditions and to exploit an aerobic metabolism either by a metabolic switch by facultative anaerobes or by growth of aerobic community members. Significant changes in community structure were detected in paddy soils after 7 days of incubation under oxic vs. anoxic conditions (Ludemann et al., 2000). We therefore assume that 10-day aeration induced the changes in community structure, which was responsible for the overall increase in hydrolytic enzyme activities. This calls for further studies to explore the dynamic changes of microbial communities in anoxic systems as affected by the duration of aeration.

Finally, the effect of medium-term aeration on the enzyme kinetics points to a potential problem: the prolonged storage (for months or years) of soil samples taken from anoxic systems may cause the slow adaptation of the microbial community to oxic conditions and to a biased estimation of enzyme activities and element turnover rates in such samples. Finally, an improved estimation of enzyme activity in anoxic environments is an important step forward in more adequately assessing the organic matter turnover in anoxic systems and in more precisely representing of these ecosystems in modern, process-based models from the local to global scale.

5. Conclusions and outlook

Our study demonstrated for the first time that the potential activity (V_{\max}) and catalytic efficiency (K_a) of phosphomonoesterase, β -glucosidase, and leucine aminopeptidase in a paddy soil were suppressed by 7-43% (V_{\max}) and 3-22% (K_a) by short-term aeration (within 2-h assay), but activated by 12-253% (V_{\max}) and 3-78% (K_a) by medium-term aeration (10-day pre-incubation). In contrast to anoxic pre-incubation, the V_{\max} and K_a values of the three studied enzymes did not

significantly change in the $-O_2$ vs. $+O_2$ assay after oxic pre-incubation. We therefore conclude that the effect of O_2 on enzyme kinetics in anoxic systems depends on the duration of aeration and reflects different mechanisms (suppression of enzymes or microbial activity vs. adaptation of microbial communities and their metabolism). Overall, short-term aeration has a higher impact on enzyme kinetics in anoxic than in oxic systems – an important observation that must be considered during enzyme assays of anoxic soils when quantitatively upscaling and predicting element and substrate turnover, i.e. in biogeochemical models.

Acknowledgements

The authors gratefully acknowledge the China Scholarship Council (CSC) for financial support for Chaoqun Wang. This study was supported by a research grant from the German Research Foundation (DFG Do 1533/3-1). This publication has been supported by the RUDN University Strategic Academic Leadership Program. We also wish to thank a technical staff member of the Department of Soil Science of Temperate Ecosystems, Susann Enzmann, for helpful hints on enzyme kinetic measurements.

References

- Alexander, M., 1977. An introduction to soil microbiology. Wiley, New York.
- Ayol, A., Filibeli, A., Sir, D., Kuzyaka, E., 2008. Aerobic and anaerobic bioprocessing of activated sludge: floc disintegration by enzymes. *Environ. Letters* 43(13), 1528–1535.
- Bai, R., Xi, D., He, J.Z., Hu, H.W., Fang, Y.T., Zhang, L.M., 2015. Activity, abundance and community structure of anammox bacteria along depth profiles in three different paddy soils. *Soil Biol. Biochem.* 91, 212–221.
- Basova, N.E., Rozengart, E.V., Khovanskikh, A.E., 2000. Kinetic analysis of the “substrate protective effect” in cholinesterases of different origin. *J. Evol. Biochem. Physiol.* 36(2), 130–137.
- Bradford, M.A., 2013. Thermal adaptation of decomposer communities in warming soils. *Front. Microbiol.* 4.
- Burns, R.G., DeForest, J.L., Marxsen, J., Sinsabaugh, R.L., Stromberger, M.E., Wallenstein, M.D., Weintraub, M.N., Zoppini, A., 2013. Soil enzymes in a changing environment: Current knowledge and future directions. *Soil Biol. Biochem.* 58, 216–234.
- Cabiscol, E., Tamarit, J., Ros, J., 2000. Oxidative stress in bacteria and protein damage by reactive oxygen species. *Int. Microbiol.* 3, 3–8.
- Deangelis, K.M., Silver, W.L., Thompson, A.W., Firestone, M.K., 2010. Microbial communities acclimate to recurring changes in soil redox potential status. *Environ. Microbiol.* 12(12), 3137–3149.
- Cao, Z., Zhu, Q., Aller, R.C., Aller, J.Y., 2011. A fluorosensor for two-dimensional measurements of extracellular enzyme activity in marine sediments. *Mar. Chem.* 123(1–4), 23–31.
- Caravaca, F., Alguacil, M.M., Torres, P., Roldán, A., 2005. Plant type mediates rhizospheric microbial activities and soil aggregation in a semiarid mediterranean salt marsh. *Geoderma* 124, 375–382.
- Cosgrove, D.J., 1980. Inositol phosphates—their chemistry, biochemistry and physiology. Amsterdam: Elsevier Scientific.
- Davidson, E.A., Samanta, S., Caramori, S.S., Savage, K., 2012. The Dual Arrhenius and Michaelis–Menten kinetics model for decomposition of soil organic matter at hourly to seasonal time scales. *Global Change Biol.* 18, 371–384.
- Deangelis, K.M., Silver, W.L., Thompson, A.W., Firestone, M.K., 2010. Microbial communities acclimate to recurring changes in soil redox potential status. *Environ. Microbiol.* 12(12), 3137–3149.
- Fenchel, T., Finlay, B.J., 1995. Ecology and evolution in anoxic worlds. Oxford

University Press, New York.

- Fenchel, T., Finlay, B., 2010. Oxygen and the spatial structure of microbial communities. *Biol. Rev.* 83(4), 553–569.
- Fenner, N., Freeman, C., 2011. Drought-induced carbon loss in peatlands. *Nat. Geosci.* 4(12), 895–900.
- Finzi, A.C., Abramoff, R.Z., Spiller, K.S., Brzostek, E.R., Darby, B.A., Kramer, M.A., Phillips, R.P., 2015. Rhizosphere processes are quantitatively important components of terrestrial carbon and nutrient cycles. *Glob. Chang. Biol.* 21, 2082–2094.
- Freeman, C., Ostle, N., Kang, H., 2001. An enzymic ‘latch’ on a global carbon store—a shortage of oxygen locks up carbon in peatlands by restraining a single enzyme. *Nature* 409, 149–149.
- German, D.P., Weintraub, M.N., Grandy, A.S., Lauber, C.L., Rinkes, Z.L., Allison, S.D., 2011. Optimization of hydrolytic and oxidative enzyme methods for ecosystem studies. *Soil Biol. Biochem.* 43 (7), 1387–1397.
- Hall, S.J., Treffkorn, J., Silver, W.L., 2014. Breaking the enzymatic latch: impacts of reducing conditions on hydrolytic enzyme activity in tropical forest soils. *Ecology* 95(10), 2964–2973.
- Hanson, H., Frohne, M., 1976. Crystalline leucine aminopeptidase from lens (α -aminoacyl-peptide hydrolase; EC 3.4.11.1). *Methods Enzymol.* 45, 504–521.
- Hartman, W.H., Ye, R., Horwath, W.R., Tringe, S.G., 2017. A genomic perspective on stoichiometric regulation of soil carbon cycling. *ISME J.* 11, 2652.
- Henry, F., Anne, T., Mohamed, S., Sophie, L.R., Patrick, D., 2018. Biochemical and microbial changes reveal how aerobic pre-treatment impacts anaerobic biodegradability of food waste. *Waste Manag.* 80, 119–129.
- Imlay, J.A., 2008. Cellular defenses against superoxide and hydrogen peroxide. *Annu. Rev. Biochem.* 77, 755–776.
- Jang, H.M., Cho, H.U., Park, S.K., Ha, J.H., Park, J.M., 2014. Influence of thermophilic aerobic digestion as a sludge pre-treatment and solids retention time of mesophilic anaerobic digestion on the methane production, sludge digestion and microbial communities in a sequential digestion process. *Water Res.* 48, 1–14.
- Keuskamp, J.A., Feller, I.C., Laanbroek, H.J., Verhoeven, J.T.A., Hefting, M.M., 2015. Short- and long-term effects of nutrient enrichment on microbial exoenzyme activity in mangrove peat. *Soil Biol. Biochem.* 81, 38–47.
- Kleber, M. 2010. What is recalcitrant soil organic matter? *Environm. Chem.* 7, 320–332.

- Krieg, N.R., Hoffman, P.S., 1986. Microaerophily and oxygen toxicity. *Annu. Rev. Microbiol.* 40, 107–130.
- Kumar, A., Shahbaz, M., Blagodatskaya, E., Kuzyakov, Y., Pausch, J., 2018. Maize phenology alters the distribution of enzyme activities in soil: field estimates. *Appl. Soil Ecol.* 125, 233–239.
- Kunito, T., Hiruta, N., Miyagishi, Y., Sumi, H., Moro, H., 2018. Changes in phosphorus fractions caused by increased microbial activity in forest soil in a short-term incubation study. *Chem. Spec. Bioavailab.* 30, 9–13.
- Ludemann, H., Arth, I., Liesack, W., 2000. Spatial changes in the bacterial community structure along a vertical oxygen gradient in flooded paddy soil cores. *Appl. Environ. Microbiol.* 66(2), 754–762.
- Ma, S., Tong, M., Yuan, S., Liu, H., 2019. Responses of microbial community structure in Fe(II)-bearing sediments to oxygenation: the role of reactive oxygen species. *ACS Earth Space Chem.* 3, 738–747.
- Martínez-Valdez, F., Komilis, D., Saucedo-Castañeda, G., Barrera, R., Sanchez, A., 2016. The effect of a short term aerobic pretreatment step on the anaerobic co-digestion of the organic fraction of municipal solid wastes: liquid extract addition versus solid phase addition. *Waste Biomass Valorization* 8, 1793–1801.
- Marx, M., Wood, M., Jarvis, S., 2001. A microplate fluorimetric assay for the study of enzyme diversity in soils. *Soil Biol. Biochem.* 33, 1633–1640.
- Matus, F., Stock, S., Eschenbach, W., Dyckmans, J., Merino, C., Nájera, F., Kuzyakov, Y., Dippold, M.A., 2019. Ferrous wheel hypothesis: abiotic nitrate incorporation into dissolved organic matter. *Geochim. Cosmochim. Acta* 245, 514–524.
- Mckew, B.A., Dumbrell, A.J., Taylor, J.D., Mcgenity, T.J., Underwood, G.J.C., 2013. Differences between aerobic and anaerobic degradation of microphytobenthic biofilm-derived organic matter within intertidal sediments. *FEMS Microbiol. Ecol.* 84(3), 495–509.
- Moat, G.A., Foster, J.W., 1988. *Microbial physiology*, 2nd edn. Wiley, New York.
- Parvin, S., Blagodatskaya, E., Becker, J.N., Kuzyakov, Y., Uddin, S., Dorodnikov, M., 2018. Depth rather than microrelief controls microbial biomass and kinetics of C-, N-, P- and S-cycle enzymes in peatland. *Geoderma* 324, 67–76.
- Pett-Ridge, J., Firestone, M.K., 2005. Redox fluctuation structures microbial communities in a wet tropical soil. *Appl. Environ. Microbiol.* 71, 6998–7007.
- Pett-Ridge, J., Silver, W.L., and Firestone, M.K., 2006. Redox fluctuations frame microbial community impacts on N-cycling rates in a humid tropical forest soil. *Biogeochemistry* 81, 95–110.
- Razavi, B.S., Blagodatskaya, E., Kuzyakov, Y., 2015. Nonlinear temperature

- sensitivity of enzyme kinetics explains canceling effect—a case study on loamy haplic luvisol. *Front. Microbiol.* 6, 1126.
- Sanaullah, M., Blagodatskaya, E., Chabbi, A., Rumpel, C., Kuzyakov, Y., 2011. Drought effects on microbial biomass and enzyme activities in the rhizosphere of grasses depend on plant community composition. *Appl. Soil Ecol.* 48(1), 38–44.
- Sinsabaugh, R.L., 2010. Phenol oxidase, peroxidase and organic matter dynamics of soil. *Soil Biol. Biochem.* 42, 391–404.
- Spohn, M., Kuzyakov, Y., 2013. Distribution of microbial- and root derived phosphatase activities in the rhizosphere depending on P availability and C allocation coupling soil zymography with ¹⁴C imaging. *Soil Biol. Biochem.* 67, 106–113.
- Tischer, A., Blagodatskaya, E., Hamer, U., 2015. Microbial community structure and resource availability drive the catalytic efficiency of soil enzymes under land-use change conditions. *Soil Biol. Biochem.* 89, 226–237.
- Unno, M., Chen, H., Kusama, S., Shaik, S., Ikeda-Saito, M., 2007. Structural characterization of the fleeting ferric peroxo species in myoglobin: experiment and theory. *J. Am. Chem. Soc.* 129(44), 13394–13395.
- Van Bodegom, P.M., Broekman, R., Van Dijk, J., Bakker, C., Aerts, R., 2005. Ferrous iron stimulates phenol oxidase activity and organic matter decomposition in waterlogged wetlands. *Biogeochemistry* 76, 69–83.
- Wang, C.Q., Xue, L., Dong, Y.H., Jiao, R.Z., 2021a. Effects of stand density on soil microbial community composition and enzyme activities in subtropical *Cunninghamia lanceolata* (Lamb.) Hook plantations. *For. Ecol. Manag.* 479, 118559.
- Wang, C., Xue, L., Dong, Y., Jiao, R., 2021b. Soil organic carbon fractions, C-cycling hydrolytic enzymes, and microbial carbon metabolism in Chinese fir plantations. *Sci. Total Environ.* 758, 143695.
- Wang, X.C., Lu, Q., 2006. Effect of waterlogged and aerobic incubation on enzyme activities in paddy soil. *Pedosphere* 16(4), 532–539.
- Wang, Y., Wang, H., He, J.S., Feng, X., 2017. Iron-mediated soil carbon response to water-table decline in an alpine wetland. *Nat. Commun.* 8, 1–9.
- Wei, L., Razavi, B.S., Wang, W., Zhu, Z., Liu, S., Wu, J., Kuzyakov, Y., Ge, T.D., 2019a. Labile carbon matters more than temperature for enzyme activity in paddy soil. *Soil Biol. Biochem.* 135, 134–143.
- Wei, X., Razavi, B.S., Hu, Y., Xu, X., Zhu, Z., & Liu, Y., Kuzyakov, Y., Li, Y., Wu, J.S., Ge, T.D., 2019b. C/P stoichiometry of dying rice root defines the spatial distribution and dynamics of enzyme activities in root-detritusphere. *Biol. Fert. Soils* 55, 251–263.

- Wen, Y., Zang, H.D., Ma, Q.X., Evans, C.D., Chadwick, D.R., Jones, D.L., 2019. Is the 'enzyme latch' or 'iron gate' the key to protecting soil organic carbon in peatlands? *Geoderma*, 349, 107–113.
- Xu, Q.L., Cai, X.J., Fu, L., Hu, Y., 2020. Space distribution of bacterial communities and substrate enzymes in vertical flow constructed wetlands. *Appl. Ecol. Environ. Res.* 18(1), 959–971.
- Yang, L., Campbell, A.N., Bhattacharyya, A., Didonato, N., Pett-Ridge, J., 2021. Differential effects of redox conditions on the decomposition of litter and soil organic matter. *Biogeochemistry* 154, 1–15.
- Zhou, Z.H., Wang, C.K., Jin, Y. 2017. Stoichiometric responses of soil microflora to nutrient additions for two temperate forest soils. *Biol. Fert. Soils* 53, 397–406.
- Zhu, Z., Ge, T., Luo, Y., Liu, S., Xu, X., Tong, C., Shibistova, O., Guggenberger, G., Wu, J., 2018. Microbial stoichiometric flexibility regulates rice straw mineralization and its priming effect in paddy soil. *Soil Biol. Biochem.* 121, 67–76.

Supplementary

Table S1 The maximum reaction rate (V_{max}) and the affinity to a substrate (K_m) of phosphomonoesterase of samples after anoxic and oxic pre-incubation in oxic (+O₂) and anoxic (-O₂) assays

		V_{max} (nmol g ⁻¹ soil h ⁻¹)					
		+O ₂ assay			-O ₂ assay		
		Seeding	Early tillering	Late tillering	Seeding	Early tillering	Late tillering
Anoxic incubation	Top	58.20±5.63	72.66±11.18	79.11±3.39	67.47±2.03	89.79±7.42	101.85±1.72
	bulk	Bb	Bab	Aa	Bb	Aa	*Aa
	Routed	81.26±12.30	92.50±4.27	86.09±8.08	88.11±4.58	99.39±2.82	109.80±5.44
		Aa	Aa	Aa	Ab	Aa	*Aa
	Bottom	49.91±2.96	79.08±0.71	75.85±5.02	60.57±1.28	88.34±12.90	99.72±7.49
	bulk	Bb	ABa	Aa	*Bb	Aa	*Aa
Oxic incubation	Top	265.67±20.45	221.37±16.5	235.10±2.28	212.57±24.3	213.97±12.4	225.77±9.48
	bulk	#Aa	2#ABb	#Bab	8#Ba	2#Ba	#Ba
	Routed	273.50±4.08	241.80±9.68	279.90±18.68	267.63±10.3	240.80±8.69	270.97±4.84
		#Aa	#Ab	#Aa	9#Aa	#Ab	#Aa
	Bottom	217.83±19.30	206.57±2.23	227.63±12.33	200.93±10.3	205.93±8.02	226.77±19.3
	bulk	#Ba	#Ba	#Ba	2#Ba	#Ba	1#Ba
		K_m (μmol g ⁻¹ soil)					
Anoxic incubation	Top	10.88±3.32	12.34±2.10	13.18±0.37	11.10±0.87	13.95±1.15	13.61±1.56
	bulk	Aa	Aa	Aa	Ba	Aa	Aa
	Routed	14.13±2.28	12.05±0.20	12.91±4.35	14.22±0.83	13.49±0.90	13.94±0.57
		Aa	Aa	Aa	Aa	Aa	Aa
	Bottom	10.54±0.70	13.39±0.30	13.57±3.79	10.77±1.00	14.66±3.77	14.88±1.10
	bulk	Aa	Aa	Aa	Ba	Aa	Aa
Oxic incubation	Top	25.65±3.26	25.94±4.81	20.49±1.86	25.47±6.80	26.56±1.51	25.07±1.99
	bulk	#Aa	#Aa	#Aa	#Aa	#Aa	#Aa
	Routed	23.75±2.59	22.62±2.44	24.26±8.46	24.62±1.75	23.79±0.89	23.84±2.10
		#Aa	#Aa	Aa	#Aa	#Aa	#Aa
	Bottom	26.19±8.59	24.51±2.40	20.84±7.03	24.22±0.76	26.47±1.46	24.57±4.21
	bulk	Aa	#Aa	Aa	#Aa	#Aa	#Aa

Note: The data are shown as the means ± standard deviations (n = 3). * and # represent significant differences (P < 0.05) between -O₂ and +O₂ assays of each compartment at each rice growth stage after oxic or anoxic pre-incubation and between oxic and anoxic pre-incubation of each compartment at each rice growth stage under a same assay condition, respectively. Different uppercase or lowercase letters represent significant differences (P < 0.05) among soil compartments at a same rice growth stage or among rice growth stages at a same compartment after anoxic or oxic pre-incubation under a same assay condition, respectively.

Table S2 The maximum reaction rate (V_{max}) and the affinity to a substrate (K_m) of β -glucosidase of samples after anoxic and oxic pre-incubation in oxic (+O₂) and anoxic (-O₂) assays

		V_{max} (nmol g ⁻¹ soil h ⁻¹)					
		+O ₂ assay			-O ₂ assay		
		Seeding	Early tillering	Late tillering	Seeding	Early tillering	Late tillering
Anoxic incubation	Top	9.07±1.26	9.38±0.66	12.81±2.10	13.34±0.33	16.29±2.33	16.71±0.72
	bulk	Ab	Bab	Aa	*Ba	*Aa	Aa
	Rooted	10.49±0.89	12.60±1.06	13.60±0.18	15.21±0.32	18.78±0.21	17.99±0.64
		Ab	Aa	Aa	*Ab	*Aa	*Aa
	Bottom	6.77±0.53	8.49±0.50	9.23±0.15	11.95±0.62	11.57±0.50	14.38±1.28
	bulk	Bb	Ba	Ba	*Cb	*Bb	*Ba
Oxic incubation	Top	20.87±0.11	21.63±0.46	24.29±1.67	20.29±1.83	21.19±0.35	24.07±0.84
	bulk	#Bb	#Bb	#Ba	#Bb	#ABb	#Ba
	Rooted	25.29±1.12	26.94±0.71	29.85±0.74	24.66±0.31	25.73±2.67	28.58±1.34
		#Ab	#Ab	#Aa	#Aa	#Aa	#Aa
	Bottom	17.21±0.76	18.30±1.47	22.80±0.57	16.83±0.43	18.27±2.90	22.60±1.74
	bulk	#Cb	#Cb	#Ba	#Cb	#Bb	#Ba
		K_m (μmol g ⁻¹ soil)					
Anoxic incubation	Top	8.70±1.31	9.56±2.24	11.19±1.55	11.35±0.79	14.19±4.03	14.53±0.44
	bulk	Aa	Aa	Aa	Aa	Aa	*Aa
	Rooted	12.13±3.75	10.76±0.55	13.47±2.51	15.08±5.55	15.13±1.18	13.56±2.82
		Aa	Aa	Aa	Aa	*Aa	Aa
	Bottom	9.00±2.86	8.73±1.64	11.09±0.62	9.12±1.87	11.10±0.65	14.22±3.92
	bulk	Aa	Aa	Aa	Aa	Aa	Aa
Oxic incubation	Top	14.74±0.83	15.96±0.71	19.82±2.75	16.27±4.94	16.73±3.06	20.26±0.46
	bulk	#Ab	#Aab	#Aa	Aa	Aa	#Aa
	Rooted	15.67±3.72	15.68±1.23	17.80±1.96	16.13±0.54	19.79±2.89	18.75±5.06
		Aa	#Aa	Aa	Aa	Aa	Aa
	Bottom	11.61±1.28	15.61±2.09	19.78±2.82	12.13±1.09	16.72±0.82	21.27±3.93
	bulk	Ab	#Aab	#Aa	Ab	#Aab	Aa

Note: The data are shown as the means ± standard deviations (n = 3). * and # represent significant differences (P < 0.05) between -O₂ and +O₂ assays of each compartment at each rice growth stage after oxic or anoxic pre-incubation and between oxic and anoxic pre-incubation of each compartment at each rice growth stage under a same assay condition, respectively. Different uppercase or lowercase letters represent significant differences (P < 0.05) among soil compartments at a same rice growth stage or among rice growth stages at a same compartment after anoxic or oxic pre-incubation under a same assay condition, respectively.

Table S3 The maximum reaction rate (V_{max}) and the affinity to a substrate (K_m) of leucine aminopeptidase of samples after anoxic and oxic pre-incubation in oxic (+O₂) and anoxic (-O₂) assays

		V_{max} (nmol g ⁻¹ soil h ⁻¹)					
		+O ₂ assay			-O ₂ assay		
		Seeding	Early tillering	Late tillering	Seeding	Early tillering	Late tillering
Anoxic incubation	Top	187.43±21.92	201.43±2.58	179.03±12.74	222.30±18.97	235.60±6.77	255.27±38.65
	bulk	Aa	ABa	Aa	Aa	*Ba	Aa
	Routed	193.87±7.77	215.70±16.99	211.77±20.24	242.83±11.87	266.63±9.72	281.97±34.55
		Aa	Aa	Aa	*Aa	*Aa	Aa
	Bottom	135.70±15.14	179.50±2.84	182.43±2.56	164.67±7.31	222.27±2.37	224.20±13.63
	bulk	Bb	Ba	Aa	Bb	*Ba	*Aa
Oxic incubation	Top	260.50±6.36	280.13±24.31	286.17±13.33	258.10±4.83	264.40±2.42	278.10±2.76
	bulk	#Ba	#Aa	#Ba	Ab	#Bb	Ba
	Routed	278.77±4.69	322.80±13.31	323.00±6.68	272.42±6.84	309.80±7.00	320.50±9.48
		#Ab	#Aa	#Aa	#Ab	#Aa	Aa
	Bottom	229.57±8.04	284.10±22.27	277.50±10.96	226.80±8.66	261.10±23.40	274.47±4.77
	bulk	#Cb	#Aa	#Ba	#Bb	Bab	#Ba
		K_m (μmol g ⁻¹ soil)					
Anoxic incubation	Top	13.28±3.58	13.73±0.91	13.89±1.00	13.24±0.69	13.50±0.77	13.75±3.85
	bulk	Aa	Aa	Aa	Aa	Aa	Aa
	Routed	15.11±0.99	13.78±2.02	13.56±4.80	14.58±0.40	13.70±1.43	13.39±1.20
		Aa	Aa	Aa	Aa	Aa	Aa
	Bottom	13.73±1.35	16.65±0.49	13.85±4.35	12.78±1.80	15.97±2.33	13.66±0.65
	bulk	Aa	Aa	Aa	Aa	Aa	Aa
Oxic incubation	Top	14.29±0.59	15.49±4.32	13.96±2.69	14.76±0.97	15.75±0.91	14.06±0.93
	bulk	Aa	Aa	Aa	Aa	Aa	Ba
	Routed	15.34±0.15	14.16±1.59	14.08±0.56	16.30±0.63	14.62±2.18	14.42±0.99
		Aa	Aa	Aa	#Aa	Aa	ABa
	Bottom	15.19±2.28	17.57±0.44	15.28±1.07	15.78±0.73	17.66±0.37	16.27±0.72
	bulk	Aa	Aa	Aa	Ab	Aa	#Aab

Note: The data are shown as the means ± standard deviations (n = 3). * and # represent significant differences (P < 0.05) between -O₂ and +O₂ assays of each compartment at each rice growth stage after oxic or anoxic pre-incubation and between oxic and anoxic pre-incubation of each compartment at each rice growth stage under a same assay condition, respectively. Different uppercase or lowercase letters represent significant differences (P < 0.05) among soil compartments at a same rice growth stage or among rice growth stages at a same compartment after anoxic or oxic pre-incubation under a same assay condition, respectively.

Table S4 Mean catalytic efficiency (K_a) and mean turnover time (T_i) of phosphomonoesterase of samples after anoxic and oxic pre-incubation in oxic (+O₂) and anoxic (-O₂) assays

		K_a (nmol h ⁻¹ μ mol ⁻¹)					
		+O ₂ assay			-O ₂ assay		
		Seeding	Early tillering	Late tillering	Seeding	Early tillering	Late tillering
Anoxic incubation	Top	5.89±1.87	5.92±0.54	6.01±0.41	6.11±0.44	6.47±0.61	7.59±1.15
	bulk	Aa	Ba	Aa	Aa	Aa	Aa
	Rooted	5.85±1.10	7.68±0.24	7.37±2.12	6.23±0.68	7.39±0.29	7.90±0.66
		Aa	Aa	Aa	Ab	Aab	Aa
	Bottom	4.77±0.57	5.91±0.19	6.11±1.99	5.67±0.44	6.26±0.92	6.73±0.58
	bulk	Aa	Ba	Aa	Aa	Aa	Aa
Oxic incubation	Top	10.48±1.17	8.81±1.58	11.57±1.02	8.68±1.32	8.06±0.18	9.04±0.48
	bulk	#Aa	Aa	*#Aa	Ba	#Ba	Ba
	Rooted	11.65±1.22	10.85±1.48	13.13±4.63	10.90±0.49	10.14±0.69	11.44±0.83
		#Aa	#Aa	Aa	#Aa	#Aa	#Aa
	Bottom	9.01±2.12	8.52±0.91	12.21±3.83	8.32±0.70	7.79±0.15	9.38±0.91
	bulk	Aa	#Aa	Aa	#Ba	Ba	#Ba
		T_i (days)					
Anoxic incubation	Top	8.49±2.21	7.80±0.66	7.66±0.54	7.54±0.57	7.15±0.67	6.20±1.03
	bulk	Aa	#Aa	#Aa	#Aa	#Aa	Aa
	Rooted	8.10±1.41	5.98±0.19	6.71±1.74	7.44±0.66	6.21±0.25	5.84±0.48
		#Aa	#Ba	Aa	#Aa	#Aab	#Ab
	Bottom	9.75±1.21	7.76±0.25	8.28±2.41	8.14±0.63	7.48±1.04	6.86±0.59
	bulk	#Aa	#Aa	Aa	#Aa	Aa	#Aa
Oxic incubation	Top	4.43±0.46	5.37±0.93	4.00±0.37	5.40±0.83	5.69±0.13	5.08±0.26
	bulk	Aa	Aa	AA	Aa	Aa	*Aa
	Rooted	3.98±0.39	4.31±0.64	3.90±1.16	4.21±0.19	4.54±0.30	4.03±0.29
		Aa	Aa	Aa	Aa	Ba	Ba
	Bottom	5.41±1.37	5.44±0.57	4.15±1.31	5.55±0.44	5.89±0.11	4.93±0.45
	bulk	Aa	Aa	Aa	Aab	Aa	Ab

Note: The data are shown as the means \pm standard deviations (n = 3). * and # represent significant differences ($P < 0.05$) between -O₂ and +O₂ assays of each compartment at each rice growth stage after oxic or anoxic pre-incubation and between oxic and anoxic pre-incubation of each compartment at each rice growth stage under a same assay condition, respectively. Different uppercase or lowercase letters represent significant differences ($P < 0.05$) among soil compartments at a same rice growth stage or among rice growth stages at a same compartment after anoxic or oxic pre-incubation under a same assay condition, respectively.

Table S5 Mean catalytic efficiency (K_a) and mean turnover time (T_t) of β -glucosidase of samples after anoxic and oxic pre-incubation in oxic (+O₂) and anoxic (–O₂) assays

		K_a (nmol h ⁻¹ μ mol ⁻¹)					
		+O ₂ assay			–O ₂ assay		
		Seeding	Early tillering	Late tillering	Seeding	Early tillering	Late tillering
Anoxic incubation	Top	1.05±0.11	1.03±0.20	1.14±0.03	1.18±0.11	1.21±0.25	1.15±0.06
	bulk	Aa	Aa	Aa	Aa	Aa	Aa
	Rooted	0.97±0.33	1.17±0.09	1.05±0.21	1.13±0.34	1.25±0.08	1.38±0.28
		Aa	Aa	Aa	Aa	Aa	Aa
	Bottom	0.83±0.25	1.00±0.12	0.84±0.05	1.36±0.24	1.04±0.04	1.07±0.22
	bulk	Aa	Aa	Aa	Aa	Aa	Aa
Oxic incubation	Top	1.42±0.08	1.36±0.04	1.24±0.15	1.36±0.38	1.31±0.25	1.19±0.05
	bulk	#Aa	Ba	Ba	Aa	Aa	ABa
	Rooted	1.69±0.31	1.73±0.16	1.69±0.14	1.53±0.06	1.34±0.30	1.61±0.31
		Aa	#Aa	#Aa	Aa	Aa	Aa
	Bottom	1.50±0.16	1.18±0.07	1.18±0.16	1.40±0.14	1.09±0.12	1.09±0.18
	bulk	#Aa	Ba	#Ba	Aa	Aa	Ba
		T_t (days)					
Anoxic incubation	Top	44.17±4.45	46.18±8.07	40.40±1.00	39.06±3.46	39.79±8.60	39.93±2.15
	bulk	#Aa	Aa	Aa	Aa	Aa	Aa
	Rooted	52.64±15.38	39.34±3.03	45.38±8.37	45.11±15.6	36.91±2.49	34.62±7.60
		Aa	#Aa	#Aa	6Aa	Aa	Aa
	Bottom	59.73±15.55	46.78±6.03	55.09±3.38	34.90±6.24	43.97±1.70	44.83±9.01
	bulk	Aa	Aa	#Aa	Aa	Aa	Aa
Oxic incubation	Top	32.37±1.79	33.81±1.04	37.37±4.53	35.99±8.44	36.14±6.32	38.63±1.69
	bulk	Aa	Ba	Aa	Aa	Aa	Aa
	Rooted	28.16±5.47	26.70±2.34	27.28±2.34	29.98±1.17	36.24±9.57	29.81±6.72
		Aa	Ca	Ba	Aa	Aa	Aa
	Bottom	30.94±3.54	38.92±2.39	39.68±5.01	33.05±3.20	42.65±4.33	43.07±6.56
	bulk	Aa	Aa	Aa	Aa	Aa	Aa

Note: The data are shown as the means \pm standard deviations ($n = 3$). * and # represent significant differences ($P < 0.05$) between –O₂ and +O₂ assays of each compartment at each rice growth stage after oxic or anoxic pre-incubation and between oxic and anoxic pre-incubation of each compartment at each rice growth stage under a same assay condition, respectively. Different uppercase or lowercase letters represent significant differences ($P < 0.05$) among soil compartments at a same rice growth stage or among rice growth stages at a same compartment after anoxic or oxic pre-incubation under a same assay condition, respectively.

Table S6 Mean catalytic efficiency (K_a) and mean turnover time (T_i) of leucine aminopeptidase of samples after anoxic and oxic pre-incubation in oxic (+O₂) and anoxic (-O₂) assays

		K_a (nmol h ⁻¹ μ mol ⁻¹)					
		+O ₂ assay			-O ₂ assay		
		Seeding	Early tillering	Late tillering	Seeding	Early tillering	Late tillering
Anoxic incubation	Top	14.84±2.68	14.72±0.76	13.02±1.85	16.76±0.63	17.49±0.77	19.35±2.85
	bulk	Aa	Aa	Aa	Aa	*ABa	Aa
	Rooted	12.91±1.22	15.82±1.41	17.45±5.20	16.66±0.81	19.65±1.88	21.44±4.46
		Aa	Aa	Aa	*Aa	Aa	Aa
	Bottom	10.07±1.97	10.79±0.36	14.28±3.54	13.08±1.41	14.23±2.18	16.50±1.80
	bulk	Aa	Ba	Aa	Ba	Ba	Aa
Oxic incubation	Top	18.28±1.09	19.44±4.88	21.19±3.67	17.55±0.98	16.84±0.99	19.87±1.40
	bulk	Aa	Aa	#Aa	Aab	ABb	ABa
	Rooted	18.17±0.22	23.11±2.88	22.97±0.71	16.74±0.84	21.75±3.74	22.29±0.95
		#Ab	#Aa	Aa	Aa	Aa	Aa
	Bottom	15.38±1.80	16.20±1.58	18.20±0.61	14.41±0.89	14.77±1.16	16.91±1.02
	bulk	#Aa	#Aa	Aa	Ba	Ba	Ba
		T_i (days)					
Anoxic incubation	Top	3.19±0.55	3.12±0.17	3.59±0.51	2.74±0.10	2.63±0.12	2.42±0.37
	bulk	Aa	*Ba	*#Aa	Ba	ABa	Aa
	Rooted	3.58±0.35	2.92±0.26	2.94±1.07	2.76±0.14	2.36±0.24	2.23±0.45
		*#Aa	#Ba	Aa	Bb	Ba	Aa
	Bottom	4.75±1.03	4.25±0.14	3.47±1.04	3.54±0.39	3.29±0.46	2.81±0.30
	bulk	*Aa	*#Aa	Aa	Aa	Aa	Aa
Oxic incubation	Top	2.52±0.16	2.49±0.54	2.22±0.35	2.62±0.14	2.73±0.16	2.32±0.16
	bulk	Aa	Aa	ABa	Bab	ABa	Bb
	Rooted	2.52±0.03	2.01±0.25	2.00±0.06	2.75±0.14	2.17±0.37	2.06±0.09
		Aa	Ab	Bb	Ba	Bb	Bb
	Bottom	3.02±0.35	2.86±0.27	2.52±0.08	3.19±0.19	3.12±0.23	2.72±0.16
	bulk	Aa	Aa	Aa	Aa	Aa	Aa

Note: The data are shown as the means \pm standard deviations ($n = 3$). * and # represent significant differences ($P < 0.05$) between -O₂ and +O₂ assays of each compartment at each rice growth stage after oxic or anoxic pre-incubation and between oxic and anoxic pre-incubation of each compartment at each rice growth stage under a same assay condition, respectively. Different uppercase or lowercase letters represent significant differences ($P < 0.05$) among soil compartments at a same rice growth stage or among rice growth stages at a same compartment after anoxic or oxic pre-incubation under a same assay condition, respectively.

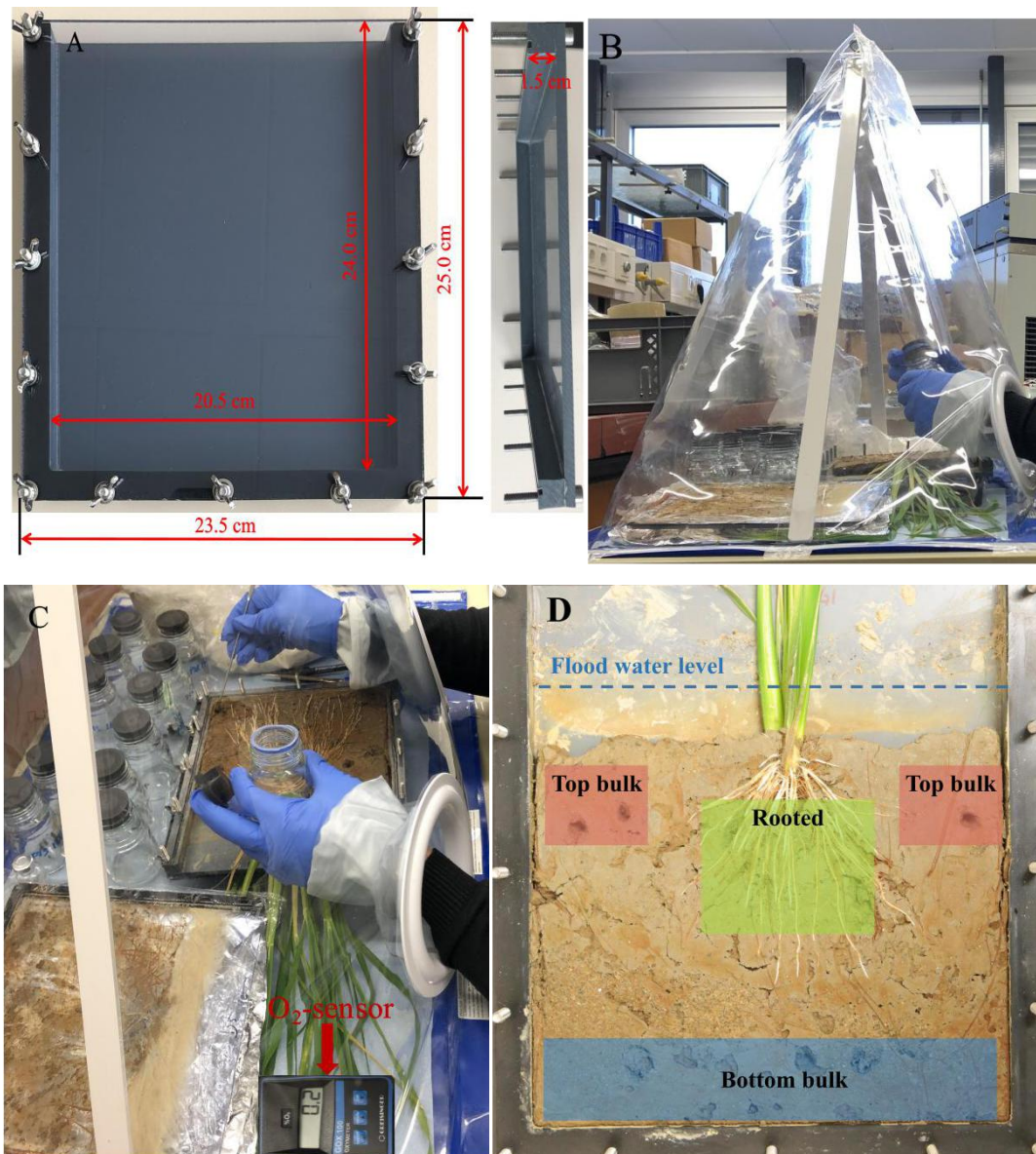


Fig. S1 The dimensions of a rhizobox with plexiglas cover on top, sealed with rubber gasket (not visible on photo) and fixed by thumbscrews (A), a portable PVC glovebox filled with N_2 and with rhizoboxes inside (B), sampling of soil from compartments of a rhizobox, glass bottles for soil suspension preparation and the level of O_2 as indicated by an O_2 -sensor (C), and the sampling locations of three soil compartments 48 hours after flood water drainage (D). The level of flooded water maintained during experiment is shown schematically by a dashed line. Shaded spots within each compartment correspond to the removed soil.

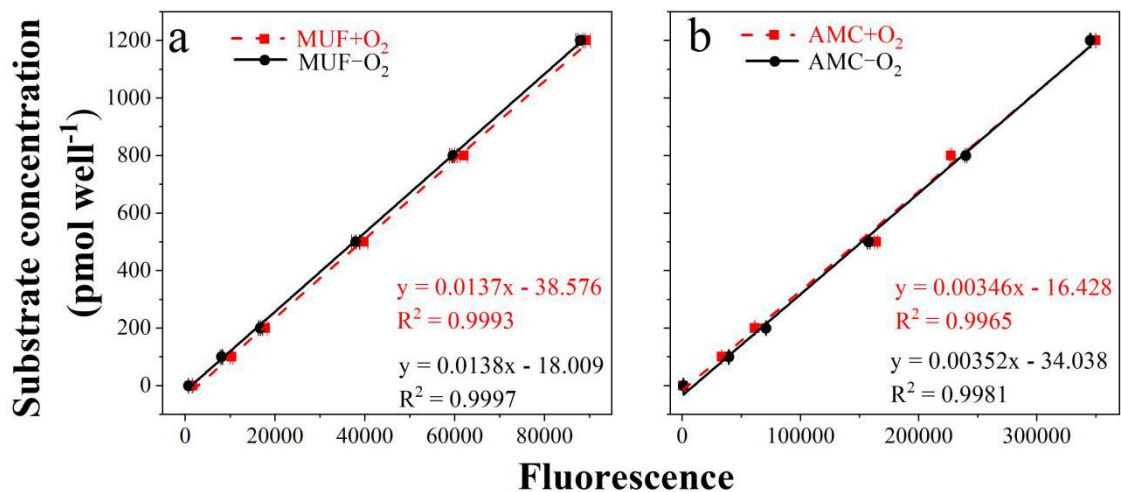


Fig. S2 Calibrations of 4-methylumbelliferone (MUF, a) and 7-amino-4-methylcoumarin (AMC, b) fluorogenic dyes under anoxic ($-O_2$) and aerobic ($+O_2$) conditions. The data are the means \pm standard deviations ($n = 6$).

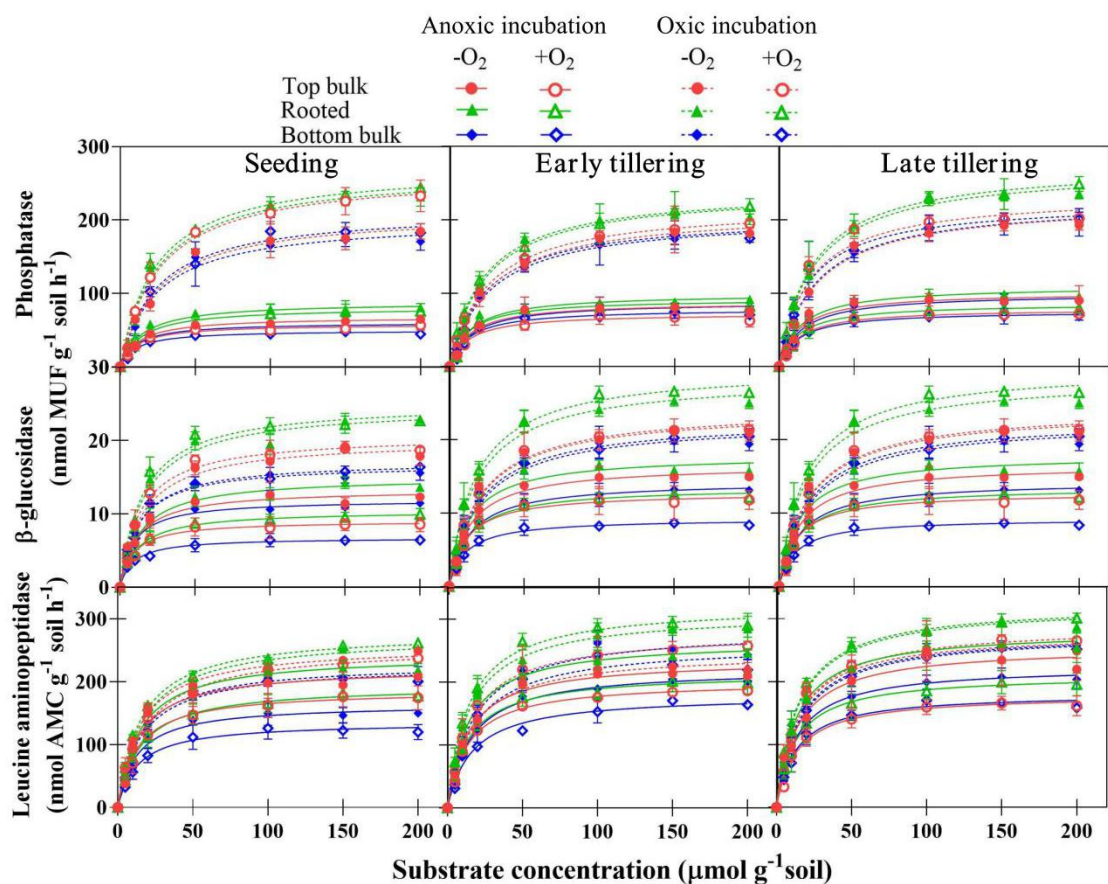


Fig. S3 The kinetics of phosphomonoesterase, β -glucosidase, and leucine aminopeptidase activities of samples after oxidic and anoxic pre-incubation at the top bulk-, rooted-, and bottom bulk soil compartments of a rhizobox in oxidic ($+O_2$) and anoxic ($-O_2$) assays. The data are the means \pm standard deviations ($n = 3$).

Study 3 Keep oxygen in check: an improved *in-situ* zymography approach for mapping anoxic hydrolytic enzyme activities in a paddy soil

Chaoqun Wang^{a,*}, Nataliya Bilyera^b, Evgenia Blagodatskaya^c, Xuechen Zhang^d, Michaela A. Dippold^{a,b}, Maxim Dorodnikov^{a,e,f}

^a Biogeochemistry of Agroecosystems, University of Goettingen, 37077 Goettingen, Germany

^b Geo-Biosphere Interactions, University of Tuebingen, 72076 Tuebingen, Germany

^c Department of Soil Ecology, Helmholtz Center for Environmental Research, 06120 Halle/Saale, Germany

^d College of Resources and Environment, Northwest A&F University, 712100 Yangling, China

^e Department of Soil Science of Temperate Ecosystems, University of Goettingen, 37077 Goettingen, Germany

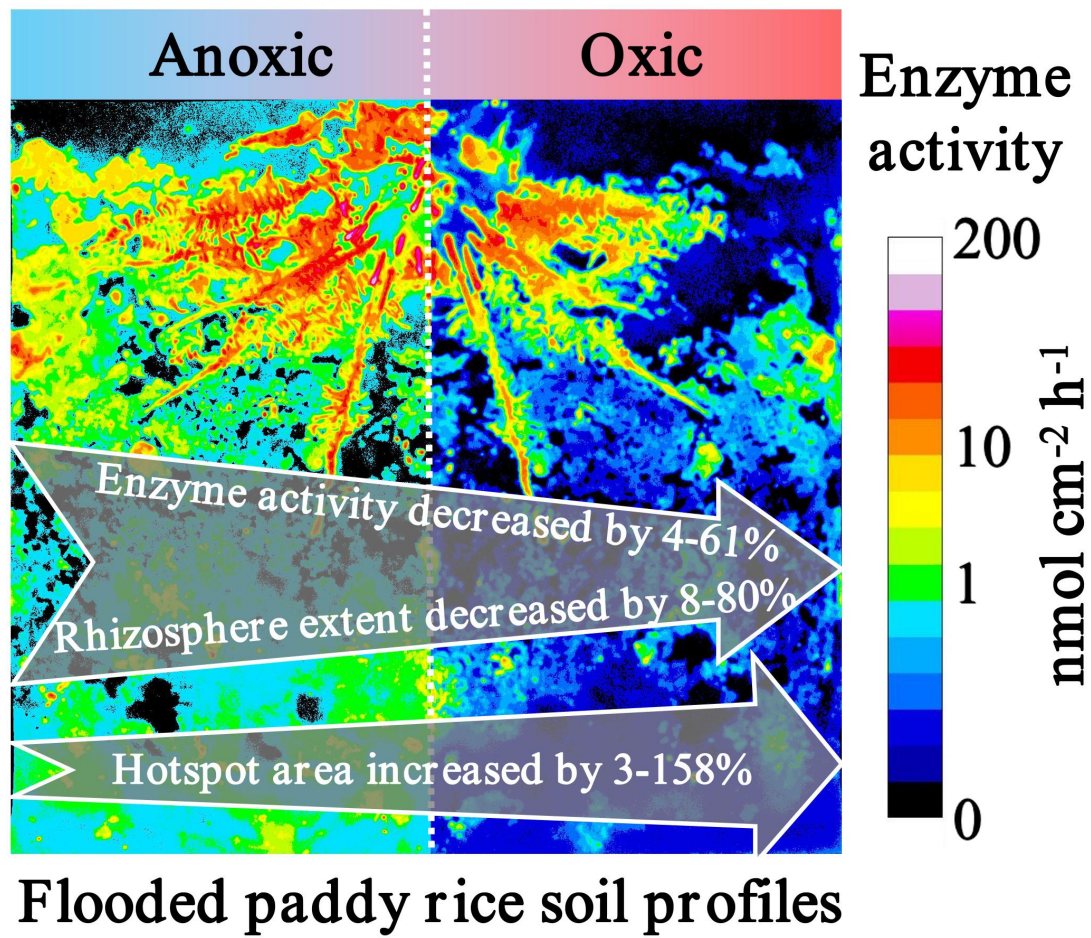
^f Institute of Landscape Ecology, University of Muenster, 48149 Muenster, Germany

* **Correspondence:** chaoqun.wang@forst.uni-goettingen.de

Status: Published in Science of the Total Environment

Wang, C.Q., Bilyera, N., Blagodatskaya, E., Zhang, X.C., Dippold, M.A., Dorodnikov, M., 2022. Keep oxygen in check: An improved *in-situ* zymography approach for mapping anoxic hydrolytic enzyme activities in a paddy soil. Science of the Total Environment 850, 158118.

Graphical abstract



Abstract: Paddy soils regularly experience redox oscillations during the wetting and draining stages, yet the effects of short-term presence of oxygen (O₂) on *in-situ* microbial hotspots and enzyme activities in anoxic ecosystems remain unclear. To fill this knowledge gap, we applied soil zymography to localize hotspots and activities of phosphomonoesterase (PME), β-glucosidase (BG), and leucine aminopeptidase (LAP) in three compartments of rice-planted rhizoboxes (top bulk, rooted, and bottom bulk paddy soil) under oxic (+O₂) and anoxic (−O₂) conditions. Short-term (35 min) aeration decreased PME activity by 13–49%, BG by 4–52%, and LAP by 12–61% as compared with −O₂ in three soil compartments. The percentage of hotspot area was higher by 3–110% for PME, by 10–60% for BG, and by 12–158% for LAP under +O₂ vs. −O₂ conditions depending on a rice growth stage. Irrespective of the aeration conditions, the rhizosphere extent of rice plants for three enzymes was generally greater under higher moisture conditions and at earlier growth stage. Higher O₂ sensitivity for the tested enzymes at bottom bulk soil versus other compartments suggested that short-term aeration during conventional zymography may lead to underestimation of nutrient mobilization in subsoil compared to top bulk soil. The intolerance of anaerobic microorganisms against the toxicity of O₂ in the cells and the shift of microbial metabolic pathways may explain such a short-term suppression by O₂. Our findings, therefore, show that anoxic conditions and soil moisture should be kept during zymography and probably other *in-situ* soil imaging methods when studying anoxic systems.

Keywords: aerobes; anaerobes; fluorogenically labelled substrates; microbial hotspots; rhizosphere; zymography

1. Introduction

Microorganisms, the main actors of biogeochemical processes, are unevenly distributed in the soil due to the high heterogeneity of bioavailable substrates (Kuzyakov and Blagodatskaya, 2015; Tecon and Or, 2017). Thus, areas with a higher labile carbon (C) input, such as rhizosphere, become microbial hotspots compared to bulk soil microzones with scarce substrate resources (Hinsinger et al., 2009). The spatial heterogeneity of microbial activities has therefore received increased attention in recent years (Baveye et al., 2018). Soil extracellular enzymes produced by microorganisms and plants mediate the biogeochemical processes (Alexander 1977; Cosgrove 1980; Wang et al., 2021a, b) and are commonly used to characterize microbial activity (Spohn et al., 2013; Tian et al., 2019). Therefore, understanding the mechanisms controlling the distribution and intensity of the enzymatic hotspots (Kuzyakov & Blagodatskaya, 2015) is of utmost importance for predicting the nutrient flows in plant-soil-microorganisms continuum.

Soil zymography, a novel *in situ* visualizing method, has been applied to reveal the distribution of enzyme activities in two-dimensional space and to localize hotspots of enzyme activities (Spohn et al., 2013; Razavi et al., 2019). Soil enzyme activities are affected by a broad range of environmental factors such as soil moisture (Sanallah et al., 2011; Bilyera et al., 2021), pH (Sinsabaugh, 2010; Ma et al., 2021), nutrient contents (Keuskamp et al., 2015), and elements stoichiometry (Hartman et al., 2017). Among the abiotic factors, the effect of oxygen (O₂) availability on enzyme activities *in situ* has not received a considerable attention, despite of the suppressive effects reported. For instance, short-term (from tens of minutes to several hours) variations in the availability of O₂ in anoxic ecosystems can cause the partial inactivation of microorganisms (Gonzalez-Flecha and Demple, 1995), which in turn may decrease enzyme activity. So, short-term aeration (for 2–2.5 h) led to the suppression of the potential activity (V_{\max}) of phosphatases, β -glucosidase, and leucine aminopeptidase in a paddy soil by 5–43% (Wang et al., 2022a, b). Also, the decrease in phosphatases and β -glucosidase activities in food waste was observed one day after exposure to atmospheric O₂ (Henry et al., 2018). Moreover, ferrous iron (Fe(II)) oxidation was suggested as a key factor mediating soil organic C mineralization in wetlands (Wang et al., 2017) and peatlands during change from anoxic to oxic conditions (Wen et al., 2019). As proposed in the ‘iron gate’ paradigm, oxidative removal of Fe(II) inactivates phenol oxidase resulting in accumulation of phenols, which inhibit the activities of hydrolytic enzymes, thus acting as a protector against C loss (Wang et al., 2017). Despite the important role of O₂, previously applied zymography method to map enzyme activities and microbial hotspots in anoxic systems including flooded rice paddy soils, was commonly conducted under oxic conditions (Ge et al., 2017; Wei et al., 2019a, b). Therefore, due to the frequently reported microbial suppression by the O₂ presence in anoxic systems, enzyme activities *in situ* measured with such a method may be underestimated. This calls for measurement of enzyme activities by zymography under natural anoxic conditions for

paddy soils, which has not been done before.

Microorganisms releasing hydrolytic enzymes and decomposing organic matter in flooded rice paddy systems can face O₂ either via (i) its diffusion belowground from atmosphere and dissolution in surface water, or (ii) delivery of O₂ belowground into rhizosphere of rice through aerenchima of plants (Larsen et al., 2015). Oxygen availability is therefore one of the strongest environmental parameters controlling microbial community structure (Deangelis et al., 2012) and consequently enzyme activities in the rice paddies. As a consequence of O₂ depletion, microaerophilic microorganisms are abundant in the rhizosphere and top bulk soil in paddy fields (Li et al., 2016; Bai et al., 2015). The strongest influence of O₂ on enzymatic hotspot distribution in paddy rice soil systems can be expected in top- and rooted soil, whereas deep bulk soil should experience long-term anoxic conditions. On the temporal scale, the spatial extent of the aerated zone in the rhizosphere has been shown to be dynamic with rice growth, as old roots cease to leak O₂, while young roots intensively release O₂ into the surrounding soil (Larsen et al., 2015). Accordingly, it can be expected that the distribution of aerobic or microaerophilic microorganisms in rhizosphere soil will depend on phenological stages of rice growth.

In this study, we adapted the conventional zymography technique developed under the ambient laboratory atmosphere (Spohn et al., 2013; Razavi et al. 2016) to the anoxic conditions by means of a portable glovebox. We mapped the activity of P, C, and N-acquiring enzymes (phosphomonoesterase (PME), β -glucosidase (BG), and leucine aminopeptidase (LAP)) under oxic (+O₂) and anoxic (-O₂) conditions during 30 days of rice growth. We hypothesized that (1) the hotspot area of enzyme activities measured under conventional oxic conditions will decrease compared to controlled anoxic conditions because of suppressive effects of the short-term aeration on hydrolytic enzymes, and (2) short-term aeration will have a higher suppressive impact on enzyme activities in bottom bulk soil compared to top bulk and rooted soil due to the natural aeration gradient of flooded rice paddy soils. Similarly, short-term aeration will have a weaker suppressive effect, especially in rooted soil, with rice growth, since the expansion of aerenchymatous roots of rice delivers O₂ belowground and causes adaptation of rhizosphere microorganisms to oxic conditions.

2. Materials and methods

2.1. Soil properties and experimental setup

The topsoil (0–20 cm) was collected in November–December 2017 from a paddy rice field located at the Changsha Agricultural and Environmental Monitoring Station, Hunan Province, China (113°19'52" E, 28°33'04" N). The soil was developed from highly weathered granite and is classified as a typical Stagnic Anthrosol (Gong et al., 2007). The soil had a pH of 6.2 and contained 13.1 g kg⁻¹ soil organic C, 1.4 g kg⁻¹ total N, 18.0 mg kg⁻¹ available N, 0.3 g kg⁻¹ total P, 3.7 mg kg⁻¹ Olsen-P, and 15.7 g kg⁻¹ total Fe (Zhu et al., 2018). After sampling, the soil was homogenized, air-dried,

and sieved < 2 mm prior the transportation to Germany.

Nine rice plants (*Oryza sativa* L. ‘Two-line hybrid rice Zhongzao 39’) were grown, each in a separate PVC-rhizobox with inner dimensions of 20.5 × 24.0 × 1.5 cm to obtain three replications for each of three enzymes (PME, BG, and LAP) measured by zymography. Rhizoboxes were made water-tight with the help of rubber sealing and screw-holders closed with a transparent removable plexiglas front cover (see Fig. S1A). One 20-day-old rice seedling was transplanted into the center of a rhizobox prefilled with 1.0 kg water-saturated soil (600 g air-dry soil 400 ml deionized water). During the experiment, the rhizoboxes were inclined by 45° so that the plant roots grew along the front removable cover. A 2–3 cm water layer was kept above soil surface in rhizoboxes by adding deionized water during the whole period of rice growth except for soil zymography dates. To prevent the microcosms destruction by the leaking water after opening, each set of rhizoboxes was preconditioned prior to the analysis: water above soil surface in the rhizoboxes was drained two days before soil zymography. Soil redox potential (E_h values) at a 5-cm soil depth ranged from –178 mV to –164 mV during two days after drainage, suggesting the effects of water drainage on O₂ diffusion from air to soil was negligible. The difference in soil moisture between stages (Fig. S2) was related to the intensification of rice plant transpiration. After zymography, all rhizoboxes were re-sealed and waterlogged until the next measurement. All seedlings were grown in a climate chamber (KBF-S 720, Binder GmbH, Tuttlingen, Germany) at 28 ± 1 °C day and 24 ± 1 °C night temperatures, 70% relative humidity, and 12-h photoperiod (08:00 to 20:00) with light intensity of 350 μmol m⁻² s⁻¹ of photosynthetically active radiation at the top of the rhizobox (LED Grow Light, GrowLED, France). After transplanting, liquid fertilizer (dissolved in water) containing 30 mg N as urea, and 25 mg K and 20 mg P as KH₂PO₄ per kg dry soil was added to the surface water in each rhizobox to maintain sufficient seedlings’ growth.

2.2. Soil zymography

To map enzyme activities at soil-root interface, we applied *in situ* imaging method – soil zymography. In contrast to the conventional zymography approach conducted under the ambient laboratory atmosphere (Spohn et al., 2013; Razavi et al. 2016), the anoxic zymography was performed here for the first time. To keep anoxic conditions during soil zymography, the rhizoboxes were placed inside a portable PVC glovebox (Captair® Pyramid Glovebox 3015-00, Erlab DFS, Saint-Maurice, France) (Fig. S1B) evacuated with a vacuum pump (Ilmvac MP 301 Vp, Ilmvac GmbH, Ilmenau, Germany) and then back-flushed with nitrogen (N₂) to O₂ concentrations below 0.2% as indicated by O₂-sensor (Greisinger GOX 100, GHM Messtechnik GmbH, Remscheid, Germany) (Fig. S1C). Six zymograms were made per rhizobox (three under –O₂ assay and three under +O₂ assay) during the experiment. A cross-test method was adopted to determine the effect of the starting conditions (oxic or anoxic) on zymography results. Briefly, zymograms from two out of the three rhizoboxes of each enzyme treatment were taken first under anoxic conditions and then repeated under oxic conditions with interval of 30 min. This treatment was termed “transition

from anoxic to oxic conditions” (Fig. S2). In turn, one remaining rhizobox per enzyme treatment was exposed first to oxic and then to anoxic zymography (“transition from oxic to anoxic conditions”) (Fig. S2). This scheme was applied for all enzymes at the seedling and late tillering stages. At the early tillering stage, the sequence of rhizoboxes was reverse for the oxic and anoxic conditions (Fig. S2). The effect of transition was evaluated as the mean of three independent measurements (see section 2.5).

Three enzyme activities (PME, BG, and LAP) were mapped by zymography at a seedling (with 1 tiller), early- (4 ± 1 tillers), and late (6 ± 1 tillers) tillering stages of rice growth, which corresponded to 10, 16–20, and 28–31 days after rice transplantation. The same set of rhizoboxes per enzyme treatment was used to map activities at three growth stages to exclude a cross-contamination by applied substrates (Fig. S2). In total, 54 zymograms (3 enzymes \times 3 rhizoboxes per enzyme \times 2 assay conditions \times 3 rice growth stages) were made during the experiment. Zymography was performed according to a growth stage of rice for all enzymes at the same date.

The activities of PME, BG, and LAP were visualized using membranes (0.45 μm pore size and 100 μm thick, Taoyuan Medical Equipment Company, China) saturated with substrates of 4-methylumbelliferyl-phosphate (for PME), 4-methylumbelliferyl- β -D-glucoside (for BG), and L-Leucine-7-amino-4-methylcomarin hydrochloride (for LAP) (all purchased from Sigma-Aldrich Co. Ltd), respectively, according to the protocol described by Razavi et al. (2016). 4-methylumbelliferyl-phosphate and 4-methylumbelliferyl- β -D-glucoside were separately dissolved to a concentration of 10 mM in MES buffer (pH 6.5), and L-Leucine-7-amino-4-methylcomarin hydrochloride was dissolved to a concentration of 10 mM in TRIZMA buffer (pH 7.2) (both buffers from Sigma-Aldrich Co. Ltd). Each of the substrates and buffer was prepared in duplicate, one portion was bubbled with N_2 for 20 minutes and then used for soil zymography under anoxic conditions in the glovebox, and the other portion without any pretreatment was used for soil zymography under oxic conditions. The saturated membrane with a size 20.5×18.0 cm fitting to a rhizobox was placed on the soil surface, covered with aluminum foil, and slightly pressed by a sand bag to achieve even attachment (Fig. S1D). A 30-min membrane exposure time (determined in a pre-experiment according to Guber et al. (2018), data not shown) was used as the optimal duration for the diffusion of substrate to the soil and/or diffusion of enzymes and 4-methylumbelliferone (MUF) or 7-amino-4-methylcomarin (AMC) back to a membrane due to water-saturated conditions. After exposure, the membranes were carefully lifted from the soil surface with tweezers and immediately photographed under ultraviolet (UV) illumination with a wavelength of 355 nm in a light-proof room with a Canon EOS 6D camera. We used the following settings: 50-cm distance from membranes to the lens of camera to take images at a resolution of $0.74 \mu\text{m pixel}^{-1}$, aperture 5.6, and ISO 12800. To define an optimal camera exposure time, the membranes were photographed at shutter speeds of 1/20, 1/25, 1/30, 1/40, 1/50, 1/60,

1/80, and 1/100 s. These speeds corresponded to exposition times of 50, 40, 33.3, 25, 16.7, 12.5, and 10 ms, respectively. We purposely omitted the time-lapse zymography (Guber et al., 2021) which enables the detection of the dynamics of enzymatic reactions and their spatial development, because we aimed to minimize the duration of the contact between enzymes and reaction products (MUF and AMC) on membranes with the presence of O₂ and thus omit any unspecific oxidation.

We conducted calibrations of zymograms under oxic and anoxic conditions. Briefly, membranes (2 × 2 cm) were uniformly saturated during 30 min either with MUF solutions at increasing concentrations of 0, 0.01, 0.2, 0.5, 1, 2, 4, 6, 10 mM or with AMC solutions at increasing concentrations of 0, 0.01, 0.02, 0.05, 0.1, 0.2, 0.5, 1, 3, 5 mM and were photographed under UV light with the same camera settings as zymograms. The amount of MUF or AMC on an area basis (nmol cm⁻²) was calculated from MUF or AMC solution volume soaked by the membrane and its size. The calibration relates enzyme activities to the gray value of zymogram fluorescence. Each of these MUF or AMC solutions was also prepared in triplicate for two sets, one set was N₂-bubbled for 20 min and then used for calibration under anoxic conditions in the glovebox, and the other set without any pretreatment was used for calibration under oxic conditions.

2.3. Image processing and analysis

Zymograms were transformed to 8-bit gray scale images in ImageJ (Schindelin et al., 2012). Then, gray values were transformed to enzyme activities based on the calibration curves for MUF or AMC concentrations. Determination and separation of hotspots and cavities (poor or no attachment areas between soil surface and membrane) in images were processed according to the method proposed by Bilyera et al. (2020) in R (version 3.5.1, R development core team, 2014). Briefly, the two Gaussian component densities were fitted to the histogram of the gray value intensity using the *normalmixEM* function in the “mixtools” package (Benaglia et al., 2009) based on the expectation-maximization (EM) algorithm. We used parameters for the component with lower mean value to threshold cavities and with higher mean value to threshold hotspots. Hotspots were mapped in red on the original image by setting the threshold value using the ImageJ, then their area was calculated. After removal of cavities from zymograms, three compartments were selected for the analysis of enzyme activities: 1) top bulk (0–6 cm) – area from the soil surface which is at least 0.5 cm away from roots, 2) rooted (0–0.4 cm from outer root boundaries), and 3) bottom bulk (12–18 cm) – the area in the lower part of a rhizobox, which is at least 0.5 cm away from roots. After selection of each compartment, each pixel except the cavities was assigned to each compartment, and then the mean activity was calculated as the enzyme activity of the compartment. The location of every compartment was fixed as selection and used for paired zymograms under oxic and anoxic conditions. We plotted the profiles of the enzyme activity distribution as a function of distance from a geometrical root center on 3–5 visible and randomly selected roots, not overlapping with each other, and without cavities within 1 cm distance away from them. The geometrical root center and not a root surface was chosen as a starting point of a profile because of the

inability to correctly define the exact root diameter due to the low resolution of light images under high moisture conditions. Importantly, the same roots were always considered for oxic and anoxic conditions. A total of 9–15 root segments from 3 rhizoboxes were analyzed as replicates for each enzyme type and rice growth stage. The rhizosphere boundaries were set using a one-way ANOVA, followed by a Tukey's HSD test, to assess the differences between independent variables (mean enzyme activity of five adjacent pixels). Significant differences ($p < 0.05$) between two adjacent groups of 5 pixels were then considered as a boundary of rhizosphere extent (Hoang et al., 2016).

2.5. Statistical analysis

A three-way ANOVA was conducted to test the effects of factors of assay condition (AC), rice growth stage (RGS), and soil compartment (SC) on enzyme activities. A one-way ANOVA, followed by a Tukey's HSD test, was used to evaluate the significant differences ($p < 0.05$) for the percentage of hotspot area either between oxic and anoxic conditions of the same rice growth stage or between rice growth stages under the same measurement condition. For the elevation of the significant effect of initial assay conditions (transition from anoxic to oxic conditions or transition from oxic to anoxic) on the percentage of hotspot area and rhizosphere extent of the three rice growth stages, the number of replicates of each tested enzyme varied from $n = 5$ (rhizoboxes, transition from anoxic to oxic conditions) to $n = 4$ (rhizoboxes, transition from oxic to anoxic). The significance of the differences ($p < 0.05$) between $-O_2$ and $+O_2$ assays depending on the initial assay conditions was tested using a one-way ANOVA. All statistical tests were conducted using SPSS (Version 21, IBM, Armonk, NY, USA).

3. Results

3.1. Enzyme activities under anoxic and oxic conditions

Enzyme activities were calculated using calibration curves of MUF (Fig. S3a, b) or AMC (Fig. S3c, d) obtained under $-O_2$ and $+O_2$ conditions followed a power function ($r^2 \sim 0.946\text{--}0.963$) with given concentrations. The assay condition, rice growth stage, and soil compartment had effects on PME activity, while BG activity was affected by rice growth stage and soil compartment ($p < 0.05$, Table 1). The activities of the three tested enzymes were essentially suppressed by the short-term shift from anoxic to oxic conditions (Fig. 1, S4). Such suppression was the most pronounced for LAP (12–61%), followed by BG (4–52%) and PME (13–49%) (Fig. 2). The overall response of enzyme activities in rooted and bottom bulk soil to short-term aeration was stronger than in top bulk soil (Fig. 2). Such a suppression effect by O_2 was better pronounced at later stages of rice growth for BG, while at seedling and late tillering stages for PME and LAP (Fig. 2). There was a decreasing trend for the relative difference in the activities of the three tested enzymes between $-O_2$ and $+O_2$ assays with the transition from oxic to anoxic vs. the transition from anoxic to oxic

zymography conditions (Fig. 1).

Table 1 Effects of assay condition (AC), rice growth stage (RGS), soil compartment (SC), and their interactions on the activities of phosphomonoesterase (PME), β -glucosidase (BG), and leucine aminopeptidase (LAP) analyzed by three-way ANOVA

	Statistic	AC	RGS	SC	AC \times RGS	AC \times SC	RGS \times SC	AC \times RGS \times SC
PME	F	39.741	215.300	17.150	18.180	0.600	11.511	0.450
	P	< 0.001	< 0.001	< 0.001	< 0.001	0.554	< 0.001	0.772
BG	F	3.700	10.466	10.810	0.555	0.081	1.530	0.073
	P	0.062	< 0.001	< 0.001	0.579	0.923	0.214	0.990
LAP	F	2.396	0.734	0.509	0.416	0.087	0.058	0.007
	P	0.130	0.487	0.605	0.663	0.917	0.993	1.000

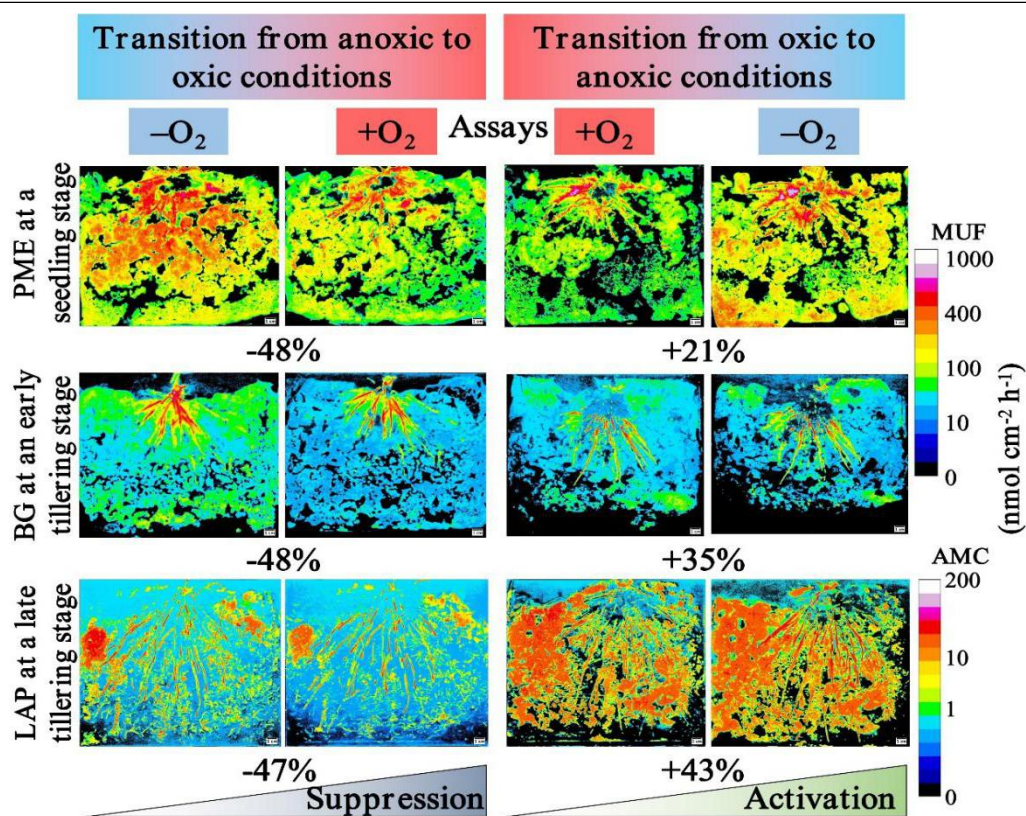


Fig. 1 Examples of zymograms with spatial distribution of phosphomonoesterase (PME), β -glucosidase (BG), and leucine aminopeptidase (LAP) activities under oxic (+O₂) and anoxic (–O₂) conditions at seedling, early-, and late tillering stages of rice growth. Cavities (poor attachment) are shown as black area. Calibration scale bars on the right side correspond to 4-methylumbelliferone (MUF) representing PME and BG activities (top) and to 7-amino-4-methylcomarin (AMC) representing LAP activity (bottom). Triangles and percentage values below images correspond either to suppression of enzyme activities due to aeration or activation of enzyme activities due to removal of O₂. For demonstration, one of three replicates and one of rice growth stages were chosen; the complete set of zymograms is shown on Fig. S3.

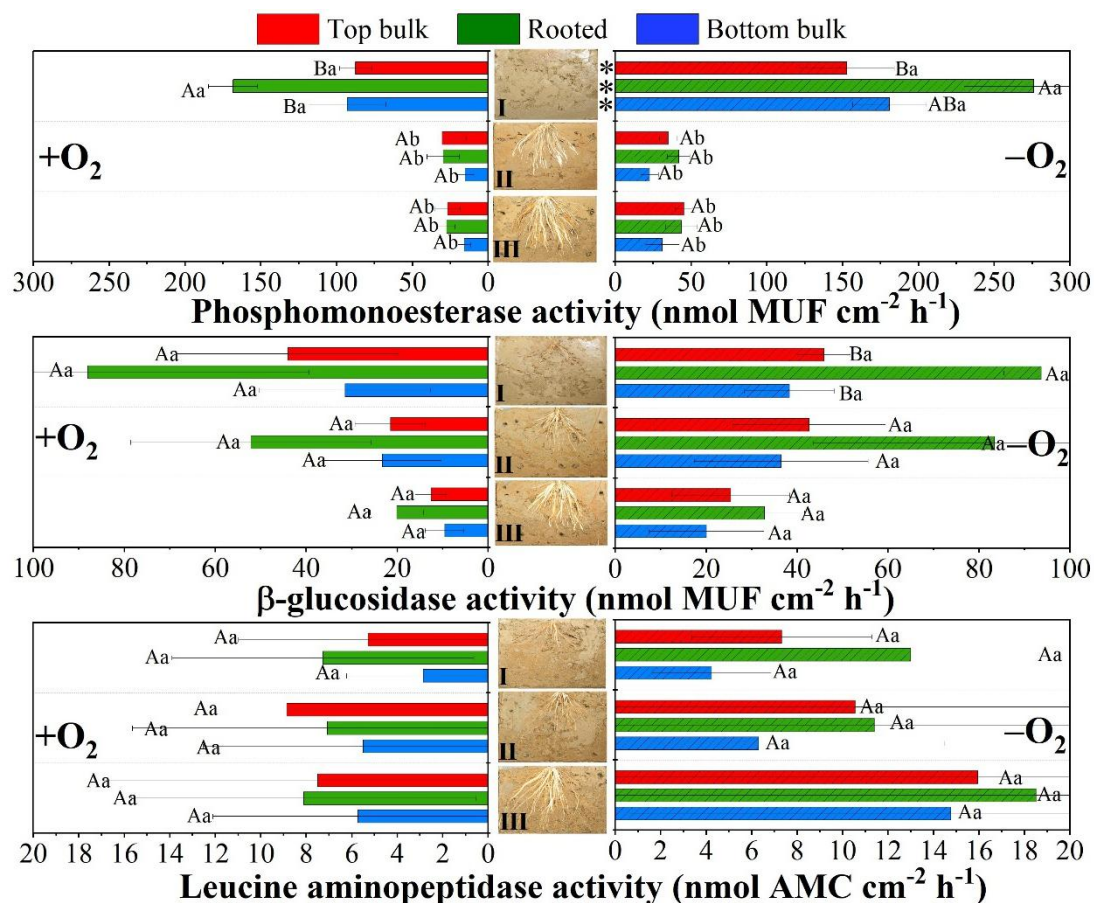


Fig. 2 The zymogram-based activities of phosphomonoesterase (PME), β -glucosidase (BG), and leucine aminopeptidase (LAP) at three soil compartments (top bulk, rooted, and bottom bulk soils) under oxic (+O₂) and anoxic (-O₂) conditions at three stages (seedling (I), early- (II) and late tillering (III) stage) of rice growth. The data are shown as the means \pm standard deviations ($n = 3$) of respective zymograms (Fig. 1 and S3). The results of effects of assay condition, rice growth stage, soil compartment, and their interactions on enzyme activities analyzed by three-way ANOVA can be found in Table 1. Different uppercase or lowercase letters represent significant differences ($p < 0.05$) among three compartments at the same rice growth stage or among three rice growth stages of each compartment, respectively. Significant differences ($p < 0.05$) between +O₂ and -O₂ assays are indicated by asterisk.

3.2. Hotspot area under anoxic and oxic conditions

The percentage of hotspot area was repeatedly higher for all enzymes under oxic vs. anoxic assay conditions. The strongest increase in hotspot area was observed for all three enzymes in +O₂ assays at seedling (59–128%) stage of rice growth compared to -O₂ assays, followed by late- (18–67%) and early (3–12%) tillering stages (Fig. 3). The relative difference in the percentage of hotspot area between -O₂ and +O₂ assays of the three tested enzymes tended to be higher with the transition from oxic to anoxic vs. the transition from anoxic to oxic conditions (Fig. S5).

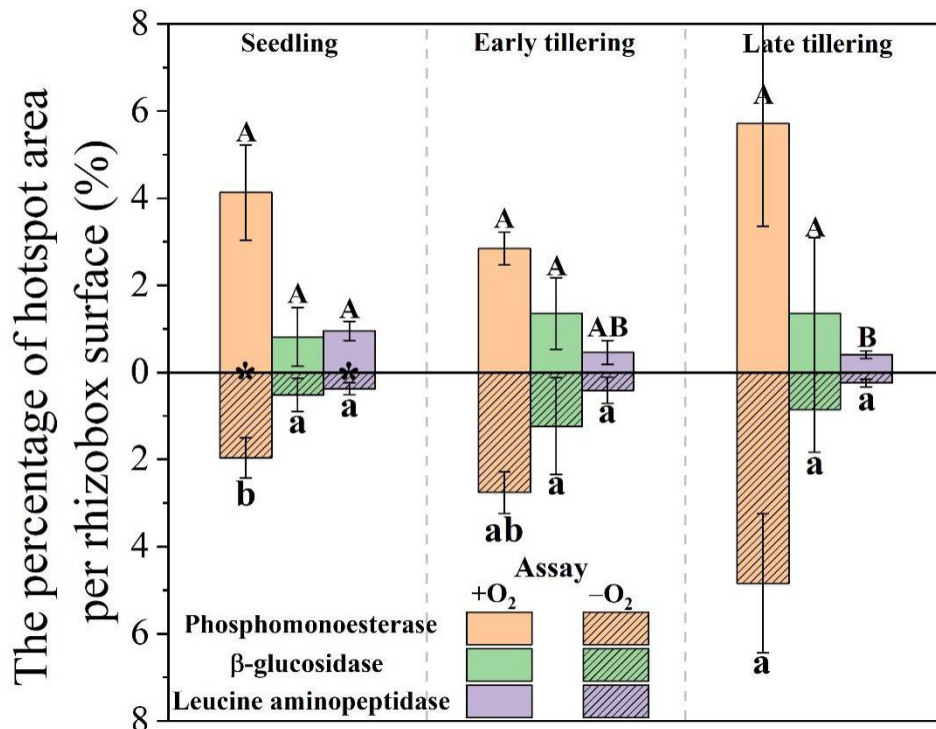


Fig. 3 The percentage of hotspot area per rhizobox surface for phosphomonoesterase, β -glucosidase, and leucine aminopeptidase under oxic (+O₂) and anoxic (-O₂) conditions at the three rice growth stages. Significant differences ($p < 0.05$) between oxic and anoxic assays are indicated by asterisk. Different uppercase or lowercase letters represent significant differences ($p < 0.05$) among three rice growth stages under +O₂ or -O₂ conditions, respectively.

3.3. Rhizosphere extent under anoxic and oxic conditions

The rhizosphere extent of PME, BG, and LAP activities from the root center were enzyme- and moisture condition specific (Fig. 4a, b, c). The distribution of hotspot area of PME as a function of distance from the geometrical root center was broader (0.9–2.7 mm) compared with that of hotspot BG (1.2–2.6 mm) and LAP (1.0–1.6 mm) activity (Fig. 4a, b, c). The rhizosphere extent of PME, BG, and LAP activities from the root center were respectively broader by 8–80%, 19–30%, and 15–32% in -O₂ assays than in +O₂ assays (Fig. 4a, b, c). With rice growth, the rhizosphere extent at tillering stage narrowed by 34–40% in +O₂ assays and 60–63% in -O₂ assays for PME activities as compared to a seedling stage, by 23–41% and 26–47% for BG, and by 14–20% and 25–30% for LAP, respectively (Fig. 4a, b, c). The relative difference in the rhizosphere extent of three tested enzymes as a function of distance from the geometrical root center between -O₂ and +O₂ assays was significantly higher with the transition from oxic to anoxic vs. the transition from anoxic to oxic conditions (Fig. 4d).

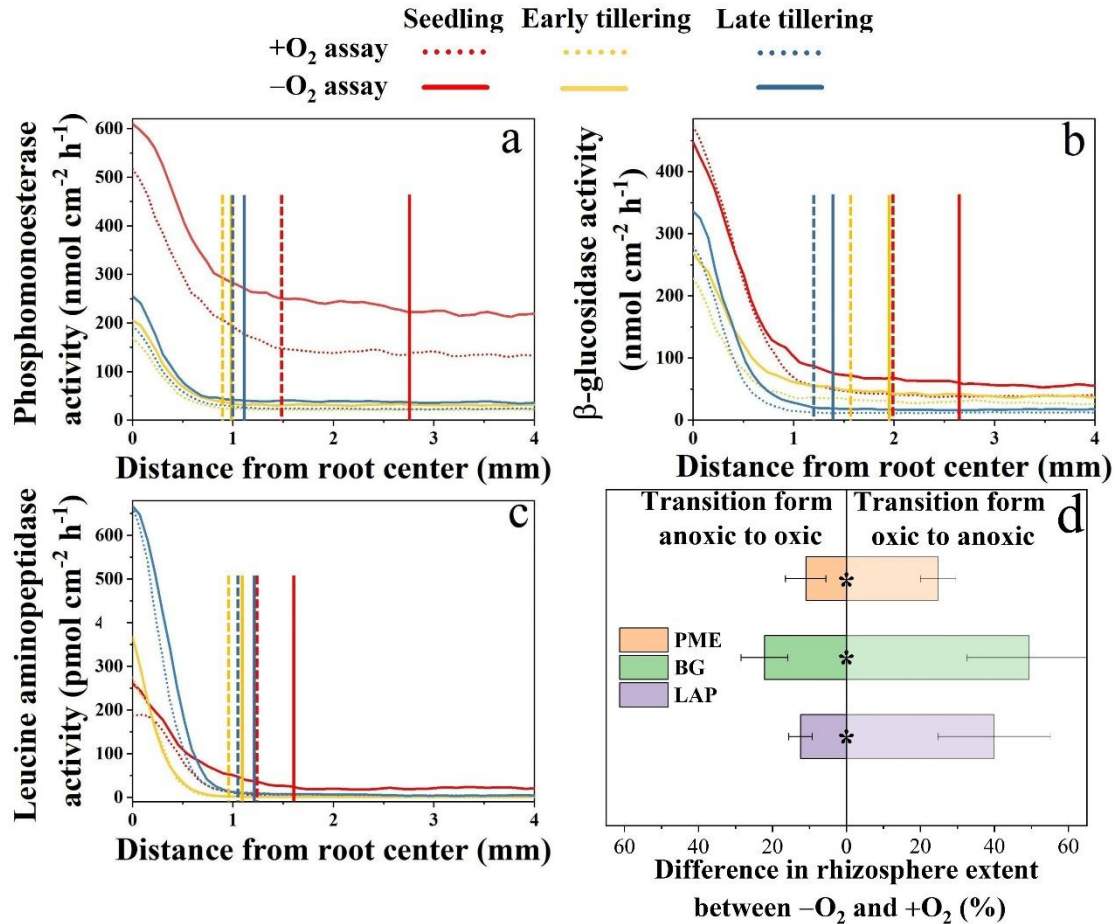


Fig. 4 The rhizosphere gradient and extent of phosphomonoesterase (a), β -glucosidase (b), and leucine aminopeptidase (c) activities as a function of distance from root center under oxic (+O₂) and anoxic (-O₂) conditions, and the difference in rhizosphere extent (%) between -O₂ and +O₂ assays depending on initial conditions – either first -O₂ and then +O₂ (transition from anoxic to oxic) or *vice versa* (transition from oxic to anoxic) (d). Each curve refers to the mean activity of each enzyme measured at 9-15 roots in the three replicated zymograms. The vertical lines (dashed for +O₂ and solid for -O₂) mark the border between rhizosphere and bulk soil as defined by one-way ANOVA. The differences in rhizosphere extent are shown as the means \pm standard deviations of the three rice growth stages (n = 5 (rhizoboxes) under the transition from anoxic to oxic conditions and n = 4 (rhizoboxes) under the transition from oxic to anoxic conditions). Significant differences ($p < 0.05$) between the transition from anoxic to oxic conditions and the transition from oxic to anoxic conditions are indicated by asterisk.

4. Discussion

4.1. Effect of short-term aeration on the spatial distribution of enzyme activities

The systematical decrease in the activities of three studied enzymes was observed under oxic vs. anoxic conditions during short-term (35 min) aeration (Fig. 2).

This is in line with the findings that the activities of hydrolytic enzymes in flooded paddy soils were lower by 5–43% under oxic vs. anoxic conditions (Wang et al., 2022a, b) and supports our first hypothesis. There are two mechanisms which may directly or indirectly be responsible for the decreased activities of hydrolytic enzymes with the increasing O₂ concentrations: (i) The directly suppressive effect of O₂ may be explained by O₂ toxicity (i.e., the formation of reactive oxygen species (ROS) including superoxide and peroxide as a result of molecular O₂ reduction) for anoxic microorganisms and reduction/loss of their ability to produce enzymes. Short-term (2.5 h) aeration increased the activities of peroxidases and phenol oxidases by 2–14 times thereby supporting the concept of increased ROS formation (Wang et al., 2022a). (ii) The indirect mechanism of the hydrolytic enzyme activities suppression by O₂ can be linked to a shift of microbial metabolic pathways under changing redox conditions (Megonigal et al., 2004; Sinsabaugh, 2010; Yang et al., 2021).

Short-term aeration increased the percentage of hotspot area for PME and LAP compared to anoxic treatment (Fig. 3). This difference was significant during the seedling stage, whereas with rice growth, the aeration did not cause any strong effect on distribution and intensity of enzyme hotspots. Therefore, the first hypothesis about a suppressive effect of short-term aeration on enzyme hotspot area was not supported. We suggest two possible reasons of such observations. (i) Enzymatic hotspots are mainly attributed to rhizosphere with overall higher microbial abundance and activity due to continuous input of root exudates as compared to the bulk soil (Kuzyakov and Blagodatskaya, 2015). Roots of wetland plants including rice are supplied via aerenchyma with atmospheric O₂ which is diffusing into the anoxic environment. Long-term availability of O₂ in the close vicinity to roots of rice should cause an adaptive effect on rhizosphere microorganisms and enzyme activities. This is why anoxic bulk soil microbial communities were suppressed by aeration during zymography, while rhizosphere microbial activities were weakly affected (Fig. 1). This explains the finding that no differences in the percentage of hotspot area were observed at a tillering stage of rice growth (Fig. 3). (ii) Another reason which can explain the increase of hotspot area with aeration is related to the algorithm of hotspots identification. Thus, we estimated a decreased threshold for the identification of hotspots by 0–12% mainly due to differences in bulk soil activities between +O₂ and -O₂ assays. By definition, the hotspot is an area of enzyme activity that is higher by three times of a standard deviation (SD) than mean enzyme activity estimated for the whole zymogram (Bilyera et al., 2020). The lower the difference between hotspot activity and the mean activity of a zymogram, the smaller is the hotspot area. This is why the difference in hotspot identification rather than actual increase in microbial metabolic activity or relatively higher concentration of substrates may explain the higher hotspot area. As a potential outcome, the models of organic matter transformation and nutrient cycling based on hotspot dynamics in anoxic ecosystems but measured under oxic conditions may presumably underestimate the enzymatic reaction rate and overestimate the area with relatively high reaction rate and substrate availability. Therefore, a systematic study addressing the issue of hotspot identification in relation to background change will be necessary to answer the

question.

Short-term aeration resulted in a narrower enzymatic rhizosphere extent as compared to anoxic assays (Fig. 4). This may have implications for other studies where the actual rhizosphere extent was most probably underestimated for paddy soils when measured under oxic conditions (Ge et al., 2017). Accordingly, incorrect rhizosphere extents will give biased input to the models established for anoxic ecosystems (Ge et al., 2017) due to the underestimation of the area with a high reaction rate on the premise that oxygen and hydrolytic enzymes are completely decoupled at a biochemical level. Generally, phosphomonoesterase and β -glucosidase had broader rhizosphere extents than leucine aminopeptidase (Fig. 4). Interestingly, the short-term aeration suppressed phosphomonoesterase and β -glucosidase more strongly than leucine aminopeptidase. This may suggest that anoxic enzyme systems of P and C cycling are more sensitive to O_2 than the N-acquiring enzymes. Current methods and models on rhizosphere processes in anoxic ecosystems (Ge et al., 2017; Wei et al., 2019a, b) did not account for short-term aeration effects on enzyme-specific activities and rhizosphere extents. Such conditions, however, are typical for e.g. paddy soils after draining or topsoil of wetlands and peatlands during drought events. Therefore, we recommend considering the potential bias in calculations when ignoring the observed short-term aeration effects on established anoxic systems.

4.2. Effects of rice growth stage and aeration conditions during zymography on enzyme activity distribution

In line with the second hypothesis, the overall higher enzyme activities were observed in the rhizosphere as compared to bulk soil under both oxic and anoxic conditions (Figs 1, 2, S4). Such an increase in enzyme activity was most likely due to intensive microbial metabolism and root exudation in the rhizosphere (Bradford et al., 2008; Kuzyakov and Blagodatskaya, 2015; Ge et al., 2017).

The activities of phosphomonoesterase and β -glucosidase decreased with rice growth, while leucine aminopeptidase activity demonstrated the opposite trend (Fig. 2). The temporal dynamics of hydrolytic enzyme activities were therefore enzyme-specific. We expected a weaker suppressive effect of the short-term aeration on the enzyme activities in rooted soil with rice growth as compared with bulk soil because of the increasing biomass of aerenchymatous roots delivering air belowground and higher adaption of rhizosphere microorganisms to O_2 (Larsen et al., 2015). Our expectations were supported by phosphomonoesterase activity (Fig. 2, top). The activities of β -glucosidase and leucine aminopeptidase in rooted soil did not differ between the tillering and the seedling stages (Fig. 2, middle and bottom). This demonstrates that the effects of root-released O_2 on enzyme activities were enzyme-specific. It is therefore unlikely that natural O_2 gradient with rice growth was a major factor affecting enzyme activities in this study. Rice plants regulate the rhizosphere processes as demonstrated by decreased rhizosphere extents with rice growth (Fig. 4). This contradicts the statement of Kuzyakov and Razavi (2019) about

the general phenomenon of rhizosphere stationarity with a plant growth that was made mostly for plants evaluated under oxic conditions. Such a changed pattern indicates either shift in root exudate quality of rice plants or change in their strategies to acquire nutrients with growth (Grossmann et al., 2011).

It is important to note that the initial conditions under which the zymography was performed – oxic or anoxic – had no effects on the enzyme activity and hotspot area (Fig. 1, S5). Therefore, we can conclude that the short-term suppressive effect of O₂ on enzymatic activities in rice paddy system is reversible. This may imply that the anoxic microbial community possesses the ability to reestablish from the suppression by short-term aeration. This is supported by the findings that microbial biomass and composition in a humid tropical forest soil did not change with short-term redox fluctuation under alternating flushing with between air and N₂ every 12 h (Pett-Ridge et al., 2006).

4.3. Which other factors do matter for soil zymography under anoxic conditions?

As shown on zymograms (Fig. 1, S4), the cavities lacking proper attachment between membrane and soil surface resulted in the absence of fluorescent signal (at 355–460 nm). Generally, a membrane attachment to the soil surface is still a methodological issue for zymography application (Razavi et al., 2019). A relatively high percentage of cavities, especially at the seedling stage, was related to the increased water content causing strong stickiness of the soil surface to the rhizoboxes cover plates. An ultimate need to open a rhizobox for zymography prevents to solve such a constraint of the method. At least, the combination of laser scanning and soil zymography could be helpful to identify areas with cavities and clearly differentiate them from the low activity areas of proper attachment (Guber et al., 2018).

Another critical factor that can affect the spatial distribution of enzyme activities during zymography is soil moisture (Guber et al., 2018; Ahmadi et al., 2018). The diffusion of substrates from the membrane to the soil surface through Brownian motion as well as products of catalysis backwards depends strongly on the soil moisture during zymography (Razavi et al., 2019). Thus, the higher soil moisture at the seedling stage could cause the broader rhizosphere extents for the three tested enzymes (Fig. S2) as compared to both tillering stages (Fig. 3). Moreover, we observed the same effect of soil moisture on rhizosphere extents for leucine aminopeptidase activity in one out of three replicates having substantially higher soil moisture (Fig. S2, S4). Still, it is important to note, that despite the observed methodological constraints the suppressive effect of O₂ on enzyme activities was generally independent from soil moisture (Fig. 2).

5. Conclusions

Short-term (35 min) aeration strongly suppressed the *in-situ* activity of anoxic hydrolytic enzymes by 4–61% in flooded paddy rice microcosms. Thus, applying zymography in natively low-oxygen systems under anoxic conditions using a

glovebox is a more accurate method to assess to enzyme activities and microbial hotspots. In addition to the activity, the enzyme-specific rhizosphere extents decreased in the presence of O₂, indicating that short-term aeration reduced the root's capacity to enhance enzyme activities in a large distance to the root, thus diminishing its capability for an extended rhizosphere area. At the same time, even slight increase in the enzymatic hotspot area with aeration was observed. Accordingly, the determination of the enzyme activity and hotspots localization in anoxic systems due to short-term aeration could cause an underestimation of the reaction rate of the biochemical processes in bulk soil and an overestimation of the microbial metabolic hotspot area in the rhizosphere. Given that a short-term aeration generally occurs in natural anoxic systems and during the measurement of samples taken from anoxic environments, it is important to consider the suppression of enzyme activities and overestimation of hotspot area by short-term O₂ exposure.

Acknowledgments

The authors gratefully acknowledge the China Scholarship Council (CSC) for financial support for Chaoqun Wang. The study was supported by the research grant from German Research Foundation (DFG Do 1533/3-1).

References

- Ahmadi, K., Razavi, B.S., Maharjan, M., Kuzyakov, Y., Kostka, S.J., Carminati, A., Zarebanadkouki, M., 2018. Effects of rhizosphere wettability on microbial biomass, enzyme activities and localization. *Rhizosphere* 7, 35–42.
- Alexander, M., 1977. *An introduction to soil microbiology*. Wiley, New York.
- Bai, R., Xi, D., He, J.Z., Hu, H.W., Fang, Y.T., Zhang, L.M., 2015. Activity, abundance and community structure of anammox bacteria along depth profiles in three different paddy soils. *Soil Biol. Biochem.* 91, 212–221.
- Baveye, P., Otten, W., Kravchenko, A., Romero, M.B., Beckers, E., Chalhoub, M., Darnault, C., Eickhorst, T., Garnier, P., Hapca, S., Kiranyaz, S., Monga, O., Muller, C., Nunan, N., Pot, V., Schlüter, S., Schmidt, H., Vogel, H.J., 2018. Emergent properties of microbial activity in heterogeneous soil microenvironments: Different research approaches are slowly converging, yet major challenges remain. *Fron. Microbiol.* 9, 1929.
- Benaglia, T., Chauveau, D., Hunter, D.R., Young, D.S., 2009. Mixtools: An R package for analyzing finite mixture models. *J. Stat. Softw.* 32, 1–29.
- Bilyera, N., Kuyzakova, I., Guber, A., Razavi, B.S., Kuzyakov, Y., 2020. How “hot” are hotspots: statistically localizing the high-activity areas on soil and rhizosphere images. *Rhizosphere* 16, 100259.
- Bilyera, N., Zhang, X.C., Duddek, P., Fan, L.C., Banfield, C.C., Schlüter, S., Carminati, A., Kaestner, A., Ahmed, M.A., Kuzyakov, Y., Dippold, M.A., Spielvogel, S., Razavi, B.S., 2021. Maize genotype-specific exudation strategies: An adaptive mechanism to increase microbial activity in the rhizosphere. *Soil Biol. Biochem.* 162, 108426.
- Cosgrove, D.J., 1980. *Inositol phosphates—their chemistry, biochemistry and physiology*. Amsterdam: Elsevier Scientific.
- Deangelis, K.M., Silver, W.L., Thompson, A.W., Firestone, M.K., 2010. Microbial communities acclimate to recurring changes in soil redox potential status. *Environ. Microbiol.* 12(12), 3137–3149.
- Ge, T.D., Wei, X.M., Razavi, B.S., Zhu, Z.K., Hu, Y.J., Kuzyakov, Y., Jones D.L., Wu, J.S., 2017. Stability and dynamics of enzyme activity patterns in the rice rhizosphere: Effects of plant growth and temperature. *Soil Biol. Biochem.* 113, 108–115.
- Gong, Z.T., Zhang, G.L., Chen, Z.C. (Eds.), 2007. *Pedogenesis and Soil Taxonomy*. Science Press, Beijing, China, pp. 613–626.
- Gonzalez-Flecha, B., Demple, B., 1995. Metabolic sources of hydrogen peroxide in aerobically growing *Escherichia coli*. *J. Biol. Chem.* 270, 13681–13687.

- Grossmann, G., Guo, W.J., Ehrhardt, D.W., Frommer, W.B., Sit, R.V., Quake, S.R., Meier, M., 2011. The RootChip: an integrated microfluidic chip for plant science. *Plant Cell* 23, 4234–4240.
- Guber, A., Kravchenko, A., Razavi, B.S., Uteau, D., Kuzyakov, Y., 2018. Quantitative soil zymography: mechanisms, processes of substrate and enzyme diffusion in porous media. *Soil Biol. Biochem.* 127, 156–167.
- Guber, A., Blagodatskaya, E., Juyal, A., Razavi, B.S., Kravchenko, A., 2021. Time-lapse approach: correcting deficiencies of 2D soil zymography. *Soil Biol. Biochem.* 157, 108225.
- Hartman, W.H., Ye, R., Horwath, W.R., Tringe, S.G., 2017. A genomic perspective on stoichiometric regulation of soil carbon cycling. *ISME J.* 11, 2652.
- Henry, F., Anne, T., Mohamed, S., Sophie, L.R., Patrick, D., 2018. Biochemical and microbial changes reveal how aerobic pre-treatment impacts anaerobic biodegradability of food waste. *Waste Manag.* 80, 119–129.
- Hinsinger, P., Bengough, A., Vetterlein, D., Young, I., 2009. Rhizosphere: biophysics, biogeochemistry and ecological relevance. *Plant Soil* 321, 117–152.
- Hoang, D.T.T., Razavi, B.S., Kuzyakov, Y., Blagodatskaya, E., 2016. Earthworm burrows: kinetics and spatial distribution of enzymes of C-, N- and P- cycles. *Soil Biol. Biochem.* 99, 94–103.
- Keuskamp, J.A., Feller, I.C., Laanbroek, H.J., Verhoeven, J.T.A., Hefting, M.M., 2015. Short- and long-term effects of nutrient enrichment on microbial exoenzyme activity in mangrove peat. *Soil Biol. Biochem.* 81, 38–47.
- Kuzyakov, Y., Blagodatskaya, E., 2015. Microbial hotspots and hot moments in soil: Concept & review. *Soil Biol. Biochem.* 83, 184–199.
- Kuzyakov, Y., Razavi, B.S., 2019. Rhizosphere size and shape: temporal dynamics and spatial stationarity. *Soil Biol. Biochem.* 135, 343–360.
- Larsen, M., Santner, J., Oburger, E., Wenzel, W.W., Glud, R.N., 2015. O₂ dynamics in the rhizosphere of young rice plants (*Oryza sativa* L.) as studied by planar optodes. *Plant Soil* 390(1), 279.
- Li, H., Yang, X., Weng, B., Su, J., Nie, S., Gilbert, J.A., Zhu, Y.G., 2016. The phenological stage of rice growth determines anaerobic ammonium oxidation activity in rhizosphere soil. *Soil Biol. Biochem.* 100, 59–65.
- Ma, X., Liu, Y., Shen, W., Kuzyakov, Y., 2021. Phosphatase activity and acidification in lupine and maize rhizosphere depend on phosphorus availability and root properties: coupling zymography with planar optodes. *Appl. Soil Ecol.* 167, 104029.
- Megonigal, J.P., Hines, M.E., and Visscher, P.T., 2004. Anaerobic metabolism: linkages to trace gases and aerobic processes. *Biogeochemistry* 8, 417–424.

- Pett-Ridge, J., Silver, W.L., Firestone, M.K., 2006. Redox fluctuations frame microbial community impacts on N-cycling rates in a humid tropical forest soil. *Biogeochemistry* 81(1), 95–110.
- R Development Core Team, 2014. R: a language and environment for statistical computing, R Foundation for Statistical Computing.
- Razavi, B.S., Zarebanadkouki, M., Blagodatskaya, E., Kuzyakov, Y., 2016. Rhizosphere shape of lentil and maize: spatial distribution of enzyme activities. *Soil Biol. Biochem.* 96, 229–237.
- Razavi, B.S., Zhang, X.C., Bilyera, N., Guber, A., Zarebanadkouki, M., 2019. Soil zymography: simple and reliable? Review of current knowledge and optimization of method. *Rhizosphere* 11, 100161.
- Sanaullah, M., Blagodatskaya, E., Chabbi, A., Rumpel, C., Kuzyakov, Y., 2011. Drought effects on microbial biomass and enzyme activities in the rhizosphere of grasses depend on plant community composition. *Appl. Soil Ecol.* 48(1), 38–44.
- Schindelin, J., Arganda-Carreras, I., Frise, E., Kaynig, V., Longair, M., Pietzsch, T., Preibisch, S., Rueden, C., Saalfeld, S., Schmid, B., Tinevez, J.Y., White, D.J., Hartenstein, V., Eliceiri, K., Tomancak, P., Cardona, A., 2012. Fiji: an open-source platform for biological-image analysis. *Nat. Methods* 9, 676–682.
- Sinsabaugh, R.L., 2010. Phenol oxidase, peroxidase and organic matter dynamics of soil. *Soil Biol. Biochem.* 42, 391–404.
- Spohn, M., Carminati, A., Kuzyakov, Y., 2013. Soil zymography – a novel *in situ* method for mapping distribution of enzyme activity in soil. *Soil Biol. Biochem.* 58, 275–280.
- Tecon, R., Or, D., 2017. Biophysical processes supporting the diversity of microbial life in soil. *FEMS Microbiol. Rev.* 41, 599–623.
- Tian, P., Razavi, B.S., Zhang, X., Wang, Q., Blagodatskaya, E., 2019. Microbial growth and enzyme kinetics in rhizosphere hotspots are modulated by soil organics and nutrient availability. *Soil Biol. Biochem.* 141, 107662.
- Wang, C., Blagodatskaya, E., Dippold, M.A., Dorodnikov, M., 2022a. Keep oxygen in check: Contrasting effects of short-term aeration on hydrolytic versus oxidative enzymes in paddy soils. *Soil Biol. Biochem.* 169, 108690.
- Wang, C., Dippold, M.A., Blagodatskaya, E., Dorodnikov, M., 2022b. Oxygen matters: Short-and medium-term effects of aeration on hydrolytic enzymes in a paddy soil. *Geoderma* 407, 115548.
- Wang, C., Xue, L., Dong, Y., Jiao, R., 2021a. Soil organic carbon fractions, C-cycling hydrolytic enzymes, and microbial carbon metabolism in Chinese fir plantations. *Sci. Total Environ.* 758, 143695.
- Wang, C., Xue, L., Jiao, R., 2021b. Soil phosphorus fractions, phosphatase activity,

- and the abundance of *phoC* and *phoD* genes vary with planting density in subtropical Chinese fir plantations. *Soil. Till. Res.* 209(4), 104946.
- Wang, Y., Wang, H., He, J.S., Feng, X., 2017. Iron-mediated soil carbon response to water-table decline in an alpine wetland. *Nat. Commun.* 8, 1–9.
- Wei, X., Ge, T., Zhu, Z., Hu, Y., Liu, S., Li, Y., Wu, J., Razavi, B., 2019a. Expansion of rice enzymatic rhizosphere: temporal dynamics in response to phosphorus and cellulose application. *Plant Soil* 445, 169–181.
- Wei, X., Razavi, B.S., Hu, Y., Xu, X., Zhu, Z., Liu, Y., Kuzyakov, Y., Li, Y., Wu, J.S., Ge, T.D., 2019b. C/P stoichiometry of dying rice root defines the spatial distribution and dynamics of enzyme activities in root-detritusphere. *Biol. Fertil. Soils* 55, 251–263.
- Wen, Y., Zang, H.D., Ma, Q.X., Evans, C.D., Chadwick, D.R., Jones, D.L., 2019. Is the ‘enzyme latch’ or ‘iron gate’ the key to protecting soil organic carbon in peatlands? *Geoderma*, 349, 107–113.
- Yang, L., Campbell, A.N., Bhattacharyya, A., Didonato, N., Pett-Ridge, J., 2021. Differential effects of redox conditions on the decomposition of litter and soil organic matter. *Biogeochemistry* 154, 1–15.

Supplementary

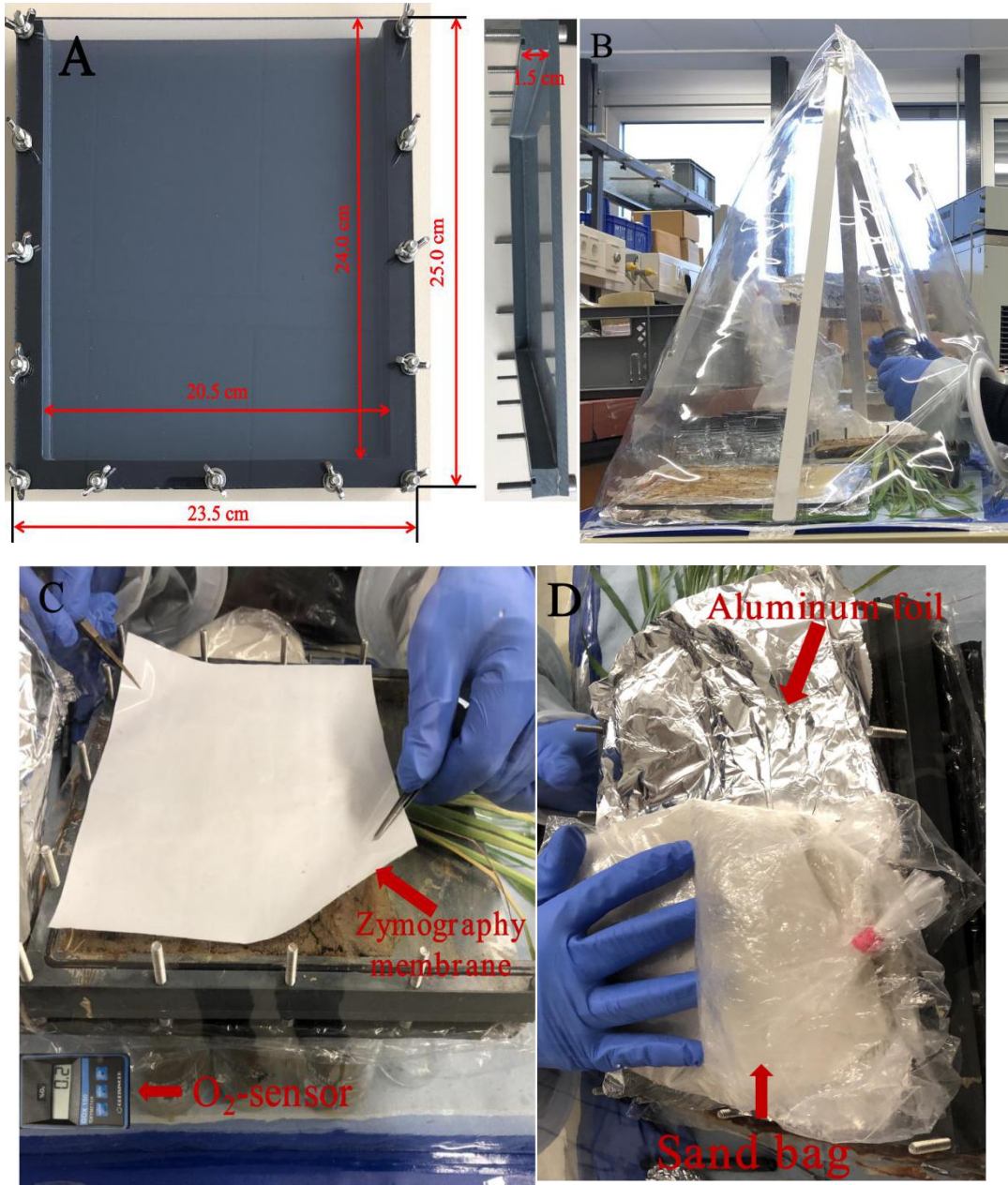


Fig. S1 The dimensions of a rhizobox with plexiglas cover on top, sealed with rubber gasket (not visible on photo) and fixed by thumbscrews (A), a portable PVC glovebox filled with N₂ and with rhizoboxes inside (B), a substrate saturated zymography membrane and the O₂ level as indicated by an O₂-sensor (C), a saturated membrane covered with an aluminum foil and pressed by a sand bag (D).

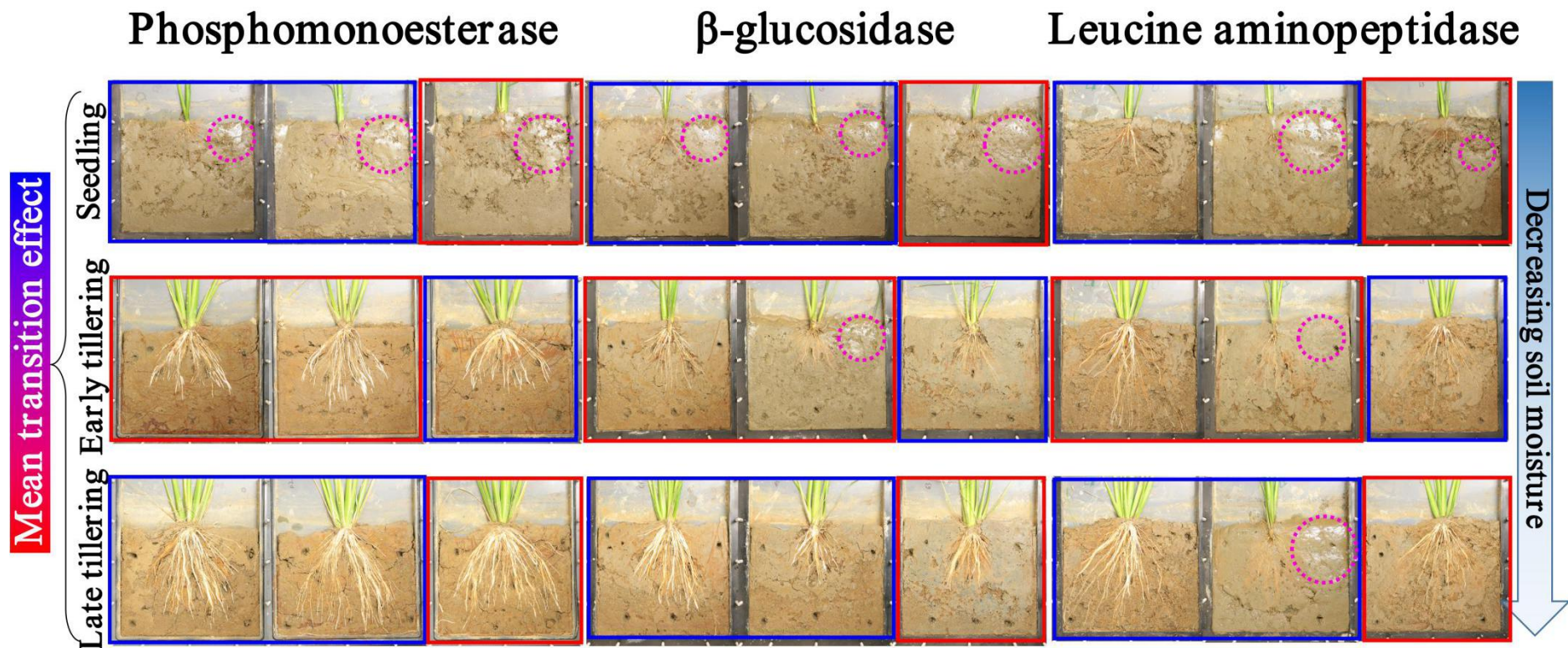


Fig. S2 Light photos of the rhizoboxes' soil surface assayed for phosphomonoesterase, β -glucosidase, and leucine aminopeptidase activities at seedling, early-, and late tillering stages of rice growth. Arrow on the right side reflects soil moisture decrease with the rice growth stages. Dashed purple circles on images indicate relatively higher moisture of soil among rice growth stages and between replicates. Rhizoboxes with blue frame were first exposed to anoxic and then to oxic zymography ("transition from anoxic to oxic conditions") during an assay. Rhizoboxes with red frame were first exposed to oxic and then to anoxic zymography ("transition from oxic to anoxic conditions"). The effect of transition was tested as the mean among rice growth stages separately for initial oxic ($n = 4$) or anoxic ($n = 5$) conditions for each of the enzymes.

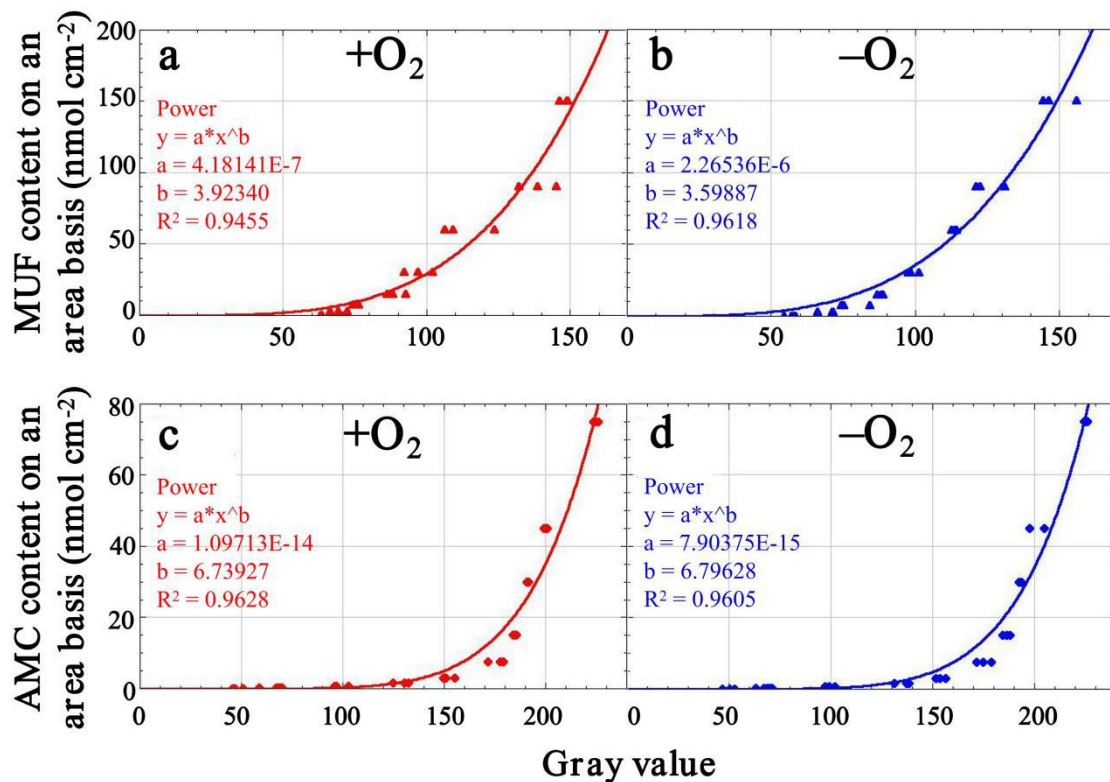


Fig. S3 Calibration curves of 4-methylumbelliferone (MUF, a and b) and 7-amino-4-methylcoumarin (AMC, c and d) gray value under anoxic (-O₂) and oxic (+O₂) conditions. There was no significant difference ($P < 0.05$) between parameters a and b of the functions under +O₂ and -O₂ for MUF and AMC.

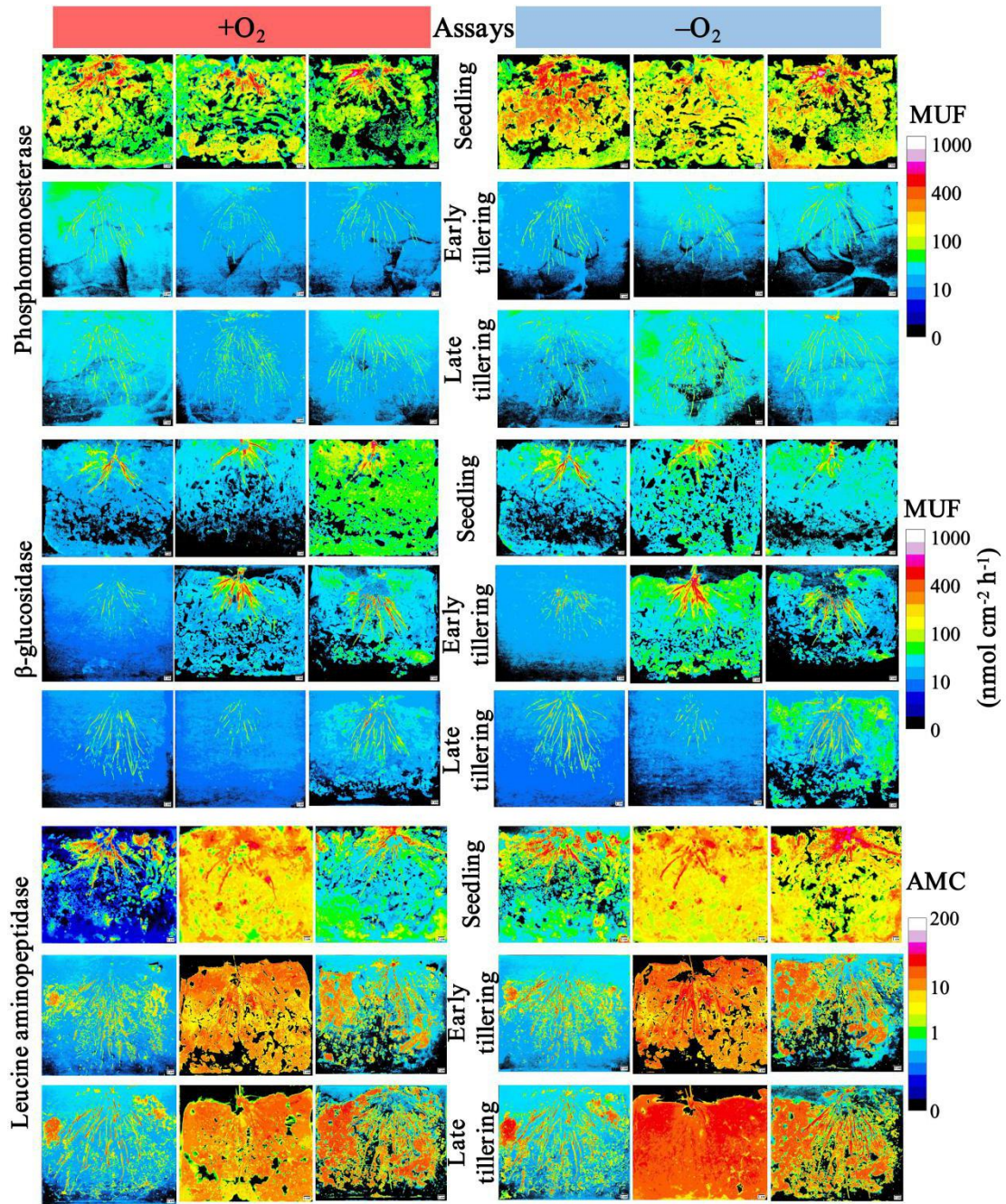


Fig. S4 Spatial distribution of phosphomonoesterase, β -glucosidase, and leucine aminopeptidase activities in oxic (+O₂) and anoxic (-O₂) assays at seedling, early-, and late tillering stages of rice growth. Cavities are shown as black area. Calibration scale bar on the right side is proportional to phosphomonoesterase and β -glucosidase activities and leucine aminopeptidase activity.

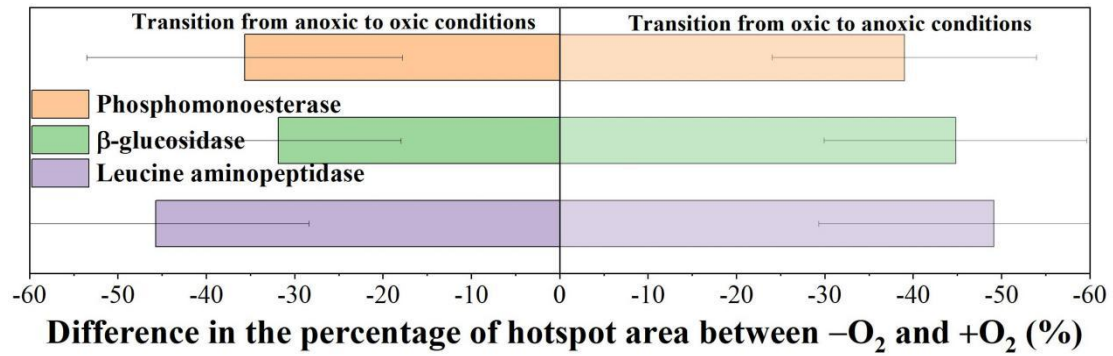


Fig. S5 The difference in the percentage of hotspot area of phosphomonoesterase, β -glucosidase, and leucine aminopeptidase between anoxic ($-O_2$) and oxic ($+O_2$) assays with different aeration conditions under which zymography was initially performed. The data are shown as the means \pm standard deviations ($n = 5$ under the transition from anoxic to oxic conditions and $n = 4$ under the transition from oxic to anoxic conditions).

Study 4 Can the reductive dissolution of ferric iron in paddy soils compensate phosphorus limitation of rice plants and microorganisms?

Chaoqun Wang^{a,*}, Lukas Thielemann^a, Michaela A. Dippold^{a,b}, Georg Guggenberger^c, Yakov Kuzyakov^{d,e}, Callum C. Banfield^{a,b}, Tida Ge^f, Stephanie Guenther^c, Patrick Bork^g, Marcus A. Horn^g, Maxim Dorodnikov^{a,d}

^a Biogeochemistry of Agroecosystems, University of Goettingen, 37077 Goettingen, Germany

^b Geo-Biosphere Interactions, University of Tuebingen, 72076 Tuebingen, Germany

^c Institute of Soil Science, Leibniz University Hannover, 30419 Hannover, Germany

^d Department of Soil Science of Temperate Ecosystems, University of Goettingen, 37077 Goettingen, Germany

^e Agricultural Soil Science, University of Goettingen, 37077 Goettingen, Germany

^f State Key Laboratory for Managing Biotic and Chemical Threats to the Quality and Safety of Agro-products, Institute of Plant Virology, Ningbo University, 315211 Ningbo, Zhejiang, China

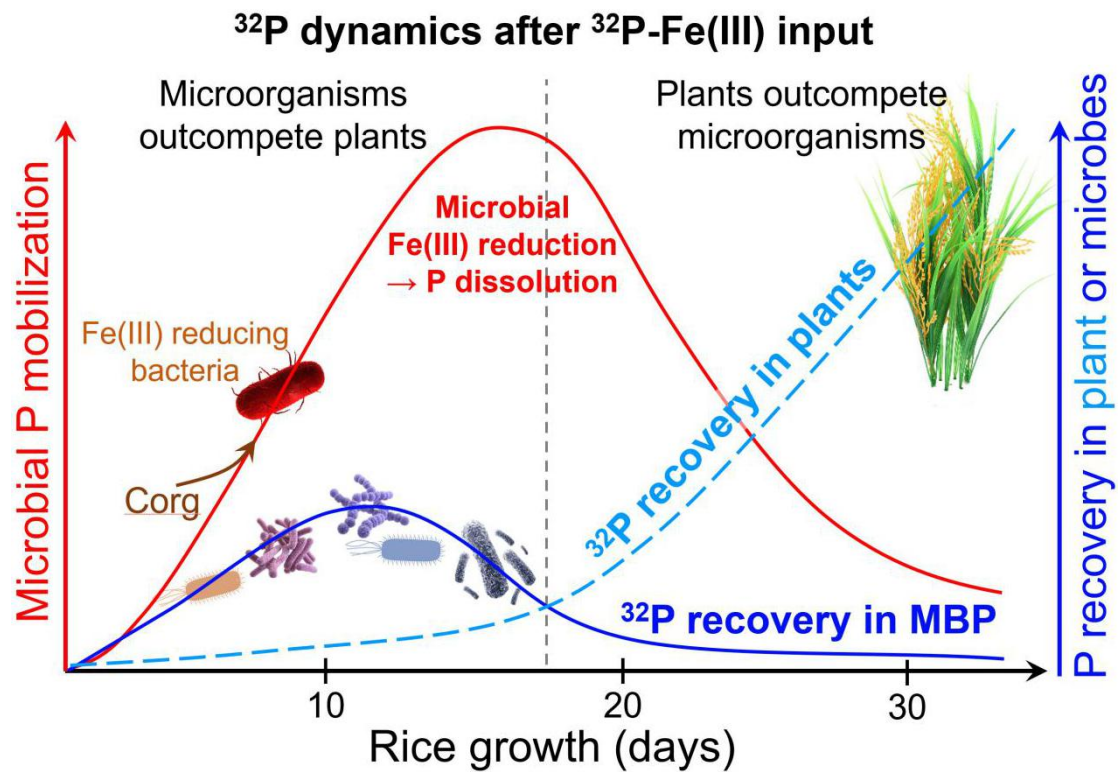
^g Institute of Microbiology, Leibniz University Hannover, 30419 Hannover, Germany

* **Correspondence:** chaoqun.wang@forst.uni-goettingen.de

Status: Published in Soil Biology and Biochemistry

Wang, C.Q., Thielemann, L., Dippold, M.A., Guggenberger, G., Kuzyakov, Y., Banfield, C.C., Ge, T.D., Guenther, S., Bork, P., Horn, M.A., Dorodnikov, M., 2022. Can the reductive dissolution of ferric iron in paddy soils compensate phosphorus limitation of rice plants and microorganisms?. *Soil Biology and Biochemistry* 168, 108653.

Graphical abstract



Conceptual scheme demonstrating the shift from microorganisms outcompeting rice plants for phosphorus to rice plants outcompeting microorganisms. Red solid line demonstrates the dynamics of microbially driven Fe(III) reduction. Blue lines show ^{32}P recovery either in rice plants (dashed line) or in microbial biomass (solid line) with rice plant growth.

Abstract: Biogeochemical cycles of phosphorus (P) and iron (Fe) are tightly interlinked, especially in highly weathered acidic subtropical and tropical soils rich in iron (oxyhydr)oxides (Fe(III)). The quantitative contribution of the reductive dissolution of Fe(III)-bound inorganic P (P_i) (Fe-P) in low-redox paddy soils may cover the demands of rice plants (*Oryza sativa* L.) and microorganisms. We hypothesized that microbially-driven Fe(III) reduction and dissolution can cover the P demand of microorganisms but not of the young rice plants when the plants' P demand is high but their root systems are not sufficiently developed. We grew pre-germinated rice plants for 33 days in flooded rhizoboxes filled with a paddy soil of low P availability. ^{32}P -labeled ferrihydrite (30.8 mg kg^{-1}) was supplied either (1) in polyamide mesh bags ($30 \mu\text{m}$ mesh size) to prevent roots from directly mobilizing Fe-P (pellets-in-mesh bag treatment), or (2) in the same pellet form but without a mesh bag to enable roots accessing the Fe-P (pellets-no-mesh bag treatment).

Without mesh bags, P_i was more available leading to increases in microbial biomass carbon (MBC) by 18–55% and nitrogen by 4–108% in rooted soil as compared to P_i pellets not directly available to roots. The maximum enzyme activities (V_{max}) of phosphomonoesterase and β -glucosidase followed this pattern. During rice root growth, day 10 to day 33, MBC and microbial biomass phosphorus (MBP) contents in both rooted and bottom bulk (15–18 cm) soil gradually decreased by 28–56% and 47–49%, respectively. In contrast to our hypothesis, the contribution of Fe-P to MBP remarkably decreased from 4.5% to almost zero from 10 to 33 days after rice transplantation, while Fe-P compensated up to 16% of the plant P uptake at 33 days after rice transplantation, thus outcompeting microorganisms. Although both plants and microorganisms obtained P_i released by Fe(III) reductive dissolution, this mechanism was not sufficient for the demand of either organism groups.

Keywords: phosphorus availability and mobilization; anoxic conditions; redox potential; Fe and P interactions; plant-microbial competition; enzyme activities

1. Introduction

Low soil phosphorus (P) contents limit the yield and productivity in many agroecosystems (Vitousek et al., 1997; Wang et al., 2021). The low P availability is particularly exacerbated in highly-weathered tropical and subtropical soils, which are acidic and rich in iron (Fe) and aluminum (Al) (oxyhydr)oxides, as well as free Fe^{3+} and Al^{3+} (Elser et al., 2007; Wang et al., 2019). This is because inorganic P (P_i) is precipitated by Fe and Al in acidic soils, or calcium (Ca) in neutral and alkaline soils or absorbed to clay mineral surfaces (Hedley et al., 1982; Cross and Schlesinger, 1995). One key strategy to alleviate the deficiency of available P_i is to solubilize the P_i precipitated on minerals or absorbed P_i , whereas the solubilized P_i must not re-precipitate with Al or Fe before it is taken up by the plant. The mobility and equilibrium concentration of P_i in acidic soils mainly depend on redox potential and pH (Shen et al., 2011).

Generally, the reductive dissolution of ferric Fe, i.e., Fe(III), is a critical factor to increase the P_i solubility at low-redox conditions after O_2 depletion in the course aerobic organic matter decomposition (Saleque et al., 1996). The P_i release from Fe minerals is commonly observed in wetland soils when the redox potential (E_h) drop below -200 mV (Ann et al., 2000). Similarly, the P_i concentration in soil solution increase when the E_h decrease from ca. $+300$ mV to -120 mV (Amarawansa et al., 2015). Not only the E_h , but also the pH controls (maximum) $\text{Fe}^{2+/3+}$ and Al^{3+} concentrations in soil solution, thereby governing the P_i precipitation if equilibrium concentrations are exceeded (Devau et al., 2009). As the solubility of Fe and Al phosphates increases with soil pH until 7.0–7.5 (Hinsinger, 2001), low-redox soils have a higher potential for P_i release when the pH is close to neutral as compared to the well-aerated acidic or alkaline soils. However, it is still changing to account for P_i release from minerals and P_i dynamics under anoxic conditions like paddy soils (Heinrich et al., 2020) due to (1) the temporal and (micro)spatial variability in redox potential, (2) the diffusive release of oxygen (O_2) by rice roots in the rhizosphere (Upreti et al., 2015), (3) the presence of alternative electron acceptors (e.g., NO_3^-) that maintain high redox potentials even in the absence of O_2 , (4) various forms of Fe(III) (oxyhydr)oxides that vary widely in their dissolution kinetics, and (5) the magnitudes of potential P sources that need to be distinguished.

Concerning P_i uptake by plants, P_i could be bound to Fe(III) in very acidic solution or following oxidation of ferrous Fe(II) by O_2 in the rhizosphere of rice and co-precipitates with ferrihydrite, goethite, and siderite (Hansel et al., 2001). In turn, Fe(III) reduction under low redox potentials ranging from -314 mV to $+14$ mV releases bound P_i into soil solution (Weber et al., 2006).

Under P_i deficiency, microorganisms compete with plants for P_i (Marschner et al., 2011). Therefore, it is important to assess the rate and amount of P_i released from Fe(III) precipitates under anoxic conditions and unravel its roles for microbial and plant growth. Plants may increase their P_i competitiveness by (1) escaping microbial

competition through rapid growth (Watt et al., 2003), (2) reducing microbial competition by decreasing the amount of exudates and so, limiting the carbon (C) source for microorganisms (Darrah, 1991), (3) increasing microbial nutrient mobilization capacity by enhancing the abundance of P-mobilizing microorganisms and/or their activities (Jorquera et al., 2008), (4) release of organic acids to desorb mineral-bound P_i and prevent P_i precipitation (Köster et al., 2020), (5) increasing the uptake of immobilized P (Kong et al., 2008; Siebner-Freibach et al., 2004), (6) release of acid phosphatase to hydrolyze organic P (P_o) (Razavi et al., 2016). Microbial growth and activity are stimulated by easily available root exudates as they provide C and energy to microorganisms and enhance microbial competitiveness of P_i (Marschner et al., 2011). At the same time, they stimulate the production of phosphatases to mobilize P from organic sources (Ge et al., 2017).

Despite low availability, organic P (P_o) plays an essential role in P cycling in soils because of its large pool size (Pistocchi et al., 2018). Phosphatases, such as acid phosphomonoesterase, alkaline phosphatase, phytase, and phosphodiesterases, mainly secreted by microorganisms and partly by plant roots (Kunito et al., 2018), are responsible for P_o hydrolysis in soil. An increase in phosphatase production by microorganisms and plant roots is generally caused by insufficient amounts of available P_i (Santos-Beneit, 2015; Vershinina and Znamenskaya, 2002) and depends on P_o content (Nannipieri et al., 2011). Given the importance of microbial release of available P_i , the phosphatase activity may be used to characterize the acceleration of P cycling mediated by plants and microorganisms. Soil P_i availability also affects C and nitrogen (N) cycling by changing soil nutrient stoichiometry (Wei et al., 2019) and by structuring microbial communities (Tang et al., 2016). For example, P_i addition increased microbial respiration by stimulating microbial activity in P-limited soils (Reed et al., 2011). Phosphate application also increased the gaseous N losses by stimulating the growth of denitrifying bacteria in paddies (Wei et al., 2017). Therefore, activities of β -glucosidase, catalyzing the last step of carbohydrate degradation and thus providing crucial C sources for microorganisms (Alexander, 1977), and leucine aminopeptidase, controlling the degradation of amide-linked polypeptides (Hanson and Frohne, 1976), reflect soil organic C and N turnover in combination with Fe and P interactions under changing redox conditions.

Based on the above, we hypothesized that (i) the direct access of Fe-P by rice roots would increase the reductive dissolution of Fe-P, (ii) microbial biomass and enzyme activities would be higher in rooted soil with more inputs of available C than in bulk soil, and (iii) microbial biomass and enzyme activities would be modified by P_i availability during rice growth. To test these hypotheses, we conducted a microcosm experiment with rice plants grown in continuously flooded paddy soil to explore the effects of P_i release from the Fe(III)-bound phase on the dynamics of microbial biomass and activities of three enzymes: phosphomonoesterase (PME), β -glucosidase (BG), and leucine aminopeptidase (LAP) under low-redox conditions. The accessibility of Fe-P by rice roots was controlled by using a mesh bag to distinguish between microbially mediated and rhizomicrobially mediated Fe-P

dissolution and P_i uptake. We adopted the Michaelis-Menten approach to assay enzyme kinetics (Marx et al., 2001) under anoxic conditions by means of a portable glovebox (Wang et al., 2022).

2. Materials and methods

2.1. Soil description

The low available P_i soil (available P_i content $< 10 \text{ mg kg}^{-1}$ according to the Chinese soil nutrient classification standard) was collected from 0–20 cm of a paddy rice field at the Changsha Agricultural and Environmental Monitoring Station, Hunan Province ($113^{\circ}19'52'' \text{ E}$, $28^{\circ}33'04'' \text{ N}$), which is located in the subtropical region of China. The annual average temperature of the region is 17.5°C , and the annual average precipitation is 1300 mm. The soil is a typical Stagnic Anthrosol developed from highly weathered granite (Gong et al., 2007), and is under paddy cultivation with double-cropping rice. The soil was collected with a corer at five locations in the field, combined, sieved through a 2 mm mesh, air-dried, and homogenized. The soil texture was 26.7% clay, 29.2% silt, and 44.2% sand. The main soil physico-chemical properties were as follows: pH 6.2, soil organic C 13.1 g kg^{-1} , total N 1.4 g kg^{-1} , available N 18.0 mg kg^{-1} , total P 0.3 g kg^{-1} , and Olsen-P 3.7 mg kg^{-1} (Zhu et al., 2018).

2.2. Experimental setup

A microcosm experiment with rice was conducted in water-tight PVC-rhizoboxes with the inner dimensions of $24.0 \times 20.5 \times 1.5 \text{ cm}$ (height \times width \times depth, Fig. S1A). The experimental design included two treatments with four replicates (eight rhizoboxes for each destructive sampling (three samplings in total) and 24 rhizoboxes in total, see section 2.3 below). The treatments represented conditions when phosphate is bound to ferric iron minerals (ferrihydrite), rendering P not directly available for plant uptake. The first treatment excluded direct contact of Fe-P by roots: the ferrihydrite pellets loaded with radioactive phosphate were put into a 30- μm polyamide mesh bag ($5.0 \times 5.0 \text{ cm}$, height \times width) (pellets-in-mesh bag treatment, Fig. 1, left side). The second treatment allowed roots to access the Fe-P in the form of pellets without mesh bag (pellets-no-mesh bag treatment, Fig. 1, right side) (see section 2.3 below). Air-dry soil (420 g) was filled into each rhizobox and saturated by deionized water for 16–24 h prior the addition of Fe-P (Fig. 1). The Fe-P pellets either in mesh bags or without were placed in the middle of the surface of the prefilled soil, and then covered with another 230 g of soil (Fig. 1). This soil was then saturated with deionized water, trapped air bubbles were removed by knocking, and one pre-cultivated rice seedling (*Oryza sativa* L. ‘Two-line hybrid rice Zhongzao 39’) was planted per rhizobox.

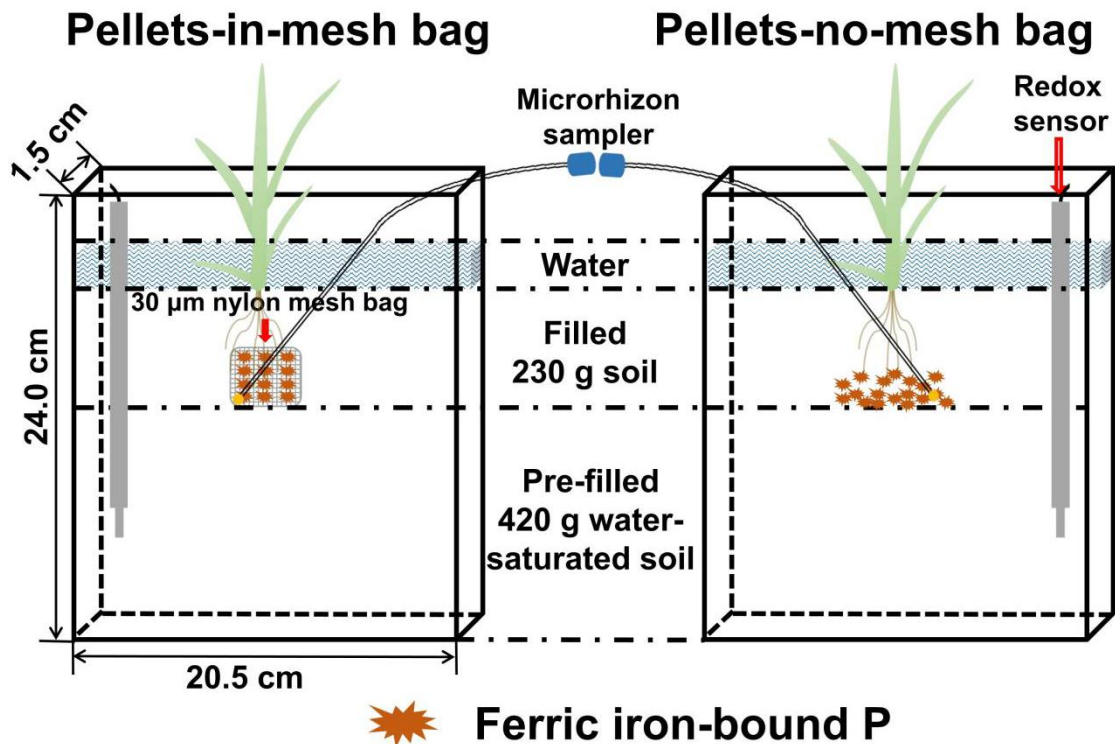


Fig. 1 Diagram of the experimental design. MicroRhizon® samplers were placed at the P-rich patch zone, and a platinum electrode for measuring redox potential (E_h) was installed in each rhizobox. Pre-filled soil corresponds to paddy soil filled into rhizoboxes 16–24 h prior the addition of ferric iron-bound P. Filled soil is the paddy soil added during Fe-P placement and rice seedlings transplantation.

All microcosms were filled with additional water to achieve 2 cm of water above the soil surface and were placed in a climate-controlled chamber (RUMED® Premium-Line P 1700, Rubarth Apparate GmbH, Germany) with $28 \pm 1^\circ\text{C}$ day temperature and $24 \pm 1^\circ\text{C}$ night temperature, 70% relative humidity, and 12-h photoperiod. The water level above the soil was maintained during the whole period of rice growth. Immediately after transplanting, 30 mg N kg^{-1} dry soil in the form of urea were applied as base fertilization.

The soil redox potential (E_h) was monitored in each rhizobox by a platinum electrode installed at 10 cm depth (Fig. 1). E_h was measured using an E_h -meter (GMH 3531, GHM Messtechnik GmbH, Germany). To measure released ^{32}P activity from Fe-P and total Fe concentration in soil solution during rice growth, 30-ml of soil solution were collected every 2–5 days during the experiment from the areas around the pellets using MicroRhizon samplers (MicroRhizons, Rhizosphere Research Products, Netherlands) in evacuated and N_2 -flushed 30-ml glass bottles (Fig. 1).

2.3. Ferric iron-P pellet preparation and labelling with ^{32}P

The Fe-P pellet was prepared by mixing 10 g of purified quartz sand as matrix and 0.7 g of synthesized ferrihydrite (Paterson, 2000) per rhizobox. The mixture was weighed into 100-ml glass centrifuge tubes and 30 ml of $3.75 \text{ g l}^{-1} \text{ K}_2\text{HPO}_4$ solution spiked with ^{32}P -labeled H_3PO_4 ($2 \text{ MBq } \mu\text{l}^{-1}$, Hartmann Analytic GmbH, Brunswick,

Germany) were added. Additionally, 2 ml of 1 M HCl was pipetted into the centrifuge tubes to increase the P adsorption efficiency. Tubes were shaken for 2 h on a roller mixer (200 rpm) and then centrifuged at $3000 \times g$ for 15 min. The activity in the supernatant was measured on a Liquid Scintillation Analyzer (LSA) (Tri-Carb® 2800 TR, PerkinElmer, Shelton, CT, USA). Briefly, 10 μ l supernatant was mixed with 10 ml scintillation cocktail (Rotiszint®eco plus, Carl Roth, Germany), then counting was conducted for 2 min. To purify the pellets, i.e., remove the non-sorbed phosphates, the supernatant was discarded, and 30 ml of deionized water were added to the tubes. The centrifugation and ^{32}P activity determination of the supernatants were repeated three more times as described.

The total amount of P_i added (20 mg rhizobox⁻¹) was equivalent to a mineral P fertilization of 80 kg ha⁻¹. The initial ^{32}P activity of the pellet was estimated based on the duration of rice growth and three destructive samplings (DS, see section 2.4. below). At the time of pellet application (t_0), approx. 5, 9, and 16 MBq of ^{32}P -labeled H_3PO_4 were employed per rhizobox to reach 3.2–3.5 MBq of ^{32}P activity at each of the destructive samplings according to the ^{32}P half-life (14.3 days). Ready pellets were weighed on an analytical balance and transferred with a spoon either to a mesh bag or directly into the soil, depending on the treatment.

2.4. Destructive sampling

Destructive samplings were conducted after 10 (DS1), 18 (DS2), and 33 (DS3) days after rice transplanting, respectively. The age of rice plants roughly corresponded to tillering stage (with 2–4 tillers) of a vegetative phase of rice growth. The distribution of rice roots at DS1 was mainly above the mesh bag or pellet, at DS2 roots were in vicinity of the mesh bag or pellet, and at DS3, they reached a depth of two cm above the bottom of the rhizoboxes. The flooding water was drained immediately before sampling. To keep anoxic conditions in the moist soil, all rhizoboxes were opened inside a portable PVC glovebox (Captair® Pyramid Glovebox 3015-00, Erlab DFS, Saint-Maurice, France) (Fig. S1B) evacuated with a vacuum pump (Ilmvac MP 301 Vp, Ilmvac GmbH, Ilmenau, Germany) and then backflushed with N_2 to achieve a level of O_2 lower than 0.4% as indicated by an O_2 -sensor (Greisinger GOX 100, GHM Messtechnik GmbH, Remscheid, Germany) (Fig. S1C).

After opening a rhizobox, the soil was collected from three compartments: top bulk (2–5 cm from soil surface), rooted (5–15 cm), and bottom bulk (15–18 cm) soil. In each compartment, soil was collected from three random locations. For microbial biomass measurements, two samples of 7–10 g of moist soil from each compartment were immediately placed in air-tight plastic bags and the soil was stored at 4°C until the next day. For enzyme kinetic assays, 0.5 g moist soil per compartment was kept in 100-ml Kimble KIMAX borosilicate laboratory glass bottles (Kimble Chase Life Science and Research Products, LLC., Meiningen, Germany), prefilled with N_2 -degassed (i.e., anoxic), deionized, and sterile water with a soil-water ratio of 1:100 (m/v). Before opening the glovebox, bottles were sealed with thick air-impermeable butyl rubber septa. Thereafter, bottles were shaken for 30 min on a shaker (200 rpm)

before enzyme activity assays.

2.5. Measurement of Fe concentration and ³²P activity in soil solution

The total Fe concentration in soil solution collected by MicroRhizons was measured after complete Fe³⁺ reduction to Fe²⁺ by 10% ascorbic acid (Elrod et al., 1991). After a 30-min reaction, 2 ml sample was mixed with 500 µl ammonium acetate buffer (pH 4.5) and 500 µl phenanthroline solution (0.5%) in a 10-mm polystyrene cuvette (Th. Geyer GmbH & Co. KG, Renningen, Germany) and then measured at 512 nm on a spectrophotometer (NanoPhotometer® NP80, Implen GmbH, Munich, Germany). Calibration was done by external FeCl₃ standards ranging from 5 to 300 µM.

The ³²P activity in the same extracted soil solution was determined on the LSA (Tri-Carb® 2800 TR, PerkinElmer, Shelton, CT, US), corrected for isotope radioactive decay during the experiment, and back-calculated to the reference date. Briefly, 0.75 ml soil solution was mixed with 10 ml scintillation cocktail (Carl Roth GmbH + Co. KG, Germany) and then counted for 5 min. The percentage of ³²P activity in soil solution derived from applied ³²P-labeled ferrihydrite-quartz-sand-pellet (%P_{mL}) was calculated according to the following equation:

$$\%P_{mL} = \frac{{}^{32}\text{P activity in water (Bq mL}^{-1})}{\text{Total } {}^{32}\text{P activity in pellets (Bq)}} \times 100 \quad (1)$$

2.6. ³²P recovery in rice plants and microorganisms, soil microbial biomass, and soil total soluble C, N, and P content

At harvest, rice roots were carefully removed from rhizoboxes and were washed free of soil with deionized water. Rice shoots were separated from roots at the soil surface by cutting. The shoot and root samples were dried in an oven at 60°C for 48 h and then milled to a fine powder in a ball mill (Retsch MM200, Retsch GmbH, Haan, Germany). To measure total P content and ³²P activity in shoots and roots, approx. 100 mg of each sample were digested with 2 ml of 65% HNO₃ at 180°C for 8 h in a PTFE digestion block. Each digested sample was filtered and filled up to 25 ml volume with MQ water. A subsample (2 ml) was used to measure the total P content by an inductively coupled plasma-optical emission spectrometry (ICP-OES) (iCAP 7000 series ICP-OES, Thermo Fisher Scientific, Dreieich, Germany). To measure the ³²P activity, 1 ml sample was mixed with 10 ml scintillation cocktail (Carl Roth GmbH + Co. KG, Germany) in a 20-ml scintillation vial, and then counted for 5 min on the LSA. The proportion of P derived from applied Fe-P (%P_{Shoot/Root}) in shoot or root total P was calculated as:

$$\%P_{\text{Shoot/Root}} = \frac{\text{Total } {}^{32}\text{P activity in shoots/roots (Bq)} \times \text{P mass in pellets (mg Bq}^{-1})}{\text{Total P in shoots/roots (mg)}} \times 100$$

(2)

Extractable microbial biomass carbon (MBC) and nitrogen (MBN) were measured using the chloroform-fumigation-extraction method (Vance et al., 1987) and were calculated according to the equation:

$$\text{MBC(MBN)} = \frac{E_C(E_N)}{k_{EC}(k_{EN})} \quad (3)$$

where k_{EC} and k_{EN} are equal to 0.45 (Brookes et al., 1985; Vance et al., 1987) and E_C and E_N are the difference between the content of organic carbon and the difference between the content of total nitrogen extracted from the fumigated and non-fumigated soils, respectively. The organic carbon and total nitrogen concentrations in each extract were measured by an elemental analyzer (Multi N/C 2100S, Analytik, Germany).

Microbial biomass phosphorus (MBP) was determined with the anion exchange resin method by adding hexanol as fumigant according to Kouno et al. (1995). The P concentration was measured by colorimetry on a spectrophotometer (NanoPhotometer® NP80, Implen, Munich, Germany). MBP was calculated as the difference between anion exchange P without hexanol and P extracted after hexanol extraction and corrected for the recovery of a P spike in each soil sample. To measure ^{32}P activity in MBP, 1 ml sample was mixed with 10 ml cocktail in a scintillation vial and then measured for 5 min on the LSA. The ^{32}P activity in MBP was also calculated as the difference in ^{32}P activity between samples extracted without and with hexanol and corrected for the recovery of a P spike in each soil sample. The proportion of P in MBP derived from applied Fe-P ($\%P_{\text{mic}}$) in each soil compartment was calculated as:

$$\%P_{\text{MBP}} = \frac{{}^{32}\text{P activity (Bq kg}^{-1}) \times \text{P mass in pellets (mg Bq}^{-1})}{\text{MBP content (mg kg}^{-1})} \times 100 \quad (4)$$

We presented the contents of organic C and N extracted from non-fumigated soils and anion exchange P without hexanol as soil total soluble C, N, and P, respectively.

2.7. Enzyme kinetic assays

The kinetics of phosphomonoesterase (PME), β -glucosidase (BG), and leucine aminopeptidase (LAP) were measured using fluorogenically labelled substrates of 4-methylumbelliferyl-phosphate, 4-methylumbelliferyl- β -D-glucoside, and L-Leucine-7-amino-4-methylcomarin hydrochloride (Sigma-Aldrich, Germany), respectively, according to Marx et al. (2001). The enzyme kinetics were assayed under anoxic conditions inside a portable PVC glovebox (Captair® Pyramid Glovebox 3015-00, Erlab DFS, Saint-Maurice, France) (Wang et al., 2022). PME activity was measured in soil samples from three destructive samplings, but the activities of BG and LAP were only measured in soil samples from DS3.

The enzyme kinetics were measured according to a Michaelis-Menten approach

with the following range of substrate concentrations 0, 5, 10, 20, 50, 100, 150, and 200 μM . Substrate and buffer were bubbled with N_2 for 20 minutes and then used for enzyme determination under anoxic conditions in the glovebox. For assays, 50 μl soil suspension, 100 μl 4-methylumbelliferone (MUF) or 7-amino-4-methylcomarin (AMC)-based substrate, and 50 μl MES or TRIZMA buffer were added into a 96-well black microplate (Brand GmbH, Wertheim, Germany). The fluorescence was repeatedly measured on a Victor 1420-050 Multi label counter (PerkinElmer, USA) after incubation of microplates during 30 min under anoxic conditions. To keep anoxic conditions during incubation, two sets of microplates were prepared with 30-min interval, so after opening of the glovebox all anoxic plates were measured simultaneously. The duration of the incubation period of substrate with soil suspension to achieve maximal fluorescence activity was determined in series of preliminary tests (data not shown). The excitation and emission wavelengths were 355 nm and 460 nm, respectively. Duration of reading per well was 1.0 sec.

Based on MUF or AMC pure substance calibrations, the rate of enzyme activities was calculated as nmol MUF/AMC per g soil (dry weight) per hour corresponded to the substrate added (in $\mu\text{mol g}^{-1}$ dry soil). The Michaelis-Menten equation was used to calculate the kinetic parameters V_{max} and K_{m} :

$$V = \frac{V_{\text{max}} \times S}{K_{\text{m}} + S} \quad (5)$$

where V is the reaction rate ($\text{nmol g}^{-1} \text{ soil h}^{-1}$), S is the substrate concentration ($\mu\text{mol g}^{-1} \text{ soil}$), V_{max} is the maximal reaction rate of enzymatic activity at saturating substrate concentration, and K_{m} is the substrate concentration at half-maximal rate ($1/2 V_{\text{max}}$). V_{max} and K_{m} were estimated using non-linear curve fitting in GraphPad Prism 8 (GraphPad Software, Inc., San Diego, USA).

2.8. Statistical analysis

A one-way ANOVA, followed by the Tukey's HSD post-hoc test, was used to test for the significant differences ($p < 0.05$) for E_{h} , the percentage of ^{32}P recovery, and Fe content either between soils with pellets in a mesh bag and without a mesh bag for the same sampling time or among sampling dates within the same treatment. A two-way ANOVA was used to test the effects of (i) the treatment (Pellets-in-mesh bag vs. Pellets-no-mesh bag) and (ii) destructive sampling on the proportion of P derived from applied Fe-P recovered in either shoot or root P, and the ratio of ^{32}P recovery in MBP in rooted soil to that in root P. A two-way ANOVA with repeated measures (destructive sampling, $n = 3$) was used to test the effects of (i) treatment (Pellets-in-mesh bag vs. Pellets-no-mesh bag) and (ii) soil compartment on MBC, MBN, MBP, soil total soluble C:N:P ratios, and V_{max} and K_{m} of PME. A two-way ANOVA was used to test the effects of (i) treatment (Pellets-in-mesh bag vs. Pellets-no-mesh bag) and (ii) soil compartment on V_{max} and K_{m} of BG and LAP. Exponential regression analysis was used to determine the relationships between E_{h} values and ^{32}P recovery in soil solution. All statistical tests were conducted using

3. Results

3.1. Soil E_h , total Fe concentration, and ^{32}P recovery in soil solution

E_h decreased in soils with and without mesh bags within six days after rice transplantation ($p < 0.05$) and then stabilized between -168 and -233 mV (Fig. 2, top row). Soil E_h was on higher in Pellets-no-mesh bag rhizoboxes than with mesh bags (Fig. 2, top row).

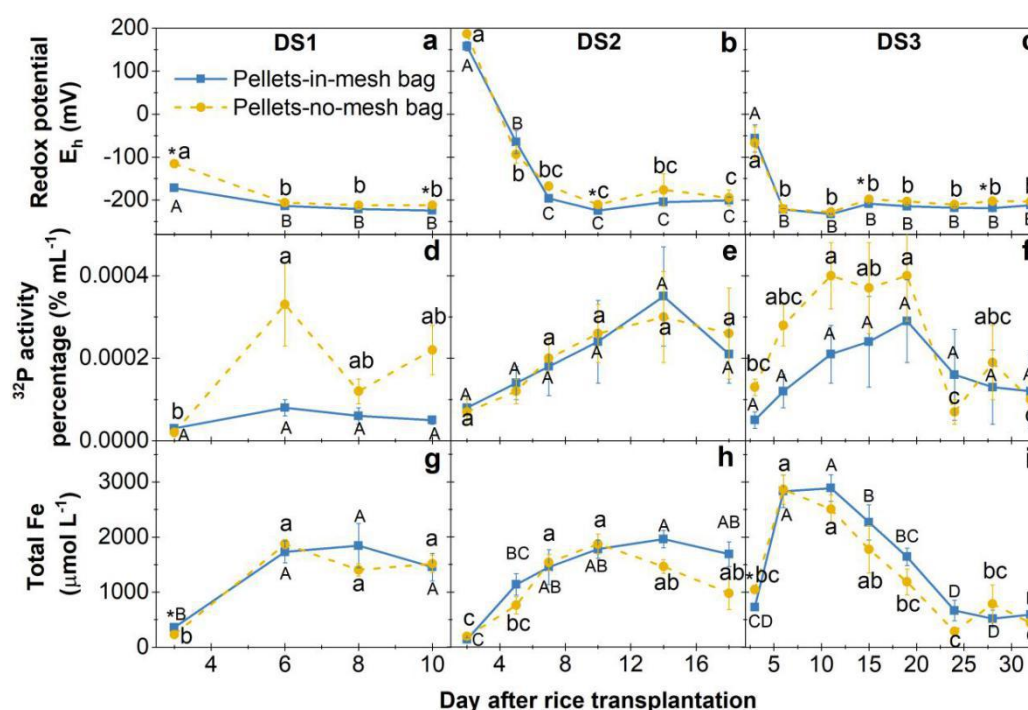


Fig. 2 Soil redox potential E_h (top), the recovery of ^{32}P (middle) and total soluble Fe concentration (bottom) in soil solution during the first (DS1), second (DS2), and third (DS3) periods of rice growth before destructive sampling. The data are the means \pm standard errors ($n = 4$). Letters represent significant differences ($p < 0.05$) among sampling dates of each period of rice growth under Pellets-in-mesh bag (uppercase) or Pellets-no-mesh bag (lowercase) treatment, respectively. Significant differences ($p < 0.05$) between Pellets-in-mesh bag and Pellets-no-mesh bag treatments are indicated by asterisk.

Dynamics of the total Fe concentration and of the ^{32}P recovered in soil solution (Fig. 2, d-i) had temporal patterns comparable to rice growth. The ^{32}P proportion in soil solution (as % from the added ^{32}P activity) was higher when Fe-P pellets were not excluded from roots by mesh bags at 10 days after seedling transplantation (DS1) and on 20 out of 33 days (DS3) (Fig. 2, middle row). The ^{32}P dynamics were similar among the three destructive samplings, especially among DS2 and DS3: there was an initial smooth slow increase till days 14–19 and then an abrupt decrease (Fig. 2, middle row). The dynamics of total Fe in soil solution matched well with soil solution

^{32}P dynamics at DS1 and DS2 (Fig. 2, middle and bottom row). At DS3, the peak of ^{32}P recovery was delayed by about 12 days after the peak of total Fe (Fig. 2, bottom row). Interestingly, the minute Fe concentration in soil solution at the end of DS3 period (days 24–33) coincided with the lowest ^{32}P recovery in both soils with and without bags (Fig. 2, bottom row).

^{32}P recovery increased with decreasing redox potential (more negative E_h values) in soil solution in Pellets-no-mesh bag rhizoboxes during 10 days after rice seedling transplantation (DS1), for 10 days out of 18 days (DS2), and for 11 days out of 33 days (DS3) (Fig. 3).

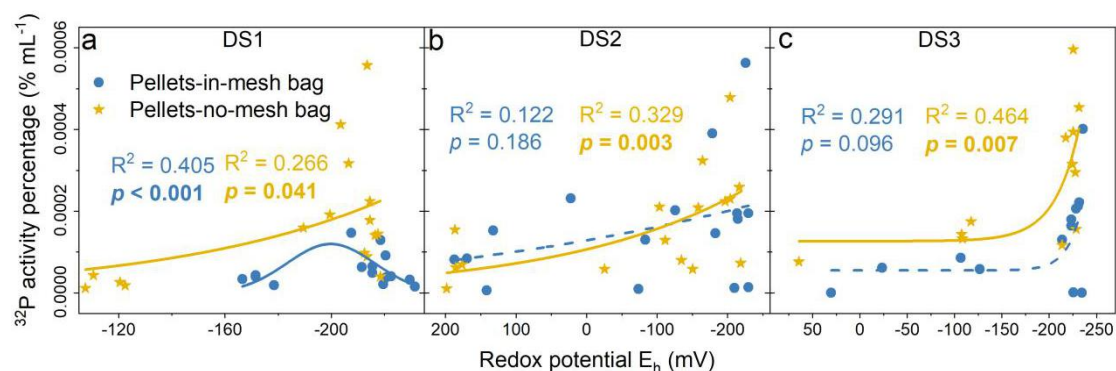


Fig. 3 Relationships between redox potential E_h and ^{32}P recovery in soil solution under Pellets-in-mesh bag and Pellets-no-mesh bag treatments in the first 10 days after rice transplantation of the 1st destructive sampling (DS1, a), 10 days of the DS2 (b), and 11 days of DS3 (c), respectively. Solid lines indicate significant non-linear correlations.

3.2. Soil microbial biomass

MBC, MBN, and MBP contents were higher in Pellets-no-mesh bag rhizoboxes as compared to the rhizoboxes with pellets in mesh bags (Fig. 4, left vs. right). The soil compartment influenced the microbial biomass contents (Fig. 4, Table S1). After 10 (DS1) and 18 (DS2) days of rice growth, the highest MBC, MBN, and MBP contents were found in rooted soil as compared to top and bottom bulk soil (Fig. 4, green vs. blue and red bars). However, the highest MBC, MBN, and MBP contents were found in top bulk soil as compared to rooted and bottom bulk soil 33 days (DS3) after rice transplantation (Fig. 4, DS3 of a, b, and c). With rice root growth, the MBC content in rooted and bottom bulk soil gradually decreased by 30–52% and 28–56% in the Pellets-in-mesh bag and Pellets-no-mesh bag soils, respectively, whereas in top bulk soil MBC contents remained stable (Fig. 4a). The highest MBN content was determined after 18 days of rice growth, but similar MBN content was detected after 10 and 33 days (Fig. 4b). MBP contents in rooted soil generally followed the MBC content pattern, i.e., with rice growth. The highest MBP content was found in the top bulk soil in Pellets-no-mesh bag rhizoboxes 33 days after seedling transplantation (Fig. 4c).

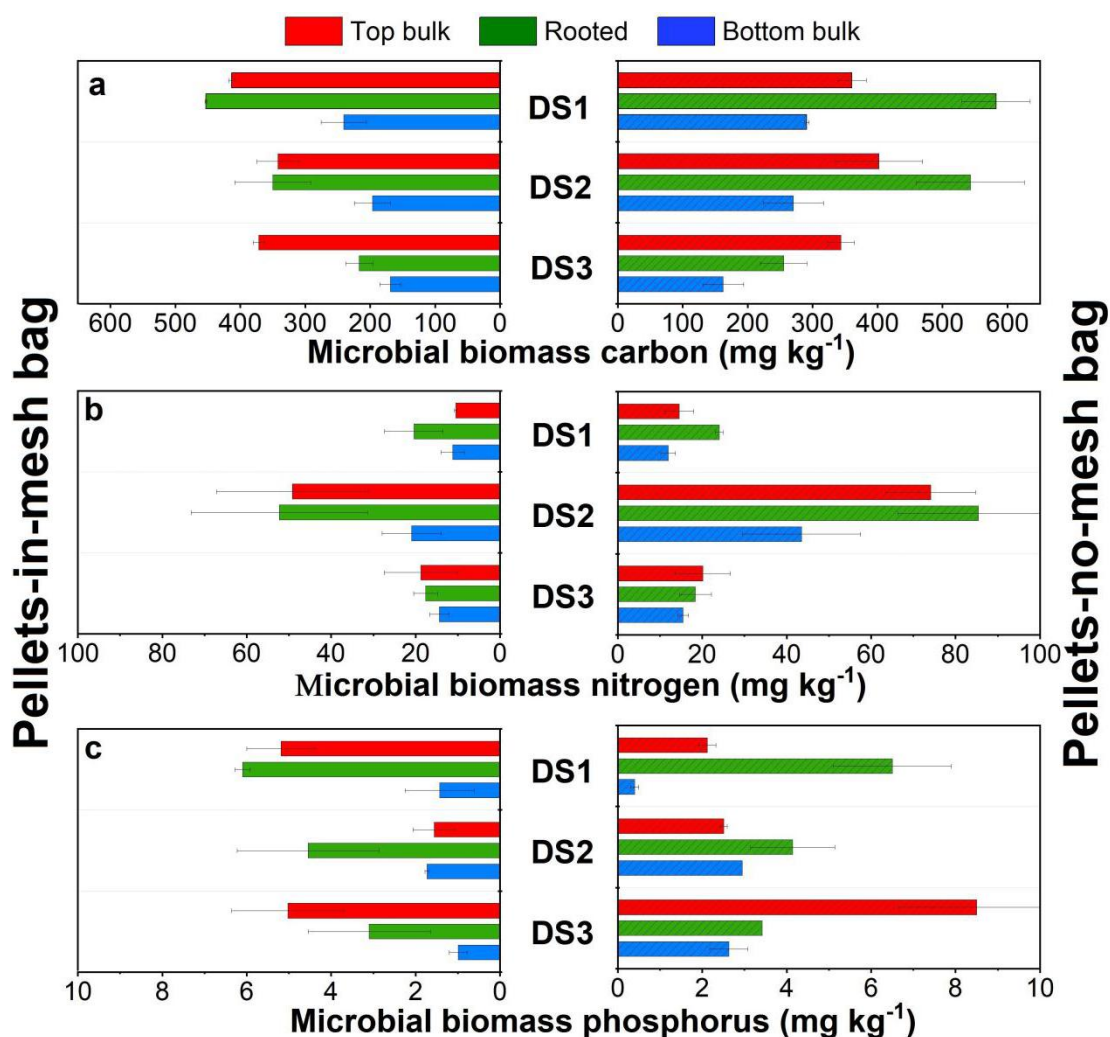


Fig. 4 Microbial biomass carbon (MBC, a), nitrogen (MBN, b), and phosphorus (MBP, c) content in the top bulk, rooted, and bottom bulk soil under Pellets-in-mesh bag (left side) and Pellets-no-mesh bag treatment (right side) of the first (DS1, 10 days), second (DS2, 18 days), and third destructive sampling (DS3, 33 days) after rice transplantation. The data are the means \pm standard errors ($n = 4$).

3.3. ^{32}P recovery in rice plants and microorganisms

The proportion of P derived from applied Fe-P differed between shoots and roots (Fig. 5a). Between 10–33 days after rice transplantation, the mobilized P increased in shoots from 0.3% to 9.3% in Pellets-in-mesh bag rhizoboxes and from 0.6% to 15% in Pellets-no-mesh bag rhizoboxes, respectively (Fig. 5a, green lines). In roots, the proportion of P derived from applied Fe-P increased from 2.5% to 16% in Pellets-no-mesh bag rhizoboxes between 10–33 days after rice transplantation (Fig. 5a, yellow and dashed line). The proportion of P derived from applied Fe-P increased from 2.3% to 11% in roots in Pellets-in-mesh bag rhizoboxes between days 10 and 18 after rice transplantation and decreased from 11% to 6.9% between days 10 and 33 (Fig. 5a, yellow and solid line). In contrast, the proportion of P derived from applied Fe-P in MBP decreased, especially in rooted soil from 4.5% to 0.03% in Pellets-no-mesh bag rhizoboxes and from 1.8% to 0.05% in Pellets-in-mesh bag

rhizoboxes (Fig. 5b, green lines). The proportion of P derived from applied Fe-P in MBP was higher in Pellets-no-mesh bag vs. Pellets-in-mesh bag rhizoboxes (Fig. 5b, dashed vs. solid line). Irrespective of the availability of the added P, the ratio of ^{32}P recovery in MBP in rooted soil to that in root P showed an abrupt decrease between 10 and 18 days after rice transplantation (Fig. 5c).

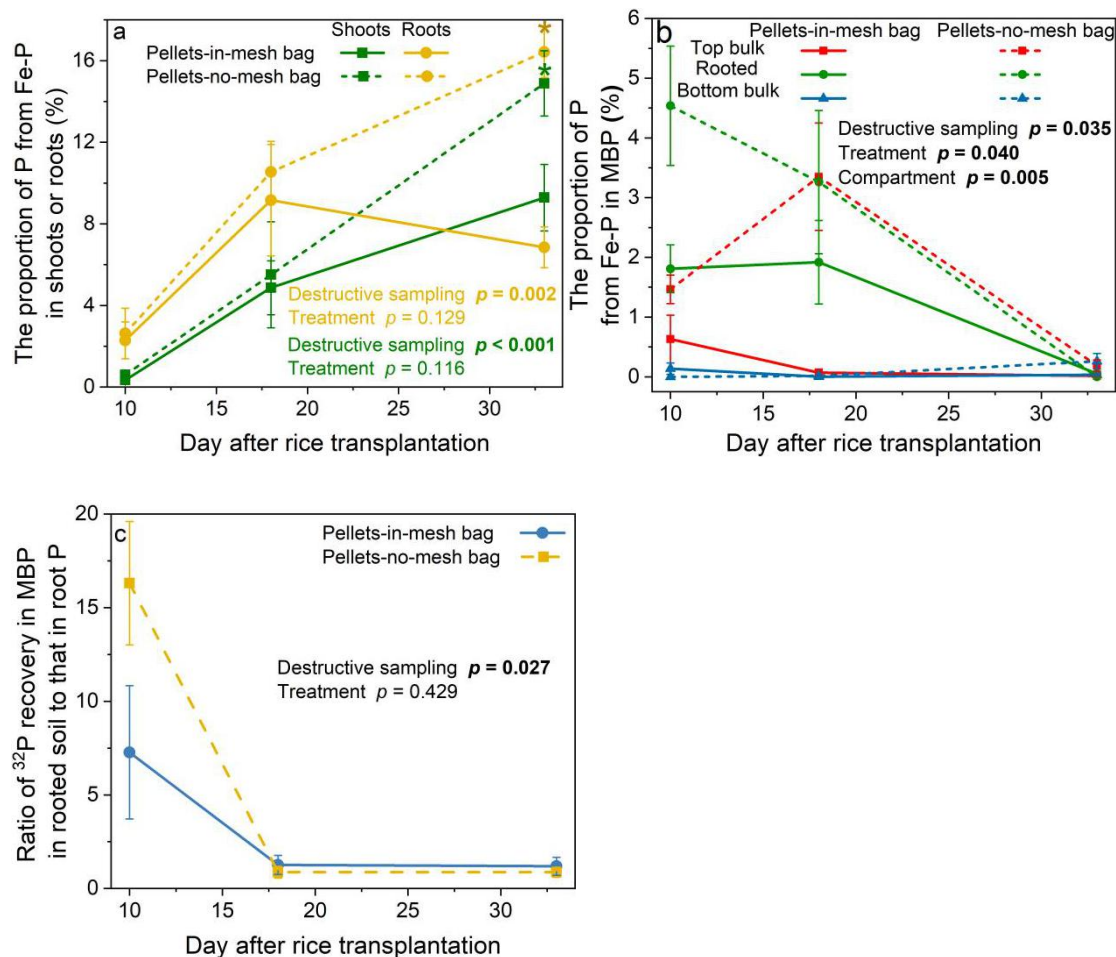


Fig. 5 Proportion of phosphorus (P) derived from applied ferric iron-bound P (Fe-P) in shoots or roots (a) and microbial biomass P (MBP, b), and the ratio of ^{32}P recovery in MBP in rooted soil and that in root P (c) under Pellets-in-mesh bag (solid lines) and Pellets-no-mesh bag treatment (dashed lines) of the first (DS1, 10 days), second (DS2, 18 days), and third destructive sampling (DS3, 33 days) after rice transplantation. The data are the means \pm standard errors ($n = 4$). Significant differences ($p < 0.05$) between Pellets-in-mesh bag and Pellets-no-mesh bag treatments are indicated by asterisk.

3.4. Enzyme kinetic parameters

Higher PME activities were measured after 18 days of rice growth in Pellets-no-mesh bag rhizoboxes as compared to the Pellets-in-mesh bag rhizoboxes (Fig. 6b). Among three compartments, 7–95% higher V_{\max} values were in rooted soil vs. bulk soil for three tested enzymes (Fig. 6). With rice root growth, the highest V_{\max} value of PME was after 18 days (DS2) from seedlings transplantation (Fig. 6b).

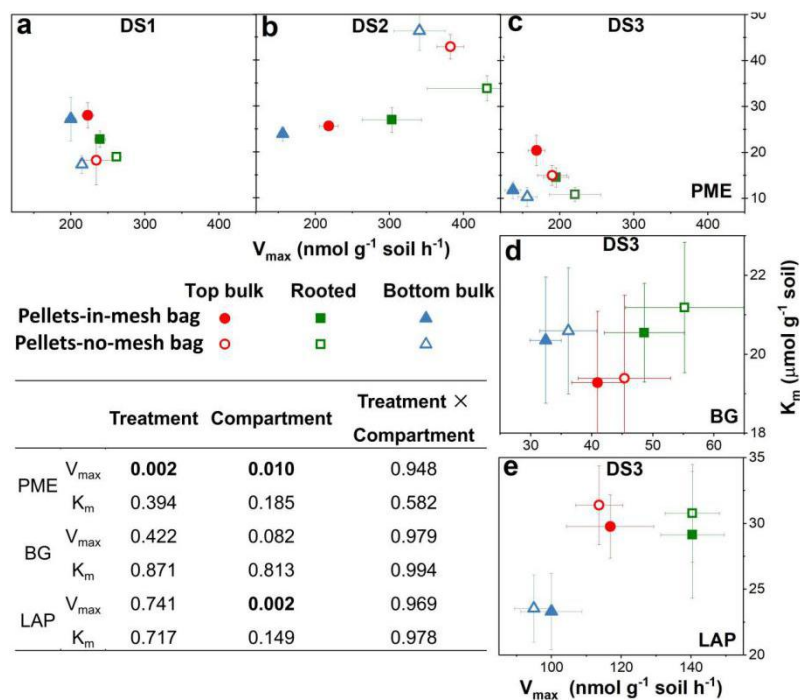


Fig. 6 Maximum reaction rate (V_{max}) and the affinity to a substrate (K_m) of phosphomonoesterase (PME, a, b, c), β -glucosidase (BG, d), and leucine aminopeptidase (LAP, e) in the top bulk, rooted, and bottom bulk soil under Pellets-in-mesh bag and Pellets-no-mesh bag treatments of the first (DS1, 10 days for PME), second (DS2, 18 days for PME), and third destructive sampling (DS3, 33 days for PME, BG, and LAP) after rice transplantation. The data are the means \pm standard errors ($n = 4$). Table inside shows p values of the effects of treatment (Pellets-in-mesh bag vs. Pellets-no-mesh bag), soil compartment, and their interactions on V_{max} and K_m of PME, BG, and LAP analyzed by a two-way ANOVA. Additionally, the V_{max} and K_m of PME were analyzed by a two-way ANOVA with repeated measures (destructive sampling, $n = 3$). The p values in bold in the table inside indicate significant effects of treatments and their interactions on V_{max} or K_m .

The higher K_m of PME in the rhizoboxes without mesh bags vs. the rhizoboxes with mesh bags was measured in top- and bottom bulk soils after 18 days (DS2) of rice growth (Fig. 6b). The K_m values of BG and LAP tended to be higher when pellets were without mesh bags vs. those in mesh bags (Fig. 6e). With rice root growth, the highest K_m of PME was detected in rooted soil 18 days after rice transplantation, especially in the rhizoboxes without mesh bags. In contrast to rooted soil, the K_m of PME in bulk soil gradually decreased by 27–57% of values in the Pellets-in-mesh bag rhizoboxes (Fig. 6).

4. Discussion

4.1. Effects of soil redox conditions on P_i release from ferric iron-bound P_i

E_h levels declined rapidly during the first six days after the seedlings were

planted into the soil, covered with water, and the exchange with atmospheric oxygen was therefore restricted. The E_h decline was primarily due to microbial respiration, which consumed O_2 faster than it diffused from the air. Starting from days 5–8, E_h stabilized between -233 and -168 mV (Fig. 2). Such low E_h values can (1) lead to Fe(III) reduction and Fe(II) dissolution (Weber et al., 2006) and (2) pave the way for the growth of Fe-reducing microorganisms that require low redox potentials (Lovely et al., 2004). Iron reducers speed up the process of Fe(III) reduction and subsequent dissolution via biocatalysis (Lovely et al., 2004). E_h values slightly increased 11–15 days after rice transplantation, which could be attributed to O_2 diffusion through growing rice roots (Larsen et al., 2015). As a result of the decreased redox potential, ferric iron-bound P_i becomes available for plants and microorganisms when Fe(III)-oxide undergoes biotic and abiotic reduction (McConnell et al., 2020). Fe(III)-oxide reduction to Fe(II) occurs at E_h ranging from -314 mV to $+14$ mV, and Fe(II) is well soluble at a pH below 7 (Weber et al., 2006). Fe(III) can function as a terminal electron acceptor under anoxic conditions for iron-reducing microorganisms catalyzing the reductive Fe dissolution and P_i release. Thus, also phosphates are released from Fe(III)-bound phases, which increases P_i availability. The availability of P_i in paddy soils (Wang et al., 2019), as well as in sediments (Xu et al., 2012; Ding et al., 2016; Wu et al., 2017; Liu et al., 2018) is strongly regulated by the redox potential and increased with Fe^{2+} concentrations. This is corroborated by the negative relationships between E_h values and ^{32}P recovery in soil solution with pellets 11 days after rice transplantation (Fig. 3).

In agreement with E_h dynamics and the Fe dissolution, the ^{32}P recovery in soil solution gradually increased in the first 15 days after rice transplantation. However, the ^{32}P recovery and total Fe concentration in soil solution started to decrease from day 13 (DS2) and this decrease was especially pronounced in the growth period following day 19 (DS3) after rice transplantation — although the E_h values remained constantly low (Fig. 2). This is most likely because rice roots increased the P_i uptake efficiency through the production of high-affinity transporters to cope with increased P_i deficiency (Lazali and Bargaz, 2017). As the Fe(III) reduction is predominately a microbially-driven process (Lovely et al., 2004), biological factors were primarily responsible for an abrupt decrease of ^{32}P recovery. Indeed, MBC contents gradually decreased especially in the rooted zone (Fig. 4a), where the Fe in soil solution was measured. To increase competitiveness, rice roots could exude allelochemicals to reduce microbial growth in the rhizosphere (Kong et al., 2008). This, in turn, may explain the slowdown of Fe(III) reduction from the pellet even under low redox conditions. Moreover, the decreased ^{32}P recovery in soil solution could also be attributed to the increased uptake of the released P_i by rice plants and microorganisms. Also, P_i re-adsorption on soil minerals, such as Al (oxyhydr)oxides in paddy soils (Yan et al., 2017), reduces the concentration of dissolved P_i , thus representing an important P_i sink also under anoxic conditions (Hinsinger, 2001).

4.2. Effects of P_i release from ferric iron-bound P_i on rice growth and microbial biomass

Limited availability of C, N, P, and their combinations can play a crucial role for microbial biomass growth and activity (Blagodatskaya and Kuzyakov, 2013). The paddy soil chosen for this experiment was P-limited (Zhu et al., 2018). We therefore expected an increase of the microbial biomass content after P release from Fe-P dissolution. This was confirmed by generally higher MBC, MBN, and MBP contents when Fe-P was root-accessible compared to the soil surrounding pellets in mesh bags (Fig. 4). Likewise, the accessibility of Fe-P to rice roots may also have facilitated their colonization with Fe reducers. This supports the first hypothesis that direct root access to Fe-P increases dissolution and P_i release leading to growth of rhizosphere microorganisms with positive feedbacks on P_i dissolution. Furthermore, microbial biomass was higher in rooted soil than in bulk soil during the first 10 to 18 days after rice transplantation (Fig. 4, DS1, DS2), which supports the second hypothesis that the inputs of available C by roots stimulate microbial growth and enzyme production but very likely also ferric iron reduction. Indeed, higher microbial biomass in the rhizosphere compared to the bulk soil is common because roots exude a great deal of labile organic substances (Kuzyakov and Blagodatskaya, 2015), such as glucose, arabinose, glucuronic acid, and amino acids (Bacilio-Jiménez et al., 2003; Wen et al., 2022). At the same time, these easily accessible C sources fuel the Fe(III) reduction.

In contrast to our expectations, above- and especially belowground rice growth at the tillering stage resulted in the decrease of MBC and MBP contents in the rooted soil (Fig. 4a, c, green bars). Such a pattern can be attributed to an increased competition between rice plants and microorganisms for the available P_i (Fig. 7). This was also visible by a gradual decrease in the ratio of ^{32}P recovery in MBP in rooted soil to that in root P (Fig. 5c). To acquire nutrients, roots that grow in nutrient-deficient soil typically follow a strategy of compensatory responses (Robinson, 1994; Farrar and Jones, 2000). This strategy entails that under nutrient limitation, plants invest in the root system to proliferate at an increased rate from nutrient-poor into nutrient-rich zones. Simultaneously, the nutrient uptake rate per unit mass of roots becomes higher (Robinson, 1994). The compensatory response may therefore strengthen the ability of rice roots to compete for the ferric-iron derived P in P-rich areas to compensate P limitation. Most likely, microbial growth was strictly limited by the strong competition with rice roots for P_i as evident from the simultaneous increase in ^{32}P recovery in plants and decreased ^{32}P recovery in MBP (Fig. 5). Additionally, the decreasing ^{32}P recovery in MBP was probably linked to the mortality and turnover of microorganisms and their necromass mineralization, thereby accelerating the release of immobilized P_i and its uptake by plants (Marschner et al., 2011; Chen et al., 2019; Loepmann et al., 2020). In contrast to upland soils, where high rhizodeposition and exudation by roots stimulate microbial growth and biomass (Gunina and Kuzyakov, 2015; Liu et al., 2019), in low-redox and anoxic flooded soil, the energy output from anaerobic respiration is much lower (Marchant et al., 2017). In addition, continuous flooding reduced the ability of the Gram-negative bacteria to use root exudates as compared to non-flooded conditions (Tian et al., 2013). Therefore, the short-term increase in P_i availability under P_i deficiency promotes plant uptake rather than microbial assimilation.

In contrast to MBC and MBP dynamics, the MBN was higher in DS2 than in DS1 and DS3 (Fig. 4). This could be attributed to nutrient stoichiometric imbalances in soil (Bai et al., 2021). In response to the latter, microbial communities regulate their biomass C:N:P ratio to adapt to the soil nutrient status. For this, microorganisms (i) mobilize and acquire nutrients that meet their demands by producing specific enzymes (Mooshammer et al., 2014), (ii) adjust their element (nutrient) use efficiencies by efficient recycling (Mooshammer et al., 2014), and (iii) intensively recycle the limiting nutrients (Chen et al., 2019; Cui et al., 2020). The occurrence of stoichiometric imbalances was supported by a gradual decrease in soluble C:P ratio with rice growth and by the lowest ratios of soluble C:N and the highest ratios of N:P in DS2 (Fig. S2). Accordingly, soil microorganisms were severely limited in C and P, additionally highlighting that the plant-microbiome interaction was driven by P limitation in our system.

4.3. Effects of P_i release from iron-bound P_i on hydrolytic enzymes

The activities of the three hydrolytic enzymes were higher in rooted soil compared to bulk soil (Fig. 6, green vs. red and blue symbols). This, along with the microbial biomass patterns (Fig. 4) supports the second hypothesis that microbial biomass and enzyme activities should be higher in rooted soil with more inputs of labile organic C than in bulk soil. This occurred even during flooding, i.e., the complete filling of all pores which facilitated the diffusion of the root exudates and therefore weakened the rhizosphere effect (Ling et al., 2022). The available P_i in soil solution is mainly controlled by the chemical equilibrium of co-precipitation/dissolution and sorption/desorption of P_i on minerals such as (oxyhydr)oxides (Helfenstein et al., 2018), microbial and plant P_i uptake, and microbial P_o mineralization by microorganisms from organic matter (Achat et al., 2016). The microbially-mediated P_i release from organic matter or from Fe-P depends on the P_i availability in soil solution, and thus on the necessity of initiating energy-consuming P_o mineralization processes such as the secretion of phosphatases by microbes (Becquer et al., 2014; Bünemann, 2015). The P_i release from the Fe-P pool was observed by higher ^{32}P recovery in soil solution (Fig. 2). This coincided with increased phosphomonoesterase activities especially in soil with restricted root access to the pellets (Fig. 2, 6). Such nutrient mining, i.e., the promotion of P_o mineralization due to an insufficient amount of P_i released from the added Fe(III)-bound P_i source—often linked to the priming effect (Kuzyakov and Blagodatskaya, 2015). In our case, roots eventually outcompeted microorganisms in P_i uptake especially when in direct access to P_i source (Fig. 7). Therefore, P deficient microbes compensated their demand from the recent plant-derived deposits and SOM-derived P_o sources. The differences in the V_{\max} between rhizoboxes with or without mesh bags were more pronounced after 18 days of rice growth (DS2) than before 10 days (DS1) or after 33 days (DS3) (Fig. 6). Importantly, the rice roots were spatially concentrated around the P_i -rich patch at DS2, just reaching the P_i -rich patch at DS1, and they had passed the P_i -rich patch at DS3, respectively. Therefore, competition for pellet-mobilized P_i was most likely the strongest during this intermediate growth stage, where the

microorganisms were most P-deficient and plants were growing rapidly.

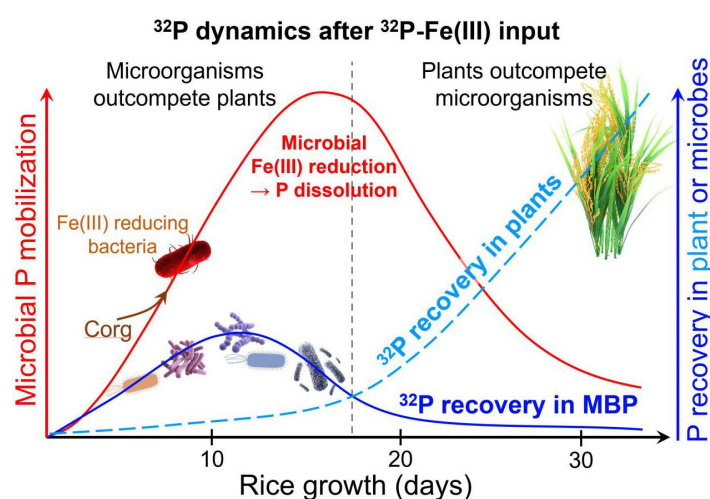


Fig. 7 Conceptual scheme demonstrating the shift from microorganisms outcompeting rice plants for phosphorus to rice plants outcompeting microorganisms. Red solid line demonstrates the dynamics of microbially driven Fe(III) reduction. Blue lines show ³²P recovery either in rice plants (dashed line) or in microbial biomass (solid line) with rice plant growth.

The increase in MBC and MBP contents did not translate to increased enzyme activities, especially in the rooted soil (Fig. 4, 6). This may be explained by the difference between the total microbial biomass mainly representing dormant species and the active microorganisms performing most of the biochemical processes (Blagodatskaya et al., 2014). The amount of available C is typically higher in rooted soil than in bulk soil, which results in a much higher fraction of active microorganisms in a physiologically alert stage (De Nobili et al., 2001). Microorganisms have adopted strategies in response to P limitation during rice growth as inferred from the affinity of the measured enzymes to respective substrates (K_m values) (Fig. 6). One of the most likely strategies of microorganisms to cope with P limitation is the increase of the affinity of their own phosphatase to the substrate (Lazali and Bargaz, 2017). This may suggest that a selection of microorganisms featuring high-affinity enzymes thrived and outcompeted those with low-affinity enzymes during rice growth (Fig. 5c). The K_m values in the rooted soil increased by 18–78% at DS2 vs. DS1, but decreased by 46–68% at DS3 vs. DS2 (Fig. 6), indicating an increase in the affinity of phosphomonoesterase to substrates with decreasing P_i availability. This confirms an increasing P competition with rice growth.

In summary, microbial biomass and enzyme activities were linked to the rice growth in this nutrient-limited low-redox environment and their dynamics were strongly depended on P_i availability. Rice plants eventually outcompeted microorganisms for P_i uptake from poorly available Fe-P. This stimulated microorganisms to forage other P sources (i.e., P_o sources) in the system where the roots had direct access to Fe-P. These findings did not only support the third hypothesis but most notably opened further perspectives for the investigation of the

contribution of P_i and P_o to the nutrition balance and competition between microorganisms and plants under changing redox conditions.

5. Conclusions

We demonstrated that the establishment of low redox conditions (E_h values between -160 and -230 mV) drove P release from the ferric iron-bound P into soil solution. The Fe(III) reduction and subsequent dissolution of Fe-P increased the P_i availability, which affected microbial biomass and phosphomonoesterase activity in the P-deficient soils. Although the E_h values corresponded to the conditions of Fe reduction, the ^{32}P recovery and the total Fe concentration in the soil solution decreased after 19 days of rice growth. Microbial biomass and enzyme activities were higher when Fe-P pellets could be accessed directly by the roots as compared to the soils with Fe-P pellets in mesh bags. This stimulation of microorganisms by the Fe-P dissolution interacts with the higher availability of easily accessible C released by roots at the surface of the pellets. This C exudation also increased the production of phosphomonoesterases leading to increased mineralization of organic P under P-deficient conditions. The intensively growing rice plants increased the competition for resources with microorganisms, which resulted in a reduction of microbial biomass, likely the mineralization of the necromass, and the recycling of P released by increased phosphomonoesterase activity. Finally, the MBN dynamics contrasted the MBC and MBP dynamics, revealing a strong C and P co-limitation. Although the released P_i by ferrihydrite reduction and dissolution is accessible to plants and microorganisms under low redox conditions, the released P_i amount was not sufficient to fully meet the P requirements of both rice plants and microorganisms. Once a threshold of root growth was passed (tillering stage), rice plants outcompeted microorganisms for the P_i uptake from the soil solution. Given that the Fe(III) reduction and Fe-P dissolution could compensate the P demand of rice plants, phosphate fertilization strategies should be adapted considering P_i mobilization from Fe (oxyhydr)oxides in paddy soils.

Acknowledgments

The authors gratefully acknowledge the China Scholarship Council (CSC) for financial support for Chaoqun Wang. This work was supported by the research grant from German Research Foundation (DO 1533/3-1; GU 406/33-1; HO4020/8-1). Michaela Dippold was funded by the Robert Bosch Junior Professorship. The authors would like to thank Bernd Kopka and Marvin Blaue of the Laboratory for Radioisotopes (LARI) of the University of Goettingen for their advice, support, and measurements. We also thank Jake Beyer and Dr. Florian Carstens for constructive advising as well as a technical staff of the Department of Agricultural Soil Science, University of Goettingen, Karin Schmidt, for microbial biomass carbon and nitrogen measurements.

References

- Achat, D.L., Pousse, N., Nicolas, M., Brédoire, F., Augusto, L., 2016. Soil properties controlling inorganic phosphorus availability: general results from a national forest network and a global compilation of the literature. *Biogeochemistry* 127, 255–272.
- Alexander, M., 1977. *An Introduction to Soil Microbiology*. Wiley, New York.
- Amarawansa, E.A.G.S., Kumaragamage, D., Flaten, D., Zvomuya, F., Tenuta, M., 2015. Phosphorus mobilization from manure-amended and unamended alkaline soils to overlying water during simulated flooding. *J. Environ. Qual.* 44(4), 1252–1262.
- Ann, Y., Reddy, K.R., Delfino, J.J., 2000. Influence of redox potential on phosphorus solubility in chemically amended wetland organic soils. *Ecol. Eng.* 14, 169–180.
- Bacilio-Jiménez, M., Aguilar-Flores, S., Ventura-Zapata, E., Pérez-Campos, E., Bouquelet, S., Zenteno, E., 2003. Chemical characterization of root exudates from rice (*Oryza sativa*) and their effects on the chemotactic response of endophytic bacteria. *Plant Soil* 249(2), 271–277.
- Becquer, A., Trap, J., Irshad, U., Ali, M.A., Plassard, C., 2014. From soil to plant, the journey of P through trophic relationships and ectomycorrhizal association. *Front. Plant Sci.* 5, 548.
- Blagodatskaya, E., Blagodatsky, S., Anderson, T.H., Kuzyakov, Y., 2014. Microbial growth and carbon use efficiency in the rhizosphere and root-free soil. *Plos One* 9.
- Blagodatskaya, E., Kuzyakov, Y., 2013. Active microorganisms in soil: critical review of estimation criteria and approaches. *Soil Biol. Biochem.* 67, 192–211.
- Brookes, P.C., Landman, A., Pruden, G., Jenkinson, D., 1985. Chloroform fumigation and the release of soil nitrogen: a rapid direct extraction method to measure microbial biomass nitrogen in soil. *Soil Biol. Biochem.* 17, 837–842.
- Bünemann, E.K., 2015. Assessment of gross and net mineralization rates of soil organic phosphorus – A review. *Soil Biol. Biochem.* 89, 82–98.
- Chen, J., Seven, J., Zilla, T., Dippold, M.A., Blagodatskaya, E., Kuzyakov, Y., 2019. Microbial C:N:P stoichiometry and turnover depend on nutrient availability in soil: a ¹⁴C, ¹⁵N and ³³P triple labelling study. *Soil Biol. Biochem.* 131, 206–216.
- Cross, A.F., Schlesinger, W.H., 1995. A literature review and evaluation of the Hedley fractionation: Applications to the biogeochemical cycle of soil phosphorus in natural ecosystems. *Geoderma* 64, 197–214.
- Cui, J., Zhu, Z., Xu, X., Liu, S., Jones, D.L., Kuzyakov, Y., Wu, J., Ge, T., 2020.

- Carbon and nitrogen recycling from microbial necromass to cope with C:N stoichiometric imbalance by priming. *Soil Biol. Biochem.* 142, 107720.
- Darrah, P.R., 1991. Models of the rhizosphere. I. Microbial population dynamics around a root releasing soluble and insoluble carbon. *Plant Soil* 133, 187–199.
- De Nobili, M., Contin, M., Mondini, C., Brookes, P.C., 2001. Soil microbial biomass is triggered into activity by trace amounts of substrate. *Soil Biol. Biochem.* 33, 1163–1170.
- Devau, N., Cadre, E.L., Hinsinger, P., Jaillard, B., Gérard, F., 2009. Soil pH controls the environmental availability of phosphorus: experimental and mechanistic modelling approaches. *Appl. Geochem.* 24, 2163–2174.
- Ding, S., Wang, Y., Wang, D., Li, Y.Y., Gong, M., Zhang, C., 2016. In situ, high-resolution evidence for iron-coupled mobilization of phosphorus in sediments. *Sci. Rep.* 6.
- Elrod, V.A., Johnson, K.S., Coale, K.H., 1991. Determination of subnanomolar levels of iron(II) and total dissolved iron in seawater by flow injection analysis with chemiluminescence detection. *Anal. Chem.* 63(9), 893–898.
- Elser, J.J., Bracken, M., Cleland, E.E., Gruner, D.S., Harpole, W.S., Hillebrand, H., Ngai, J.T., Seabloom, E.W., Shurin, J.B., Smith, J.E., 2007. Global analysis of nitrogen and phosphorus limitation of primary producers in freshwater, marine and terrestrial ecosystems. *Ecol. Lett.* 10(12), 1135–1142.
- Farrar, J.F., Jones, D.L., 2000. The control of carbon acquisition by roots. *New Phytol.* 147, 43–53.
- Ge, T., Wei, X., Razavi, B.S., Zhu, Z., Hu, Y., Kuzyakov, Y., Jones, D., Wu, J., 2017. Stability and dynamics of enzyme activity patterns in the rice rhizosphere: Effects of plant growth and temperature. *Soil Biol. Biochem.* 113, 108–115.
- Gong, Z.T., Zhang, G.L., Chen, Z.C. (Eds.), 2007. *Pedogenesis and Soil Taxonomy*. Science Press, Beijing, China, pp. 613–626.
- Gunina, A., Kuzyakov, Y., 2015. Sugars in soil and sweets for microorganisms: review of origin, content, composition and fate. *Soil Biol. Biochem.* 90, 87–100.
- Hansel, C.M., Fendorf, S., Sutton, S., Newville, M., 2001. Characterization of Fe plaque and associated metals on the roots of mine-waste impacted aquatic plants. *Environ. Sci. Technol.* 35, 3863–3868.
- Hanson, H., Frohne, M., 1976. Crystalline leucine aminopeptidase from lens (α -aminoacyl-peptide hydrolase; EC 3.4.11.1). *Methods Enzymol.* 45, 504–521.
- Hedley, M.J., Stewart, J.W.B., Chauhan, B.S., 1982. Changes in inorganic and organic soil phosphorus fractions induced by cultivation practices and by laboratory incubations. *Soil Sci. Soc. Am. J.* 46, 970–976.

- Heinrich, L., Rothe, M., Braun, B., Hupfer, M., 2020. Transformation of redox-sensitive to redox-stable iron-bound phosphorus in anoxic lake sediments under laboratory conditions. *Water Res.* 189, 116609.
- Helfenstein, J., Jegminat, J., McLaren, T.I., Frossard, E., 2018. Soil solution phosphorus turnover: derivation, interpretation, and insights from a global compilation of isotope exchange kinetic studies. *Biogeosciences* 15, 105–114.
- Hinsinger, P., 2001. Bioavailability of soil inorganic P in the rhizosphere as affected by root-induced chemical changes: a review. *Plant Soil* 237, 173–195.
- Jorquera, M.A., Hernandez, M.T., Rengel, Z., Marschner, P., de la Luz Mora, M., 2008. Isolation of culturable phosphobacteria with both phytate-mineralization and phosphate-solubilization activity from the rhizosphere of plants grown in a volcanic soil. *Biol. Fert. Soils* 44, 1025–1044.
- Kong, C.H., Wang, P., Zhao, H., Xu, X.H., Zhu, Y.D., 2008. Impact of allelochemicals exuded from allelopathic rice on the soil microbial community. *Soil Biol. Biochem.* 40, 1862–1869.
- Köster, M., Stock, S.C., Nájera, F., Abdallah, K., Gorbushina, A., Prietzel, J., Matus, F., Klysubun, W., Boy, J., Kuzyakov, Y., Dippold, A.M., Spielvogel, S., 2020. From rock eating to vegetarian ecosystems—disentangling processes of phosphorus acquisition across biomes. *Geoderma* 388, 114827.
- Kouno, K., Tuchiya, Y., Ando, T., 1995. Measurement of soil microbial biomass phosphorus by an anion exchange membrane method. *Soil Biol. Biochem.* 27, 1353–1357.
- Kunito, T., Hiruta, N., Miyagishi, Y., Sumi, H., Moro, H., 2018. Changes in phosphorus fractions caused by increased microbial activity in forest soil in a short-term incubation study. *Chem. Spec. Bioavailab.* 30, 9–13.
- Kuzyakov, Y., Blagodatskaya, E., 2015. Microbial hotspots and hot moments in soil: concept & review. *Soil Biol. Biochem.* 83, 184–199.
- Larsen, M., Santner, J., Oburger, E., Wenzel, W.W., Glud, R.N., 2015. O₂ dynamics in the rhizosphere of young rice plants (*Oryza sativa* L.) as studied by planar optodes. *Plant Soil* 390 279–292.
- Lazali, M., Bargaz, A., 2017. Examples of belowground mechanisms enabling legumes to mitigate phosphorus deficiency. In *Legume Nitrogen Fixation in Soils with Low Phosphorus Availability*; Springer: Berlin/Heidelberg, Germany, pp. 135–152.
- Ling, N., Wang, T., Kuzyakov, Y., 2022. Rhizosphere bacteriome structure and functions. *Nat. Commun.* 13, 836.
- Liu, H., Ding, Y., Zhang, Q., Liu, X., Xu, J., Li, Y., Di, H., 2019. Heterotrophic nitrification and denitrification are the main sources of nitrous oxide in two paddy

- soils. *Plant Soil* 445, 55–69.
- Liu, Q., Ding, S., Chen, X., Sun, Q., Chen, M., Zhang, C., 2018. Effects of temperature on phosphorus mobilization in sediments in microcosm experiment and in the field. *Appl. Geochem.* 88, 158–166.
- Loeppmann, S., Breidenbach, A., Spielvogel, S., Dippold, M. A., Blagodatskaya, E., 2020. Organic nutrients induced coupled C-and P-cycling enzyme activities during microbial growth in forest soils. *Front. For. Glob. Change* 3, 100.
- Lovley, D.R., Holmes, D.E., Nevin, K.P., 2004. Dissimilatory Fe(III) and Mn(IV) reduction. *Adv. Microb. Physiol.* 49, 219–286.
- Marchant, H.K., Ahmerkamp, S., Lavik, G., Tegetmeyer, H.E., Graf, J., Klatt, J.M., Holtappels, M., Walpersdorf, E., Kuypers, M.M.M., 2017. Denitrifying community in coastal sediments performs aerobic and anaerobic respiration simultaneously. *ISME J.* 11, 1799–1812.
- Marschner, P., Crowley, D., Rengel, Z., 2011. Rhizosphere interactions between microorganisms and plants govern iron and phosphorus acquisition along the root axis – model and research methods. *Soil Biol. Biochem.* 43, 883–894.
- Marx, M., Wood, M., Jarvis, S., 2001. A fluorimetric assay for the study of enzyme diverooted soility in soils. *Soil Biol. Biochem.* 33, 1633–1640.
- McConnell, C.A., Kaye, J.P., Kemanian, A.R., 2020. Reviews and Syntheses: Ironing out wrinkles in the soil phosphorus cycling paradigm. *Biogeosciences* 17, 5309–5333.
- Mooshammer, M., Wanek, W., Zechmeister-Boltenstern, S., Richter, A., 2014. Stoichiometric imbalances between terrestrial decomposer communities and their resources: Mechanisms and implications of microbial adaptations to their resources. *Front. Microbiol.* 5, 22.
- Nannipieri, P., Giagnoni, L., Landi, L., Renella, G., 2011. Role of phosphatase enzymes in soil. In: Bünemann, E., Oberson, A., Frossard, E. (Eds.), *Phosphorus in Action. Soil Biology*, Vol. 26. Springer, Berlin, Heidelberg, pp. 215–243.
- Paterson, E., 2000. Iron oxides in the laboratory. preparation and characterization. *Clay Miner.* 27(3), 393–393.
- Pistocchi, C., Mészáros, É., Tamburini, F., Frossard, E., and Bünemann, E.K., 2018. Biological processes dominate phosphorus dynamics under low phosphorus availability in organic horizons of temperate forest soils. *Soil Biol. Biochem.*, 126, 64–75.
- Razavi B.S., Zarebanadkouki M., Blagodatskaya E., Kuzyakov Y. 2016. Rhizosphere shape of lentil and maize: Spatial distribution of enzyme activities. *Soil Biol. Biochem.* 96, 229–237.
- Reed, S., Vitousek, P., Cleveland, C., 2011. Are patterns in nutrient limitation

- belowground consistent with those aboveground: results from a 4 million year chronosequence. *Biogeochemistry* 106, 323–336.
- Robinson, D., 1994. The responses of plants to non-uniform supplies of nutrients. *New Phytol.* 127, 635–674.
- Saleque, M.A., Abedin, M.J., Bhuiyan, N.I., 1996. Effect of moisture and temperature regimes on available phosphorus in wetland rice soils. *Commun. Soil Sci. Plant Anal.* 27, 2017–2023.
- Santos-Beneit, F., 2015. The Pho regulon: a huge regulatory network in bacteria. *Front. Microbiol.* 6, 402.
- Shen, J.B., Yuan, L.X., Zhang, J.L., Li, H.J., Bai, Z.H., Chen, X.P., Zhang, W.F., Zhang, F.S., 2011. Phosphorus dynamics: from soil to plant. *Plant Physiol.* 156(3), 997–1005.
- Siebner-Freibach, H., Hadar, Y., Chen, Y., 2004. Interaction of iron chelating agents with clay minerals. *Soil Sci. Soc. Am. J.* 68, 470–480.
- Tang, Y.Q., Zhang, X.Y., Li, D.D., Wang, H.M., Chen, F.S., Fu, X.L., Fang, X.M., Sun, X.M., Yu, G.R., 2016. Impacts of nitrogen and phosphorus additions on the abundance and community structure of ammonia oxidizers and denitrifying bacteria in Chinese fir plantations. *Soil Biol. Biochem.* 103, 284–293.
- Tian, J., Dippold, A.M., Pausch, J., Blagodatskaya, E., Fan, M.S., Li, X.L., Kuzyakov, Y., 2013. Microbial response to rhizodeposition depending on water regimes in paddy soils. *Soil Biol. Biochem.* 65, 195–203.
- Upreti, K., Joshi, S.R., McGrath, J., Jaisi, D.P., 2015. Factors controlling phosphorus mobilization in a Coastal Plain tributary to the Chesapeake Bay. *Soil Sci. Soc. Am. J.* 79, 826–837.
- Vance, E., Brookes, P., Jenkinson, D., 1987. An extraction method for measuring soil microbial biomass C. *Soil Biol. Biochem.* 19, 703–707.
- Vershinina, O., Znamenskaya, L., 2002. The Pho regulons of bacteria. *Microbiology* 71, 497–511.
- Vitousek, P.M., Farrington, H., 1997. Nutrient limitation and soil development: experimental test of a biogeochemical theory. *Biogeochemistry* 37, 63–75.
- Wang, C.Q., Dippold, M.A., Blagodatskaya, E., Dorodnikov, M., 2022. Oxygen matters: Short- and medium-term effects of aeration on hydrolytic enzymes in a paddy soil. *Geoderma* 407, 115548.
- Wang, C.Q., Xue, L., Jiao, R.Z., 2021. Soil phosphorus fractions, phosphatase activity, and the abundance of *phoC* and *phoD* genes vary with planting density in subtropical Chinese fir plantations. *Soil. Till. Res.* 209(4), 104946.
- Wang, Y., Yuan, J.H., Chen, H., Zhao, X., Wang, D., Wang, S.Q., Ding, S.M., 2019.

- Small-scale interaction of iron and phosphorus in flooded soils with rice growth. *Sci. Total Environ.* 669, 911–919.
- Watt, M., McCully, M.E., Kirkegaard, J.A., 2003. Soil strength and rate of root elongation alter the accumulation of *Pseudomonas* spp. and other bacteria in the rhizosphere of wheat. *Funct. Plant Biol.* 30, 483–491.
- Weber, K.A., Achenbach, L.A., Coates, J.D., 2006. Microorganisms pumping iron: anaerobic microbial iron oxidation and reduction. *Nat. Rev. Microbiol.* 4(10), 752–764.
- Wei, X.M., Hu, Y.J., Peng, P.Q., Zhu, Z.K., Atere, C.T., O'Donnell, A.G., Wu, J.S., Ge, T.D., 2017. Effect of P stoichiometry on the abundance of nitrogen-cycle genes in phosphorus-limited paddy soil. *Biol. Fertil. Soils* 53, 767–776.
- Wei, X.M., Razavi, B.S., Hu, Y.J., Xu, X.L., Zhu, Z.K., Liu, Y.H., Kuzyakov, Y., Li, Y., Wu, J.S., Ge, T.D., 2019. C/P stoichiometry of dying rice root defines the spatial distribution and dynamics of enzyme activities in root-detritusphere. *Biol. Fertil. Soils* 55, 251–263.
- Wen, T., Yu, G., Hong, W., Yuan, J., Niu, G., Xie, P., Sun, F., Guo, L., Kuzyakov, Y., Shen, Q., 2022. Root exudate chemistry affects soil carbon mobilization via microbial community reassembly. *Fundam. Res.* (in press). <https://doi.org/10.1016/j.fmre.2021.12.016>
- Wu, T., Wang, G., Zhang, Y., Kong, M., Zhao, H., 2017. Determination of mercury in aquatic systems by DGT device using thiol-modified carbon nanoparticle suspension as the liquid binding phase. *New J. Chem.* 41, 10305–10311.
- Xu, D., Wu, W., Ding, S., Sun, Q., Zhang, C., 2012. A high-resolution dialysis technique for rapid determination of dissolved reactive phosphate and ferrous iron in pore water of sediments. *Sci. Total Environ.* 421–422, 245–252.
- Yan, X., Wei, Z., Hong, Q., Lu, Z., Wu, J., 2017. Phosphorus fractions and sorption characteristics in a subtropical paddy soil as influenced by fertilizer sources. *Geoderma* 295, 80–85.
- Zhu, Z., Ge, T., Luo, Y., Liu, S., Xu, X., Tong, C., Shibistova, O., Guggenberger, G., Wu, J., 2018. Microbial stoichiometric flexibility regulates rice straw mineralization and its priming effect in paddy soil. *Soil Biol. Biochem.* 121, 67–76.

Supplementary

Table S1 The effects of treatment (Pellets-in-mesh bag vs. Pellets-no-mesh bag), soil compartment, and their interactions on microbial biomass carbon (MBC) and nitrogen (MBN) analyzed by two-way ANOVA with repeated measures (destructive sampling, $n = 3$)

	Statistic	Treatment	Compartment	Treatment \times Compartment
MBC	F	1.484	14.075	0.334
	P	0.263	0.004	0.727
MBN	F	2.771	1.330	1.307
	P	0.157	0.344	0.349

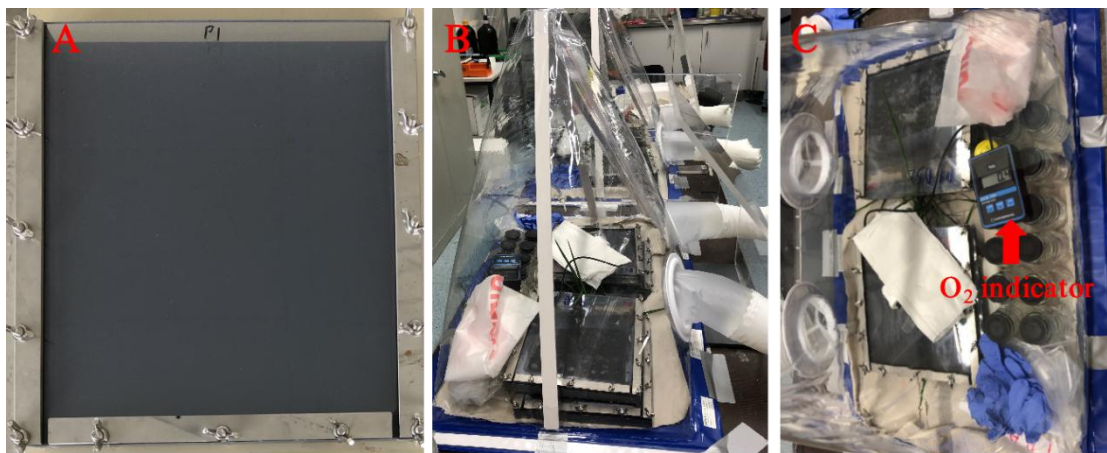


Fig. S1 The construction of a rhizobox with plexiglas cover on top, sealed with rubber gasket (not visible on photo) and fixed by thumbscrews (A), a portable PVC glovebox filled with N_2 and with rhizoboxes inside (B), the level of O_2 as indicated by an O_2 -sensor (C).

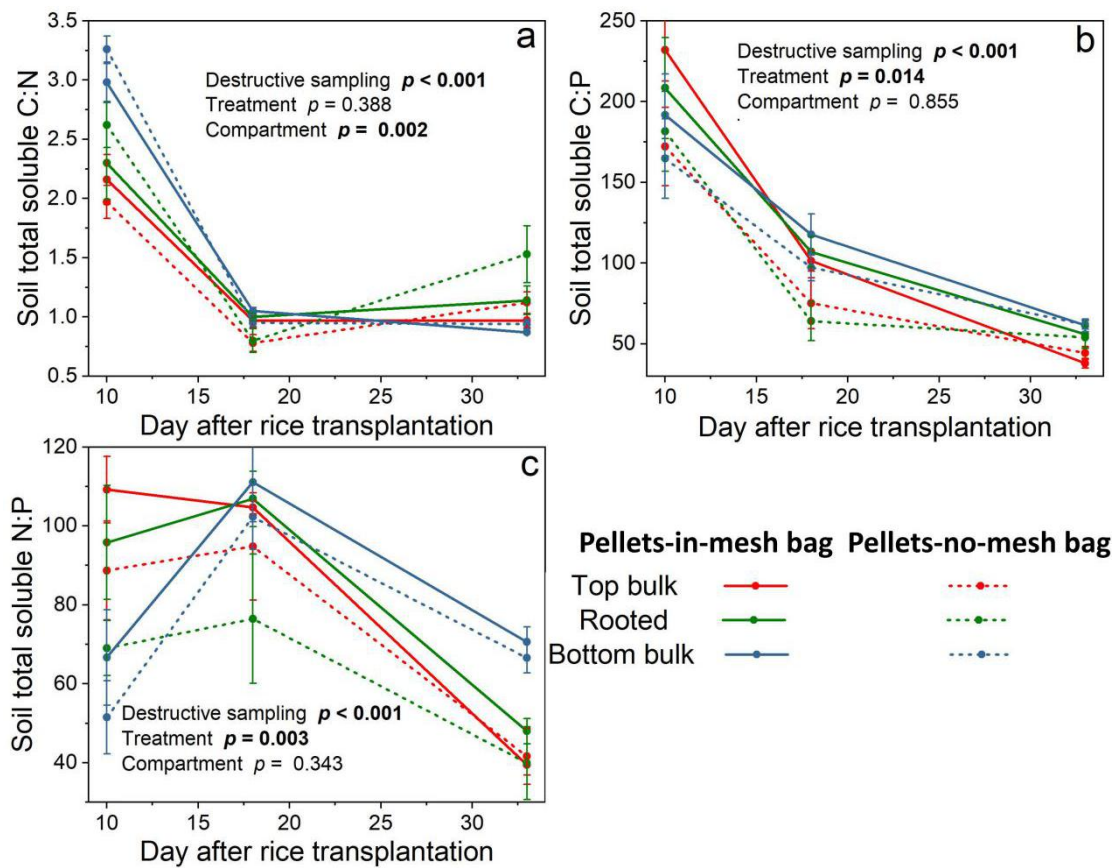


Fig. S2 Soil total soluble carbon (C):nitrogen (N):phosphorus stoichiometries in the top bulk, rooted, and bottom bulk soil under the Pellets-in-mesh bag and Pellets-no-mesh bag treatment in the first (DS1, 10 days), second (DS2, 18 days), and third destructive sampling (DS3, 33 days) after rice transplantation. The data are the means \pm standard errors ($n = 4$).

Study 5 Microbial iron reduction compensates for phosphorus limitation in paddy soils

Chaoqun Wang^{a,*}, Lukas Thielemann^a, Michaela A. Dippold^{a,b}, Georg Guggenberger^c, Yakov Kuzyakov^{d,e,f}, Callum C. Banfield^{a,b}, Tida Ge^g, Stephanie Guenther^c, Patrick Bork^h, Marcus A. Horn^h, Maxim Dorodnikov^{a,d,#}

^a Biogeochemistry of Agroecosystems, University of Goettingen, 37077 Goettingen, Germany

^b Geo-Biosphere Interactions, University of Tuebingen, 72076 Tuebingen, Germany

^c Institute of Soil Science, Leibniz University Hannover, 30419 Hannover, Germany

^d Department of Soil Science of Temperate Ecosystems, University of Goettingen, 37077 Goettingen, Germany

^e Agricultural Soil Science, University of Goettingen, 37077 Goettingen, Germany

^f Peoples Friendship University of Russia (RUDN University), 117198 Moscow, Russia

^g State Key Laboratory for Managing Biotic and Chemical Threats to the Quality and Safety of Agro-products, Institute of Plant Virology, Ningbo University, 315211 Ningbo, Zhejiang, China

^h Institute of Microbiology, Leibniz University Hannover, 30419 Hannover, Germany

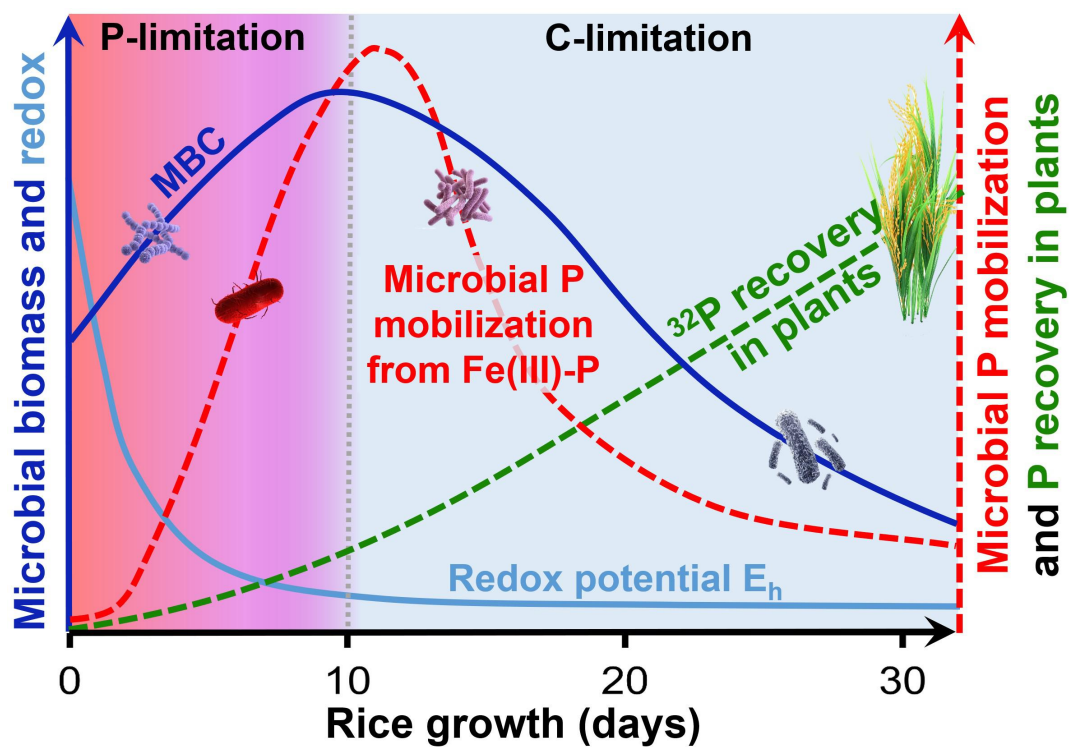
[#] now at: Institute for Landscape Ecology, University of Münster, 48149 Münster, Germany

* **Correspondence:** chaoqun.wang@forst.uni-goettingen.de

Status: Published in Science of the Total Environment

Wang, C.Q., Thielemann, L., Dippold, M.A., Guggenberger, G., Kuzyakov, Y., Banfield, C.C., Ge, T.D., Guenther, S., Bork, P., Horn, M.A., Dorodnikov, M., 2022. Microbial iron reduction compensates for phosphorus limitation in paddy soils. Science of the Total Environment 837, 155810.

Graphical abstract



Conceptual scheme demonstrating the shift from P-limitation to C-limitation for microorganisms during 33 days of rice growth. Blue lines show either microbial biomass C (MBC) or redox potential E_h dynamics with rice growth. Red dashed line demonstrates the dynamics of microbially-mediated Fe(III) reduction. Green dashed line shows ^{32}P recovery in rice plants with rice plant growth.

Abstract: Limitation of rice growth by low phosphorus (P) availability is a widespread problem in tropical and subtropical soils because of the high content of iron (Fe) (oxyhydr)oxides. Ferric iron-bound P (Fe(III)-P) can serve as a P source in paddies after Fe(III) reduction to Fe(II) and corresponding H_2PO_4^- release. However, the relevance of reductive dissolution of Fe(III)-P for plant and microbial P uptake is still an open question. To quantify this, ^{32}P -labeled ferrihydrite ($30.8 \text{ mg P kg}^{-1}$) was added to paddy soil microcosms with rice to trace the P uptake by microorganisms and plants after Fe(III) reduction. Nearly 2% of ^{32}P was recovered in rice plants, contributing 12% of the total P content in rice shoots and roots after 33 days. In contrast, ^{32}P recovery in microbial biomass decreased from 0.5% to 0.08% of ^{32}P between 10–33 days after rice transplantation. Microbial biomass carbon (MBC) and dissolved organic C content decreased from day 10 to 33 by 8–54% and 68–77%, respectively, suggesting that the microbial-mediated Fe(III) reduction was C-limited. The much faster decrease of MBC in rooted (by 54%) vs. bulk soil (8–36%) reflects very fast microbial turnover in the rice rhizosphere (high C and oxygen inputs) resulting in the mineralization of the microbial necromass. In conclusion, Fe(III)-P can serve as small but a relevant P source for rice production and could partly compensate plant P demand. Therefore, the P fertilization strategies should consider the P mobilization from Fe (oxyhydr)oxides in flooded paddy soils during rice growth. An increase in C availability for microorganisms in the rhizosphere intensifies P mobilization, which is especially critical at early stages of rice growth.

Keywords: phosphorus isotopes; phosphorus pools and availability; ferric iron reduction; redox potential; land use in subtropics; plant-microbial competition

1. Introduction

Low phosphorus (P) availability limits plant production, especially in acidic tropical and subtropical soils that are strongly weathered and residually enriched in iron (Fe) and aluminum (Al) (LeBauer et al., 2008; Turner et al., 2018; Hou et al., 2020; Wang et al., 2021). The application of fertilizers derived from non-renewable rock phosphates is the most important agricultural strategy to cope with P limitation for plants (Menezes-Blackburn et al., 2017). However, only 10–25% of applied P is taken by crops within the growing season (Zhang et al. 2008; Syers et al., 2008); the remainder is retained mainly by sorption on metal (Fe, Al) (oxyhydr)oxides in acidic soils (Bindraban et al., 2020). Moreover, the rock phosphate used to produce P fertilizers is a non-renewable resource and will inevitably be depleted in the future (Cordell et al., 2009). Therefore, in-depth understanding of the P mobilization and recycling mechanisms is of significance to prevent the overuse of mineral P fertilizers and to sustain crop yields.

Rice (*Oryza sativa* L.) cultivated on flooded paddy fields is one of the predominant global food sources (Fairhurst and Dobermann, 2002). Inorganic P in paddy soils largely appears in the form of ferric Fe phosphates (Fe(III)-P), which accounts for approximately 30% of the total P in the soils where rice has been planted for more than 20 years (Darilek, 2010). Phosphorus availability increases in flooded paddy soils with low redox potentials due to the Fe(III) reduction and dissolution (Rabeharisoa et al., 2012). Understanding the contribution of the reductive dissolution of Fe(III)-P to compensate for the P limitation in paddy soils is an important strategy to simultaneously reduce the use of P fertilizers and maintain rice yield. However, knowledge gaps in tracing the dynamic of P released from Fe(III)-P dissolution in paddy soils are associated with (1) alternative electron acceptors (e.g., NO_3^-) that maintain high redox potentials even in the absence of O_2 and (2) various forms of Fe(III) (oxyhydr)oxides with considerable differences in their dissolution kinetics.

The mobilization and equilibrium of Fe(III)-P depend mainly on the biota, i.e., dissimilatory Fe(III)-reducing microorganisms (Lovely et al., 2004), and abiotic factors including redox potential (Schmidt et al., 2011) as well as pH (Devau et al., 2009). Under flooded conditions, Fe(III) is the most common terminal electron acceptor for anaerobic microorganisms to maintain their metabolism, especially in strongly weathered acidic soils (Weber et al., 2006; Sánchez-Alcalá et al., 2011). Microbial biomass decrease is one of the main reasons for the slowdown in reductive dissolution of Fe(III)-P in flooded paddy soils (Wang et al., 2022). However, large uncertainties exist regarding the compensation of microbially mediated reduction of Fe(III) for P release during the rice growth due to (1) the disproportionality between the decrease in soil redox potential and the Fe(III) reduction with the H_2PO_4^- release and (2) competition for P between microorganisms and rice plants under P deficiency (Wei et al., 2021b). Microbial-mediated reduction of Fe(III) is strongly affected by dissolved organic carbon (DOC), which is used as a substrate and an energy source by

microorganisms in paddy soils (Kögel-Knabner et al., 2010; Liu et al., 2022). Increased DOC accelerates the reductive dissolution of Fe(III) (oxyhydr)oxides mediated by microorganisms (Scalenghe et al., 2002; Rakotoson et al., 2015; Maranguit et al., 2017). Some DOC species carry redox-sensitive functional groups (Fimmen et al., 2007) and serve as an electron shuttle between bacteria and iron oxides (Lovley et al., 1998; Yu and Kuzyakov, 2021). Thus, P released by Fe(III) reduction mediated by microorganisms will be stimulated in soils with high labile C availability under reducing conditions.

Although many studies have reported the increase in P bioavailability after Fe(III) reduction in flooded soils, the subsequent P uptake by rice and thus the relevance of P release for plant growth has not yet been demonstrated. Using microcosms with rice plants grown in a continuously flooded paddy soil, we traced the dynamics of P uptake by plants and competition between plants and microorganisms based on ^{32}P -labeling of Fe(III)-P 33 days after rice transplantation. We hypothesized that (1) reductively dissolving Fe(III)-P contributes to the P nutrition of plants and microorganisms; (2) the P limitation in highly weathered paddy soils results in fierce competition between rice plants and microorganisms; and (3) the competitiveness of microorganisms for P strongly depends on C availability. The results of the study can be highly relevant for the explanation of soil P cycling mechanisms under anoxic conditions and should be considered for the development of P fertilization strategies.

2. Materials and methods

2.1. Soil description and experimental setup

The soil was collected from a paddy rice field (depth of 0–20 cm) after the second rice harvest (November–December 2017) at the Changsha Agricultural and Environmental Monitoring Station, Hunan Province (113°19'52" E, 28°33'04" N). The station is located in an area with typical Stagnic Anthrosols derived from highly weathered granite in the Subtropical Region of China (Gong et al., 2007). The annual average temperature is 17.5°C, and the annual average precipitation is 1300 mm. The main soil physicochemical properties were: pH 6.2, soil organic C 13.1 g kg⁻¹, total N 1.4 g kg⁻¹, available N 18.0 mg kg⁻¹, total P 0.3 g kg⁻¹, Olsen-P 3.7 mg kg⁻¹, and total Fe 15.7 g kg⁻¹ (Zhu et al., 2018). The soil was sieved through a 2 mm mesh, air-dried, and homogenized prior to the transportation to Germany.

A microcosm experiment with growing rice was set in water-tight PVC rhizoboxes (24 in total) with inner dimensions of 24.0 (height) × 20.5 (width) × 1.5 cm (depth) (Fig. S1A). To mimic field conditions when mineral P is bound to Fe(III) minerals (i.e. ferrihydrite) and thus is not directly available for plant uptake, Fe(III)-P was placed as pellets into all rhizoboxes (see section 2.2 below). In detail, 420 g of air-dried soil was prefilled and saturated by deionized water in each rhizobox 16–24 h prior addition of Fe(III)-P pellets (Fig. S2). The Fe(III)-P pellets were placed at the center of rhizoboxes on the surface of prefilled soil, then covered with 230 g of

remaining soil (Fig. S2). This soil was saturated with water, trapped air bubbles were removed by knocking, and one pre-germinated rice seedling (*O. sativa* L. ‘Two-line hybrid rice Zhongzao 39’; seedlings with similar size were selected) was planted at 1 cm depth below the surface. All rhizoboxes with transplanted rice seedlings were filled with water to a depth of 2 cm above the soil surface and left growing in a climate chamber (RUMED® Premium-Line P 1700, Rubarth Apparate GmbH, Germany) with $28 \pm 1^\circ\text{C}$ day and $24 \pm 1^\circ\text{C}$ night temperatures, 70% relative humidity, and 12 h photoperiod. A water layer above the soil surface was maintained during the entire rice growth, except during destructive sampling dates (see section 2.3 below). Immediately after transplanting, the nutrient solution was applied at a rate of 30 mg N (as urea) per kg dry soil as background fertilizer.

Soil redox potential (E_h) was monitored in each rhizobox by a platinum electrode installed at 10 cm depth (Fig. S2). E_h was measured using an E_h -meter (GMH 3531, GHM Messtechnik GmbH, Germany). A soil solution was collected every 2–5 days during the experiment from the area of pellet placement using Microrhizon samplers (MicroRhizons, Rhizosphere Research Products, Netherlands) and pre-evacuated N_2 -flushed 30-mL glass bottles (Fig. S2).

2.2. *Fe(III)-P pellet preparation and labelling with ^{32}P*

To prepare Fe(III)-P pellets, 10 g of purified Quartz-sand (as matrix) and 0.7 g of synthesized ferrihydrite (Paterson, 2000) per rhizobox were weighed into a 100-mL glass centrifuge tube and then mixed well by hand. We added 30 ml of 3.75 g L^{-1} K_2HPO_4 solution spiked with ^{32}P -labeled H_3PO_4 (Hartmann Analytic GmbH, Braunschweig, Germany) to each centrifuge tube. Additionally, 2 ml of 1 M HCl (pH 4) was added to pellets to increase the P absorbance efficiency. All tubes were shaken for 2 h on a rotator (200 rpm) and then centrifuged at $3000 \times g$ for 15 min. The activity in the supernatant was measured on a Liquid Scintillation Analyser (LSA) (Tri-Carb® 2800 TR, PerkinElmer, Shelton, CT, USA). Briefly, 10 μL supernatant was mixed with 10 mL scintillation cocktail (Rotiszint®eco plus, Carl Roth, Germany), then counting was conducted for 2 min. To purify pellets, the supernatant was removed, and 30 mL of deionized water was added to each tube. Thereafter, centrifugation and ^{32}P activity determination were repeated as described above. Prepared pellets were weighed on a balance into a petri-dish, then put into rhizoboxes using a spoon. In total, 20 mg P equivalent to mineral P fertilization of 80 kg ha^{-1} was added to each rhizobox. The initial ^{32}P activity of the pellet was estimated based on the duration of rice growth and planned three destructive samplings (see section 2.3 below). At the time of pellet application (t_0), approximately 5, 9, and 16 MBq of ^{32}P were employed per rhizobox with 2.0, 3.6, and 6.4 μL of $\text{H}_3^{32}\text{PO}_4$, respectively, to reach approximately 3.2–3.5 MBq of activity at each of destructive samplings, considering the ^{32}P half-life of 14.3 days.

2.3. *Destructive soil sampling*

Destructive sampling with eight rhizoboxes per sampling was conducted 10, 18, and 33 days after rice transplantation, respectively. The age of rice plants

approximately corresponded to tillering stage (with 2–4 tillers) of a vegetative phase of rice growth. The distribution of rice root systems at the time of three destructive samplings was as follows: mainly at the upper part of pellets at the 1st sampling, at the area of the pellet position at the 2nd sampling, and at the very bottom of the rhizobox at the 3rd sampling. The flooding water was drained before each sampling. To maintain anoxic conditions in the moist soil, all the rhizoboxes were opened inside a portable PVC glovebox (Captair® Pyramid Glovebox 3015-00, Erlab DFS, Saint-Maurice, France) (Fig. S1B) evacuated with a vacuum pump (Ilmvac MP 301 Vp, Ilmvac GmbH, Ilmenau, Germany), then back-flushed with nitrogen to a level of O₂ lower than 0.4% as indicated by an O₂-sensor (Greisinger GOX 100, GHM Messtechnik GmbH, Remscheid, Germany) (Fig. S1C). After the opening of a rhizobox, the soil was collected from three compartments: top bulk (2–5 cm), rooted (5–15 cm), and bottom bulk (15–18 cm) (Fig. S1D). In each compartment, soil was collected from three random locations, placed in an air-tight plastic bag, mixed into one sample of approximately 30 g moist weight, stored at 4°C for one day, and then used to measure microbial biomass carbon (MBC), microbial biomass phosphorus (MBP), and soil total dissolved C, nitrogen (N), and P.

2.4. Measurement of total Fe concentration and ³²P activity in soil solution

To measure total Fe concentration in soil solution, 10% ascorbic acid was used to completely reduce Fe³⁺ to Fe²⁺ for 30 min (Elrod et al., 1991). Then, a 2 ml sample was mixed with 500 µl ammonium acetate buffer (pH 4.5) and 500 µl phenanthroline solution (0.5%) in a cuvette and measured at 512 nm on a spectrophotometer (NanoPhotometer® NP80, IMPLLEN). Calibration was completed after the same procedure with FeCl₃ at increasing concentrations of 0, 5, 10, 25, 50, 100, 200, and 300 µM.

The ³²P activity in soil solution was determined in the Liquid Scintillation Analyser (LSA) (Tri-Carb® 2800 TR) and corrected for isotope decay. Briefly, 0.75 mL soil solution was mixed with 10 mL cocktail in a scintillation vial, and the activity was measured for 5 min. The percentage of P per liter soil solution derived from applied ³²P-labeled Fe(III)-P (%P) was calculated as:

$$\%P = (^{32}\text{P activity per liter solution [Bq]} / ^{32}\text{P activity in Fe(III)-P [Bq]}) * 100 \quad (1)$$

2.5. Plant ³²P uptake, microbial biomass, and soil dissolved C, N, and P

After harvest, shoots and roots were dried in an oven at 60°C for 48 h and then milled. Approximately 3 mg milled sample was used to measure C and nitrogen (N) contents in shoots or roots by an N/C analyzer (Multi N/C 2100S, Analytik-Jena, Germany). To measure total P content and ³²P activity in shoots and roots, ca. 100 mg of each sample was digested with 2 ml of 65% HNO₃ at 180°C for 8 h. Each digested sample was filled up to 25 ml volume with deionized water. We used 2 ml sample to measure total P content by an inductively coupled plasma-optical emission spectrometry (ICP-OES) (iCAP 7000 series ICP-OES, Thermo Fisher Scientific, Dreieich, Germany). ³²P activity was measured in 1 mL subsample similarly to the

way described above. The proportion of P derived from applied Fe(III)-P (%) in shoot or root total P was calculated as:

$$\text{Fe(III)-derived P (\%)} = ({}^{32}\text{P activity [Bq]} * \text{P mass in pellets [mg Bq}^{-1}\text{]} / \text{total P in shoots or roots [mg]}) * 100 \quad (2)$$

Soil MBC was measured using the chloroform-fumigation-extraction method (Vance et al., 1987) and was calculated as:

$$\text{MBC} = E_C / k_{EC} \quad (3)$$

Where k_{EC} is equal to 0.45 and E_C is the difference between the content of organic C extracted from the fumigated and non-fumigated soils. The organic C contents in each extract were measured by an N/C analyzer. Soil MBP was determined with the anion exchange resin method by adding hexanol as fumigant according to Kouno et al. (1995). The P concentration was measured with the colorimetric method on a spectrophotometer (NanoPhotometer® NP80, IMPLLEN, Munich, Germany). MBP was calculated as the difference between anion exchange P without hexanol and P extracted with hexanol, corrected by the recovery of a P spike in each soil sample. The ${}^{32}\text{P}$ in MBP was measured (see above) and calculated as the difference in ${}^{32}\text{P}$ activity between samples extracted without and with hexanol, corrected by the recovery of a P spike in each soil sample. The proportion of P in MBP derived from applied Fe(III)-P (%) was calculated as:

$$\text{MBP}_{\text{Fe(III)-P}} (\%) = ({}^{32}\text{P activity [Bq]} * \text{P mass in pellets [mg Bq}^{-1}\text{]} / \text{MBP [mg]}) * 100 \quad (4)$$

We present the content of organic C extracted from non-fumigated soils and anion exchange P without hexanol as soil dissolved C and P, respectively. Dissolved N was extracted with 0.5 M K_2SO_4 and measured by an N/C analyzer.

2.6. Statistical analysis

One-way ANOVA, followed by the Tukey HSD test, was conducted to evaluate the significant differences ($p < 0.05$) for E_h , total Fe concentration, the percentage of ${}^{32}\text{P}$ recovery in soil solution, the proportion of applied Fe(III)-P in plant and MBP, and the recovery rate of applied Fe(III)-P in plant and MBP between three sampling dates. Two-way ANOVA was used to test the effects of rice growth and soil compartment on dissolved C and P, MBC, MBP, and the proportion of P derived from applied Fe(III)-P in shoots, roots, and MBP. A linear regression analysis was used to determine the relationships between soil dissolved C:N:P ratios and shoot or root C:N:P. All statistical tests, as well as the linear regression analysis, were conducted using SPSS (Version 21, IBM, Armonk, NY, USA).

3. Results

3.1. Redox potential E_h and ${}^{32}\text{P}$ recovery in soil solution

Soil E_h decreased within six days after rice transplantation and then stabilized

between -207 and -218 mV after 10 days (Fig. 1a). Total dissolved Fe concentration and the ^{32}P recovery in soil solution showed similar dynamics during rice growth (Fig. 1b, c). Total soluble Fe concentration increased from 592 to 1624 μM within six days after rice transplantation, stabilized between 6–14 days, then abruptly decreased down to the initial level (Fig. 1b). The ^{32}P recovery reached a maximum of 0.32% L^{-1} within 10 days after rice transplantation, generally following similar dynamics to that of the total Fe in soil solution (Fig. 1c), and 0.01 – 0.08% applied ^{32}P were released into soil solution.

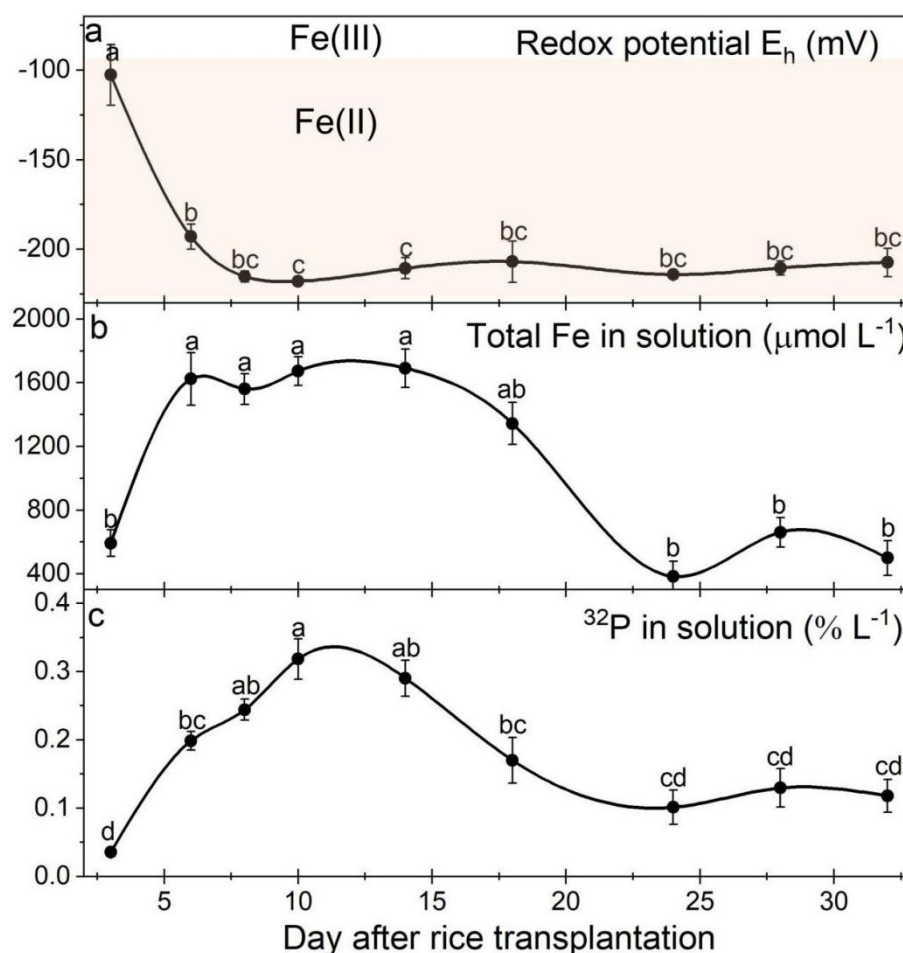


Fig. 1 Dynamics of soil redox potential E_h (a), total iron (Fe) concentration (b), and ^{32}P recovery in soil solution (c, based on Eq.1) after rice transplantation. The data are mean \pm standard error ($n = 24$ during 10 days after rice transplantation, $n = 16$ during 10–18 days, and $n = 8$ during 18–32 days). Lowercase letters represent significant differences ($p < 0.05$) among the three sampling dates. The orange shaded area in ‘a’ shows the redox potential area where Fe(III) or Fe(II) exists at a soil pH of 6.2.

3.2 Soil dissolved C and P, microbial biomass C and P

Dissolved C decreased abruptly by 61–64% from day 10 to day 18 after rice transplantation, then slightly decreased by a further 10–40% from day 18 to day 33 (Fig. 2a). Dissolved P decreased by 11–41% from day 10 to day 18 after rice transplantation, then increased by 24–49% from day 18 to day 33 (Fig. 2b).

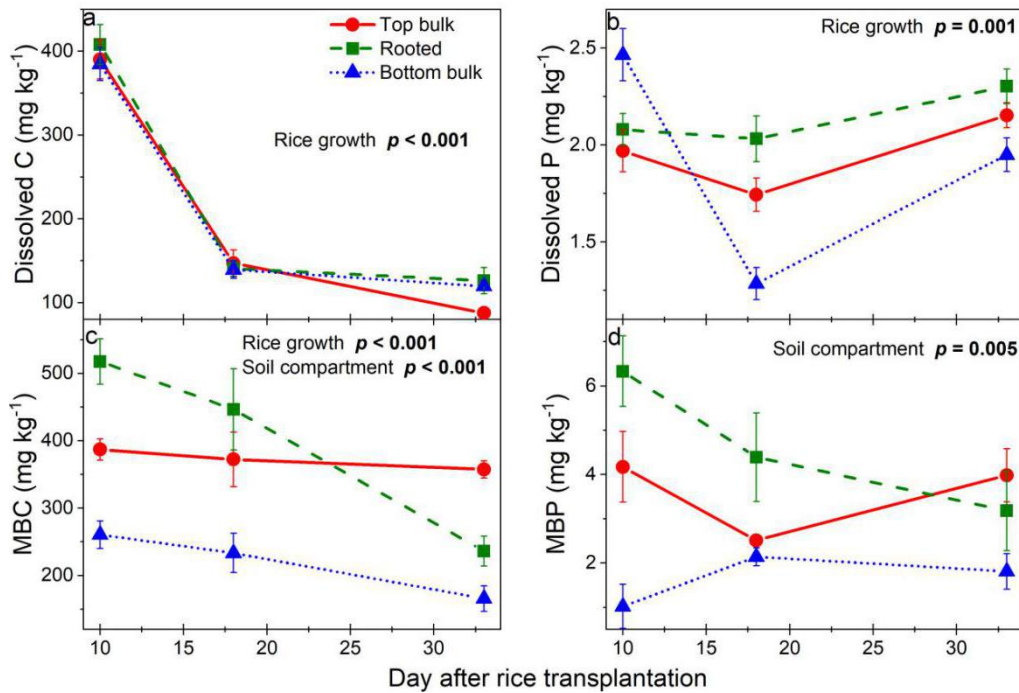


Fig. 2 Dissolved carbon (C; a) and phosphorus (P; b), and microbial biomass carbon (MBC; c) and phosphorus (MBP; d) at the top bulk-, rooted-, and bottom bulk soil in rhizoboxes after 10, 18, and 33 days of rice growth. The data are mean \pm standard error ($n = 8$). The p values show the effects of rice growth or soil compartment on the respective parameter.

MBC decreased by 8%, 54%, and 36% at top bulk, rooted, and bottom bulk soils from day 10 to day 33 after rice transplantation, respectively (Fig. 2c). MBP in rooted soil decreased by 50% with rice growth from day 10 to day 33 (Fig. 2d). MBP in the top bulk soil decreased by 55% during 10–18 days after rice transplantation, and then increased by 242% during 18–33 days (Fig. 2d). However, MBP in bottom bulk soil part of the rhizoboxes increased by 110% during 10–18 days after rice transplantation, then decreased by 15% during 18–33 days (Fig. 2d).

3.3. ^{32}P recovery from applied Fe(III)-P in plant and microbial biomass

The recovery of ^{32}P from the applied Fe(III)-P in plants increased from 0.1% to 1.9% of the applied ^{32}P between 10–33 days after rice transplantation (Fig. 3, black solid line). The corresponding ^{32}P uptake rate in plants 33 days after rice transplantation increased with rice growth and reached $0.06\% \text{ day}^{-1}$ of applied ^{32}P (Fig. 3, red solid line). In contrast, the recovery of applied Fe(III)- ^{32}P in MBP decreased from 0.5% to 0.08% between 10–33 days after rice transplantation (Fig. 3, black dashed line). Similarly, the recovery rate of applied Fe(III)- ^{32}P in MBP decreased with rice growth and was lower than $0.003\% \text{ day}^{-1}$ 33 days after rice transplantation (Fig. 3, red dashed line).

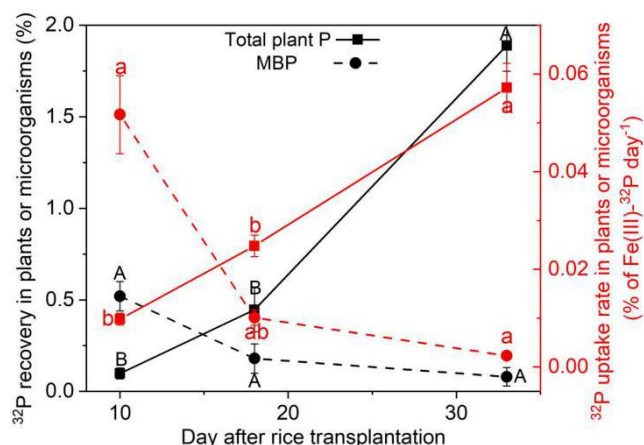


Fig. 3 ^{32}P recovery from applied ferric iron-bound phosphorus ($\text{Fe(III)-}^{32}\text{P}$) in plant (black solid line) and microbial biomass (MBP, black dashed line, left Y-axis) and the uptake rate of $\text{Fe(III)-}^{32}\text{P}$ in total plant P (red solid line) and MBP (red dashed line, right Y-axis). The data are mean \pm standard error ($n = 8$). Uppercase or lowercase letters represent significant differences ($p < 0.05$) in the recovery of $\text{Fe(III)-}^{32}\text{P}$ in total plant P and MBP or the recovery rate of $\text{Fe(III)-}^{32}\text{P}$ in total plant P and MBP among three sampling dates, respectively.

The proportion of P derived from Fe(III)-P in shoots smoothly increased from 0.4% to 12% 33 days after rice transplantation (Fig. 4a). In contrast, the proportion of P derived from Fe(III)-P in roots strongly increased from 2.5% to 10.9% of applied ^{32}P during 10–18 days after rice transplantation, and then slightly increased from 10.9% to 11.6% during 18–33 days (Fig. 4a). The proportion of P derived from Fe(III)-P in MBP in rooted and bottom bulk soil decreased from 3.4% to 0.07% and from 0.08% to 0.004% during 10–33 days after rice transplantation, respectively (Fig. 4b). The proportion of P derived from Fe(III)-P in MBP in top bulk soil increased from 0.9% to 1.2% during 10–18 days after rice transplantation, and then decreased from 1.2% to 0.007% during 18–33 days (Fig. 4b).

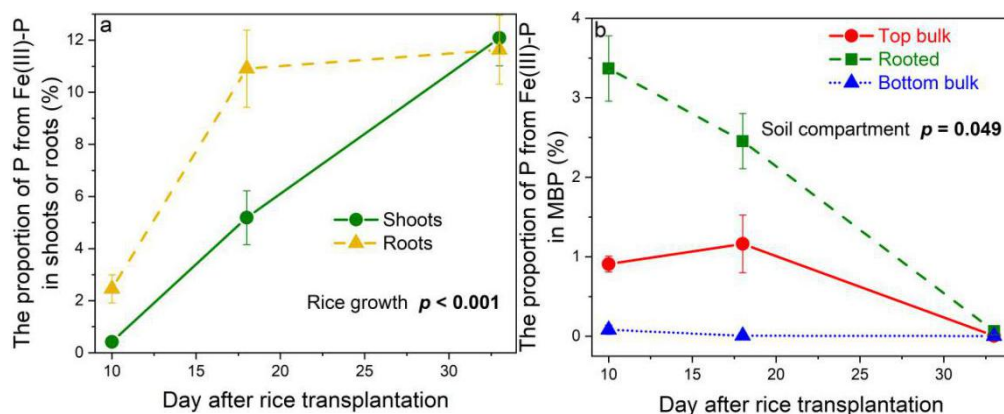


Fig. 4 Proportion of total phosphorus (P) from the applied ferric iron-bound P (Fe(III)-P) to total P in plant shoots and roots (a, based on Eq. 2) or total P in microbial biomass (MBP, b, based on Eq. 3). The data are mean \pm standard error ($n = 8$).

3.4. Relationships between shoot or root C:N:P and total dissolved C:N:P in soil

Negative relationships were observed between root C:N and total dissolved C:N and between root C:P and total soluble C:P in rooted soil (Fig. 5a, b). Both shoot and root N:P ratios increased with the N:P ratio in rooted soil (Fig. 5c).

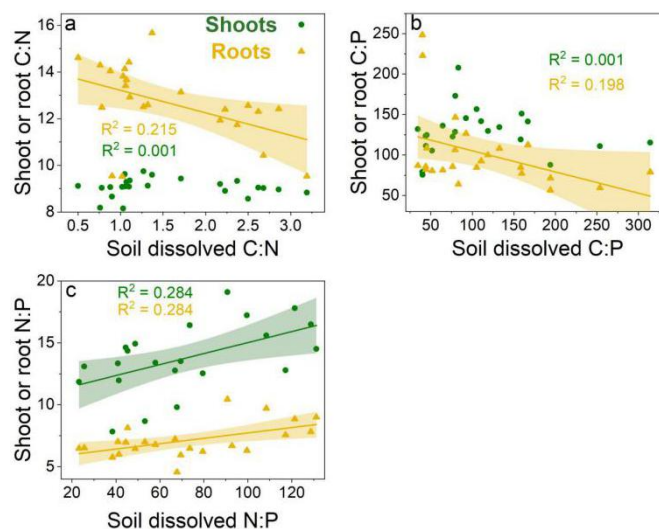


Fig. 5 Relationships between shoot (green) and root (yellow) C:N, C:P, and N:P ratios to the respective ratios in dissolved organic matter in rooted soil ($n = 24$). Solid lines indicate linear correlations significant at $p < 0.05$.

4. Discussion

4.1. Contribution of reductive dissolution of Fe(III)-P to P nutrition of rice plants and microorganisms

Previous studies have shown that less than 20% of the applied P fertilizers are recovered in rice plants under conventional flooded land use (Yu et al., 2021), and the rest of the applied P is accumulated in the soil (Sattari et al., 2012). The Fe(III)-P accounts for approximately 30% of the total P in paddy soils (Darilek, 2010), but the reductive dissolution of Fe(III)-P under anoxic conditions can increase P bioavailability. Here, approximately 2% of applied Fe(III)- 32 P was recovered in rice plants and microbial biomass after 33 days (Fig. 3, solid line). The proportion of assimilated phosphate-P derived from Fe(III)-P accounted for 12% of the total P in shoot and root biomass 33 days after rice transplantation (Fig. 4a). This result supports our first hypothesis that the reductive dissolution of Fe(III)-P contributes with a relevant proportion to the P nutrition of rice plants and microorganisms. Consequently, Fe-bound phosphates serve as an important P source for rice plants which must be considered in strategies to improve fertilizer management.

The reduction of Fe(III) to Fe(II) occurs via either biotic or abiotic mechanisms (Li et al., 2012). Biologically, Fe(III)-reducing microorganisms (e.g., *Geobacter* spp.) can reduce Fe(III) through direct (Lovley, 1995) or indirect (Lovley, 1998) pathways

coupling the oxidation of organic matter in paddy soils (Hori et al., 2010; Yu and Kuzyakov, 2021). To reduce Fe(III), Fe(III)-reducing microorganisms can (1) come into direct contact with Fe(III) oxides, (2) use actively produced or naturally occurring electron-shuttling compounds, e.g. quinones or humic acids that permit electron transfer to Fe(III) oxides which microorganisms cannot directly contact, and/or (3) use Fe(III) chelators dissolving Fe(III) from minerals and that shuttle Fe(III) to the microbes. Therefore, considering the primary role of soil Fe(III)-reducing microorganisms, we expected that P mobilization would correlate with the microbial biomass content. Such an expectation was supported by similar dynamics of MBC content, E_h values, and total Fe content in soil solutions (Fig. 1, 2). Indeed, initially high MBC contents were accompanied by a strong increase in soluble Fe content and a corresponding sharp decrease in E_h values. Accordingly, the increase in ^{32}P recovery in soil solution reflects gradual microbial-mediated Fe(III) reduction within the first 10 days after rice transplantation. However, rice growth leads to a decrease of MBC content (Fig. 2c). Such a decrease can be attributed to (1) increased competition between rice plants and microorganisms for the available P as confirmed by the gradual decrease of ^{32}P recovery in MBP (Fig. 3) (Wei et al., 2019), and (2) the shift from aerobic to anaerobic microbial communities after flooding (Tian et al., 2013). For example, there is clear evidence that flooding decreases the biomass of aerobes (Unger et al., 2009) and fungal abundance (Drenovsky et al., 2004; Wei et al., 2022). With the consumption of dissolved oxygen after flooding, microorganisms capable of anaerobic respiration shift to alternative electron acceptors, e.g. NO_3^- , Fe(III), and Mn(IV), for their metabolic demands (Unger et al., 2009). The increasing Fe(III) concentrations in soil solution during the initial growth phase of rice indicates an increasing abundance or activity of Fe-reducing bacteria. However, stabilization of ^{32}P recovery in soil solution 24 days after rice transplantation (Fig. 1c) indicates a dynamic equilibrium between P release from Fe(III) reduction and P uptake by plants and microorganisms.

The reductive dissolution of Fe(III)-P depends on the redox potential, since Fe(III) oxides are redox-sensitive (Li et al., 2012). Reductive dissolution of Fe(III)-P can occur at E_h values between -314 mV and $+14$ mV (Weber et al., 2006). Therefore, we expected that the amount of P released from the Fe(III)-bound phase into the soil solution would increase with decreasing E_h values. This prediction was partially supported by the opposite E_h dynamics and the ^{32}P recovery in soil solution within the first 10 days (Fig. 1a, c). However, thereafter, ^{32}P recovery decreased under steadily low E_h values (between -207 and -218 mV) 10 days after rice transplantation (Fig. 1a, c). This indicates most likely that (1) the redox potential *per se* can only regulate the sorption surface for P, regardless of the reductive dissolution of Fe oxides as proposed in the “ $\text{Fe}^{\text{III}}\text{-Fe}^{\text{II}}$ redox wheel” paradigm (Li et al., 2012; Matus et al., 2019), and (2) the reduction of Fe(III) to Fe(II) was predominately controlled by biotic mechanisms other than the redox potential 10 days after rice transplantation. Decreased ^{32}P recovery in soil solution is most likely due to (1) increased P uptake efficiency of rice plants through high-affinity transporters to cope with increased P deficiency (Lazali and Bargaz, 2017), (2) the slowdown of Fe(III) reduction due to decreased microbial

abundance as indicated by the MBC content (Fig. 2c), and (3) P co-precipitation and re-adsorption on soil minerals (Hinsinger, 2001).

4.2. Competition of rice plants with microorganisms for phosphorus

A strong decrease in microbial biomass during rice growth (Fig. 2c) and the opposite dynamics of the ^{32}P in plant and microbial biomass (Fig. 3) revealed a strong competition between plants and microorganisms for P. These findings corroborated the second hypothesis that the P limitation results in competition between rice plants and microorganisms. Moreover, microorganisms were strongly limited by C availability, as indicated by a 3–4 times decrease in dissolved C during rice growth (Fig. 2a). We speculate that the microbial demand for C was neither covered from rhizodeposition nor compensated from the soil organic matter (SOM) decomposition. The C limitation of microbial growth and activity has been widely reported in P-deficient terrestrial systems (Demoling et al., 2007; Maranguit et al., 2017), as well as in paddy soils (Rakotoson et al., 2014; 2015). Low redox and anoxic conditions strongly retard the SOM decomposition especially in paddy soils (Freeman et al., 2001; Wang et al., 2017; Wei et al., 2021a). Moreover, the decrease in total soluble C in the rooted soil was similarly strong as in the bulk soil (Fig. 2a, green), but resulted in the highest decrease of MBC in the rooted vs. bulk soil (Fig. 2c, green). This result further implies that microbial growth was strictly limited by the strong competition with roots for nutrients – most likely P, as evident from the simultaneous increased ^{32}P recovery in plants and decreased ^{32}P recovery in microbial biomass (Fig. 4). In addition, C:N and C:P ratio in roots decreased with the respective increase of those in soil solution, suggesting the plant but not the microbial nutrient uptake is controlling the nutrient availability (Fig. 5). The dissolved P increased by the end of the experiment (Fig. 2b). We speculate that C limitation combined with plant outcompetition for P are the strongest limiting factors for microorganisms. Therefore, the data support the third hypothesis that microbial competitiveness strongly depends on C availability (Fig. 6).

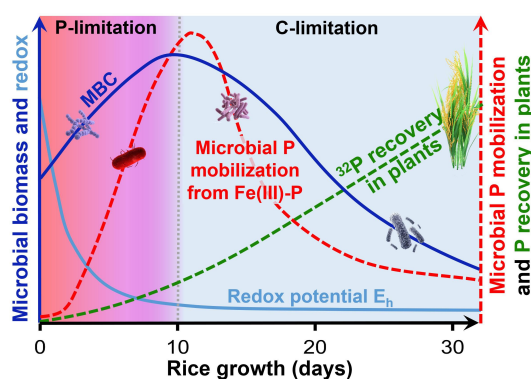


Fig. 6 Conceptual scheme demonstrating the shift from P-limitation to C-limitation for microorganisms during 33 days of rice growth. Blue lines show either microbial biomass C (MBC) or redox potential E_h dynamics with rice growth. Red dashed line demonstrates the dynamics of microbially-mediated Fe(III) reduction. Green dashed line shows ^{32}P recovery in rice plants with rice plant growth.

5. Conclusions

The reductive dissolution of Fe(III)-P is an important P source to increase P availability and contribute to rice plant and microbial P nutrition. The microbially mediated Fe(III) reduction depends on C availability and O₂ consumption rather than P availability in paddy soils. The shift from aerobic to anaerobic microbial community after flooding and the decrease in dissolved C content reduced the microbial biomass and subsequent Fe(III) reduction. Increased P uptake by plants to cope with increased P deficiency resulted in an abrupt decline in ³²P recovery in soil solution between 14 and 24 days after rice transplantation. The stabilization of ³²P recovery in soil solution 24 days after rice transplantation indicates a dynamic equilibrium between P release from Fe(III) reduction and P uptake by plants and microorganisms. Remarkably, the rate of microbial biomass decline was faster in rooted than in bulk soil, suggesting that rice plants outcompeted microorganisms for P as well as fast microbial turnover, whereas P and C co-limitation might lead to a microbial necromass mineralization to reutilize limiting nutrients. In summary, the reductive dissolution of Fe(III)-P contributed to 12% of the total rice plant P uptake and is therefore an important P source, which is necessary to consider in fertilization strategies.

Acknowledgments

The authors gratefully acknowledge the China Scholarship Council (CSC) for financial support for Chaoqun Wang. This work was supported by the research grant from German Research Foundation (DFG Do 1533/3-1; GU 406/33-1; HO4020/8-1). Michaela Dippold was funded by the Robert Bosch Junior Professorship. The authors would like to thank Bernd Kopka and Marvin Blaue of the Laboratory for Radioisotopes (LARI) of the University of Goettingen for their advice, support, and measurements. We also thank Jake Beyer and Dr. Florian Carstens for constructive advising as well as a technical staff of the Department of Agricultural Soil Science, University of Goettingen, Karin Schmidt, for microbial biomass carbon measurement.

References

- Bindraban, P.S., Dimkpa, C.O., Pandey, R., 2020. Exploring phosphorus fertilizers and fertilization strategies for improved human and environmental health. *Biol. Fert. Soil.* 56, 299–317.
- Cordell, D., Drangert, J.O., White, S., 2009. The story of phosphorus: global food security and food for thought. *Glob. Environ. Change* 19, 292–305.
- Darilek, J.L., 2010. Effect of land use conversion from rice paddies to vegetable fields on soil phosphorus fractions. *Pedosphere* 2, 137–145.
- Demoling, F., Figueroa, D., Bååth, E., 2007. Comparison of factors limiting bacterial growth in different soils. *Soil Biol. Biochem.* 39, 2485–2495.
- Devau, N., Cadre, E.L., Hinsinger, P., Jaillard, B., Gérard, F., 2009. Soil pH controls the environmental availability of phosphorus: experimental and mechanistic modelling approaches. *Appl. Geochem.* 24, 2163–2174.
- Drenovsky, R.E., Vo, D., Graham, K.J., Scow, K.M., 2004. Soil water content and organic carbon availability are major determinants of soil microbial community composition. *Microb. Ecol.* 48, 424–430.
- Elrod, V.A., Johnson, K.S., Coale, K.H., 1991. Determination of subnanomolar levels of iron(II) and total dissolved iron in seawater by flow injection analysis with chemiluminescence detection. *Anal. Chem.* 63(9), 893–898.
- Fairhurst, T.H., Dobermann, A., 2002. Rice in the global food supply. *Better Crops International* 16.
- Freeman, C., Ostle, N., Kang, H., 2001. An enzymatic “latch” on a global carbon store. *Nature* 409, 149.
- Gong, Z.T., Zhang, G.L., Chen, Z.C. (Eds.), 2007. *Pedogenesis and Soil Taxonomy*. Science Press, Beijing, China, pp. 613–626.
- Hinsinger, P., 2001. Bioavailability of soil inorganic P in the rhizosphere as affected by root-induced chemical changes: a review. *Plant Soil* 237, 173–195.
- Hori, T., Müller, A., Igarashi, Y., Conrad, R., Friedrich, M.W., 2010. Identification of iron-reducing microorganisms in anoxic rice paddy soil by ¹³C-acetate probing. *ISME J.* 4, 267–278.
- Hou, E., Luo, Y., Kuang, Y., Chen, C., Wen, D., 2020. Global meta-analysis shows pervasive phosphorus limitation of aboveground plant production in natural terrestrial ecosystems. *Nat. Commun.* 11, 637.
- Kögel-Knabner, I., Amelung, W., Cao, Z.H., Fiedler, S., Frenzel, P., Jahn, R., Kalbitz, K., Kölbl, A., Schloter, M., 2010. Biogeochemistry of paddy soils. *Geoderma* 157, 1–14.

- Kouno, K., Tuchiya, Y., Ando, T., 1995. Measurement of soil microbial biomass phosphorus by an anion exchange membrane method. *Soil Biol. Biochem.* 27, 1353–1357.
- Lazali, M., Bargaz, A., 2017. Examples of belowground mechanisms enabling legumes to mitigate phosphorus deficiency. In *Legume Nitrogen Fixation in Soils with Low Phosphorus Availability*; Springer: Berlin/Heidelberg, Germany, pp. 135–152.
- LeBauer, D.S., Treseder, K.K., 2008. Nitrogen limitation of net primary productivity in terrestrial ecosystems is globally distributed. *Ecology* 89, 371–379.
- Li, Y., Yu, S., Strong, J., Wang, H., 2012. Are the biogeochemical cycles of carbon, nitrogen, sulfur, and phosphorus driven by the “Fe^{III}-Fe^{II} redox wheel” in dynamic redox environments? *J. Soil. Sediment.* 12, 683–693.
- Liu, Q., Li, Y., Liu, S., Gao, W., Zhang, G., Xu, H., Zhu, Z., Ge, T., Wu, J., 2022. Anaerobic primed CO₂ and CH₄ in paddy soil are driven by Fe reduction and stimulated by biochar. *Sci. Total. Environ.* 808, 151911.
- Lovley, D.R., 1995. Microbial reduction of iron, manganese, and other metals. *Adv. Agron.* 54, 175–231.
- Lovley, D.R., Fraga, J.L., Blunt-Harris, E.L., Hayes, L.A., Phillips, E.J.P., Coates, J.D., 1998. Humic substances as a mediator for microbially catalyzed metal reduction. *Acta Hydrochim. Hydrobiol.* 26, 152–157.
- Lovley, D.R., Holmes, D.E., Nevin, K.P., 2004. Dissimilatory Fe(III) and Mn(IV) reduction. *Adv. Microb. Physiol.* 49, 219–286.
- Maranguit, D., Guillaume, T., Kuzyakov, Y., 2017. Effects of flooding on phosphorus and iron mobilization in highly weathered soils under different land-use types: short-term effects and mechanisms. *Catena* 158, 161–170.
- Matus, F., Stock, S., Eschenbach, W., Dyckman, J., Merino, C., Nájera, F., Köster, M., Kuzyakov, Y., Dippold, M.A., 2019. Proof of the Ferrous Wheel Hypothesis: Abiotic nitrate incorporation in dissolved organic matter. *Geochimica et Cosmochimica Acta* 245, 514–524.
- Menezes-Blackburn, D., Giles, C., Darch, T., George, T.S., Blackwell, M., Stutter, M., Shand, C., Lumsdon, D., Cooper, P., Wendler, R., Brown, L., Almeida, D.S., Wearing, C., Zhang, H., Haygarth, P.M., 2017. Opportunities for mobilizing recalcitrant phosphorus from agricultural soils: a review. *Plant Soil* 427, 1–12.
- Rakotoson, T., Six, L., Razafimanantsoa, M.P., Rabeharisoa, L., Smolders, E., 2015. Effects of organic matter addition on phosphorus availability to flooded and nonflooded rice in a P-deficient tropical soil: a greenhouse study. *Soil Use Manag.* 31, 10–18.
- Paterson, E., 2000. Iron oxides in the laboratory. preparation and characterization.

- Clay Miner. 27(3), 393–393.
- Rabeharisoa, L., Razanakoto, O.R., Razafimanantsoa, M.P., Rakotoson, T., Amery, F., Smolders, E., 2012. Larger bioavailability of soil phosphorus for irrigated rice compared with rainfed rice in madagascar: results from a soil and plant survey. *Soil Use Manage.* 28, 448–456.
- Rakotoson, T., Six, L., Razafimanantsoa, M.P., Rabeharisoa, L., Smolders, E., 2015. Effects of organic matter addition on phosphorus availability to flooded and nonflooded rice in a P-deficient tropical soil: a greenhouse study. *Soil Use Manag.* 31, 10–18.
- Sánchez-Alcalá, I., del Campillo, M.C., Torrent, J., Straub, K.L., Kraemer, S.M., 2011. Iron (III) reduction in anaerobically incubated suspensions of highly calcareous agricultural soils. *Soil Sci. Soc. Am. J.* 75, 2136–2146.
- Sattari, S.Z., Bouwman, A.F., Giller, K.E., Ittersum, M.V., 2012. Residual soil phosphorus as the missing piece in the global phosphorus crisis puzzle. *Proceed. Natl. Acad. Sci. USA.* 109(16), 6348.
- Scalenghe, R., Edwards, A., Ajmone Marsan, F., Barberis, E., 2002. The effect of reducing conditions on the solubility of phosphorus in a diverse range of European agricultural soils. *Eur. J. Soil Sci.* 53, 1–9.
- Schmidt, H., Eickhorst, T., Tippkoetter, R., 2011. Monitoring of root growth and redox conditions in paddy soil rhizotrons by redox electrodes and image analysis. *Plant Soil* 341, 221–232.
- Syers, J.K., Johnston, A.E., Curtin, D., 2008. Efficiency of soil and fertilizer phosphorus use. *FAO Fertilizer and Plant Nutrition Bulletin* 18.
- Tian, J., Dippold, M., Pausch, J., Blagodatskaya, B., Fan, M., Li, X., Kuzyakov, Y., 2013. Microbial response to rhizodeposition depending on water regimes in paddy soils. *Soil Biol. Biochem.* 65, 195–203.
- Turner, B.L., Brenes-Arguedas, T., Condit, R., 2018. Pervasive phosphorus limitation of tree species but not communities in tropical forests. *Nature* 555, 367–370.
- Unger, I.M., Kennedy, A.C., Muzika, R.-M., 2009. Flooding effects on soil microbial communities. *Appl. Soil Ecol.* 42, 1–8.
- Vance, E., Brookes, P., Jenkinson, D., 1987. An extraction method for measuring soil microbial biomass C. *Soil Biol. Biochem.* 19, 703–707.
- Wang, C., Thielemann, L., Dippold, M.A., Guggenberger, G., Kuzyakov, Y., Banfield, C.C., Ge, T.D., Guenther, S., Bork, P., Horn, M.A., Dorodnikov, M., 2022. Can the reductive dissolution of ferric iron in paddy soils compensate phosphorus limitation of rice plants and microorganisms?. *Soil Biol. Biochem.* 168, 108653.
- Wang, C., Xue, L., Jiao, R., 2021. Soil phosphorus fractions, phosphatase activity, and the abundance of *phoC* and *phoD* genes vary with planting density in

- subtropical Chinese fir plantations. *Soil Till. Res.* 209(4), 104946.
- Wang, Y., Wang, H., He, J.S., Feng, X., 2017. Iron-mediated soil carbon response to water-table decline in an alpine wetland. *Nat. Commun.* 8, 15972.
- Weber, K., Achenbach, L., Coates, J., 2006. Microorganisms pumping iron: anaerobic microbial iron oxidation and reduction. *Nat. Rev. Microbiol.* 4, 752–764.
- Wei, L., Ge, T., Zhu, Z., Ye, R., Peñuelas, J., Li, Y., Lynn, T. M., Jones, D. L., Wu, J., Kuzyakov, Y., 2022. Paddy soils have much higher microbial biomass than upland soils: Review of origin, mechanisms, and drivers. *Agr. Ecosyst. Environ.* 326, 107798.
- Wei, L., Ge, T.D., Zhu, Z.K., Luo, Y., Yang, Y., Xiao, M., Yan, Z., Li, Y., Wu, J., Kuzyakov, Y., 2021a. Comparing carbon and nitrogen stocks in paddy and upland soils: Accumulation, stabilization mechanisms, and environmental drivers. *Geoderma* 398, 115121.
- Wei, X., Hu, Y., Cai, G., Yao, H., Ye, J., Sun, Q., Veresoglou, S. D., Li, Y., Zhu, Z., Guggenberger, G., Chen, X., Su, Y., Li, Y., Wu, J., Ge, T., 2021b. Organic phosphorus availability shapes the diversity of *phoD*-harboring bacteria in agricultural soil. *Soil Biol. Biochem.* 161: 108364.
- Wei, X., Hu, Y., Razavi, B. S., Zhou, J., Shen, J., Nannipieri, P., Wu, J., Ge, T., 2019. Rare taxa of alkaline phosphomonoesterase-harboring microorganisms mediate soil phosphorus mineralization. *Soil Biol. Biochem.* 131, 62–70.
- Yu, G.H., Kuzyakov, Y., 2021. Fenton chemistry and reactive oxygen species in soil: Abiotic mechanisms of biotic processes, controls and consequences for carbon and nutrient cycling. *Earth-Sci. Rev.* 214, 103525.
- Yu, X., Keitel, C., Dijkstra, F.A., 2021. Global analysis of phosphorus fertilizer use efficiency in cereal crops. *Glob. Food Secur.* 29(2), 100545.
- Zhu, Z., Ge, T., Luo, Y., Liu, S., Xu, X., Tong, C., Shibistova, O., Guggenberger, G., Wu, J., 2018. Microbial stoichiometric flexibility regulates rice straw mineralization and its priming effect in paddy soil. *Soil Biol. Biochem.* 121, 67–76.

Supplementary

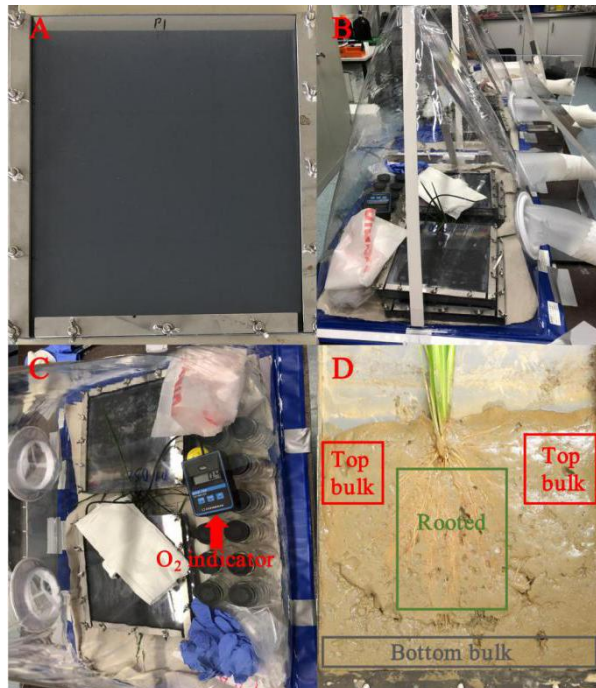


Fig. S1 The construction of a rhizobox with plexiglas cover on top, sealed with rubber gasket (not visible on photo) and fixed by thumbscrews (A), a portable PVC glovebox filled with N₂ and with rhizoboxes inside (B), the level of O₂ as indicated by an O₂-sensor (C), and the locations of three compartments (top bulk, rooted, and bottom bulk) in rhizoboxes (D).

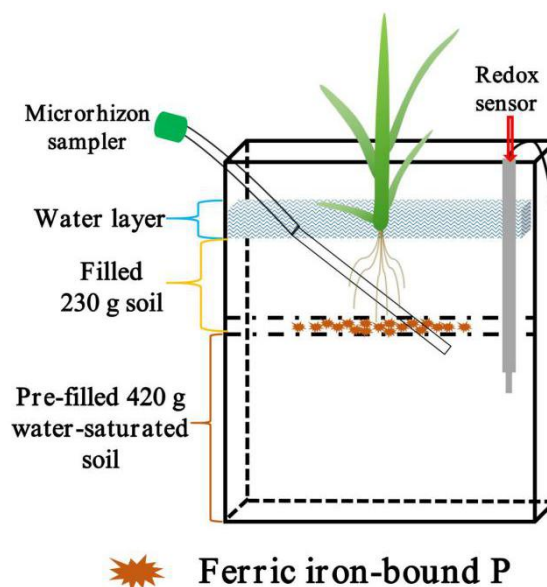


Fig. S2 Layout of the experimental design. Microrhizon samplers were placed at the P-rich patch zone, and a platinum electrode for measuring redox potential E_h was installed in each rhizobox.

Study 6 Reductive dissolution of iron phosphate modifies rice root morphology in phosphorus-deficient paddy soils

Chaoqun Wang^{a,*}, Lukas Thielemann^a, Michaela A. Dippold^{a,b}, Georg Guggenberger^c, Yakov Kuzyakov^{d,e,f}, Callum C. Banfield^b, Tida Ge^g, Stephanie Guenther^c, Maxim Dorodnikov^{a,d,h}

^a Biogeochemistry of Agroecosystems, University of Goettingen, 37077 Goettingen, Germany

^b Geo-Biosphere Interactions, University of Tuebingen, 72076 Tuebingen, Germany

^c Institute of Soil Science, Leibniz University Hannover, 30419 Hannover, Germany

^d Agricultural Soil Science, University of Goettingen, 37077 Goettingen, Germany

^e Department of Soil Science of Temperate Ecosystems, University of Goettingen, 37077 Goettingen, Germany

^f Peoples Friendship University of Russia (RUDN University), 117198 Moscow, Russia

^g State Key Laboratory for Managing Biotic and Chemical Threats to the Quality and Safety of Agro-products, Institute of Plant Virology, Ningbo University, 315211 Ningbo, Zhejiang, China

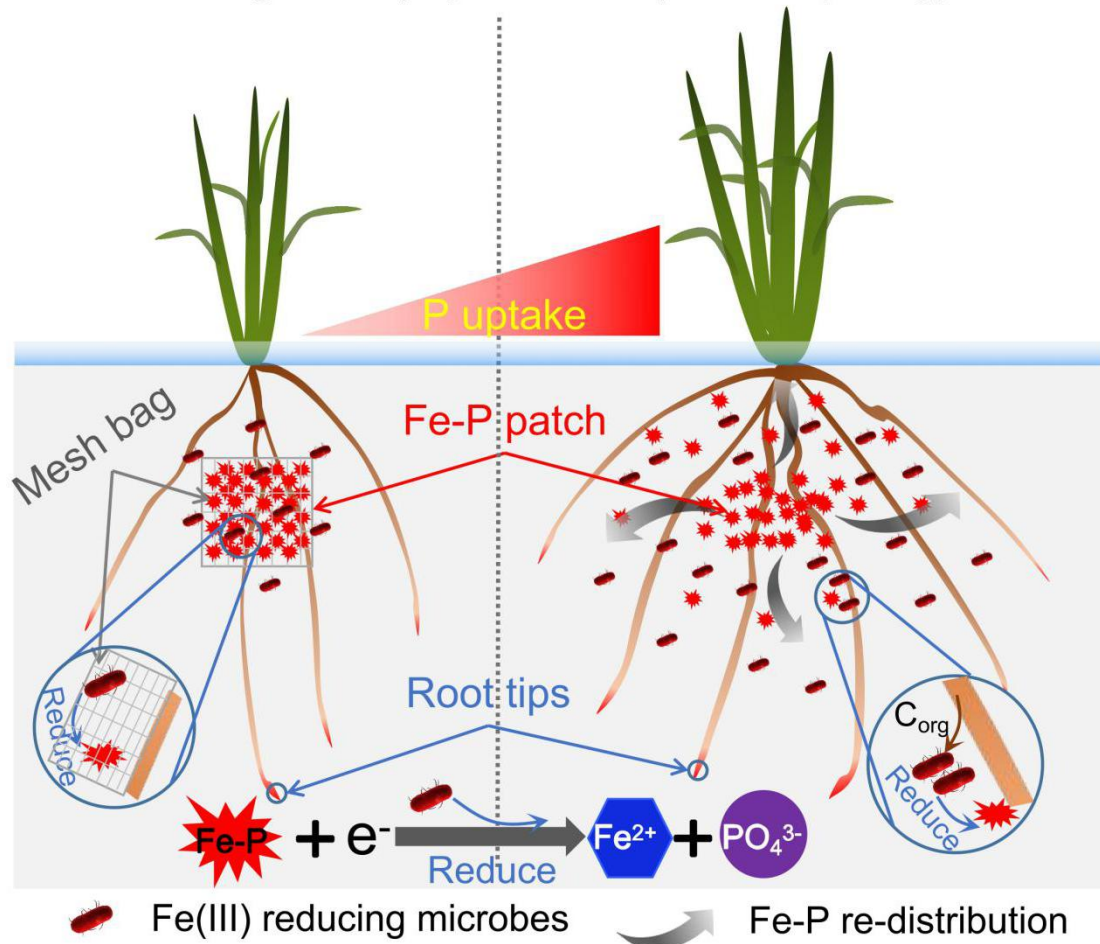
^h Institute of Landscape Ecology, University of Muenster, 48149 Muenster, Germany

* **Correspondence:** chaoqun.wang@forst.uni-goettingen.de

Status: Under review in Soil Biology and Biochemistry

Graphical abstract

Reductive dissolution of Fe-P changes rice (*Oryza sativa* L.) root morphology



A schematic diagram of the effects of direct accessibility of ferric iron-bound phosphate (Fe-P) by rice roots on root architecture under low phosphate conditions. With the application of Fe-P directly to the soil, Fe-P pellet re-distribution resulted in a large area, where roots were directly in contact with Fe-P. When Fe-P was not restricted by mesh bags, roots could provide carbon to Fe-reducing microorganisms to boost microbial growth and activity (blue circles).

Abstract: Root morphology reflects plant adaptations to phosphorus (P) deficiency. We hypothesized that changes in rice root morphology reflect P deficiency decrease after ferric iron (Fe(III))-bound phosphate (Fe-P) dissolution in low-redox paddy soils. We developed a novel *in-situ* ³²P phosphor-imaging approach under flooding to estimate P uptake by rice roots released from Fe-P dissolution. ³²P-labeled ferrihydrite (31 mg P kg⁻¹) was supplied either (1) in polyamide mesh bags (30 μm mesh size) to prevent roots but not microorganisms from direct Fe-P mobilization, or (2) directly mixed with soil to enable roots and microorganisms unrestricted access to the Fe-P. The establishment of low redox conditions (E_h values between -176 and -224 mV) drove the reductive dissolution of Fe-P. Rice root-derived organic acids alone were unable to control Fe-P dissolution, and Fe(III) reduction is predominately a microbially-mediated process. Direct root access to Fe-P raised both the number and mean diameter of crown roots and root tips, and increased P uptake by 149–231%. Crown root elongation rate, ³²P activities along roots and root tips were 5–133% higher when roots directly accessed Fe-P. Plant-derived organic acids alone did not cause Fe-P dissolution, suggesting Fe(III) reduction is a predominately microbially-mediated process. Iron accumulation on roots was depended on the rice growth stage, but not on their access to Fe-P. Roots' access to Fe-P increased rice crown roots elongation and branching and increased P accessibility under P deficiency.

Keywords: ³²P imaging; ferric iron reduction; iron accumulation; phosphorus isotopes; root architecture; root tips

1 Introduction

Limited crop productivity due to poor soil phosphorus (P) availability is widespread (Veneklaas et al., 2012), especially in tropical and subtropical regions where soils are generally strongly weathered, acidic, and rich in free Fe^{3+} and Al^{3+} , which tightly binds P in plant-inaccessible forms (Vitousek et al., 2010). Long-term P fertilizer applications have resulted in a build-up of a soil P ‘bank’, which is retained mainly by sorption on Fe and Al (oxyhydr)oxides in acidic soils (Hedley et al., 1982). For example, ferric iron (Fe(III))-bound P (Fe-P) accounts for up to 30% of the total P in flooded paddy soils, on which rice has been cultivated for more than 20 years (Darilek, 2010). The reductive dissolution of Fe(III) could be key to increase of the P solubility at low-redox conditions (Saleque et al., 2004). Importantly, Fe(III)-oxide reduction to Fe(II) occurs at redox potential (E_h) from -314 mV to $+14$ mV, and Fe(II) is well soluble at a pH below 7 (Weber et al., 2006). Thus, Fe mineral dissolution would in consequence release absorbed and immobilized P, making it accessible to plants (Wang et al., 2022a, 2022b). Therefore, we aimed to clarify the quantitative relevance of Fe-P as a P source enabling a more sustainable future rice production in flooded paddy soils.

Plants evolved various adaptations to cope with P limitation including morphological and physiological modifications (Lynch et al., 2019). Root growth and development play key roles in the improvement of foraging and exploitation (Walk et al., 2006; Sun et al., 2018). For soil foraging improvement (i.e. exploring a larger soil volume more effectively), plants can (1) increase the production of axial roots (Sun et al., 2018), (2) increase root density (Postma et al., 2014), (3) increase root hair length and density (Miguel et al., 2015), (4) decrease root diameter to achieve a relatively higher surface area, thus increasing the exploited soil volume (Gahoonia et al., 2001), (5) shallow axial root growth angles (Walk et al., 2006), and (6) reduce root metabolic costs (Barber, 1984). To increase P mobilization, roots concentrate in P-rich areas and locally increase exudation rates (Lynch, 2011). For example, P adsorbed to soil particles can be mobilized by organic acids, such as citrate, malate, and oxalate (Gerke et al., 2000). However, how plant roots under anoxic conditions, such as rice plants in flooded paddy soils, adopt additional mechanisms to increase the utilization of Fe-P remains unclear. This is because the Fe-P displays contrasting availabilities depending on redox potentials, and a magnitude of factors such as O_2 release by roots leading to a high spatio-temporal variability in redox potentials in paddy soils.

Phosphorus deficiency induces the formation of Fe plaques on rice root surfaces because of the oxidation of Fe(II) to Fe(III) by O_2 release by roots and subsequent precipitation of Fe oxide on the root surface (Armstrong, 1964; Liu et al., 2008). Iron plaques were induced on root surfaces under low P conditions ($13 \mu\text{M}$ P in hydroponic culture) for one day (Ding et al., 2018). Importantly, the Fe plaques can accumulate ions from the medium, thus severing as a nutrient pool and contributing to P uptake by rice (Zhang et al., 1998; Liu et al., 2004). For example, the increase of Fe

plaques content raised P concentration in rice plants, suggesting that P in Fe plaques can be taken by the plant to decrease P deficiency (Wang et al., 2019).

Generally, root tips are more sensitive to P limitation than other root zones, especially at the early root system development stage (Fletcher et al., 2020). Nutrient limitations may induce changes in root morphology, such as increased root branching (Postma et al., 2014), which would result in more root tips. One additional exuding root tip of wheat increased the citrate-driven P uptake rate by one percent under P deficiency (Fletcher et al., 2020). The rice root system largely consists of crown roots, which are nutrient limitation-sensitive (Rose et al., 2013). Crown roots of rice plants play a key role in P uptake, and rice genotypes with more crown roots often perform better under low P conditions (Wissuwa et al., 2020). This is because crown roots have a greater capability of P uptake than other root types due to their density of root hairs implying a larger surface area per unit root length (Kuppe et al., 2022). Physiological and molecular responses of crown roots and root tips to P availability have solely been documented in oxic systems. However, mobilization and spatio-temporal P dynamics (as induced by reductive Fe(III) dissolution) in anoxic systems likely differ from the dynamics in oxic systems. Root system responses to these fluctuating P availabilities are not yet clear.

Innovative imaging methodologies, like phosphor imaging, enable to document qualitatively and quantitatively the development of root systems *in situ* (Sakuraba et al., 2018). This helps to uncover and visualize the response dynamics of roots to low P availability. However, it has been challenging to image roots at low redox conditions, as phosphor imaging best requires direct contact imaging plates and the soil surface. Previous, rhizoboxes had to be opened for imaging, thereby completely changing the redox state of the soil.

To explore the effects of the reductive dissolution of Fe(III) on rice root growth and to quantitatively assess the allocation dynamics of P released from Fe-P with root growth, we developed and applied a novel disturbance-free ³²P-imaging method for low-redox conditions and combined it with mesh-bag approach to distinguish between direct and indirect root accessibility to Fe-P. We hypothesized that (1) the direct accessibility of Fe-P by rice roots stimulates crown roots growth due to increased plant P foraging and uptake, (2) Fe accumulation on roots resulting in Fe plaque formation is promoted by direct accessibility of Fe-P by rice roots and increases with rice growth because of the longer period of Fe(II) flux to the root and Fe(III) precipitation in oxic rhizosphere caused by diffused O₂ released from roots.

2 Materials and methods

2.1 Soil description

The soil used in this experiment was collected from 0–20 cm of a paddy rice field at the Changsha Agricultural and Environmental Monitoring Station, Hunan Province (113°19'52" E, 28°33'04" N), which is located in subtropical region of

China. The mean annual temperature of the region is 17.5 °C, and the mean annual precipitation is 1300 mm. The soil is a typical Stagnic Anthrosol developed from highly weathered granite (Gong et al., 2007), and has been under paddy cultivation with double-cropping rice. According to the Chinese soil nutrient classification standard, the soil was limited by available P (available P content < 10 mg kg⁻¹). The soil was collected with an auger from five random locations in the field, combined, sieved through a 2-mm mesh, air-dried, and homogenized. The main soil physicochemical properties were as follows: pH 6.2, soil organic C 13.1 g kg⁻¹, total N 1.4 g kg⁻¹, available N 18.0 mg kg⁻¹, total P 0.3 g kg⁻¹, Olsen-P 3.7 mg kg⁻¹, and 15.7 g kg⁻¹ total Fe (Zhu et al., 2018).

2.2 Experimental setup

A microcosm experiment with rice was conducted in water-tight PVC-rhizoboxes with inner dimensions of 24.0 (height) × 20.5 (width) × 1.5 cm (depth) (Fig. S1A). A transparent, colorless, and 0.2-mm thin rigid-PVC film (Modulor Material Total, Berlin, Germany) was installed approximately 2 mm below the sturdy plexiglass front cover of the rhizobox (see section 2.4 below) (Fig. S1B). This 2-mm gap (and the good seal) allowed to insert the moisture-sensitive imaging plate with minimum scatter.

The experimental design included two treatments with four replicates and three destructive samplings (8 rhizoboxes for each destructive sampling, 24 rhizoboxes in total, see section 2.5. below). Radiosotopically-labelled Fe(III)-bound phosphate (Fe-P) was added to both treatments: (1) To avoid direct contact of the roots and the labeled Fe-P was first put into a polyamide mesh bag (30 µm mesh size, 5.0 × 5.0 cm, height × width) (Pellets-in-mesh bag treatment). (2) To allow roots access to the Fe-P, the Fe-P was added to the soil as pellets, i.e., without mesh bag (Pellets-no-mesh bag treatment) (see section 2.3. below).

In both treatments, air-dry soil (420 g) was filled into the rhizoboxes and saturated with deionized water 16–24 h prior addition of Fe-P (Fig. S2). The Fe-P in mesh bags or pellets were placed in the center of the rhizoboxes on the surface of the pre-filled soil, and then covered with an additional 230 g of air-dried soil (Fig. S2). The soil was saturated with water, trapped air bubbles were removed by knocking, and one pre-germinated rice seedling (*Oryza sativa* L. ‘Two-line hybrid rice Zhongzao 39’) was transplanted.

All microcosms were filled with water to 2 cm above the soil surface and left growing in a climate chamber (RUMED® Premium-Line P 1700, Rubarth Apparate GmbH, Germany) with 28 ± 1 °C day temperature and 24 ± 1 °C night temperatures, 70% relative humidity, and 12 h photoperiod. The water layer above the soil surface was maintained throughout except for destructive sampling dates under anoxic conditions (see section 2.5. below). Immediately after transplanting, 30 mg N as urea per kg dry soil was applied as background fertilization.

Soil redox potential (E_h) was monitored in each rhizobox by a platinum electrode

installed at 10 cm depth (Fig. S2) using an E_h -meter (GMH 3531, GHM Messtechnik GmbH, Germany). Soil solution from the Fe-P area was collected every 2–5 days using Microrhizon® samplers (MicroRhizons, Rhizosphere Research Products, Netherlands) (Fig. S2) and pre-evacuated and N_2 -flushed 30-ml glass bottles.

2.3 Ferric iron-P pellet preparation and labelling with ^{32}P

The Fe-P pellets were each prepared by mixing 10 g of purified quartz sand as matrix and 0.7 g of synthesized ferrihydrite (Paterson, 2000) per rhizobox. The mixture was weighed into 100-ml glass centrifuge tubes and 30 ml of 3.75 g l⁻¹ K_2HPO_4 solution spiked with ^{32}P -labeled H_3PO_4 (Hartmann Analytic GmbH, Braunschweig, Germany) were added. Additionally, 2 ml of 1 M HCl were pipetted into centrifuge tubes to increase the P adsorption efficiency. Tubes were agitated for 2 h on a shaker (200 rpm) and then centrifuged at 3000 × g for 15 min. Then, the activity in the supernatant was measured on a Liquid Scintillation Analyzer (LSA; Tri-Carb® 2800 TR, PerkinElmer, Shelton, CT, USA). Briefly, 10 µl supernatant were mixed with 10 ml scintillation cocktail (Rotiszint®eco plus, Carl Roth, Germany), then counted for 2 min. To purify pellets and remove the non-adsorbed P, the supernatant was discarded, and the pellet washed three times by adding 30 ml of deionized water, shaking for 15 min on a shaker (200 rpm), and centrifugation at 3000 × g for 15 min. The activity of the combined supernatants was subtracted from the initially applied ^{32}P activity. The ferrihydrite sorbed between 90–97% of the ^{32}P .

The total amount of P added (20 mg rhizobox⁻¹) was equivalent to a mineral-P fertilization of 80 kg ha⁻¹. The initially applied ^{32}P activities were estimated based on varying durations of rice growth and the planned three destructive samplings (DS; see section 2.5. below): At the time of pellet application, the target activities of ^{32}P were 5, 9, and 16 MBq (for DS1, DS2, and DS3, respectively) to achieve 3.2–3.5 MBq of activity at each of destructive samplings considering the ^{32}P half-life and to achieve comparable image qualities. Pellets were added with a spoon either to a mesh bag or directly as pellets depending on a treatment (see above).

2.4 ^{32}P imaging

For the imaging of the ^{32}P activity distribution (showing the total P mobilized from the Fe-P) in rice roots and soil over time, a phosphor imaging plate (20 × 40 cm; BAS-IP MS 2040 E, Cytiva, Marlborough, MA, USA) was inserted into the gap between the PVC film and the front cover of each rhizobox (Fig. S1B). Exposure in the dark was 1 h. The imaging system Fujifilm FLA-5100 (FUJIFILM Life Science, Stamford, CT, USA) was used to read the plates with a spatial resolution of 100 µm. The emitted β^- radiation from the decay of ^{32}P was stored in 16-bit digital images and converted (log-linearization) to standardized photo-stimulated luminescence (PSL) units (Fuji Photo Film Co. Ltd. 2003).

To transform PSL values into ^{32}P activities, we conducted a calibration based on imaging known ^{32}P activities. Briefly, 3.75 g of the soil used in the experiment were uniformly saturated with 1.5 ml of ^{32}P -labeled H_3PO_4 solution and filled into a well of

a 48-well microplate (Brand GmbH, Wertheim, Germany). The activities of ^{32}P -labeled H_3PO_4 solutions ranged from 0 to 112 kBq ml^{-1} . The microplate was covered by the same transparent PVC film used in rhizoboxes. A phosphor imaging plate was placed on the membrane, exposed in dark for 1 h, and read on the imaging system FLA-5100 with a resolution of $100 \mu\text{m}$.

2.5 Destructive sampling

Destructive sampling of all four replicates of each treatment (8 rhizoboxes in total) was conducted after 10 (DS1), 18 (DS2), and 33 (DS3) days after rice transplanting, respectively. These dates of rice plants roughly corresponded to a tillering stage (with 2–4 tillers) of a vegetative phase of rice growth. Rice roots in DS1 were distributed above the mesh bag or pellet location, in DS2 were growing around the mesh bag or pellets, and in DS3 reached the bottom of a rhizobox. To keep the soil anoxic conditions during sampling, rhizoboxes were drained only just before sampling and opened inside a portable PVC glovebox (Captair® Pyramid Glovebox 3015-00, Erlab DFS, Saint-Maurice, France) (Fig. S1C), which was repeatedly evacuated with a vacuum pump (Ilmvac MP 301 Vp, Ilmvac GmbH, Ilmenau, Germany) and then back-flushed with pure nitrogen (99.999%) to achieve a concentration of O_2 lower than 0.4% as indicated by an O_2 -sensor (Greisinger GOX 100, GHM Messtechnik GmbH, Remscheid, Germany) (Fig. S1C).

After opening of a rhizobox (by removing the front cover), rice roots were carefully removed from rhizoboxes and washed free of soil with deionized water. Rice shoots were separated from roots at the soil surface. The shoot and root samples were dried in an oven at $60 \text{ }^\circ\text{C}$ for 48 h and then milled. Then, the soil was collected from three compartments: top bulk soil (2–5 cm), rooted soil (5–15 cm), and bottom bulk soil (15–18 cm) (Fig. S1D). In each compartment, soil was collected from three random locations. For microbial biomass measurements, two samples of 7–10 g moist soil from each compartment were immediately put in air-tight plastic bags and kept at $4 \text{ }^\circ\text{C}$ until the next day.

2.6 Measurement of Fe concentration and ^{32}P activity in soil solution

Total Fe concentrations in soil solution collected by Microrhizons® were measured after complete Fe^{3+} reduction to Fe^{2+} by 10% ascorbic acid for 30 min (Elrod et al., 1991). A 2-ml sample was mixed with 500 μl ammonium acetate buffer (pH 4.5) and 500 μl phenanthroline solution (0.5%) in a cuvette and then measured at 512 nm on a spectrophotometer (NanoPhotometer® NP80, Implen GmbH, Munich, Germany). Calibration was done by external FeCl_3 standards ranging from 5 to 300 μM .

The ^{32}P activity in soil solution was determined on a LSA (Tri-Carb® 2800 TR, PerkinElmer, Shelton, CT, US) and corrected for isotope radioactive decay. Briefly, 0.75 ml solution was mixed with 10 ml scintillation cocktail (Rotiszint®eco plus, Carl Roth, Germany) and then counting was conducted during 5 min. The specific ^{32}P recovery ($\% \text{P L}^{-1}$) in soil solution derived from applied ferrihydrite-quartz-sand-pellet

was calculated according to the following equation:

$$\%P \text{ L}^{-1} = \frac{{}^{32}\text{P activity in solution (Bq L}^{-1})}{\text{Total } {}^{32}\text{P activity in pellets (Bq)}} \times 100 \quad (1)$$

2.7 ${}^{32}\text{P}$ recovery in rice plants and microorganisms, microbial biomass carbon, and dissolved C content in soil

To measure total P content and ${}^{32}\text{P}$ activity in shoots and roots, approximately 100 mg of dried and ground sample were digested with 2 ml of 65% HNO_3 at 180 °C for 8 h, then filtered and filled up to 25 ml final volume with deionized water. 2 ml sample were used to measure total P content by an inductively coupled plasma-optical emission spectrometry (ICP-OES; iCAP 7000 series ICP-OES, Thermo Fisher Scientific, Dreieich, Germany). To measure the ${}^{32}\text{P}$ activity, 1 ml sample was mixed with 10 ml scintillation cocktail (Rotiszint®eco plus, Carl Roth, Germany) in a 20-ml scintillation vial, and then was counted for 5 min on a LSA. The proportion of P derived from applied Fe-P ($\%P_{\text{Shoot, Root}}$) in shoot or root total P was calculated as:

$$\%P_{\text{Shoot, Root}} = \frac{\text{Total } {}^{32}\text{P activity in shoots, roots (Bq)} \times \text{P mass in pellets (mg Bq}^{-1})}{\text{Total P in shoots, roots (mg)}} \times 100$$

(2)

Extractable microbial biomass carbon (MBC) was measured using the chloroform-fumigation-extraction method (Vance et al., 1987) and was calculated according to the equation:

$$\text{MBC} = \frac{E_C}{k_{EC}} \quad (3)$$

where k_{EC} is equal to 0.45 and E_C is the difference between the content of dissolved organic C extracted from the fumigated and non-fumigated soils, respectively. The organic C concentration in each aqueous extract was measured by an elemental analyzer (Multi N/C 2100S, Analytik, Germany). We presented the content of organic C extracted from non-fumigated soils as soil total dissolved C.

Microbial biomass phosphorus (MBP) was determined by the anion exchange resin method by using 1-hexanol as a fumigant according to Kouno et al. (1995). The P concentration in the samples was determined colorimetrically (NanoPhotometer® NP80, Implen, Munich, Germany). MBP was calculated as the difference between resin-P with and without hexanol fumigation and corrected for the recovery of a P spike in each soil sample. To measure the Fe-P-derived ${}^{32}\text{P}$ activity in MBP, 1 ml sample was mixed with 10 ml scintillation cocktail in a 20-ml scintillation vial and then measured for 5 min on the LSA. The ${}^{32}\text{P}$ activity in MBP was also calculated as the difference in ${}^{32}\text{P}$ activity between samples extracted with and without hexanol and corrected by the recovery of a P spike in each soil sample. The proportion of P in

MBP derived from applied Fe-P ($\%P_{\text{MBP}}$) in each soil compartment was calculated as:

$$\%P_{\text{MBP}} = \frac{{}^{32}\text{P activity (Bq kg}^{-1}) \times \text{P mass in pellets (mg Bq}^{-1})}{\text{MBP content (mg kg}^{-1})} \times 100 \quad (4)$$

2.8 Image processing

Image processing was performed with an open-source software Fiji (Schindelin et al., 2012). The PSL values were transformed to ${}^{32}\text{P}$ activities based on the calibration and corrected for isotope radioactive decay. All images of each rhizobox were aligned by defining one image the reference and applying geometric transformations to other images. The visible roots on the images were counted as totally available roots number because the rhizoboxes were kept at an angle of 45° and all roots have been growing along the front cover of rhizoboxes. The crown root elongation rate (cm day^{-1}) was calculated from the root length with respect to the displacement of root apex for the exact duration of root growth. Here and below, three crown roots not overlapping with each other on an image were randomly selected. The same crown roots were always considered for all images of each rhizobox. A total of twelve crown root segments from four rhizoboxes per treatment were analyzed as replicates. We plotted the profiles of ${}^{32}\text{P}$ activity as a function of distance from a geometrical crown root center at a position of 1 cm away from root tips. For every crown root, the profile of mean ${}^{32}\text{P}$ activity was presented as a function of distance from a crown root center determined at given pixels from a root center (Zarebanadkouki et al., 2016) assuming radial symmetry of a crown root. The boundaries between root and soil were set using a one-way ANOVA, followed by a Tukey's HSD test, to assess the differences between the independent variables (mean ${}^{32}\text{P}$ activity of five adjacent pixels). Significant differences ($p < 0.05$) between two adjacent groups of 5 pixels were considered the boundary between root and soil (Hoang et al., 2016). To explore ${}^{32}\text{P}$ activity distribution along the root, we also plotted the profiles of ${}^{32}\text{P}$ activity as a function of distance along a crown root through a root tip to the soil by drawing a segment line. The same segment line was moved horizontally at a distance of approximately 3 mm from the crown root surface to plot the profiles of ${}^{32}\text{P}$ activity as a function of distance with soil depth. Such a 3 mm distance was chosen to avoid the effect of ${}^{32}\text{P}$ activity radial distribution and to minimize the difference in background ${}^{32}\text{P}$ activity distribution. The ${}^{32}\text{P}$ activity of each pixel along a crown root through a root tip to the soil was calculated as the difference in the ${}^{32}\text{P}$ activity of each corresponding pixel in two profiles. The boundaries between root and root tip and between root tip and soil were determined using a one-way ANOVA as described above. Root tip diameter of each root was calculated as a distance from the boundary between root and root tip to the boundary between root tip and soil.

2.9 Statistical analysis

A two-way ANOVA was used to test the effects of (i) the Fe- ${}^{32}\text{P}$ placement (Pellets-in-mesh bag vs. Pellets-no-mesh bag) and (ii) rice growth (sampling dates) on

the E_h , ^{32}P recovery in soil solution, total Fe content in soil solution, root number, crown root diameter, crown root elongation rate, root tip number and diameter, rooted soil area, ^{32}P recovery in shoots or roots, the ratio of ^{32}P recovery in MBP to that in roots, and Fe content in shoots or roots. A two-way ANOVA with repeated measures (destructive sampling, $n = 3$) was used to test the effects of (i) Fe- ^{32}P placement (Pellets-in-mesh bag vs. Pellets-no-mesh bag) and (ii) soil compartment on ^{32}P recovery in MBP, MBC, and soil total dissolved C. To determine the increase in root number, root tip number and diameter, crown root elongation rate, and the increase in rooted soil area during rice growth, linear regression analysis was used to determine the relationships between root number, root tip number, or rooted soil area to sampling dates. Normality and homogeneity of variance of the residuals were verified by a quantile-quantile (QQ) plot and by a plot of fitted values versus residuals in R (v.4.0.4), respectively. Exponential non-linear regression analysis was used to determine the relationships between crown root elongation rate or root tip diameter and sampling dates. All statistical tests were conducted using SPSS (Version 21, IBM, Armonk, NY, USA).

3 Results

3.1 Redox potential (E_h), total Fe concentration, and ^{32}P recovery in soil solution

Soil E_h decreased within the first six days after rice transplantation and then stabilized between -176 and -224 mV (Fig. 1a). Soil E_h was overall higher in the rhizoboxes, in which pellets were distributed in soil rather than in mesh bags (Fig. 1a).

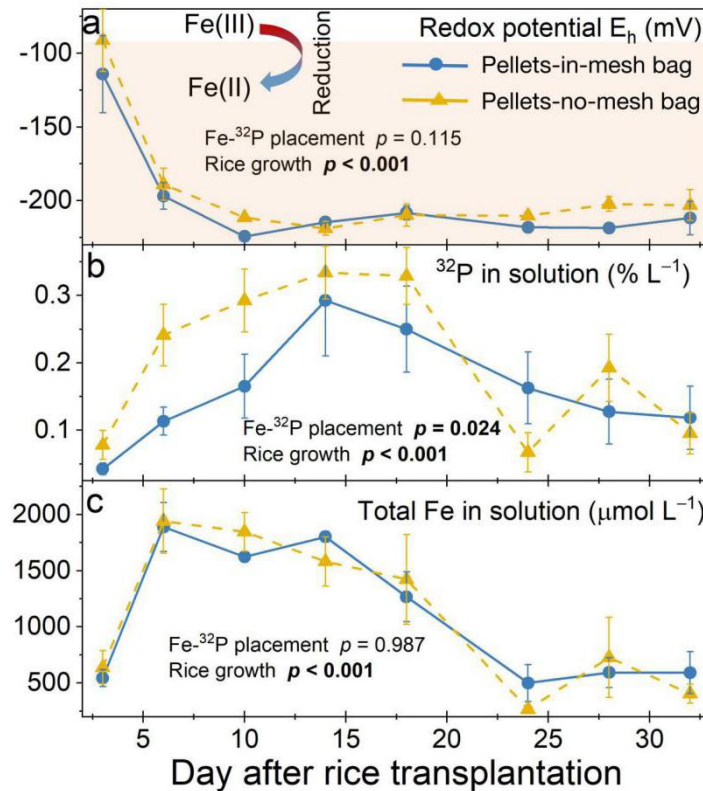


Fig. 1 Soil redox potential E_h (a), ^{32}P recovery (b), and total soluble Fe concentration (c) in soil solution after rice transplantation. The data are the means \pm standard errors ($n = 24$ during 10 d after rice transplantation, $n = 16$ during 14–18 d, and $n = 8$ during 24–32 d) and are modified from Wang et al., 2022. Soil Bio. Biochem., Fig.2. The orange shaded area in a, b, and c shows the redox potential area where Fe(III) or Fe(II) exist for the soil pH of 6.2.

The relative ^{32}P recovery in soil solution was higher when Fe-P was applied directly to the soil as compared to Fe-P pellets excluded from roots in mesh bags (Fig. 1b). The ^{32}P recovery in soil solution initially smoothly increased till days 14–19 and then dropped abruptly (Fig. 1b). The total Fe concentration in soil solution abruptly increased from ~ 500 to $\sim 1900 \mu\text{M}$ within six days after rice transplantation, stabilized between 6–14 days, and then decreased down to the initial level (Fig. 1c).

3.2 Responses of roots and root tips to P release from Fe-P

Placing pellets directly into the soil strongly increased the number and diameter of roots and root tips as compared to when pellets were kept in mesh bags (Fig. 2, 3, 4a, b, d, e). The number and increase rate of crown roots were higher than those of root tips (Fig. 4f). However, crown root elongation rates exponentially decreased from 15 to 32 days after rice transplantation (Fig. 4c). The crown root diameters strongly decreased when roots grew through the pellet zone (Fig. 4b, 15–24 days). The root tip diameter remained constant during the second and the third week of rice growth, but abruptly decreased 28–32 days after rice transplantation when roots approached the bottom of rhizoboxes (Fig. 4e).

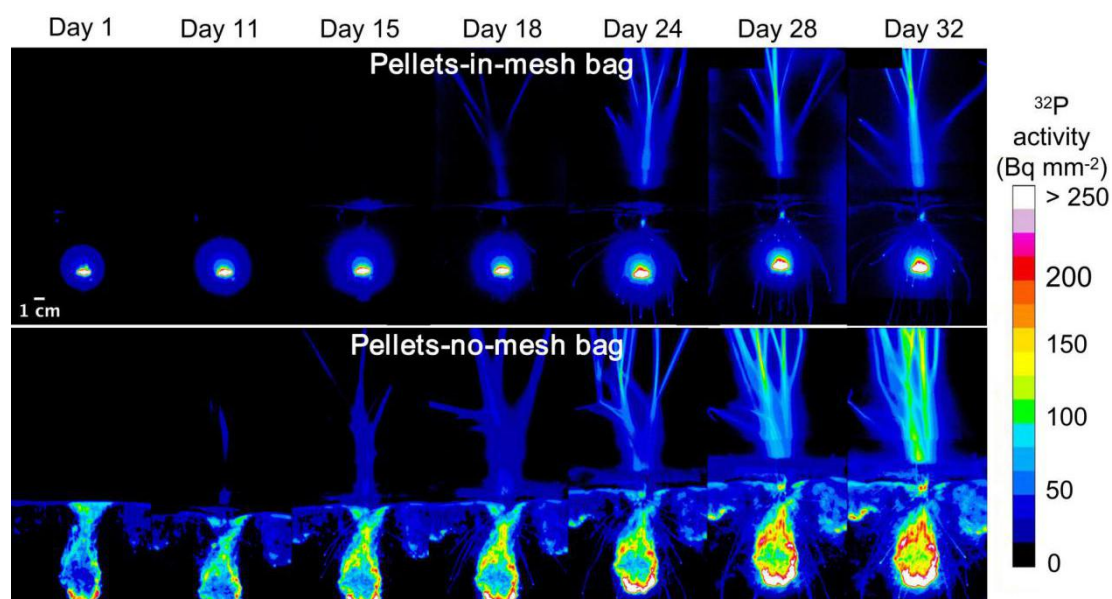


Fig. 2 Examples of spatial distribution of ^{32}P activities during 32 days of the experiment under Pellets-in-mesh bag (top) or Pellets-no-mesh bag (bottom) treatment. Calibration scale bar on the right side represents ^{32}P activity per mm^{-2} . For demonstration, one of four replicates of each treatment was chosen.

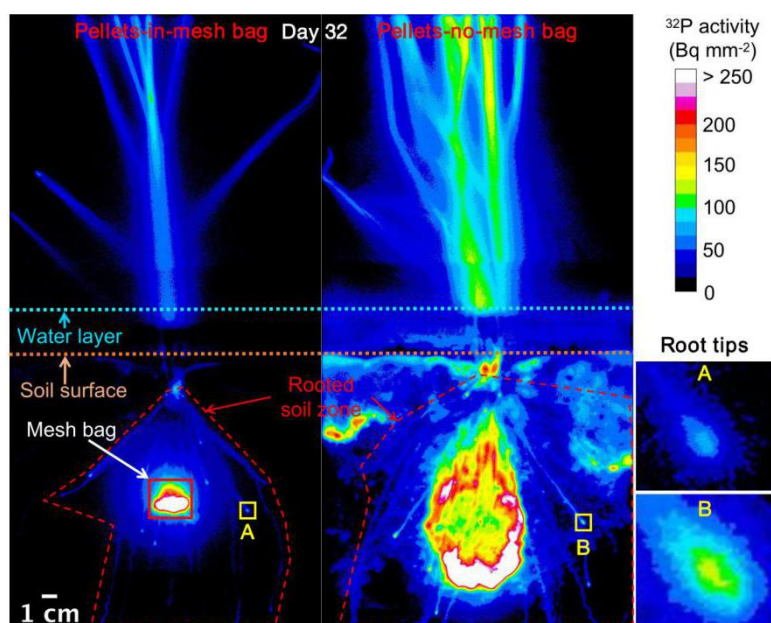


Fig. 3 Examples of spatial distribution of ^{32}P activities (in Bq per mm^{-2} of rhizobox area) under Pellets-in-mesh bag (left side) or Pellets-no-mesh bag (right side) treatment. Calibration scale bar on the right side represents ^{32}P activity. For demonstration, one of four replicates of each treatment at 32 d after rice transplantation was chosen; full set of images of these two rhizoboxes demonstrating the dynamics of spatial distribution of ^{32}P activities are shown on Fig. 2. Red dashed lines represent borders of the maximally rooted zone of rice under two treatments. A or B is an example of root tip under Pellets-in-mesh bag or Pellets-no-mesh bag treatment, respectively.

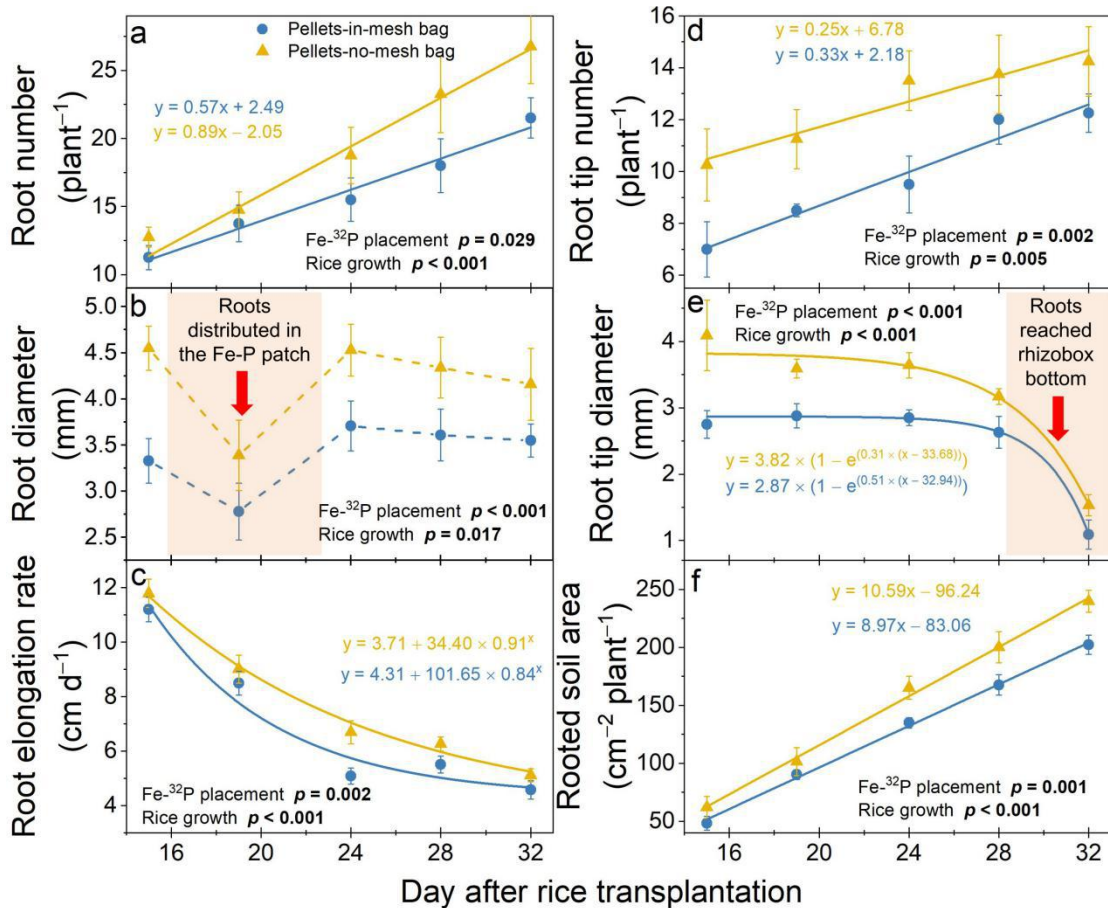


Fig. 4 Detectable root number on the soil surface (a), crown root diameter (b), crown root elongation rate (c), detectable root tip number on the soil surface (d), root tip diameter (e), and maximally rooted soil area (f) under Pellets-in-mesh bag (blue lines) and Pellets-no-mesh bag (yellow lines) treatments calculated from rhizoboxes of the third destructive sampling (DS3, 33 days) at 15, 19, 24, 28, and 32 d after rice transplantation. The data are means \pm standard errors ($n = 4$). Solid lines indicate correlations significant at $p < 0.05$. The orange shaded area in b and e shows the period when most of crown roots distributed either in the applied Fe-P patch (b) or towards the rhizobox bottom (e).

3.3 ³²P dynamics in rice roots

³²P activities along crown roots were 32–133% higher in the rhizoboxes without mesh bags compared to rhizoboxes with mesh bags (Fig. 2, 3, 5). There was also an impact of mesh bag placement on ³²P activities in root tips (36–89% difference), which was lower than the differences along the root axis (Fig. 2, 3, 5). Irrespective of the placement of Fe-P pellets, the ³²P activities along the root tips showed a ³²P peak around day 28 (Fig. 5). However, pellets in direct contact with soil delayed the ³²P activity peak along the crown roots by 4 days (Fig. 5). The ³²P activities were higher in root tips than in the rest of the roots. The differences in ³²P activities between root tips and roots decreased gradually from 306% to 87% in the rhizoboxes with mesh bags, and from 184% to 103% in the rhizoboxes without mesh bags from day 15 to day 32 (Fig. 5).

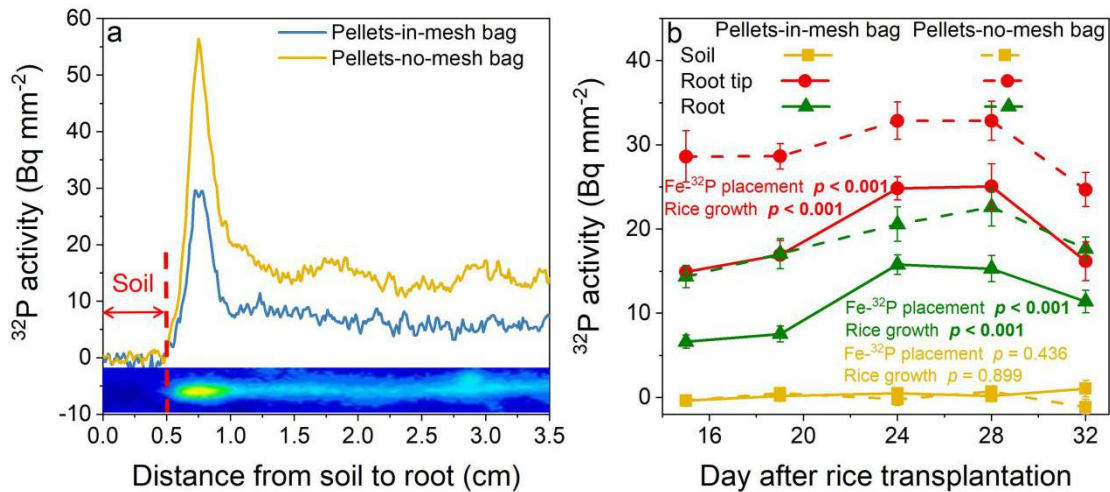


Fig. 5 (a) Examples of the profiles of ^{32}P activity as a function of distance along soil through a root rip to crown root (see inlet as an example on subFig. a) under Pellets-in-mesh bag (blue lines) and Pellets-no-mesh bag (yellow lines) treatments calculated from rhizoboxes for the third destructive sampling (DS3, 33 days) at 24 d after rice transplantation. (b) Mean ^{32}P activities in soil (0–0.5 cm away from root tip), root tips, and roots (0–3 cm away from root tip) under Pellets-in-mesh bag (solid lines) and Pellets-no-mesh bag (dashed lines) treatments calculated from rhizoboxes for the third destructive sampling (DS3, 33 days) at 15, 19, 24, 28, and 32 d after rice transplantation. Data are radial means \pm standard errors ($n = 12$).

The radial distribution of ^{32}P activities as a function of distance from the crown root center was more homogeneous in the rhizoboxes with mesh bags vs. the rhizoboxes without mesh bags (Fig. 6). ^{32}P activities were higher near the crown root center and decreased towards the outer root tissues (Fig. 6). The gradient of ^{32}P activities from root center to outer tissue was most pronounced around day 24 compared to the other dates (Fig. 6).

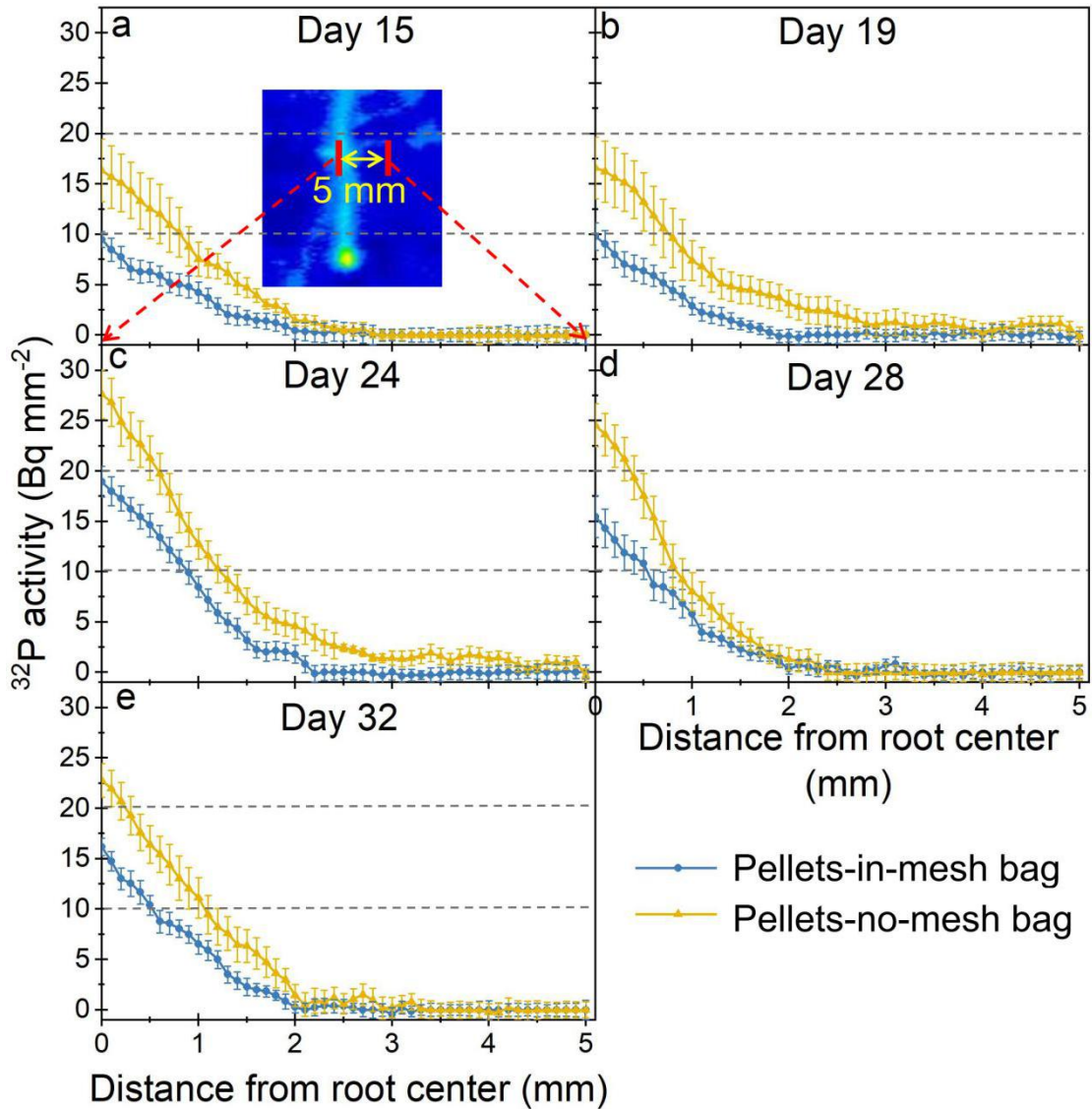


Fig. 6 Radial profiles of ^{32}P activities as a function of the distance from the crown root center at a position of ca. 1 cm away from root tips under Pellets-in-mesh bag (blue lines) and Pellets-no-mesh bag (yellow lines) treatments calculated from rhizoboxes for the third destructive sampling (DS3, 33 days) at 15 (a), 19 (b), 24 (c), 28 (d), and 32 (e) d after rice transplantation. Data are the means \pm standard errors ($n = 12$).

3.4 ^{32}P recovery in microorganisms and plants and Fe content in plants

The ^{32}P recovery in microbial biomass P (MBP) was higher in the rhizoboxes, where Fe-P pellets were distributed in soil as compared to those with mesh bags (Fig. 7a, dashed vs. solid line). ^{32}P recovery in MBP decreased with rice growth, especially in rooted soil from 0.7% to 0.1% in the Pellets-no-mesh bag rhizoboxes, and from 0.2% to 0.04% in the Pellets-in-mesh bag rhizoboxes from day 10 to day 33 of rice growth (Fig. 7a, green lines).

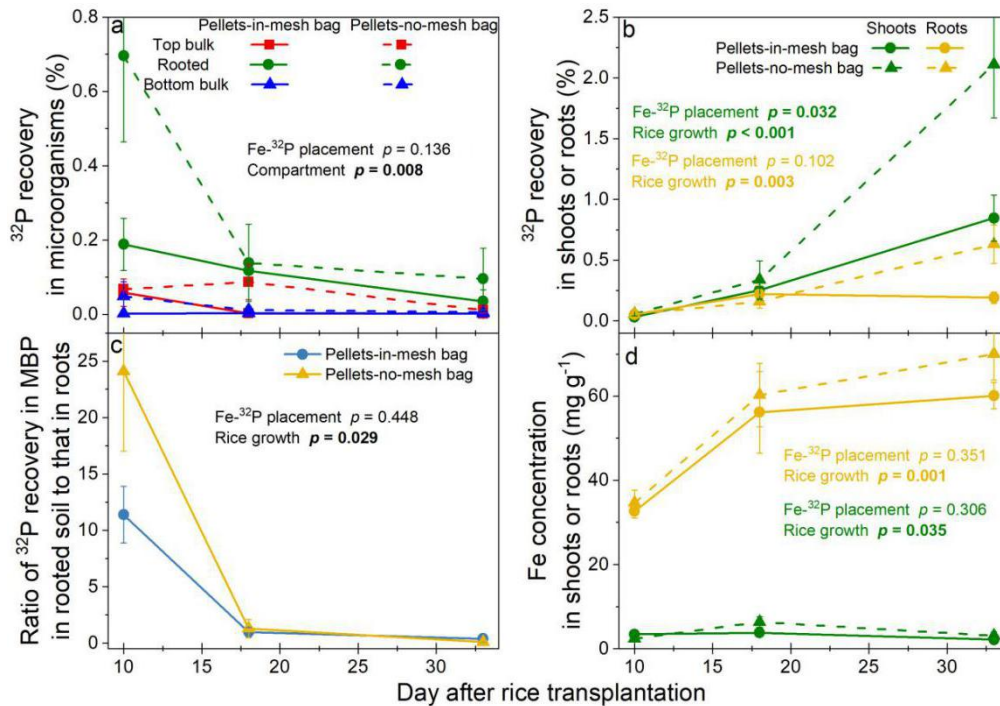


Fig. 7 ^{32}P recovery from applied ferric iron-bound phosphate ($\text{Fe-}^{32}\text{P}$) in microbial biomass (MBP, a) and shoots or roots (b), the ratio of ^{32}P recovery in MBP in rooted soil and that in roots (c), and Fe content in shoots or roots (d) under Pellets-in-mesh bag and Pellets-no-mesh bag treatments of the first (DS1, 10 d), second (DS2, 18 d), and third destructive sampling (DS3, 33 d) after rice transplantation. The data are the means \pm standard errors ($n = 4$).

^{32}P recoveries in shoots and roots were 149% and 231% higher in the rhizoboxes without mesh bags vs. the rhizoboxes with mesh bags 33 days after rice transplantation, respectively (Fig. 7b). With rice growth, ^{32}P recovery in shoots increased by 8-fold from day 10 to day 18 and 3-fold from day 18 to day 33 in the rhizoboxes with mesh bags (Fig. 7b). In contrast, ^{32}P recovery in shoots constantly increased from up to 37 times from day 10 to day 33 in the rhizoboxes without mesh bags (Fig. 7b). Compared to shoots, ^{32}P recovery in roots peaked around day 18 in the rhizoboxes with mesh bags but gradually increased by 12 times in the rhizoboxes without mesh bags (Fig. 7b).

Irrespective of the accessibility of the added P, the ratio of ^{32}P in MBP in rooted soil to ^{32}P in roots showed a marked drop between 10 and 18 days after rice transplantation (Fig. 7c). No differences in Fe content either in shoots or roots were observed between the two treatments (Fig. 7d).

4 Discussion

4.1 Redox- and microbially-driven Fe-P reductive dissolution

The Fe redox cycle (“Fe(III)–Fe(II) redox wheel”) linking Fe(III) reduction and

Fe(II) oxidation, is governed by ambient E_h /pH, microbial activity (Li et al., 2012), and availability of alternative electron acceptors (Fan et al., 2021). This is confirmed in our experiment from a rapid E_h decrease accompanied by a strong increase in soluble Fe in the first six days after rice transplantation (Fig. 1a, c). The E_h decrease during the first ten days after the soil was submerged was due to microbial respiration, which depleted O_2 faster than it diffused back from the air. In agreement with the E_h dynamics, the Fe(III) reductive dissolution led to a release of sorbed labeled P into soil solution as observed a gradual increase of ^{32}P recovery in soil solution within 15–18 days of rice transplantation (Fig. 1b). Although the E_h values remained constantly low 15 days after rice transplantation, the ^{32}P recovery and Fe concentration in soil solution started to decrease (Fig. 1). This is most likely due to (1) an increased P uptake by rice roots through high-affinity transporters to cope with increased P deficiency (Lazali and Bargaz, 2017), and (2) P re-adsorption on soil minerals such as aluminum (oxyhydr)oxides providing additional redox-independent binding sites for P (Hinsinger, 2001). Additionally, the decrease of MBC especially in the rooted zone with rice growth (Fig. S3a) may result in a slowdown of Fe-P reductive dissolution. A decrease in MBC is likely accompanied by a decrease in the abundance of dissimilatory Fe(III)-reducing microorganisms using Fe(III) as an electron acceptor (Lovely et al., 2004; Fan et al., 2021). The MBC decreased because of (1) the shift from aerobic to anaerobic microbial communities after flooding (Tian et al., 2013), (2) increased competition between plants and microorganisms for the available P (Wei et al., 2019) as observed by the gradual decrease in the ratio of ^{32}P recovery in MBP (Fig. 7a, c), and (3) C limitation of microbial growth and activity as the dissolved organic C strongly decreased from day 10 to day 18 after rice transplantation (Fig. S3b). However, why does the dissolved organic C (and by that MBC) decrease with root development?

4.2 Effects of P release from Fe-P on roots and root tips

Phosphate availability can impact rice root architecture (Shimizu et al., 2004; Yang and Finnegan, 2010). We expected an increase in the crown root growth with P release after the reductive dissolution of Fe(III) since the selected paddy soil was strongly P-limited. This was confirmed by the higher number of roots and root tips and faster crown root elongation, when Fe-P was root-accessible compared to the Fe-P pellets in mesh bags (Fig. 2, 3, 4). ^{32}P activities along the crown roots and the root tips were higher in the rhizoboxes without mesh bags compared to the rhizoboxes with mesh bags (Fig. 5, 6). These results support the first hypothesis that direct root accessibility of Fe-P stimulates crown root growth and P uptake. The reductive dissolution of Fe-P increased root foraging by increasing the soil volume exploited by the root system without mesh bag vs. with mesh bags (Fig. 4f). In turn, a higher number of crown roots indicates more intensive root foraging. This was also shown in P-limited upland soils, when a greater number of roots and higher root density increased P acquisition by maize (*Zea mays*) phenotypes (Jia et al., 2018). Remarkably, the crown root elongation rate strongly decreased between 15–24 days after rice transplantation and then slowly decreased from days 24 to 32 (Fig. 4c). This

is contrasting previous findings that P deficiency increased root elongation rates with rice growth (Shimizu et al., 2004; Wissuwa et al., 2005; Panigrahy et al., 2009; Ding et al., 2018). Moreover, the crown root diameter was lower on day 19 than on other dates (Fig. 4b). Notably, the roots were spatially concentrated in the vicinity of the Fe-P pellets 15–19 days after rice transplantation (Fig. 2). Therefore, rice roots may indirectly increase P foraging from soil by slowing down the downward root growth, where there are lower P contents, and by increasing the surface area in contact with the soil by decreasing the root diameter once a P hotspot in soils. In agreement to this hypothesis, the mean crown root diameter was lower on day 19 than on other dates (Fig. 4b).

Plant roots exude P-solubilizing agents to mobilize P adsorbed to soil particles (Hinsinger, 2001; Richardson et al., 2011; Koester et al., 2021). Organic acid anions, such as citrate, malate, and oxalate, can lower the soil pH, thus increasing P solubilization (Oburger et al., 2011). However, the P solubilization may only be affected when the content of organic acids is higher than $10 \mu\text{mol g}^{-1}$ soil (Gerke et al., 2000). The typical exudation rate of organic acids for rice roots at the tillering stage is reported to be approximately $2.4 \mu\text{mol h}^{-1} \text{g}^{-1}$ of dry root biomass (Aulakh et al., 2001). At this rate, rice roots may only exude $0.015 \mu\text{mol organic acids g}^{-1}$ soil considering 5 h half-life time of these compounds (Kirk et al., 1999) and an average 0.4 g dry root biomass 33 days after rice transplantation in our experiment. Therefore, microbial oxidization of organic acids exuded by rice roots is unlikely to be a major factor in maintaining Fe(III) as the primary electron acceptor. This is in line with the findings that a rate of $0.73 \mu\text{mol cm}^{-1}$ of root h^{-1} of organic acid exudation is needed to increase P uptake (McKay Fletcher et al., 2021).

In a parallel experiment, we have assessed the potential of organic acids to desorb P bound to the ferrihydrite without any microbial contribution by increasing concentrations of the mixture of most abundant organic acids released by rice roots within 3 h (Fig. S4a). Less than 0.2% P was released from Fe-P by 200 μM organic acids, the maximal reported acid concentration in soil solution induced by rice roots at a tillering stage (Kirk et al., 1999; Aulakh et al., 2001). While, this maximal organic acid mixture of 200 μM resulted in a sharp decline in pH, the acids only desorbed approximately 1.1% of P (Fig. S4). This further suggests that plant-derived organic acids alone may not control Fe-P dissolution and that Fe(III) reduction is predominately a microbially-mediated process (Lovely et al., 2004). Therefore, the higher ^{32}P recovery in roots in the soil without mesh bags may be mostly attributed to the increased colonization of rice roots with Fe reducers compared to the pellets isolated in mesh bags (Fig. 8). This interpretation, however, needs further experimental confirmation by microbiological measurements.

Reductive dissolution of Fe-P
changes rice (*Oryza sativa* L.) root morphology

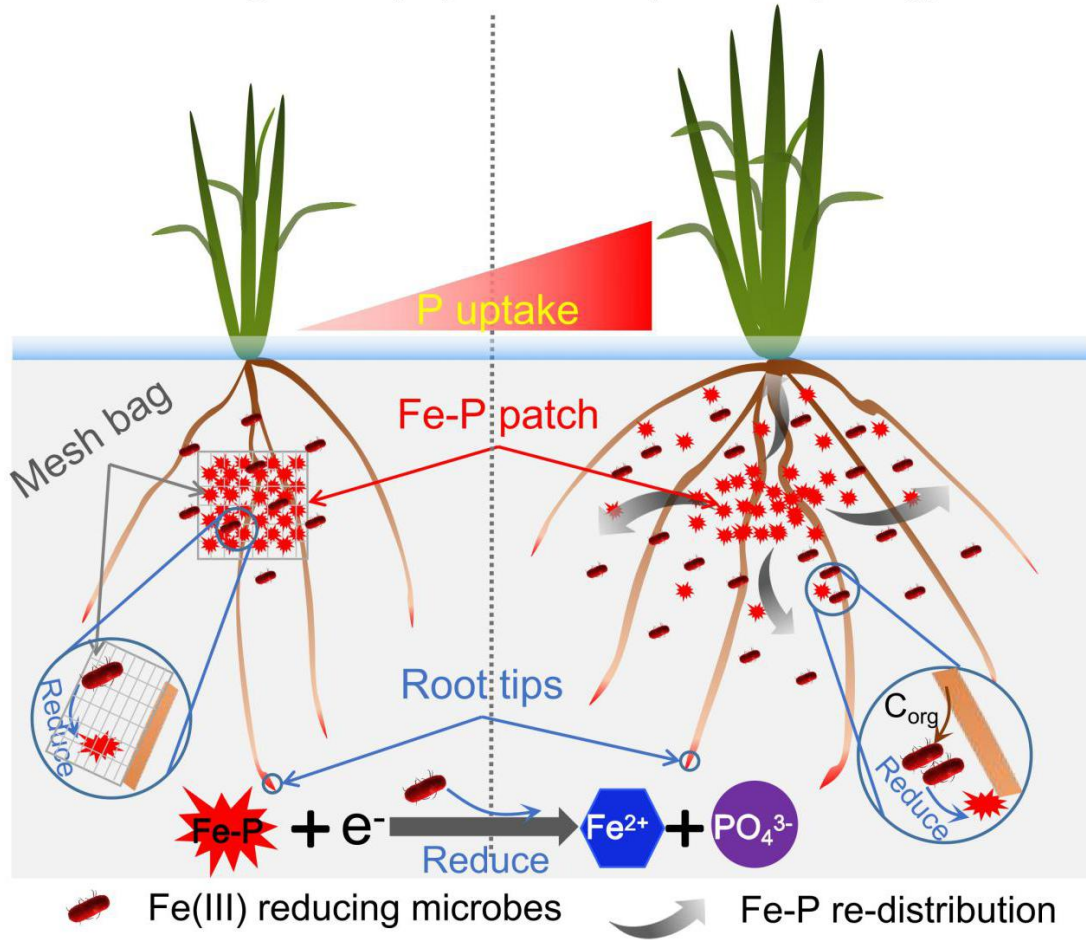


Fig. 8 A schematic diagram of the effects of direct accessibility of ferric iron-bound phosphate (Fe-P) by rice roots on root architecture under low phosphate conditions. With the application of Fe-P directly to the soil, Fe-P pellet re-distribution resulted in a large area, where roots were directly in contact with Fe-P. When Fe-P was not restricted by mesh bags, roots could provide carbon to Fe-reducing microorganisms to boost microbial growth and activity (blue circles).

Direct accessibility of Fe-P by rice roots increased the number of root tips, suggesting an increase in crown root density. Root growth slows down dramatically when root tips reach low P patches (Linkohr et al., 2002). Such a response of root tips to low P contents was confirmed by an abrupt decrease of root tip diameter during 28–32 days after rice transplantation when crown roots reached the very bottom of rhizoboxes (Fig. 4e). These findings can be explained by local responses of roots to P limitation leading to root growth reduction and higher root density (Sánchez-Calderón et al., 2005). Although P uptake by slow-growing root tips decreased (Fig. 4e, 5b), roots were still growing 32 days after rice transplantation at a rate of 4.6–5.1 cm d⁻¹ (Fig. 4c). Therefore, the reductive dissolution of Fe-P induced rice crown roots mainly grown and distributed in localized Fe-P patches. This implies that localized

phosphate fertilization will increase P uptake efficiency, decrease P fixation by soil particles and so, and reduce the P fertilizer demand in rice production.

4.3 Effects of Fe accumulation on P uptake by roots

Iron availability plays an important role in root growth under low P availabilities (Ward et al., 2008; Onaga et al., 2016). Low P conditions induced the expression of the ferritin gene *AtFER1* in roots (Misson et al., 2005) as a result of increased Fe(II) availability (Hirsch et al., 2006). One adaptive strategy of plants to P deficiency is to increase the uptake of P-complexation metals that sequester P in soils (Mission et al., 2005), thus increasing Fe accumulation on the surface of rice roots as iron plaques because of aerenchym O₂ diffusion (Liu et al., 2008; Fu et al., 2014). Ferric iron precipitation on the root surface because of Fe(II) oxidation by diffused O₂ in the rhizosphere is also one of the main reasons for Fe accumulation on the rhizoplane (Fu et al., 2014). Moreover, Fe accumulation coincides with deposition sites of callose regulating root development (Zavaliev et al., 2011). Therefore, root growth is controlled by such antagonistic interactions of P and Fe availability. The toxic effect of Fe, even at low concentrations as 10 μM of Fe²⁺ (Péret et al., 2011), could decrease the root growth rate under low P conditions (Ward et al., 2008). In contrast, when the medium contained Fe under high P (Müller et al., 2015) or did not contain Fe under low P (Svistoonoff et al., 2007), the root growth rate was not reduced. However, underlying mechanisms how Fe regulates root growth under low P conditions remain unclear. No differences in Fe content either in shoots or in roots would not support the second hypothesis that direct accessibility of Fe-P by rice roots may stimulate Fe accumulation in roots. This is supported by the findings that Fe plays only a small role in rice root architecture under low P conditions (Ding et al., 2018). Irrespective of the form of Fe-P application, Fe contents in roots increased with rice growth, thus supporting the hypothesis that Fe accumulation depends on the rice growth stage. This can be attributed to the formation of Fe plaque that contributes to the uptake of P and the accumulation of Fe on the rice root surface (Liu et al., 2008; Fu et al., 2014).

5 Conclusions

Direct accessibility of Fe-P by rice roots changed root morphology of rice plants. The application of Fe-P pellets directly to the soil increased crown root elongation and P uptake by roots as compared to the soils with Fe-P pellets kept in mesh bags. Thus, the reductive dissolution of Fe-P can mitigate P limitation and thereby increase the P uptake by rice plants. Placement of pellets directly into the soil induced rice roots' adaptation by increasing the number of crown roots, expanding crown root distribution, and decreasing crown root elongation rates and diameters. All these increased P acquisition by roots from this extended hotspot of P availability. Organic acids exuded by rice roots were unable to control the reductive dissolution of Fe-P, and Fe(III) reduction is primarily a microbially-mediated process. Iron accumulation on root surface was independent of the accessibility of Fe-P by rice roots but depended on the growth stage, most probably as a result of the Fe plaque formation on

root surface. Increased root tip numbers raised P uptake by roots from soil with the application of Fe-P pellets without mesh bags. Very low P uptake by the growing tips when they reached the bottom of the rhizobox reduced the elongation rate of crown roots. In conclusion, the reductive dissolution of ferrihydrite-bound P under low redox conditions can not only serve as a P source to increase P uptake by rice roots, but also increased rice root growth and induced root morphological changes. Therefore, rice varieties with extended crown root densities will increase P uptake when P is limiting in paddy soils.

Acknowledgments

The authors would like to thank Bernd Kopka and Marvin Blaue of the Laboratory for Radioisotopes (LARI) of the University of Goettingen for their advice, support, and measurements. We also thank Jake Beyer and Dr. Florian Carstens for constructive advice.

References

- Armstrong, W., 1964. Oxygen diffusion from the roots of some British bog plants. *Nature* 204, 801–802.
- Aulakh, M., Wassmann, R., Bueno, C., Kreuzwiser, J., Rennenberg, H., 2001. Characterization of root exudates at different growth stages of ten rice (*Oryza sativa* L.) cultivars. *Plant Biology* 3, 139–148.
- Barber, S., 1984. Soil nutrient bioavailability: a mechanistic approach. New York, NY, USA: John Wiley & Sons Inc.
- Darilek, J.L., 2010. Effect of land use conversion from rice paddies to vegetable fields on soil phosphorus fractions. *Pedosphere* 2, 137–145.
- Ding, Y., Wang, Z.G., Ren, M.L., Zhang, P., Li, Z.N., Chen, S., Ge, G.L., Wang, Y.L., 2018. Iron and callose homeostatic regulation in rice roots under low phosphorus. *BMC Plant Biology* 18, 326.
- Elrod, V.A., Johnson, K.S., Coale, K.H., 1991. Determination of subnanomolar levels of iron(II) and total dissolved iron in seawater by flow injection analysis with chemiluminescence detection. *Analytical Chemistry* 63(9), 893–898.
- Fan, L., Schneider, D., Dippold, M.A., Poehelm, A., Wu, W., Gui, H., Ge, T., Wu, J., Thiel, V., Kuzyakov, Y., Dorodnikov, M., 2021. Active metabolic pathways of anaerobic methane oxidation in paddy soil. *Soil Biology and Biochemistry* 156, 108215.
- Fletcher, M.K., Ruiz, S.A., Dias, T.G.S., Petroselli, C., Roose, T., 2020. Linking root structure to functionality: the impact of root system architecture on citrate enhanced phosphate uptake. *New Phytologist* 227, 376–391.
- Fu, Y.Q., Yang, X.J., Wu, D.M., Shen, H., 2014. Effect of phosphorus on reddish brown iron plaque on root surface of rice seedlings and their nutritional effects. *Scientia Agricultura Sinica* 47, 1072–1085.
- Gahoonia, T.S., Nielsen, N.E., Joshi, P.A., Jahoor, A., 2001. A root hairless barley mutant for elucidating genetics of root hairs and phosphorus uptake. *Plant and Soil* 235, 211–219.
- Gerke, J., Beißner, L., Römer, W., 2000. The quantitative effect of chemical phosphate mobilization by carboxylate anions on P uptake by a single root. I. The basic concept and determination of soil parameters. *Journal of Plant Nutrition and Soil Science* 163, 207–212.
- Gong, Z.T., Zhang, G.L., Chen, Z.C., 2007. *Pedogenesis and Soil Taxonomy*. Science Press, Beijing, China, pp. 613–626.
- Hedley, M.J., Stewart, J.W.B., Chauhan, B.S., 1982. Changes in inorganic and

- organic soil phosphorus fractions induced by cultivation practices and by laboratory incubations. *Soil Science and Society of America Journal* 46, 970–976.
- Hinsinger, P., 2001. Bioavailability of soil inorganic P in the rhizosphere as affected by root-induced chemical changes: a review. *Plant and Soil* 237, 173–195.
- Hirsch, J., Marin, E., Floriani, M., Chiarenza, S., Richaud, P., Nussaume, L., Thibaud, M.C., 2006. Phosphate deficiency promotes modification of iron distribution in *Arabidopsis* plants. *Biochimie* 88(11), 1767–1771.
- Hoang, D.T.T., Razavi, B.S., Kuzyakov, Y., Blagodatskaya, E., 2016. Earthworm burrows: kinetics and spatial distribution of enzymes of C-, N- and P- cycles. *Soil Biology and Biochemistry* 99, 94–103.
- Jia, X.C., Liu, P., Lynch, J.P., 2018. Greater lateral root branching density in maize improves phosphorus acquisition from low phosphorus soil. *Journal of Experimental Botany* 69, 4961–4970.
- Kirk, G.J.D., Santos, E.E., Santos, M.B., 1999. Phosphate solubilization by organic anion excretion from rice growing in aerobic soil: rates of excretion and decomposition, effects on rhizosphere pH and effects on phosphate solubility and uptake. *New Phytologist* 142, 185–200.
- Koester, M., Stock, S., Nájera, F., Abdallah, K., Gorbushina, A., Prietzel, J., Matus, F., Klysubun, W., Boy, J., Kuzyakov, Y., Dippold, M., Spielvogel, S., 2021. From rock eating to vegetarian ecosystems—disentangling processes of phosphorus acquisition across biomes. *Geoderma* 388, 114827.
- Kuppe, C.W., Kirk, G.J., Wissuwa, M., Postma, J.A., 2022. Rice increases phosphorus uptake in strongly sorbing soils by intra-root facilitation. *Plant, Cell and Environment* 45(3), 884–899.
- Kouno, K., Tuchiya, Y., Ando, T., 1995. Measurement of soil microbial biomass phosphorus by an anion exchange membrane method. *Soil Biology and Biochemistry* 27, 1353–1357.
- Lazali, M., Bargaz, A., 2017. Examples of belowground mechanisms enabling legumes to mitigate phosphorus deficiency. In *Legume Nitrogen Fixation in Soils with Low Phosphorus Availability*; Springer: Berlin/Heidelberg, Germany, pp. 135–152.
- Li, Y., Yu, S., Strong, J., Wang, H., 2012. Are the biogeochemical cycles of carbon, nitrogen, sulfur, and phosphorus driven by the “Fe^{III}-Fe^{II} redox wheel” in dynamic redox environments? *Journal of Soil and Sediment* 12, 683–693.
- Linkohr, B.I., Williamson, L.C., Fitter, A.H., Leyser, H.O., 2002. Nitrate and phosphate availability and distribution have different effects on root system architecture of *Arabidopsis*. *Plant Journal* 29(6), 751–760.

- Liu, W.J., Hu, Y., Zhu, Y.G., Gao, R.T., Zhao, Q.L., 2008. The mechanisms of iron plaque formation on the surface of rice roots induced by phosphorus starvation. *Plant Nutrition and Fertilizer Science* 14, 22–27.
- Liu, W.J., Zhu, Y.G., Smith, F.A., Smith, S.E., 2004. Do phosphorus nutrition and iron plaque alter arsenate (As) uptake by rice seedlings in hydroponic culture?. *New Phytologist* 162(2), 481–488.
- Lovley, D.R., Holmes, D.E., Nevin, K.P., 2004. Dissimilatory Fe(III) and Mn(IV) reduction. *Advance in Microbial Physiology* 49, 219–286.
- Lynch, J.P., 2011. Root phenes for enhanced soil exploration and phosphorus acquisition: tools for future crops. *Plant Physiology* 156, 1041–1049.
- Lynch, J.P., 2019. Root phenotypes for improved nutrient capture: an underexploited opportunity for global agriculture. *New Phytologist* 223, 548–564.
- McKay Fletcher, D.M., Shaw, R., Sánchez-Rodríguez, A.R., Daly, K.R., van Veelen, A., Jones, D.L., Roose, T., 2021. Quantifying citrate-enhanced phosphate root uptake using microdialysis. *Plant and Soil* 461, 69–89.
- Miguel, M.A., Postma, J.A., Lynch, J.P., 2015. Phene synergism between root hair length and basal root growth angle for phosphorus acquisition. *Plant Physiology* 167, 1430–1439.
- Misson, J., Raghothama, K.G., Jain, A., Jouhet, J., Block, M.A., Bligny, R., Ortet, P., Creff, A., Somerville, S., Rolland, N., Doumas, P., Nacry, P., Herrerra, L., Nussaume, L., Thibaud, M.C., 2005. A genome-wide transcriptional analysis using *Arabidopsis thaliana* Affymetrix gene chips determined plant responses to phosphate deprivation. *Proceeding of the National Academy of Sciences* 102(33), 11934–11939.
- Müller, J., Toev, T., Heisters, M., Teller, J., Moore, K., Hause, G., Dinesh, D.C., Bürstenbinder, K., Abel, S., 2015. Iron-dependent callose deposition adjusts root meristem maintenance to phosphate availability. *Developmental Cell* 33, 216–230.
- Oburger, E., Jones, D.L., Wenzel, W.W., 2011. Phosphorus saturation and pH differentially regulate the efficiency of organic acid anion-mediated P solubilization mechanisms in soil. *Plant and Soil* 341, 363–382.
- Onaga, G., Dramé, K.N., Ismail, A.M., 2016. Understanding the regulation of iron nutrition: can it contribute to improving iron toxicity tolerance in rice? *Functional Plant Biology* 43, 709–726.
- Panigrahy, M., Nageswara, R.D., Sarla, N., 2009. Molecular mechanisms in response to phosphate starvation in rice. *Biotechnology Advances* 27(4), 389–97.
- Paterson, E., 2000. Iron oxides in the laboratory: preparation and characterization. *Clay Minerals* 27(3), 393–393.

- Péret, B., Clément, M., Nussaume, L., Desnos, T., 2011. Root developmental adaptation to phosphate starvation: better safe than sorry. *Trends in Plant Science* 16, 442–450.
- Postma, J.A., Dathe, A., Lynch, J.P., 2014. The optimal lateral root branching density for maize depends on nitrogen and phosphorus availability. *Plant Physiology* 166, 590–602.
- Richardson, A.E., Lynch, J.P., Ryan, P.R., Delhaize, E., Smith, F.A., Smith, S.E., Harvey, P.R., Ryan, M.H., Veneklaas, E.J., Lambers, H., Oberson, A., Culvenor, R.A., Simpson, R.J., 2011. Plant and microbial strategies to improve the phosphorus efficiency of agriculture. *Plant and Soil* 349, 121–156.
- Rose, T.J., Impa, S.M., Rose, M.T., Pariasca-Tanaka, J., Mori, A., Heuer, S., Johnson-Beebout, S.E., Wissuwa, M., 2013. Enhancing phosphorus and zinc acquisition efficiency in rice: a critical review of root traits and their potential utility in rice breeding. *Annals of Botany* 112(2), 331–345.
- Sakuraba, Y., Kanno, S., Mabuchi, A., Monda, K., Iba, K., Yanagisawa, S., 2018. A phytochrome-B-mediated regulatory mechanism of phosphorus acquisition. *Nature Plants* 4(12), 1089–1101.
- Saleque, M.A., Naher, U.A., Islam, A., Pathan, A.B.M.B.U., Hossain, A.T.M.S., Meisner, C.A., 2004. Inorganic and organic phosphorus fertilizer effects on the phosphorus fractionation in wetland rice soils. *Soil Science and Society of America Journal* 68(5), 1635–1644.
- Sánchez-Calderón, L., López-Bucio, J., Chacón-López, A., Cruz-Ramirez, A., Nieto-Jacobo, F., Dubrovsky, J.G., Herrera-Estrella, L., 2005. Phosphate starvation induces a determinate developmental program in the roots of *Arabidopsis thaliana*. *Plant and Cell Physiology* 46, 174–184.
- Schindelin, J., Arganda-Carreras, I., Frise, E., Kaynig, V., Longair, M., Petzsch, T., Preibisch, S., Rueden, C., Saalfeld, S., Schmid, B., Tinevez, J.Y., White, D.J., Hartenstein, V., Eliceiri, K., Tomancak, P., Cardona, A., 2012. Fiji: an open-source platform for biological-image analysis. *Nature Methods* 9(7), 676–682.
- Shimizu, A., Yanagihara, S., Kawasaki, S., Ikehashi, H., 2004. Phosphorus deficiency-induced root elongation and its QTL in rice (*Oryza sativa* L.). *Theoretical and Applied Genetics* 109(7), 1361–1368.
- Sun, B., Gao, Y., Lynch, J., 2018. Large crown root number improves topsoil foraging and phosphorus acquisition. *Plant Physiology* 177, 90–104.
- Svistonoff, S., Creff, A., Reymond, M., Sigoillot-Claude, C., Ricaud, L., Blanchet, A., Nussaume, L., Desnos, T., 2007. Root tip contact with low-phosphate media reprograms plant root architecture. *Nature Genetics* 39, 792.
- Tian, J., Dippold, M., Pausch, J., Blagodatskaya, B., Fan, M., Li, X., Kuzyakov, Y.,

2013. Microbial response to rhizodeposition depending on water regimes in paddy soils. *Soil Biology and Biochemistry* 65, 195–203.
- Vance, E., Brookes, P., Jenkinson, D., 1987. An extraction method for measuring soil microbial biomass C. *Soil Biology and Biochemistry* 19, 703–707.
- Veneklaas, E.J., Lambers, H., Bragg, J., Finnegan, P.M., Raven, J.A., 2012. Opportunities for improving phosphorus-use efficiency in crop plants. *New Phytologist* 195(2), 306–320.
- Vitousek, P.M., Porder, S., Houlton, B.Z., Chadwick, O.A., 2010. Terrestrial phosphorus limitation: mechanisms, implications, and nitrogen-phosphorus interactions. *Ecological Applications* 20, 5–15.
- Walk, T.C., Jaramillo, R., Lynch, J.P., 2006. Architectural tradeoffs between adventitious and basal roots for phosphorus acquisition. *Plant and Soil* 279, 347–366.
- Wang, C.Q., Thielemann, L., Dippold, M.A., Guggenberger, G., Kuzyakov, Y., Banfield, C.C., Ge, T.D., Guenther, S., Bork, P., Horn, M.A., Dorodnikov, M., 2022a. Can the reductive dissolution of ferric iron in paddy soils compensate phosphorus limitation of rice plants and microorganisms? *Soil Biology and Biochemistry* 168, 108653.
- Wang, C.Q., Thielemann, L., Dippold, M.A., Guggenberger, G., Kuzyakov, Y., Banfield, C.C., Ge, T.D., Guenther, S., Bork, P., Horn, M.A., Dorodnikov, M., 2022b. Microbial iron reduction compensates for phosphorus limitation in paddy soils. *Science of the Total Environment* 837, 155810.
- Wang, Y., Yuan, J.H., Chen, H., Zhao, X., Wang, D., Wang, S.Q., Ding, S.M., 2019. Small-scale interaction of iron and phosphorus in flooded soils with rice growth. *Science of the Total Environment* 669, 911–919.
- Ward, J.T., Lahner, B., Yakubova, E., Salt, D.E., Raghothama, K.G., 2008. The effect of iron on the primary root elongation of *Arabidopsis* during phosphate deficiency. *Plant Physiology* 147, 1181–1191.
- Weber, K.A., Achenbach, L.A., Coates, J.D., 2006. Microorganisms pumping iron: anaerobic microbial iron oxidation and reduction. *Nature Review in Microbiology* 4(10), 752–764.
- Wei, X., Hu, Y., Razavi, B.S., Zhou, J., Shen, J., Nannipieri, P., Wu, J., Ge, T., 2019. Rare taxa of alkaline phosphomonoesterase-harboring microorganisms mediate soil phosphorus mineralization. *Soil Biology and Biochemistry* 131, 62–70.
- Wissuwa, M., Gamat, G., Ismail, A.M., 2005. Is root growth under phosphorus deficiency affected by source or sink limitations? *Journal of Experimental Botany* 56(417), 1943–50.
- Wissuwa, M., Gonzalez, D., Watts-Williams, S.J., 2020. The contribution of plant

traits and soil microbes to phosphorus uptake from low-phosphorus soil in upland rice varieties. *Plant and Soil* 448(1), 523–537.

Yang, X.J., Finnegan, P.M., 2010. Regulation of phosphate starvation responses in higher plants. *Annals of Botany* 105(4), 513–526.

Zarebanadkouki, M., Ahmed, M.A., Carminati, A., 2016. Hydraulic conductivity of the root-soil interface of lupin in sandy soil after drying and rewetting. *Plant and Soil* 398, 267–280.

Zavaliev, R., Ueki, S., Epel, B.L., Citovsky, V., 2011. Biology of callose (β -1,3-glucan) turnover at plasmodesmata. *Protoplasma* 248, 117–130.

Zhang, X., Zhang, F., Mao, D., 1998. Effect of iron plaque outside roots on nutrient uptake by rice (*Oryza sativa* L.). Zinc uptake by Fe-deficient rice. *Plant and soil* 202(1), 33–39.

Zhu, Z., Ge, T., Luo, Y., Liu, S., Xu, X., Tong, C., Shibistova, O., Guggenberger, G., Wu, J., 2018. Microbial stoichiometric flexibility regulates rice straw mineralization and its priming effect in paddy soil. *Soil Biology and Biochemistry* 121, 67–76.

Supplementary

Experiment: Effects of organic acids on phosphate release from ferric iron-bound phosphates (Fe-P)

1. Ferric iron- P_i pellet preparation and labelling with ^{33}P

We replaced ^{32}P -labeled H_3PO_4 with ^{33}P -labeled H_3PO_4 (Hartmann Analytic GmbH, Braunschweig, Germany) to prepare Fe- ^{33}P pellets. The Fe- ^{33}P pellets were prepared as described for the preparation of Fe- ^{32}P pellets (see section 2.3 in Manuscript). To mimic the rhizobox microcosms, the experiment was downscaled to the 50-ml falcon tubes. Therefore, 15 g soil, 0.4 g Fe-P pellets, and 15 ml deionized water per falcon were filled into each falcon tube (three replicates). At the time of pellet application, ca. 42 kBq ^{33}P were employed to each falcon tube.

2. Organic acid mixture preparation

The composition and proportion of organic acids (shown in Table S1) released by rice roots at a tillering stage were derived from Kirk et al. (1999) and Aulakh et al. (2011). Thus, 200 μM as 100% of organic acid mixture were assumed to be produced by each rice plant per day. Organic acid mixtures were prepared at increasing concentrations of 100, 200, 400, and 2000 μM .

3. ^{33}P recovery in soil solution

1.5 ml of each organic acid mixture were pipetted into each falcon tube containing ^{33}P -labeled Fe-P pellets and soil. Falcon tubes were shaken on a rotator (200 rpm) for 45, 90, and 180 min, respectively. Then, the activity in the soil solution was measured on a Liquid Scintillation Analyzer (LSA) (Tri-Carb® 2800 TR, PerkinElmer, Shelton, CT, USA). Briefly, 30 μl supernatant was mixed with 10 ml scintillation cocktail (Rotiszint®eco plus, Carl Roth, Germany), then counting was conducted for 2 min.

Table S1 Composition and proportion of organic acids used for the preparation of organic acid mixture

Composition	Malic acid	Tataric acid	Succinic acid	Citric acid	Lactic acid
Concentration ($\mu mol\ plant^{-1}\ d^{-1}$)	42.51	5.03	5.42	4.15	2.13
Proportion (%)	71.75	8.49	9.15	7.01	3.60

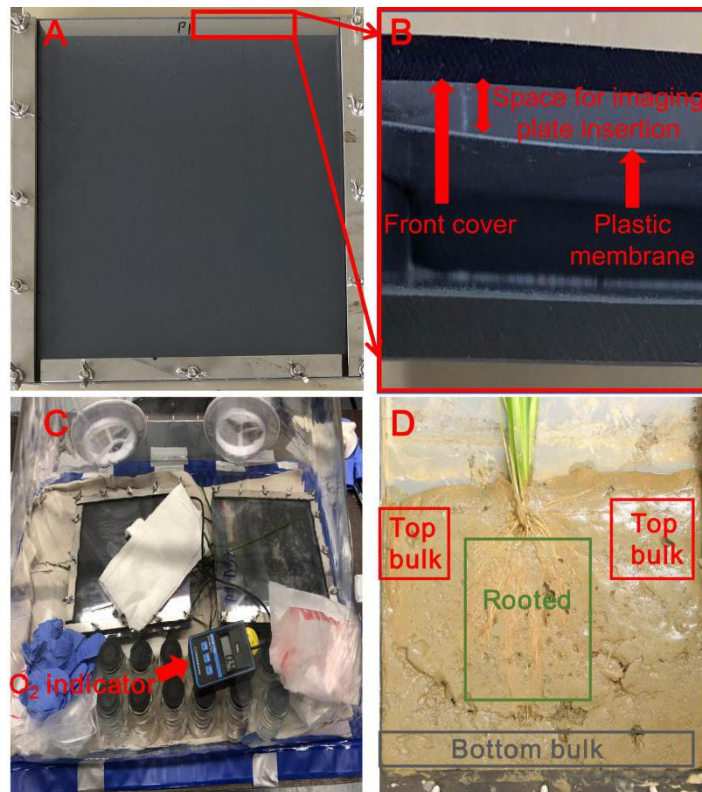


Fig. S1 The construction of a rhizobox with plexiglas cover on top, sealed with rubber gasket (not visible on photo) and fixed by thumbscrews (A), a transparent colorless rigid-PVC membrane (0.2 mm) installed below the front cover of the rhizobox to enable insertion of an imaging plate (B), the level of O₂ inside a portable PVC glovebox filled with N₂ during destructive sampling of rhizoboxes (level of O₂ is indicated by an O₂-sensor) (C), and the locations of three compartments (top bulk, rooted, and bottom bulk) in rhizoboxes from where soil samples were collected (D).

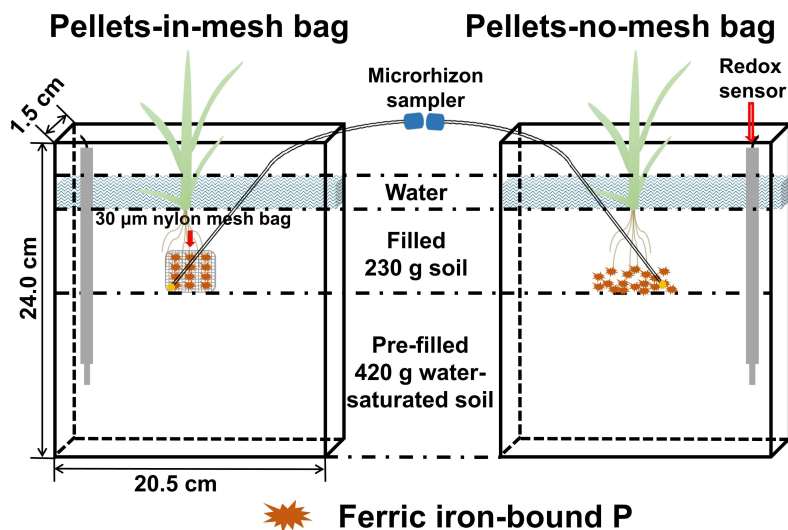


Fig. S2 Diagram of the experimental design. Microrhizon® samplers were placed at the Pi-rich patch zone, and a platinum electrode for measuring redox potential (E_h) was installed in each rhizobox.

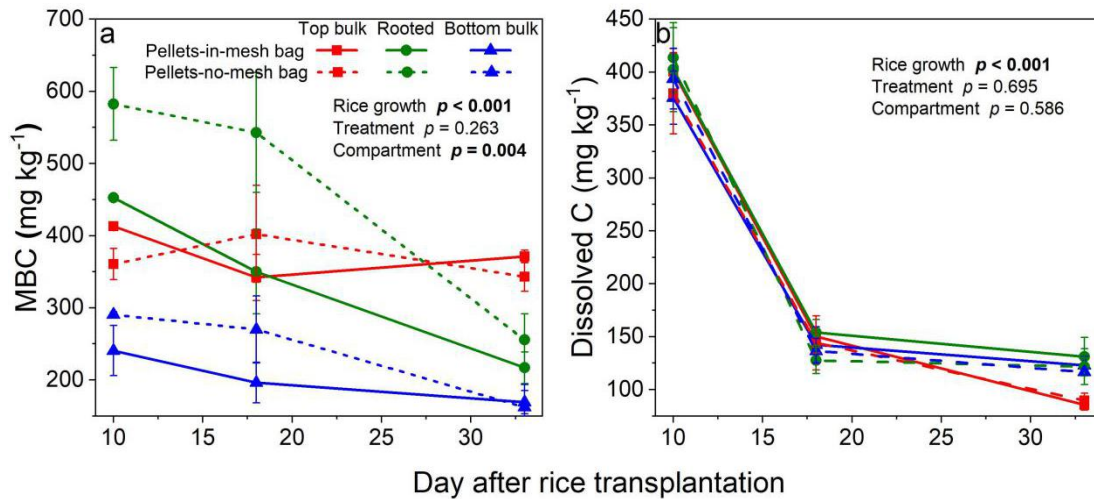


Fig. S3 Microbial biomass carbon (MBC, a) and dissolved carbon (b) at the top bulk-, rooted-, and bottom bulk soil in rhizoboxes after 10, 18, and 33 d of rice growth. The data are the means \pm standard errors ($n = 4$).

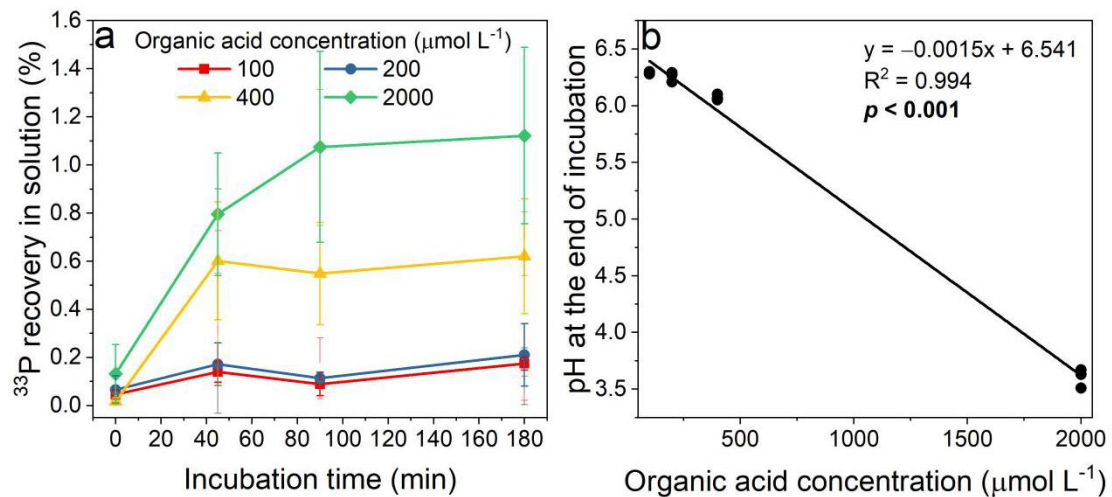


Fig. S4 ^{33}P recovery in the solution with increasing concentrations of organic acids during a 3-h incubation (a) and pH dynamics in the solution with increasing concentrations of organic acids (b).

References

- Aulakh, M., Wassmann, R., Bueno, C., Kreuzwiser, J., Rennenberg, H., 2001. Characterization of root exudates at different growth stages of ten rice (*Oryza sativa* L.) cultivars. *Plant Biol.* 3, 139–148.
- Kirk, G.J.D., Santos, E.E., Santos, M.B., 1999. Phosphate solubilization by organic anion excretion from rice growing in aerobic soil: rates of excretion and decomposition, effects on rhizosphere pH and effects on phosphate solubility and uptake. *New Phytol.* 142, 185–200.

Study 7 The wetter the better: continuous flooding promoted phosphorus uptake by rice from ³³P-organic and ³²P-inorganic phosphorus sources compared to alternate wetting and drying

Chaoqun Wang^{a,*}, Michaela A. Dippold^{a,b}, Georg Guggenberger^c, Yakov Kuzyakov^{d,e}, Callum C. Banfield^b, Stephanie Guenther^c, Maxim Dorodnikov^{a,d,f}

^a Biogeochemistry of Agroecosystems, University of Goettingen, 37077 Goettingen, Germany

^b Geo-Biosphere Interactions, University of Tuebingen, 72076 Tuebingen, Germany

^c Institute of Soil Science, Leibniz University Hannover, 30419 Hannover, Germany

^d Department of Soil Science of Temperate Ecosystems, University of Goettingen, 37077 Goettingen, Germany

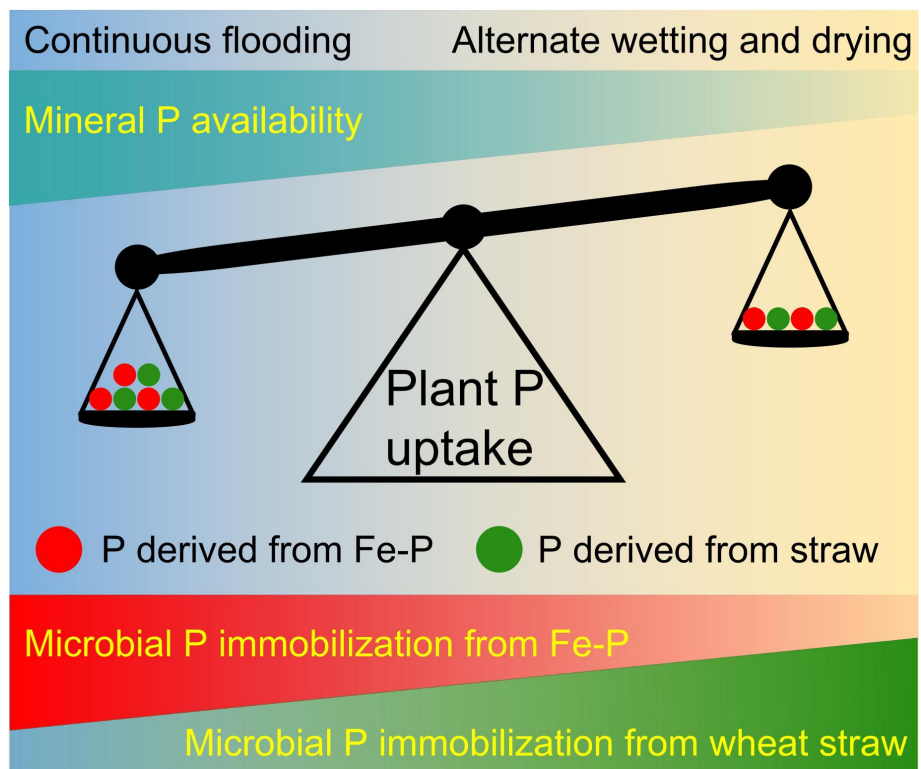
^e Agricultural Soil Science, University of Goettingen, 37077 Goettingen, Germany

^f Institute of Landscape Ecology, University of Muenster, 48149 Muenster, Germany

* **Correspondence:** chaoqun.wang@forst.uni-goettingen.de

Status: In preparing

Graphical abstract



Abstract: The quantitative contributions of the reductive dissolution of ferric iron (Fe(III))-bound phosphate (Fe-P) (inorganic phosphorus (P_i)) and organic P (P_o) mineralization to the P nutrition of rice plants (*Oryza sativa* L.) and microorganisms under continuous flooding (CF) vs. alternate wetting and drying (AWD) regime in paddy soils are urgent research questions. To address them, we grew pre-germinated rice plants in rhizoboxes filled with a paddy soil of poor P availability under CF and AWD water regimes for 40 days. ^{32}P -labeled ferrihydrite (30 mg P kg^{-1}) and ^{33}P -labeled wheat straw (10 g straw kg^{-1}) to trace the preferential P_i - P_o uptake by plants and microorganisms depending on a water regime. Compared to AWD, CF strongly increased Fe(III) reduction- and wheat straw mineralization-derived P which released P to the soil solution. The proportions of P derived from Fe-P and wheat straw in rice plants were 43–64% higher under CF vs. AWD regime. The proportion of P derived from Fe-P to microbial biomass P (MBP) was 5–45% higher but the contribution of wheat straw to MBP was 6–18% lower under CF vs. AWD regime. The effects of water regimes were most pronounced in top bulk soil where microbial biomass and phosphomonoesterase activities were 9–56% higher under CF vs. AWD regime. The contribution of Fe-P was 72–78% lower but wheat straw contribution to MBP was 16–42% higher in rooted soil than in bulk soil, suggesting a strong competition between plants and microorganisms for P. The Fe-P and wheat straw compensated up to 36% and 40% of the plant and microbial P uptake at day 40 after rice transplantation, respectively. Relatively high contribution of P_o to the total P nutrition of plants and microorganisms calls for the adaptation of the P fertilization strategies in paddy soils to avoid excess chemical P fertilizer inputs especially under continuous water flooding.

Keywords: Fe and P interactions; phosphorus availability and mobilization; phosphorus isotopes; plant-microbial competition; redox potential; enzyme activities

1. Introduction

Finite and dwindling phosphate rock reserves, the main source of phosphorus (P) fertilizer, becomes increasingly a threat to crop yield and productivity of agroecosystems (Cordell et al., 2009; Sattari et al., 2012; Yu et al., 2021). Although P fertilizer decreases P deficiency, only 10–25% of applied P is taken by crops within the growing season (Syers et al., 2008); most of the rest is retained mainly by sorption on iron (Fe) and aluminum (Al) (oxyhydr)oxides in acidic soils or on calcium in alkaline soils (Bindraban et al., 2020). Retention of P is most pronounced in well-weathered tropical and subtropical soils because of the presence of abundant Fe^{3+} and Al^{3+} and strong acidic conditions (Saleque et al., 2004). For example, ferric Fe (Fe(III))-bound phosphates (Fe-P) in paddy soils can account for approximately 30% of the total P in these soils where rice has been cultivated for more than 20 years (Darilek, 2010). One key strategy to meet long-term P demand is to solubilize inorganic P (P_i) precipitated or absorbed on minerals. Despite the increasing accumulation of P_i in soils with P fertilizer application, we still lack the knowledge to what extent and under what conditions P_i retained by soil particles can contribute to the P nutrition of plants and microorganisms.

Rice (*Oryza sativa* L.) is one of the predominant food sources and is mainly cultivated on flooded paddy soils (Fairhurst and Dobermann, 2002). The P deficiency is lower in flooded paddy soils because Fe(III) reduction increases the P_i solubility at low-redox conditions (redox potential ranging from -314 mV to $+14$ mV) (Saleque et al., 1996; Weber et al., 2006). Thus, the Fe–P compensated 16% of the rice plant P uptake 33 days after rice transplantation in a continuous flooding (CF) paddy soil (Wang et al., 2022c). However, rice cultivation faces the challenge of freshwater limitation because of population growth, climate change, and water pollution (Belder et al., 2005; Wu et al., 2017). Alternate wetting and drying (AWD) regime as a water-saving technique has been adopted for rice cultivation on paddy soils (Bouman and Tuong, 2001; Chen et al., 2021). The release of P_i from the reductive dissolution of Fe-P may potentially be retarded by the AWD regime as oxygen (O_2) diffusion from air to soil will maintain Fe-P in drying periods (Olsen and Court, 1982; Forber et al., 2018). However, the dynamics of P availability caused by AWD regime, especially the duration of drying and wetting phases, are not yet clearly conclusive.

The reductive dissolution of Fe-P is predominately a microbial process and depends on the carbon (C) availability for microorganisms (Maranguit et al., 2017; Wang et al., 2022d). Generally, crop straw is an important source of both organic C and P (P_o) (Gupta et al., 2007). Accordingly, straw incorporation is expected to not only improve C availability for microorganisms but also accelerate Fe(III) reduction and P_o mineralization in soil under low O_2 conditions. Indeed, rice straw incorporation improved Fe(III) reduction and P availability in flooded paddy soils (Rakotoson et al., 2014). The Fe-P dissolution increased phosphomonoesterase activities in a P-deficient flooded paddy soil (Wang et al., 2022c), suggesting microorganisms compensate for their P demand from P_o sources. However, contrasting effects of the AWD regime on

phosphatase activities have been documented (Zornoza et al., 2006; Chen et al., 2021). Thus, the AWD regime increased P availability through accelerated release of immobilized P as a result of microbial necromass mineralization (Blackwell et al., 2010). In contrast, the increased C availability for microorganisms under the AWD regime stimulated microbial biomass and accelerated the microbial immobilization of P from the soil solution (Butterly et al., 2009). Together, attempts have been made to explore the effects of different water regimes on the rates of P_o mineralization and Fe-P dissolution. However, to the best of knowledge, there are no quantitative estimations available of the contribution of Fe(III) reduction and P_o (i.e. crop straw) mineralization to the P uptake by plants and microorganisms under CF and AWD water regimes.

To fill these apparent knowledge gaps, we conducted a mesocosm experiment with rice plants grown either in continuous flooding or alternate wetting and drying paddy soils to explore the effects of such water regimes on the dynamics of P release from the Fe-P and wheat straw. We applied double labeling approach to quantify contribution of $^{32}P_i$ and $^{33}P_o$ to the total P uptake. We hypothesized that (i) the AWD regime decreases mineral P availability because of increasing P sorption capacity of soils after drying, (ii) the AWD regime increases the contribution of P_o to P nutrition of microorganisms and rice plants, and (iii) the contribution of P_o to P demand of microorganisms will be higher in rooted soil than in bulk soil because of a strong plant-microorganism competition. The ultimate novelty of the study is the quantitative estimation of the contributions of P derived from different sources to microbial and plant P nutrition which is useful for the development of fertilization strategies in rice crop production.

2. Materials and methods

2.1. Soil description

The low available P_i soil (available P_i content $< 10 \text{ mg kg}^{-1}$ according to the Chinese soil nutrient classification standard) was collected from 0–20 cm of a paddy rice field at the Changsha Agricultural and Environmental Monitoring Station, Hunan Province, China (113°19'52" E, 28°33'04" N). This region is characterized by a subtropical monsoon climate with an annual average temperature of 17.5°C and an annual average precipitation of 1300 mm. The soil is a typical Stagnic Anthrosol developed from highly weathered granite (Gong et al., 2007), and is under paddy cultivation with double-cropping rice. The soil was collected with a corer at five locations in the field, combined, sieved through a 2 mm mesh, air-dried, and homogenized. The soil texture was 26.7% clay, 29.2% silt, and 44.2% sand. The main soil physico-chemical properties were as follows: pH 6.2, soil organic C 13.1 g kg^{-1} , total N 1.4 g kg^{-1} , available N 18.0 mg kg^{-1} , total P 0.3 g kg^{-1} , Olsen-P 3.7 mg kg^{-1} , and total Fe 15.7 g kg^{-1} (Zhu et al., 2018).

2.2. Experimental setup

A microcosm experiment was conducted in water-tight PVC-rhizoboxes with inner dimensions of 24.0 (height) × 20.5 (width) × 1.5 cm (depth) (Fig. 1). The experimental design included two water regimes with four replicates (eight rhizoboxes in total). Air-dry soil (600 g) was filled into each rhizobox and saturated with deionized water. Two water regimes included: (i) continuous flooding (CF), the rhizoboxes were filled with water to a depth of 2–3 cm from the soil surface for the entire experimental period 40 days, and (ii) alternate wetting and drying (AWD), the rhizoboxes were flooded for 10 days as described above for CF, then drained the surface water and left drying for 10 days, two wetting and drying cycles were employed over 40 days.

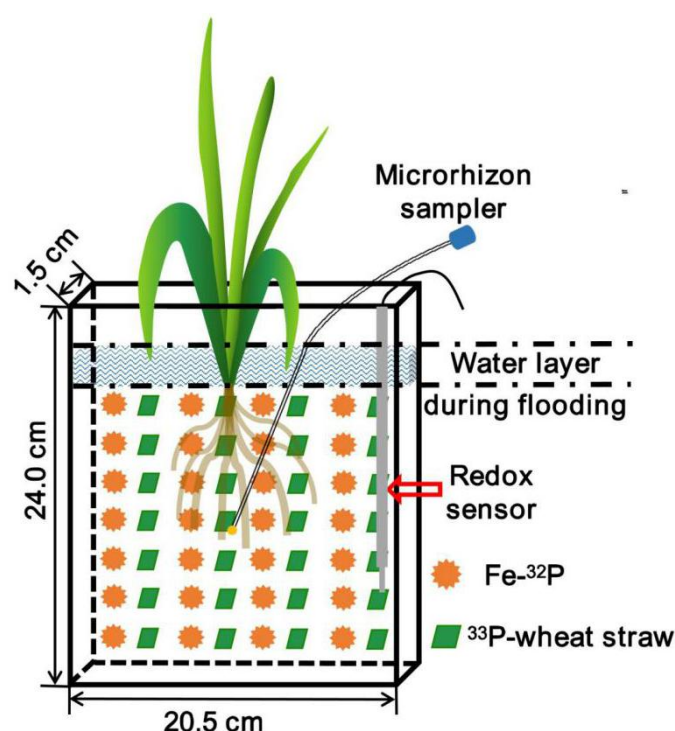


Fig. 1 Diagram of the experimental design. ^{32}P -labeled ferrihydrite (Fe-P) and ^{33}P -labeled wheat straw were evenly mixed with the soil. The rhizoboxes were filled with water to a depth of 2–3 cm from soil surface from day 1 to day 40 under continuous flooding and at wetting phase from day 11 to day 20 and from day 31 to day 40 under alternate wetting and drying regime. Microrhizon samplers were placed at the middle of rhizoboxes, and a platinum electrode for measuring redox potential (E_h) was installed in each rhizobox.

All mesocosms were kept in a climate chamber (RUMED® Premium-Line P 1700, Rubarth Apparate GmbH, Germany) with $28 \pm 1^\circ\text{C}$ day temperature and $24 \pm 1^\circ\text{C}$ night temperature, 70% relative humidity within the first 10 days, 35% relative humidity from day 11 to day 40 to mimic gradually drier climate conditions, and 12-h photoperiod. Immediately after rhizobox establishing, 30 mg N kg^{-1} dry soil as urea were applied as background fertilization.

The soil redox potential (E_h) was monitored in each rhizobox by a platinum electrode installed at 10 cm depth (Fig. 1). E_h was measured using an E_h -meter (GMH 3531, GHM Messtechnik GmbH, Germany). To measure the activities of ^{32}P and ^{33}P , the concentrations of Fe(II) and Fe(III), and the concentrations of dissolved C, N, and P in soil solution with rice growth, 10-ml soil solution was collected every 3–4 days during the experiment from the middle areas of rhizoboxes using MicroRhizon samplers (MicroRhizons, Rhizosphere Research Products, Netherlands) in prevacuated and N_2 -flushed 10-ml glass bottles (Fig. 1).

2.3. Ferric iron bound-P (Fe-P) preparation and labeling with ^{32}P

The Fe-P pellet was prepared by mixing 10 g of purified quartz sand as a matrix and 0.7 g of synthesized ferrihydrite (Paterson, 2000) per rhizobox. The mixture was weighed into 100-ml glass centrifuge tubes, and 30 ml of $3.75 \text{ g l}^{-1} \text{ K}_2\text{HPO}_4$ solution spiked with ^{32}P -labeled H_3PO_4 ($2 \text{ MBq } \mu\text{l}^{-1}$, Hartmann Analytic GmbH, Braunschweig, Germany) were added. Additionally, 2 ml of 1 M HCl were pipetted into the centrifuge tubes to increase the P adsorption efficiency. Tubes were homogenized for 2 h on a roller mixer (200 rpm) and then centrifuged at $3000 \times g$ for 15 min. The activity in the supernatant was measured on a Liquid Scintillation Analyzer (LSA) (Tri-Carb® 2800 TR, PerkinElmer, Shelton, CT, USA). Briefly, 10 μl supernatant were mixed with 10 ml scintillation cocktail (Rotiszint®eco plus, Carl Roth, Germany), then counting was conducted for 2 min. To purify the pellets, i.e., remove the non-adsorbed phosphates, the supernatant was discarded, and 30 ml of deionized water were added to the tubes. The centrifugation and ^{32}P activity determination of the supernatants were repeated three more times as described.

The total amount of P_i added ($20 \text{ mg rhizobox}^{-1}$) was equivalent to a mineral P fertilization of 85 kg ha^{-1} . The initial ^{32}P activity of the pellet was estimated based on the duration of rice growth. At the time of pellet application (t_0), approximately 20 MBq of ^{32}P -labeled H_3PO_4 were employed per rhizobox to reach ca. 2.5 MBq of ^{32}P activity at the destructive sampling according to the ^{32}P half-life (14.3 days).

2.4. Wheat straw preparation and labeling with ^{33}P

Twenty pre-cultivated wheat seedlings (*Triticum turgidum* L.) were grown in 5-l PVC buckets filled with 2 l nutrient solution culture containing 1.4 mM NH_4NO_3 , 0.5 mM K_2SO_4 , 1 mM CaCl_2 , 1.6 mM $\text{MgSO}_4 \cdot 7\text{H}_2\text{O}$, 0.04 mM NaH_2PO_4 , 0.15 μM MnCl_2 , 0.5 μM $(\text{NH}_4)_6\text{Mo}_7\text{O}_{24}$, 20 μM H_3BO_3 , 0.15 μM $\text{ZnSO}_4 \cdot 7\text{H}_2\text{O}$, 0.15 μM $\text{CuSO}_4 \cdot 5\text{H}_2\text{O}$, 35 μM FeCl_3 (Kim et al., 2005). To uniformly label the different organs of wheat plants with ^{33}P , phosphorus as NaH_2PO_4 was applied at a rate of 0.04 and 0.08 mM in the solution during 1–13 and 14–20 days after wheat transplanting, respectively. The nutrient solution was amended with ^{33}P -labeled H_3PO_4 ($370 \text{ kBq } \mu\text{l}^{-1}$, Hartmann Analytic GmbH, Braunschweig, Germany) on days 1, 7, and 14. The nutrient solution was fully removed and refilled on days 7 and 14. This labeling method minimized the immediate uptake and storage of ^{33}P as P_i only in plant leaves (Siebers et al., 2019). The time interval for the labeling was set as a 5% threshold of ^{33}P activity remaining in the nutrient solution. To obtain sufficient wheat plant biomass with required ^{33}P

activity, plants were harvested 20 days after transplanting. Wheat plants were dried at 60°C for 48 h and cut into < 1 mm. Approximately 3 mg wheat straw were used to measure C and nitrogen (N) contents by an N/C analyzer (Multi N/C 2100S, Analytik-Jena, Germany). To measure element concentrations and ³³P activity in wheat straw, 6 samples each approximately 100 mg straw were digested with 2 ml of 65% HNO₃ at 180°C for 8 h. Each digested sample was filtered and filled up to 25 ml volume with deionized water. To measure ³³P activity, 1 ml sample was mixed with 10 ml scintillation cocktail (Carl Roth GmbH + Co. KG, Germany) in a 20-ml scintillation vial, and then counted for 2 min on a Liquid Scintillation Analyzer (LSA) (Tri-Carb® 2800 TR, PerkinElmer, Shelton, CT, USA). A subsample (2 ml) was used to measure element concentrations by an inductively coupled plasma-optical emission spectrometry (ICP-OES) (iCAP 7000 series ICP-OES, Thermo Fisher Scientific, Dreieich, Germany). Total C, N, and P contents in wheat straw were 363.3 mg g⁻¹, 33.3 mg g⁻¹, and 3.5 mg g⁻¹, respectively.

2.5. Destructive sampling

Soil samples were collected from three compartments: top bulk (0–4 cm from soil surface), rooted (4–12 cm), and bottom bulk (12–16 cm) soil (Fig. S1). In each compartment, soil was collected from three random locations. For microbial biomass measurements, two samples of 7–10 g of moist soil from each compartment were immediately placed in air-tight plastic bags and the soil was stored at 4°C until the next day. For phosphomonoesterase (PME) kinetic assays, approximately 0.5 g moist soil was kept in 100-ml Kimble KIMAX borosilicate laboratory glass bottles (Kimble Chase Life Science and Research Products, LLC., Meiningen, Germany) filled with deionized and sterile water with a soil-water ratio of 1:100 (*m/v*). Thereafter, bottles were shaken for 30 min on a shaker (200 rpm) before enzyme activity assays.

2.5. Measurement of Fe(II) and Fe(III) concentrations and ³²P and ³³P activities in soil solution

To measure Fe(II) concentration in soil solution, 2 ml of a sample were mixed with 500 µl ammonium acetate buffer (pH 4.5) and 500 µl phenanthroline solution (0.5%) in a 10-mm polystyrene cuvette (Th. Geyer GmbH & Co. KG, Renningen, Germany) and then measured at 512 nm on a spectrophotometer (NanoPhotometer® NP80, Implen GmbH, Munich, Germany). Then, 200 µl 10% ascorbic acid were added to each cuvette to completely reduce Fe(III) to Fe(II) after a 30-min reaction. Total Fe concentration was measured as Fe(II) as above (Elrod et al., 1991). Fe(III) concentration was calculated as the difference between total Fe and Fe(II) concentrations. Calibration was done by external FeCl₃ standards ranging from 5 to 300 µM.

The ³²P and ³³P activities in extracted soil solution were determined using a dual-labeling (³²P/³³P) counting procedure on the LSA (Tri-Carb® 2800 TR, PerkinElmer, Shelton, CT, US), corrected for respective isotope radioactive decays, and back-calculated to the reference date. Briefly, 1 ml soil solution was mixed with 10 ml scintillation cocktail (Carl Roth GmbH + Co. KG, Germany) and then counted

for 10 min. The percentage of ^{32}P or ^{33}P activity in soil solution derived from applied ^{32}P -labeled ferrihydrite-quartz-sand-pellet or ^{33}P -labelled wheat straw (%P per rhizobox) was calculated according to the following equation:

$$\%P = \frac{{}^{32}\text{P}/{}^{33}\text{P} \text{ activity in solution (Bq ml}^{-1}) \times \text{Solution volume (ml)}}{\text{Applied } {}^{32}\text{P}/{}^{33}\text{P} \text{ activity in rhizobox (Bq)}} \times 100 \quad (1)$$

where soil solution volume was estimated by soil moisture.

2.6. Soil microbial biomass measurement

Extractable microbial biomass carbon (MBC) and nitrogen (MBN) were measured using the chloroform-fumigation-extraction method (Vance et al., 1987) and were calculated according to the equation:

$$\text{MBC(MBN)} = \frac{E_C(E_N)}{k_{EC}(k_{EN})} \quad (2)$$

where k_{EC} and k_{EN} are equal to 0.45 (Brookes et al., 1985; Vance et al., 1987) and E_C and E_N are the difference between the content of organic C and the difference between the content of total N extracted from the fumigated and non-fumigated soils, respectively. The organic C and total N contents in each extract were measured by an elemental analyzer (Multi N/C 2100S, Analytik, Germany).

Microbial biomass phosphorus (MBP) was measured according to Brookes et al. (1984). Phosphorus was extracted with 0.5 M NaHCO_3 solution and was measured with the colorimetric method on a spectrophotometer (NanoPhotometer[®] NP80, Implen, Munich, Germany). A conversion factor of 0.40 and the recovery of a P spike in each soil sample were used to calculate MBP by calculating the difference between the content of P extracted from the fumigated and non-fumigated soils.

2.7. Enzyme kinetic assays

The PME kinetic was measured using fluorogenically labelled substrate of 4-methylumbelliferyl-phosphate (Sigma-Aldrich Co. Ltd) according to Marx et al. (2001). The PME kinetic was measured according to a Michaelis-Menten approach with the following range of substrate concentrations 0, 5, 10, 20, 50, 100, 150, and 200 μM . For assays, 50 μl soil suspension, 100 μl 4-methylumbelliferyl-phosphate, and 50 μl MES (2-(N-morpholino) ethanesulfonic acid) buffer (pH 6.5) were added into a 96-well black microplate (Brand GmbH, Wertheim, Germany). The fluorescence was repeatedly measured on a Victor 1420-050 Multi label counter (PerkinElmer, USA) at 0, 30, 60, 90, 120 min after incubation of microplates. The excitation and emission wavelengths were 355 nm and 460 nm, respectively. Duration of reading per well was 0.1 s.

Based on 4-methylumbelliferyl (MUF) pure substance calibration, the rate of PME activities was calculated as nmol MUF per g soil (dry weight) per hour

corresponded to the substrate added (in $\mu\text{mol g}^{-1}$ soil). The Michaelis-Menten equation was used to calculate the kinetic parameters V_{max} and K_m :

$$V = \frac{V_{\text{max}} \times S}{K_m + S} \quad (3)$$

where V is the reaction rate ($\text{nmol g}^{-1} \text{ soil h}^{-1}$), S is the substrate concentration ($\mu\text{mol g}^{-1}$ soil), V_{max} is the maximal reaction rate of enzymatic activity at saturating substrate concentration, and K_m is the substrate concentration at half-maximal rate ($1/2 V_{\text{max}}$). V_{max} and K_m were estimated using non-linear curve fitting in GraphPad Prism 8 (GraphPad Software, Inc., San Diego, USA).

2.8. ^{32}P and ^{33}P recovery in rice plants and microorganisms

At harvest, rice roots were carefully removed from rhizoboxes and were washed free of soil with deionized water. Rice shoots were separated from roots at the soil surface. The shoot and root samples were dried in an oven at 60°C for 48 h and then milled in a ball mill (Retsch MM200, Retsch GmbH, Haan, Germany). To measure total P content and the activities of ^{32}P and ^{33}P in shoots and roots, approximately 100 mg of each sample was digested with 2 ml of 65% HNO_3 at 180°C for 8 h. Each digested sample was filtered and filled up to 50 ml volume with deionized water. Subsample (2 ml) was used to measure the total P content by an inductively coupled plasma-optical emission spectrometry (ICP-OES) (iCAP 7000 series ICP-OES, Thermo Fisher Scientific, Dreieich, Germany). To measure ^{32}P and ^{33}P activities, 1 ml sample was mixed with 10 ml scintillation cocktail (Carl Roth GmbH + Co. KG, Germany) in a 20-ml scintillation vial, and then counted for 10 min on the LSA. The measured ^{32}P and ^{33}P activities were corrected for respective isotope radioactive decays and back-calculated to the reference date. The proportion of P derived from applied Fe-P or wheat straw ($\%P_{\text{Shoot/Root}}$) in shoot or root total P was calculated as:

$$\%P_{\text{Shoot/Root}} = \frac{\text{Total } ^{32}\text{P}/^{33}\text{P} \text{ activity in shoots/roots (Bq)} \times \text{P mass in pellets/straw (mg Bq}^{-1}\text{)}}{\text{Total P in shoots/roots (mg)}} \times 100 \quad (4)$$

where Total $^{32}\text{P}/^{33}\text{P}$ activity in shoots/roots is the activity (Bq) at the reference date, and P mass in pellets/straw is the specific mass of labeled P in pellets/straw and calculated by dividing total P by total $^{32}\text{P}/^{33}\text{P}$ activity in pellets/straw (mg Bq^{-1}).

To measure ^{32}P and ^{33}P activities in MBP, 1 ml P extraction sample (see above 2.6) was mixed with 10 ml cocktail in a scintillation vial and then measured for 5 min on the LSA. The measured ^{32}P and ^{33}P activities were corrected for respective isotope radioactive decays and back-calculated to the reference date. The ^{32}P and ^{33}P activities in MBP were calculated as the differences in ^{32}P and ^{33}P activities between samples extracted without and with fumigation and corrected by the recovery of a P spike in each soil sample. The proportion of P in MBP derived from applied Fe-P or wheat straw ($\%P_{\text{MBP}}$) in each soil compartment was calculated as:

$$\%P_{\text{MBP}} = \frac{{}^{32}\text{P}/{}^{33}\text{P} \text{ activity (Bq kg}^{-1}) \times \text{P mass in pellets/straw (mg Bq}^{-1})}{\text{MBP content (mg kg}^{-1})} \times 100 \quad (5)$$

where ${}^{32}\text{P}/{}^{33}\text{P}$ activity is the activity (Bq) in MBP at the reference date, and P mass in pellets/straw is the specific mass of labeled P in pellets/straw and calculated by dividing total P by total ${}^{32}\text{P}/{}^{33}\text{P}$ activity in pellets/straw (mg Bq^{-1}).

2.9. Statistical analysis

A one-way ANOVA, followed by the Tukey's HSD post-hoc test, was used to test the significance of differences ($p < 0.05$) of the V_{max} and K_m values of PME between water regimes (CF vs. AWD) or between soil compartments under each water regime and for the proportion of P derived from applied Fe-P and wheat straw in shoots and roots P between water regimes. A two-way ANOVA was used to test the effects of (i) water regime and (ii) rice growth on the E_h values, the percentage of ${}^{32}\text{P}$ and ${}^{33}\text{P}$ recovery, the concentrations of Fe(II) and Fe(III), and the concentrations of dissolved C, N, and P in soil solution. A two-way ANOVA was used to test the effects of (i) water regime (CF vs. AWD) and (ii) soil compartment on the contents of MBC, MBN, and MBP and the proportions of P derived from applied Fe-P and wheat straw in MBP. Exponential regression analysis was used to determine the relationships between E_h values and ${}^{32}\text{P}$ recovery and between E_h values and ${}^{33}\text{P}$ recovery in soil solution. All statistical tests were conducted using SPSS (Version 21, IBM, Armonk, NY, USA).

3. Results

3.1. Soil E_h , the recovery of ${}^{32}\text{P}$ and ${}^{33}\text{P}$, and the concentrations of Fe(II) and Fe(III) in soil solution

Soil E_h decreased under both CF and AWD regimes within ten days after rice transplantation (Fig. 2a). Soil E_h stabilized between -151 and -195 mV from day 10 to day 40 under CF regime (Fig. 2a). Alternate wetting and drying regime strongly increased soil E_h at drying phases (during 11–20 and 31–40 days) and decreased soil E_h after flooding (during 1–10 and 21–30 days) (Fig. 2a).

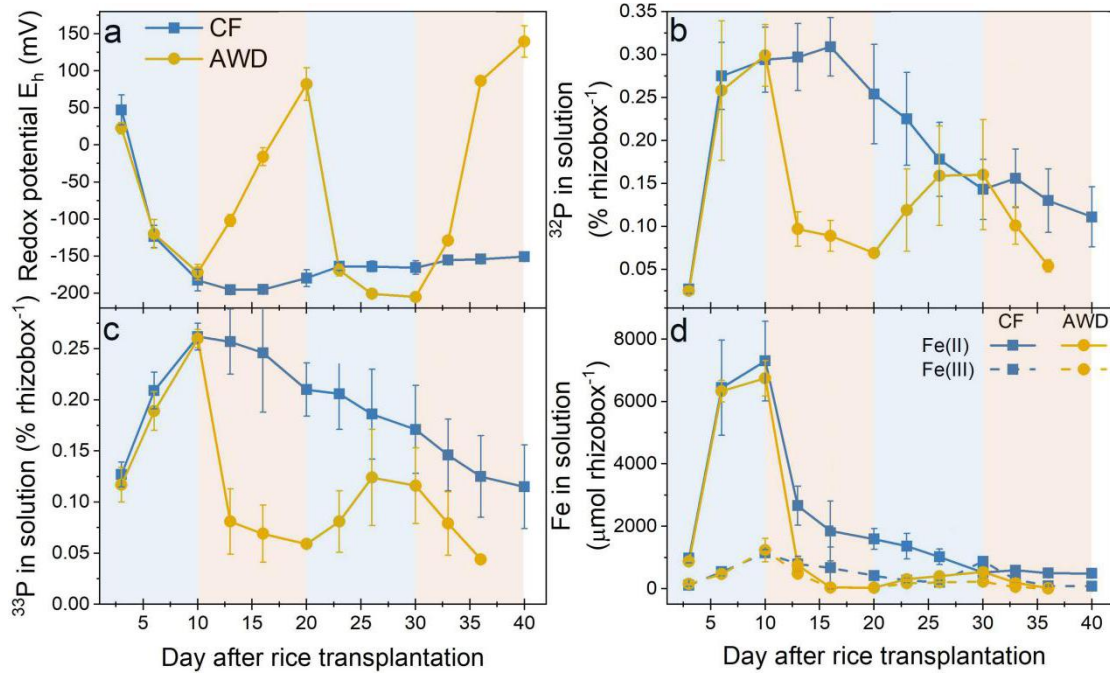


Fig. 2 Soil redox potential E_h (a), the recovery of ^{32}P (b) and ^{33}P (c), and the concentrations of Fe(II) (solid lines) and Fe(III) (dash lines) (d) in soil solution under continuous flooding (CF) (blue lines) and alternate wetting and drying (AWD) (yellow lines) regimes. The blue and orange shaded areas show the wetting and drying phases under AWD regime, respectively. Under AWD regime, the absence of data on day 40 indicates failure of soil solution collection due to increased evaporation and rice plant transpiration. The data are the means \pm standard errors ($n = 4$). Two-way ANOVA revealed significant effects ($p < 0.001$) of water regimes and rice growth on E_h values, the proportions of ^{32}P and ^{33}P , and the concentrations of Fe(II) and Fe(III) in soil solution.

Alternate wetting and drying regime decreased the ^{32}P and ^{33}P proportions in soil solution (as % from the added ^{32}P and ^{33}P activities) compared to continuous flooding regime (Fig. 2b, c). Under CF, the ^{32}P proportion abruptly decreased from day 16 to day 30, and the ^{33}P proportion smoothly decreased after day 10 (Fig. 2c). Under AWD, the peaks of ^{32}P and ^{33}P proportions in soil solution coincided with the onset of soil drainage (day 10 and day 30) (Fig. 2b, c).

Alternate wetting and drying decreased Fe(II) and Fe(III) concentrations compared to continuous flooding (Fig. 2d). Under CF, the peaks of Fe(II) and Fe(III) were only observed on day 10 (Fig. 2d, blue lines). In contrast, the peaks of Fe(II) under AWD were observed on day 10 and day 30 (Fig. 2d, yellow lines).

The ^{32}P and ^{33}P proportions in soil solution increased with decreasing redox potential (more negative E_h values) under two water regimes (Fig. 3).

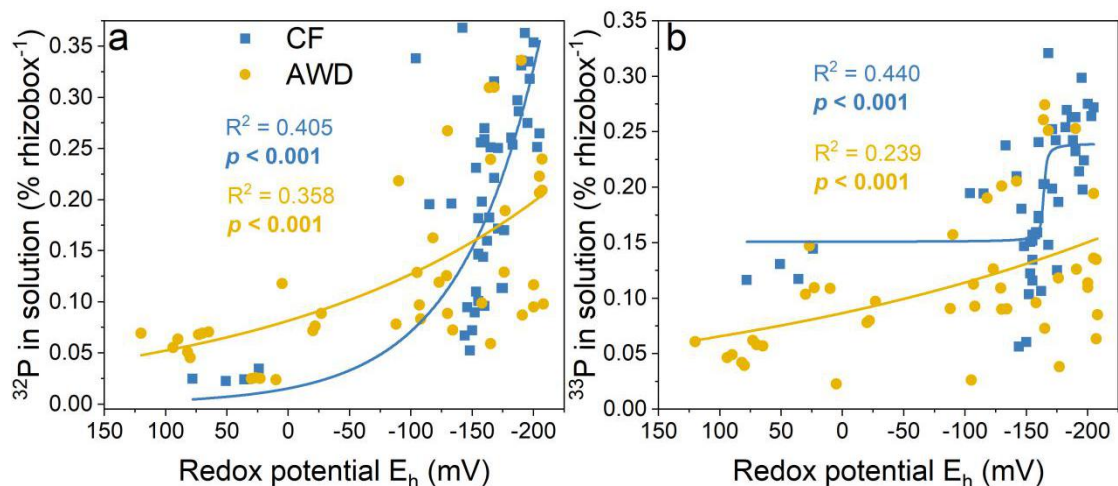


Fig. 3 Relationships between redox potential (E_h values) and either ^{32}P (a) or ^{33}P (b) proportions in soil solution under continuous flooding (CF) and alternate wetting and drying (AWD) regimes.

3.2. Soil microbial biomass and phosphomonoesterase kinetic parameters

Alternate wetting and drying pronouncedly decreased MBC and MBN contents in top bulk soil as compared to continuous flooding (Fig. 4a, b). However, water regimes had no effects on MBP content (Fig. 4c). The highest MBC, MBN, and MBP contents were found in rooted soil as compared to bulk soils (Fig. 4).

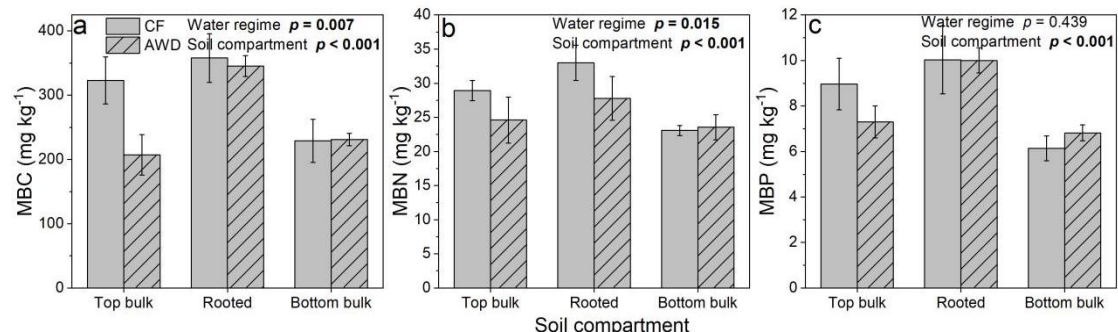


Fig. 4 Microbial biomass carbon (MBC, a), nitrogen (MBN, b), and phosphorus (MBP, c) contents in the top bulk, rooted, and bottom bulk soils under continuous flooding (CF) and alternate wetting and drying (AWD) regimes. The data are the means \pm standard errors ($n = 4$). The p values show the effects of water regime or rice growth on the respective parameter.

The PME activity was 9% higher in top bulk soil but was 14–18% lower in rooted and bottom bulk soil under CF vs. AWD regime (Fig. 5). Among three compartments, 15–50% higher V_{\max} values were found in rooted soil vs. bulk soil (Fig. 5). The affinity of PME to substrates (K_m values) was 4–28% lower under CF vs. AWD regime (Fig. 5). The K_m values of PME were 22–76% higher in rooted soil as compared to bulk soil (Fig. 5).

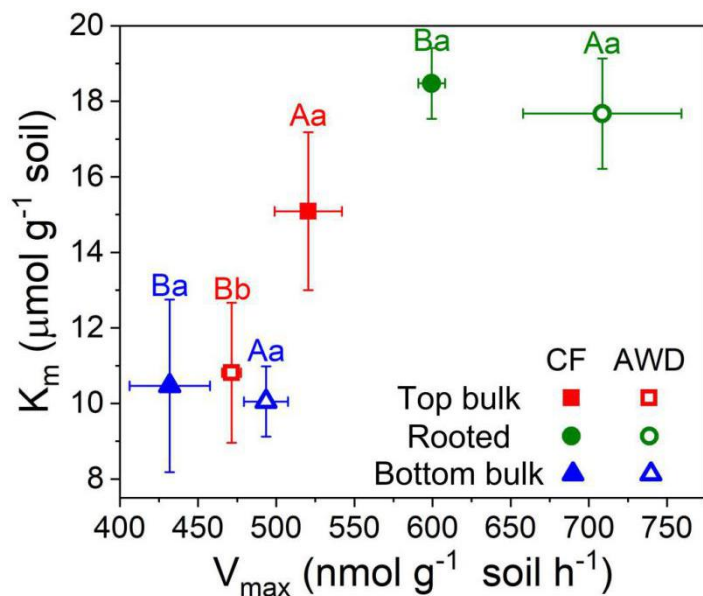


Fig. 5 Maximum reaction rate (V_{max}) and the affinity to a substrate (K_m) of phosphomonoesterase (PME) in the top bulk, rooted, and bottom bulk soil under continuous flooding (CF) (filled symbols) and alternate wetting and drying (AWD) (open symbols) regimes. The data are the means \pm standard errors ($n = 4$). Uppercase and lowercase letters represent significant differences ($p < 0.05$) in V_{max} and K_m between CF and AWD regimes, respectively. Significant differences ($p < 0.05$) in V_{max} and K_m values among the soil compartments were observed.

3.3. ³²P and ³³P recovery in rice plants and microorganisms

The Fe-P dissolution and wheat straw mineralization contributed up to 16% and 20% of the plant P uptake and up to 15% and 35% of microbial P uptake at day 40 after rice transplantation, respectively (Fig. 6). The proportions of P derived from applied Fe-P and wheat straw in shoots and roots were 43–64% higher under CF vs. AWD regime (Fig. 6a, b). Similarly, the proportion of P derived from applied Fe-P in MBP was 5–45% higher under CF vs. AWD regime (Fig. 6c). In contrast, the proportion of P derived from applied wheat straw in MBP was 6–18% higher under AWD vs. CF regime (Fig. 6d). Among three soil compartments, the proportion of P derived from applied Fe-P in MBP was 72–78% higher in bulk soil than in rooted soil (Fig. 6c). In contrast, the proportion of P derived from applied wheat straw in MBP was 16–42% higher in rooted soil than in bulk soil (Fig. 6d).

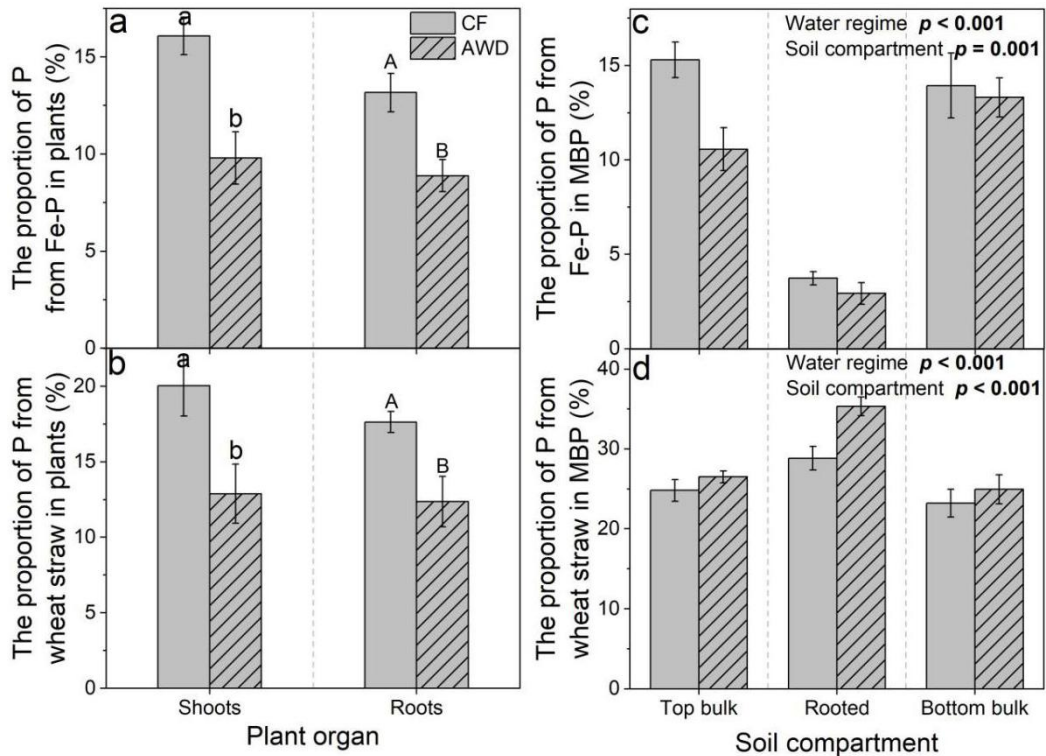


Fig. 6 Proportions of phosphorus (P) derived from applied ferric iron-bound P (Fe-P) and wheat straw in shoots or roots (a, b) and microbial biomass P (MBP, c, d) under continuous flooding (CF) and alternate wetting and drying (AWD) regimes. The data are the means \pm standard errors ($n = 4$). Uppercase or lowercase letters represent significant differences ($p < 0.05$) in the proportions of P derived from applied Fe-P and wheat straw in shoots or roots between CF and AWD regimes, respectively. The p values show the effects of water regime or rice growth on the respective parameter.

4. Discussion

4.1. Effects of water regimes on Fe-P dissolution and wheat straw mineralization

The ^{32}P proportion in soil solution was higher under CF vs. AWD regime (Fig. 2b), supporting the first hypothesis that AWD decreases mineral P solubilization (Fig. S2c). The rate of P release from the reductive dissolution of Fe-P depends on the activities of Fe reducers (Lovley et al., 2004; Wang et al., 2022c, d), redox potential (Schmidt et al., 2011; Wang et al., 2022c, d), and soil pH (Devau et al., 2009). Soil flooding expelled most of O_2 and restricted the exchange with atmospheric O_2 , thus decreasing rapidly E_h values during the first 10 days under both water regimes and from day 20 to day 23 under AWD regime (Fig. 2a). Low redox potentials (E_h values ranging from -314 mV to $+14$ mV) reflect the conditions for abiotic Fe-P dissolution (Weber et al., 2006) which pave the way for the growth of Fe reducers (Lovely et al., 2004). This is confirmed by the negative relationships between E_h values and ^{32}P proportions in the soil solution (Fig. 3a). Despite E_h values under CF regime were ranging from -195 mV to -151 mV from day 10 to day 40 (Fig. 2a), the ^{32}P and ^{33}P

proportions in soil solution started to decrease from day 16 and day 10 after rice transplantation, respectively (Fig. 2b, c). This can be attributed to several co-running processes: (i) increased P uptake by rice plants and microorganisms (Lazali and Bargaz, 2017), (ii) decreased microbial biomass because of the shift from aerobic to anaerobic microbial communities after flooding (Tian et al., 2013), and (iii) P co-precipitation and re-adsorption on soil minerals (Hinsinger, 2001).

Under AWD, the dynamics of ^{32}P proportion in soil solution showed an opposite pattern to E_h dynamics (Fig. 2a, b). This is because the reductive dissolution of Fe-P is redox-sensitive (Li et al., 2012). A rapid shift to oxidative conditions (high redox potentials) may decrease Fe-P dissolution and increase P_i re-adsorption on soil minerals during drying periods (Yan et al., 2017), thus decreasing P solubility and availability. The ^{33}P proportion in soil solution depended on the wheat straw mineralization by microorganisms, microbial and plant P uptake, and chemical processes of sorption/desorption of P on soil particles. The rate of P_o transformation from wheat straw is generally controlled by phosphatases (Cosgrove, 1980). Higher phosphomonoesterase activities in rooted soil where soil solution was collected were observed under AWD vs. CF regime (Fig. 5). Therefore, P release from P_o mineralization was expected to be increased under AWD vs. CF regime. However, the AWD decreased the ^{33}P proportion in soil solution compared to CF regime (Fig. 2c). Moreover, the ^{33}P proportions in soil solution were negatively related to E_h values (Fig. 3b), and contrasting patterns of the dynamics of E_h values and ^{33}P proportions were observed under AWD regime (Fig. 2a, c). This suggests that a significant fraction of the released P after wheat straw mineralization during AWD was mainly bound to the soil solid phase because of the increased P sorption capacity of soils after drying (Olsen and Court, 1982). Accordingly, soil water status is more important as a control of the release of P from P_o mineralization, and straw addition is unlikely to fully overcome P deficiency, especially under AWD regime.

4.2. Effects of water regimes on microbial biomass and phosphomonoesterase activities

Contrasting effects of water regimes on microbial biomass have been documented for the variety of soils (Mondini et al., 2002; Nandi, 2020). Our results showed that the effects of water regimes on microbial biomass were soil depth-dependent (Fig. 4). The decrease of microbial biomass in top bulk soil under AWD is most likely because microorganisms have not yet adapted to the AWD stress (Sawada et al., 2019; Bagheri-Novair, et al., 2020). Only the microorganisms with adaption strategies such as production of spores or cysts can survive drought stress (Blackwell et al., 2010). This is why AWD reduced microbial biomass in top bulk soil. However, AWD had less effects on microbial biomass in rooted and bottom bulk soil compared to top bulk soil (Fig. 4). This is because the soil experiences less swings in soil moisture with increasing depth (Brady and Weil, 2002). Nutrient availability plays a key role for the growth and activity of microorganisms. We found that dissolved C and N concentrations in soil solution were no longer different from day 23 to day 36 despite of contrasting water regimes (Fig. S2a, b). This is most likely due

to the provision of labile C by wheat straw decomposition which ultimately governed the microbial biomass (Yuan and Yue, 2012).

Phosphomonoesterase activities in top bulk soil were higher under CF vs. AWD regime (Fig. 5), thus following microbial biomass patterns (Fig. 4). Alternate wetting and drying regime increased phosphomonoesterase activities in rooted and bottom bulk soils (Fig. 5), although no differences in MBP were observed between two water regimes (Fig. 4c). This was coinciding with decreased ^{32}P and ^{33}P proportions in soil solution under AWD vs. CF regime (Fig. 2b, c). The contribution of P derived from Fe-P dissolution to MBP was lower in rooted soil than in bulk soil (Fig. 4c), suggesting a strong competition between rice plants and microorganisms for the available P. Accordingly, P-deficient microorganisms may increase the secretion of phosphomonoesterase mobilizing P_o to compensate for their P demand. This is supported by 18% higher phosphomonoesterase activities (V_{max}) in rooted soil under AWD vs. CF regime (Fig. 5). Microbial biomass and phosphomonoesterase activities were higher in rooted soil than in bulk soil (Fig. 3, 5), suggesting that microbial growth and activity were promoted by root exudates that provide easily available C sources (Marschner et al., 2011).

One strategy adopted by microorganisms to cope with P deficiency is increasing the affinity of their own phosphatases to the substrate (i.e., decreasing K_m values) (Lazali and Bargaz, 2017). The K_m values of PME was 4–28% higher under CF vs. AWD regime (Fig. 5), suggesting that a selection of microorganisms producing high-affinity phosphatases thrived and outcompeted those with low-affinity phosphatases under fluctuating redox potentials. Thus, the adaptation of microbial metabolism to AWD is a potential mechanism for regulating P_o transformation when soil moisture fluctuates (Wang et al., 2022a, b).

4.3. Effects of water regimes on the contributions of Fe-P and wheat straw to P demands of rice plants and microorganisms

Continuous flooding increased the contribution of Fe-P to rice plant and microbial P uptake (Fig. 6a, c) because of the increased rates of the reductive dissolution of Fe-P under low-redox conditions after flooding (Fig. 2a, b). In contrast to our expectations, AWD regime decreased the contribution of wheat straw-derived P to the P nutrition of rice plants compared to CF regime (Fig. 6b). Thus, our second hypothesis that AWD regime induces higher contributions of P_o to rice plant P demand was not confirmed. However, the hypothesis that AWD regime increases the contribution of P_o to microbial P nutrition was supported by 5–64% higher ^{33}P proportions in MBP under AWD vs. CF regime (Fig. 6d). This means that microorganisms immobilized most P derived from wheat straw mineralization to their biomass, thus decreasing P availability to plants (Fig. 7). Phosphorus uptake by rice plants is controlled not only by the P availability in soil solution, but also by the processes of P transport to the roots (Jungk and Claasen, 1989). Apparently, continuous flooding increased plant available P by the improved P diffusion compared to alternate wetting and drying regime (Fig. 7).

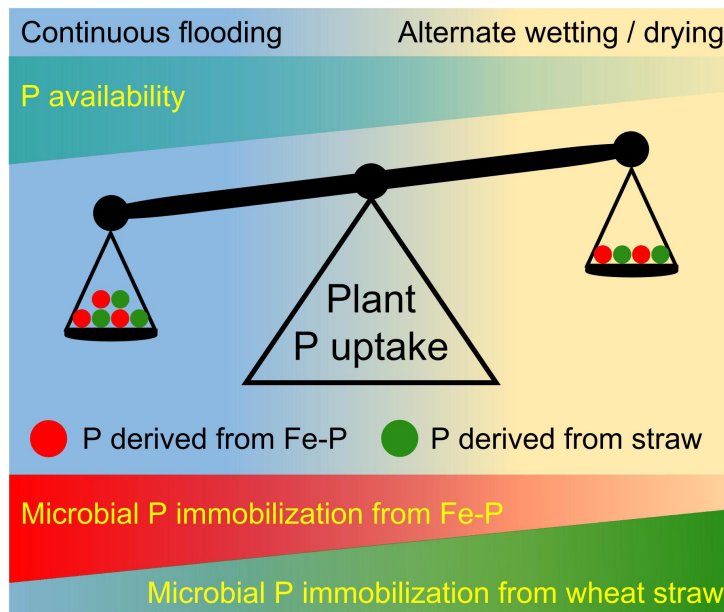


Fig. 7 Conceptual scheme demonstrating the effects of water regimes on mineral phosphorus (P) availability and the contributions of ferric iron-bound P (Fe-P) and wheat straw-driven P to P uptake by rice plants and microorganisms. Trapezoids with color gradients demonstrate either the relative P availability in soil solution or the relative contributions of Fe-P and wheat straw to microbial biomass P from high (dark) to low (light).

72–78% lower contributions of Fe-P and 16–42% higher contributions of wheat straw-driven P to MBP were observed in rooted soil vs. bulk soil (Fig. 6c, d). Thus, the third hypothesis that microorganisms compensate for their P demand from P_o sources under a strong plant-microorganism competition was supported. Microorganisms appear to be more competitive for P_o than rice plants, and rice plants are more competitive than microorganisms for P released from the reductive dissolution of Fe-P (Fig. 7). Finally, these findings opened further perspectives for estimating the contributions of Fe-P and P_o to rice grains under different water regimes.

5. Conclusions

Continuous flooding increased the release of P from both Fe-P and wheat straw into the soil solution. The effects of water regimes on microbial biomass and phosphomonoesterase activities were soil depth-dependent. Alternate wetting and drying induced drought stress on microorganisms in top bulk soil, thus reducing microbial biomass and phosphomonoesterase activities. Despite water regimes had no effects on MBP contents, AWD increased phosphomonoesterase activities in rooted and bottom bulk soil. This can be attributed to decreased P availability caused by higher P sorption on mineral phases of soils after drying and increased competition between rice plants and microorganisms for P. Continuous flooding promoted the contributions of P released from Fe-P dissolution and wheat straw decomposition to P

nutrition. Rice plants outcompeted microorganisms for P released from the reductive dissolution of Fe-P, and microorganisms increased the immobilization of wheat straw-derived P to their biomass. The released P amount by Fe-P dissolution and wheat straw decomposition contributed up to 36% and 40% of the plant and microbial P demand, respectively. Thus, phosphate fertilization strategies should be adapted considering the rates of P mobilization from Fe (oxyhydr)oxides and straw under different water regimes in paddy soils.

Acknowledgments

The authors gratefully acknowledge the China Scholarship Council (CSC) for financial support for Chaoqun Wang. This work was supported by the research grant from German Research Foundation (DO 1533/3-1; GU 406/33-1) and the RUDN University Strategic Academic Leadership Program. Michaela Dippold was funded by the Robert Bosch Junior Professorship. The authors would like to thank Jan Muhr and Marvin Blaue of the Laboratory for Radioisotopes (LARI) of the University of Goettingen for their advice, support, and measurements. We also thank Jake Beyer and Dr. Florian Carstens for constructive advising as well as a technical staff of the Department of Agricultural Soil Science, University of Goettingen, Karin Schmidt, for microbial biomass carbon and nitrogen measurements.

References

- Bagheri-Novair, S., Hosseini, H.M., Etesami, H., Razavipour, T., Lajayer, B.A., Astatkie, T., 2020. Short-term soil drying–rewetting effects on respiration rate and microbial biomass carbon and phosphorus in a 60-year paddy soil. *3 Biotech* 10(11), 1–11.
- Belder, P., Bouman, B.A.M., Cabangon, R., Guoan, L., Quilang, E.J.P., Li, Y., Spiertz, J.H.J., Tuong, T.P., 2004. Effect of water-saving irrigation on rice yield and water use in typical lowland conditions in Asia. *Agricultural Water Management* 65, 193–210.
- Bindraban, P.S., Dimkpa, C.O., Pandey, R., 2020. Exploring phosphorus fertilizers and fertilization strategies for improved human and environmental health. *Biology and Fertility of Soils* 56, 299–317.
- Blackwell, M.S.A., Brookes, P.C., de la Fuente-Martinez, N., Gordon, H., Murray, P.J., Snars, K.E., Williams, J.K., Bol, R., Haygarth, P.M., 2010. Phosphorus solubilization and potential transfer to surface waters from the soil microbial biomass following drying-rewetting and freezing-thawing. *Advances in Agronomy* 106, 1–35.
- Bouman, B.A.M., Tuong, T.P., 2001. Field water management to save water and increase its productivity in irrigated lowland rice. *Agricultural Water Management* 49, 11–30.
- Brady, N., Weil, R., 2002. *The Nature and Properties of Soils*, Pearson Education, Inc, Upper Saddle River, NJ, p. 960.
- Brookes, P.C., Landman, A., Pruden, G., Jenkinson, D., 1985. Chloroform fumigation and the release of soil nitrogen: a rapid direct extraction method to measure microbial biomass nitrogen in soil. *Soil Biology and Biochemistry* 17, 837–842.
- Brookes, P.C., Powlson, D.S., Jenkinson, D.S., 1984. Phosphorus in the soil microbial biomass. *Soil Biology and Biochemistry* 16, 169–175.
- Butterly, C.R., Bünemann, E.K., McNeill, A.M., Baldock, J.A., Marschner, P., 2009. Carbon pulses but not phosphorus pulses are related to decreases in microbial biomass during repeated drying and rewetting of soils. *Soil Biology and Biochemistry* 41, 1406–1416.
- Chen, H., Jarosch, K.A., Mészáros, É., Frossard, E., Zhao, X., Oberson, A., 2021. Repeated drying and rewetting differently affect abiotic and biotic soil phosphorus (P) dynamics in a sandy soil: A ³³P soil incubation study. *Soil Biology and Biochemistry* 153, 108079.
- Cordell, D., Drangert, J.O., White, S., 2009. The Story of Phosphorus: Global food security and food for thought. *Global Environmental Change* 19, 292–305.

- Cosgrove, D.J., 1980. *Inositol Phosphates—Their Chemistry, Biochemistry and Physiology*. Elsevier Scientific, Amsterdam.
- Darilek, J.L., 2010. Effect of land use conversion from rice paddies to vegetable fields on soil phosphorus fractions. *Pedosphere* 2, 137–145.
- Devau, N., Cadre, E.L., Hinsinger, P., Jaillard, B., Gérard, F., 2009. Soil pH controls the environmental availability of phosphorus: experimental and mechanistic modelling approaches. *Applied Geochemistry* 24, 2163–2174.
- Elrod, V.A., Johnson, K.S., Coale, K.H., 1991. Determination of subnanomolar levels of iron(II) and total dissolved iron in seawater by flow injection analysis with chemiluminescence detection. *Analytical Chemistry* 63(9), 893–898.
- Fairhurst, T., Dobermann, A., 2002. Rice in the global food supply. *World* 5, 454–349.
- Forber, K.J., Withers, P.J.A., Ockenden, M.C., Haygarth, P.M., 2018. The phosphorus transfer continuum: a framework for exploring effects of climate change. *Agricultural and Environmental Letters* 3, 180036.
- Gong, Z.T., Zhang, G.L., Chen, Z.C. (Eds.), 2007. *Pedogenesis and Soil Taxonomy*. Science Press, Beijing, China, pp. 613–626.
- Gupta, R.K., Ladha, J.K., Singh, J., Singh, G., Pathak, H., 2007. Yield and phosphorus transformations in a rice–wheat system with crop residue and phosphorus management. *Soil Science Society of America Journal* 71(5), 1500–1507.
- Hinsinger, P., 2001. Bioavailability of soil inorganic P in the rhizosphere as affected by root- induced chemical changes: a review. *Plant and Soil* 237, 173–195.
- Jungk, A., Claassen, N., 1989. Availability in soil and acquisition by plant as the basis for phosphorus and potassium supply to plants. *Zeitschrift für Pflanzenernährung und Bodenkunde* 152(2), 151–157.
- Kim, D.W., Rakwal, R., Agrawal, G.K., Jung, Y.H., Shibato, J., Jwa, N.S., Iwahashi, Y., Iwahashi, H., Kim, D.H., Shim, I., Usui, K., 2005. A hydroponic rice seedling culture model system for investigating proteome of salt stress in rice leaf. *Electrophoresis* 26(23), 4521–4539.
- Lazali, M., Bargaz, A., 2017. Examples of belowground mechanisms enabling legumes to mitigate phosphorus deficiency. *Legume Nitrogen Fixation in Soils With Low Phosphorus Availability*. Springer, Berlin/Heidelberg, Germany, pp. 135–152.
- Li, Y., Yu, S., Strong, J., Wang, H., 2012. Are the biogeochemical cycles of carbon, nitrogen, sulfur, and phosphorus driven by the “FeIII-FeII redox wheel” in dynamic redox environments? *Journal of Soils and Sediments* 12, 683–693.
- Lovley, D.R., Holmes, D.E., Nevin, K.P., 2004. Dissimilatory Fe(III) and Mn(IV)

- reduction. *Advances in Microbial Physiology* 49, 219–286.
- Maranguit, D., Guillaume, T., Kuzyakov, Y., 2017. Effects of flooding on phosphorus and iron mobilization in highly weathered soils under different land-use types: short-term effects and mechanisms. *Catena* 158, 161–170.
- Marschner, P., Crowley, D., Rengel, Z., 2011. Rhizosphere interactions between microorganisms and plants govern iron and phosphorus acquisition along the root axis – model and research methods. *Soil Biology and Biochemistry* 43, 883–894.
- Marx, M., Wood, M., Jarvis, S., 2001. A fluorimetric assay for the study of enzyme diverooted soility in soils. *Soil Biology and Biochemistry* 33, 1633–1640.
- Mondini, C., Contin, M., Leita, L., De Nobili, M., 2002. Response of microbial biomass to air-drying and rewetting in soils and compost. *Geoderma* 105, 111–124.
- Nandi, S., 2020. Microbial biomass carbon and organic carbon fractions in paddy soil as influenced by rice stubble management. *International Journal of Microbiology Research* 12, 1871–1874.
- Olsen, R., Court, M., 1982. Effect of wetting and drying of soils on phosphate adsorption and resin extraction of soil phosphate. *Journal of Soil Science* 33, 709–717.
- Paterson, E., 2000. Iron oxides in the laboratory. Preparation and characterization. *Clay Minerals* 27, 393.
- Rakotoson, T., Amery, F., Rabeharisoa, L., Smolders, E., 2014. Soil flooding and rice straw addition can increase isotopic exchangeable phosphorus in P-deficient tropical soils. *Soil Use and Management* 30, 189–197.
- Saleque, M.A., Abedin, M.J., Bhuiyan, N.I., 1996. Effect of moisture and temperature regimes on available phosphorus in wetland rice soils. *Communications in Soil Science and Plant Analysis* 27, 2017–2023.
- Saleque, M.A., Naher, U.A., Islam, A., Pathan, A.B.M.B.U., Hossain, A.T.M.S., Meisner, C.A., 2004. Inorganic and organic phosphorus fertilizer effects on the phosphorus fractionation in wetland rice soils. *Soil Science Society of America Journal* 68, 1635–1644.
- Sattari, S.Z., Bouwman, A.F., Giller, K.E., van Ittersum, M.K., 2012. Residual soil phosphorus as the missing piece in the global phosphorus crisis puzzle. *Proceedings of the National Academy of Sciences of the United States of America* 109, 6348–6353.
- Sawada, K., Funakawa, S., Kosaki, T., 2019. Immediate and subsequent effects of drying and rewetting on microbial biomass in a paddy soil. *Soil Science and Plant Nutrition* 65(1), 28–35.

- Schmidt, H., Eickhorst, T., Tippkoetter, R., 2011. Monitoring of root growth and redox conditions in paddy soil rhizotrons by redox electrodes and image analysis. *Plant and Soil* 341, 221–232.
- Siebers, N., Hofmann, D., Schiedung, H., Landsrath, A., Ackermann, B., Gao, L., Mojzeš, P., Jablonowski, N.D., Nedbal, L., Amelung, W., 2019. Towards phosphorus recycling for agriculture by algae: Soil incubation and rhizotron studies using ³³P-labeled microalgal biomass. *Algal Research* 43, 101634.
- Syers, J.K., Johnston, A.E., Curtin, D., 2008. Efficiency of soil and fertilizer phosphorus use. *FAO Fertilizer and Plant Nutrition Bulletin*. 18.
- Tian, J., Dippold, M., Pausch, J., Blagodatskaya, B., Fan, M., Li, X., Kuzyakov, Y., 2013. Microbial response to rhizodeposition depending on water regimes in paddy soils. *Soil Biology and Biochemistry* 65, 195–203.
- Vance, E., Brookes, P., Jenkinson, D., 1987. An extraction method for measuring soil microbial biomass C. *Soil Biology and Biochemistry* 19, 703–707.
- Wang, C.Q., Blagodatskaya, E., Dippold, M.A., Dorodnikov, M., 2022a. Keep oxygen in check: Contrasting effects of short-term aeration on hydrolytic versus oxidative enzymes in paddy soils. *Soil Biology and Biochemistry* 169, 108690.
- Wang, C.Q., Dippold, M.A., Blagodatskaya, E., Dorodnikov, M., 2022b. Oxygen matters: Short-and medium-term effects of aeration on hydrolytic enzymes in a paddy soil. *Geoderma* 407, 115548.
- Wang, C.Q., Thielemann, L., Dippold, M.A., Guggenberger, G., Kuzyakov, Y., Banfield, C.C., Ge, T.D., Guenther, S., Bork, P., Horn, M.A., Dorodnikov, M., 2022c. Can the reductive dissolution of ferric iron in paddy soils compensate phosphorus limitation of rice plants and microorganisms?. *Soil Biology and Biochemistry* 168, 108653.
- Wang, C.Q., Thielemann, L., Dippold, M.A., Guggenberger, G., Kuzyakov, Y., Banfield, C.C., Ge, T.D., Guenther, S., Bork, P., Horn, M.A., Dorodnikov, M., 2022d. Microbial iron reduction compensates for phosphorus limitation in paddy soils. *Science of The Total Environment* 155810.
- Weber, K.A., Achenbach, L.A., Coates, J.D., 2006. Microorganisms pumping iron: anaerobic microbial iron oxidation and reduction. *Nature Reviews Microbiology* 4, 752–764.
- Wu, X.H., Wang, W., Yin, C.M., Hou, H.J., Xie, K.J., Xie, X.L., 2017. Water consumption, grain yield, and water productivity in response to field water management in double rice systems in China. *PLoS ONE* 12, e0189280.
- Yan, X., Wei, Z., Hong, Q., Lu, Z., Wu, J., 2017. Phosphorus fractions and sorption characteristics in a subtropical paddy soil as influenced by fertilizer sources. *Geoderma* 295, 80–85.

- Yu, X., Keitel, C., Dijkstra, F.A., 2021. Global analysis of phosphorus fertilizer use efficiency in cereal crops. *Global Food Security* 29, 100545.
- Yuan, B.C., Yue, D.X., 2012. Soil microbial and enzymatic activities across a chronosequence of Chinese pine plantation development on the Loess Plateau of China. *Pedosphere* 22, 1–12.
- Zhu, Z., Ge, T., Luo, Y., Liu, S., Xu, X., Tong, C., Shibistova, O., Guggenberger, G., Wu, J., 2018. Microbial stoichiometric flexibility regulates rice straw mineralization and its priming effect in paddy soil. *Soil Biology and Biochemistry* 121, 67–76.
- Zornoza, R., Guerrero, C., Mataix-Solera, J., Arcenegui, V., García-Orenes, F., Mataix-Beneyto, J., 2006. Assessing air-drying and rewetting pre-treatment effect on some soil enzyme activities under Mediterranean conditions. *Soil Biology and Biochemistry* 38, 2125–2134.

Supplementary

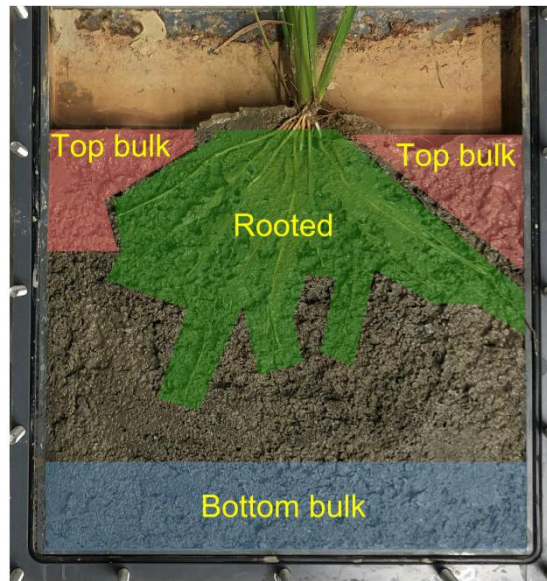


Fig. S1 Sampling locations in three soil compartments including top bulk, rooted, and bottom bulk soils

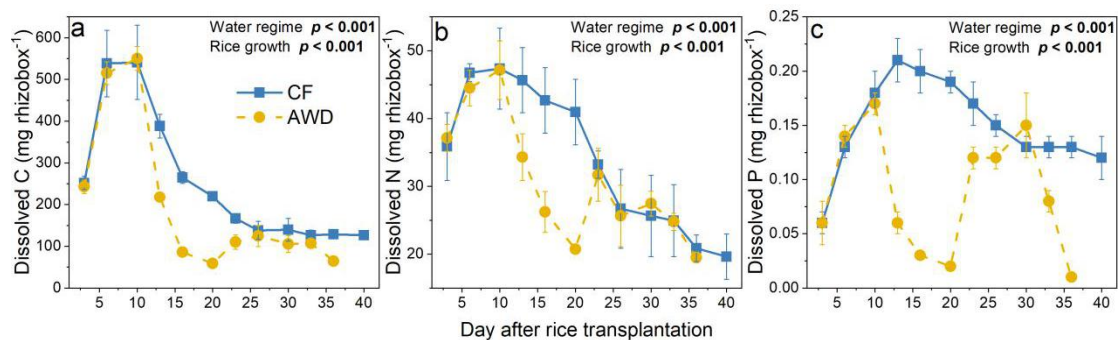


Fig. S2 Dynamics of dissolved carbon (C; a), nitrogen (N; b) and phosphorus (P; c) concentrations in soil solution under continuous flooding (CF; blue and solid line) and alternate wetting and drying (AWD; yellow and dashed line) regimes. Under AWD regime, the absence of data on day 40 indicates failure of soil solution collection due to increased evaporation and rice plant transpiration. The data are mean \pm standard error ($n = 4$). The p values show the effects of water regime or rice growth on the respective parameter.

Curriculum vitae

First name, last name: Chaoqun, Wang

Date and place of birth: 1993.06.12, Henan Province, China

Nationality: Chinese

Email: chaoqun.wang@forst.uni-goettingen.de

Education and degrees

- **Georg-August-Universität Göttingen, Germany** 2019–2022
PhD student in Biogeochemistry of Agroecosystems
Advisors: Prof. Michaela A. Dippold, Dr. Maxim Dorodnikov, Prof. Georg Guggenberger
Thesis title: Biogeochemical mechanisms of P and C cycling in rice-paddy systems driven by enzymatic reactions and the Fe(III)-Fe(II) redox wheel
- **Chinese Academy of Forestry, China** 2016–2019
MSc. in Soil Science
Advisor: Prof. Ruzhen Jiao
Thesis title: Study on soil properties change of Chinese fir plantation based on stand age effect and stand density effect
- **Qiqihar University, China** 2012-2016
BSc. in Biotechnology
Thesis title: Response of proteome of phthalate-degrading bacteria to dimethyl phthalate pollution

Publications

- Wang C.Q.**, Blagodatskaya E., Dippold M.A., Dorodnikov M., 2022. Keep oxygen in check: contrasting effects of short-term aeration on hydrolytic versus oxidative enzymes in paddy soils. *Soil Biology and Biochemistry* 169, 108690.
- Wang C.Q.**, Dippold M., Blagodatskaya E., Dorodnikov M., 2022. Oxygen matters: Short- and medium-term effects of aeration on hydrolytic enzymes in a paddy soil. *Geoderma* 407, 115548.
- Wang, C.Q.**, Bilyera, N., Blagodatskaya, E., Zhang, X., Dippold, M.A., Dorodnikov, M. (2022). Keep oxygen in check: An improved *in-situ* zymography approach for mapping anoxic hydrolytic enzyme activities in a paddy soil. *Science of the*

Total Environment 850, 158118.

Wang C.Q., Thielemann L., Dippold M.A., Guggenberger G., Kuzyakov Y., Banfield C.C., Ge T.D., Guenther S., Bork P., Horn M.A., Dorodnikov M., 2022. Can the reductive dissolution of ferric iron in paddy soils compensate phosphorus limitation of rice plants and microorganisms? *Soil Biology and Biochemistry* 168, 108653.

Wang C.Q., Thielemann L., Dippold M.A., Guggenberger G., Kuzyakov Y., Banfield C.C., Ge T.D., Guenther S., Bork P., Horn M.A., Dorodnikov M., 2022. Microbial iron reduction compensates for phosphorus limitation in paddy soils. *Science of the Total Environment* 837, 155810.

Presentations at conferences

Oral presentation: An improved method for extracellular enzyme assays in paddy soil: a comparative study under aerobic and anaerobic conditions

European Geoscience Union 2021, online

Oral presentation: Can ferric iron reduction in paddy soils compensate phosphorus limitation of rice plants and microorganisms?

European Geoscience Union 2022, Vienna, Austria

Declaration

I hereby declare, to the best of my knowledge and belief, that this thesis contains no material previously published or written by another person, except where due reference has been made in the text of the thesis. This thesis contains no material which has been accepted or definitely rejected for the award of any other doctoral degree at any university.

Erklärung

Hiermit erkläre ich, die vorliegende Arbeit selbst verfasst, keine anderen als die angegebenen Quellen und Hilfsmittel benutzt sowie alle wörtlich und sinngemäß übernommenen Stellen in der Arbeit gekennzeichnet zu haben. Ferner erkläre ich, dass ich nicht anderweitig mit oder ohne Erfolg versucht habe, eine Dissertation einzureichen oder mich einer Doktorprüfung zu unterziehen.